Identification of Membrane Associated Proteins as Potential Markers for the DLKP Clonal Subpopulations

Andrew McCann

PhD **2016**

Identification of Membrane Associated Proteins as Potential Markers for the DLKP Clonal Subpopulations

A thesis submitted for the degree of Ph.D.

by

Andrew McCann, B.Sc. (Hons)

The research work described in this thesis was performed under the supervision of

Dr. Anne-Marie Larkin, Dr. Joanne Keenan and

Prof. Martin Clynes

School of Biotechnology
National Institute for Cellular Biotechnology
Dublin City University

September 2016

I hereby certify that this material, which I now submit for assessment on the programme of study leading to the award of Ph.D. is entirely my own work and that I have exercised reasonable care to ensure that the work is original, and to does not to the best of my knowledge breach any law of copyright, and has not been taken from the work of others save and to the extent that such work has been cited and acknowledged within the text of my work.

Signed: _____ **ID No.:** 10113444

Date: _____

Acknowledgements

I will be forever grateful to Professor Martin Clynes for giving me the opportunity to do a Ph.D in the NICB. Martin took a chance on me 6 years ago and I feel I owe a huge debt to him for this incredible experience. Over the years Martin has shown me a new way of thinking and has influenced me to speak my mind, which not only allowed me to grow as a scientist but more importantly as a person as well. Thanks to you, the NICB has been a great place to work in.

I am also very grateful to my supervisor Dr. Annemarie Larkin, who has constantly helped and guided me through this process. From the start you have had to endure constant knocking on your door followed by a quick question, that never turned out to be quick. Both Professor Martin Clynes and Dr. Annemarie Larkin you both have offered me constant encouragement, help, advice, guidence and most of all support over the last six years. There were rocky times for me and without this support I wouldn't have made it through.

I would like to acknowledge the many people in the center who have made a huge impact on me both personally and professionally throughout my Ph.D. For the first two years I worked very closely with Dr. Joanne Keenan, who through her in depth knowledge and teaching, you coached me on everything from invasion assays to anoikis assays and prepared me for what was to come. A huge thanks goes out to Dr. Paul Dowling, who with conveying a simple idea at my transfer, helped change the direction of this project. I would also like to thank Michael Henry for his lengthy input into the world of mass spectrometry, you made it sound so easy. There are a number of people, along with Dr. Annemarie Larkin, who directed and made the *in vivo* study happen, so a special thanks goes to Professor Robert Straubinger and Ms. Ninfa Straubinger, University at Buffalo, who provided their unrivaled expertise. Also a huge thanks to Dr. Sandra Roche and Dr. Fiona O'Neill for communicating the results of the study with me and helping me put it all together. A big thanks to Professor Susan Kennedy and Damian Tiernan, Royal Victoria Eye and Ear Hospital for taking the time to examine and offer a pathologists view on the xenografts. I would also like to thank Mr. Vincent Lynch for offering a surgeons view on the animal study, but also for his weekly visits and chats throughout the last number of years.

Working in G116 with Dr. Helena Joyce was an absolute pleasure, you offered unbiased input and direction on my project when it was needed, but was always available to listen to my woes. Also Edel McAuley, you have been in the lab everyday through a number of my meltdowns and you have also helped me in so many other ways throughout the years. I cannot thank both of you enough! A big thanks goes to Kerrie Evans for help with the SPR transfections and to Leah Quinn for her help with immunoblots. I would also like to thank Dr. Finbarr O'Sullivan and Dr. Clair Gallagher, you guys were the two people who I could reply on for help with the flourescent microscope. I would like to thank Creina

Slator for consoling me when things got the better of me. Gemma, thanks for providing me with pancreatic and breast cancer cell lines when needed. To Orla for your help deconstructing and simplifying Micks mass spectrometry lectures. Everyone on the first and second floors who I constantly badgered for help and anyone else that I may have forgotten.

To the staff past and present, who made the day to day things easier to bare. From Gillian for her excellent organisation of the prep room to Carol, Mairead, Emer, Geraldine and Yvonne for running everything so smoothly from the front office, with you guys around any problem is a problem solved!

Finally, there are some close family and friends which I would like to acknowledge. I would like to thank Barbara Bates, Lisa Fergus and Lorna Eggers for our 11 years of friendship which certainly made me stronger throughout this Ph.D. You guys have always encouraged me to stick with it and I owe you guys so much for that. Barbara, I reached level 10, its endgame! Also thanks to Nelson Moody and John O'Brien for listening to me when I had drained the life out of everyone else. You all offered a distraction from the work when one was needed.

I would like to thank my parents Gertrude and Andy, who from the day I was born have always supported and encouraged me to do whatever I wanted and never stood in my way. You guys did well to raise two doctors in the one family. A big thank you has to go to my sister Sinead, who is the only one in my family that understands what it takes to do a Ph.D. Our intense Ph.D chats are finally coming to an end Sinead and in a strange way I will miss them. I would also like to thank Derek White who did his best to challenge and understand my work.

I've saved the best until last. Chris, my fiancé and husband to be. So far you have had to endure a relationship like no other. We met when I was a student and 9 years later I'm still a student. You have been there from the start, offered so much love, support and encouragement and you have had to listen to so much more than anyone else. This process has certainly tested us as a couple but I feel we are closer than ever. Next year we will finally get to start our married life together and I look forward to see what the next chapter will bring for us.

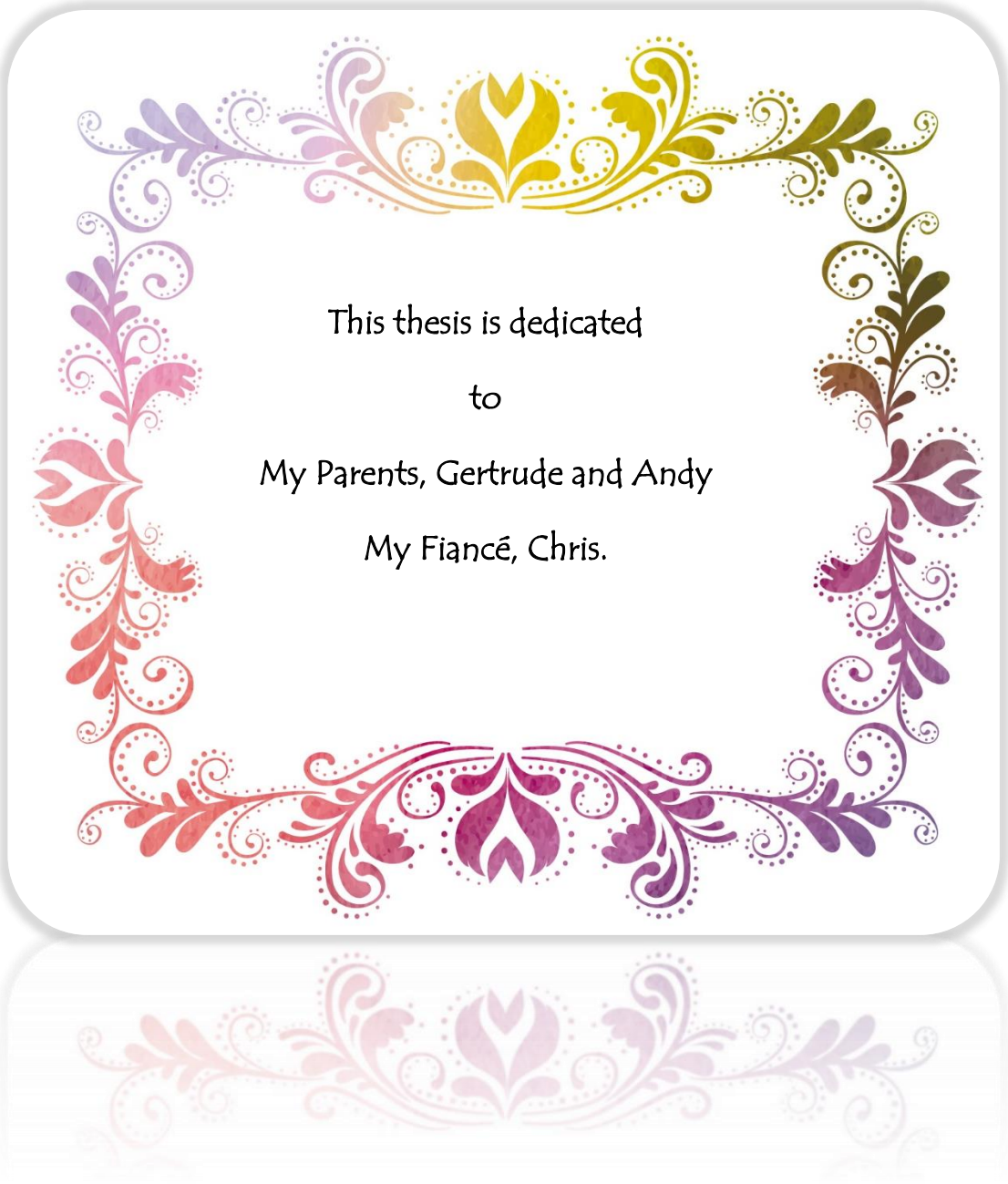
This thesis is dedicated
to
My Parents, Gertrude and Andy
My Fiancé, Chris.

I would like to remember a number of people who passed away during the course this Ph.D.:

My aunt, Rita McCann

Our close Neighbour, Dermot Hazard

My uncle, Sean McCann

My uncle, Eamon Briscoe

Extended family member, Sheila White

Abbreviations

%	-	Percentage
AACR	-	American Association for Cancer Research
Ab	-	Antibody
AC	-	Adenocarcinoma
ACN	-	Acetonitrile
AD	-	Adenocarcinoma
Ag	-	Antigen
AHNAK	-	Neuroblast differentiation-associated protein
ALCAM	-	Activated leukocyte cell adhesion molecule
ALK	-	Anaplastic Lymphoma Receptor Tyrosine Kinase
ATCC	-	American Tissue Culture Collection
ATP	-	Adenosine Triphosphate
BAC	-	Bronchioloalveolar carcinoma
BCRP	-	Breast cancer resistant protein
BH_4	-	5,6,7,8-Tetrahydrobiopterin
BL	-	Basal-like
BrdU	-	Bromodeoxyuridine
BSA	-	Bovine Serum Albumin
CM	-	Conditioned Medium
CSC	-	Cancer Stem Cell
cSCLC	-	Combined Small Cell Lung Carcinoma
Ctrl	-	Control
Da	-	Dalton
DAB	-	Diaminobenzidine
DCU	-	Dublin City University
DFMO	-	D, L-alpha-difluoromethylornithine
DMEM	-	Dulbeccos Modified Eagles Media
DMSO	-	Dimethyl Sulfoximide
DNA	-	Deoxyribonucleic Acid
DSMZ	-	Deutsche Sammlung von Mikroorganismen und Zellkulturen
ECACC	-	European Collection of Animal Cell Cultures
ECL	-	Enhanced Chemiluminescence
ECM	-	Extra Cellular Matric
EDTA	-	Ethylene Diamine Tetra-acetic Acid

EGFR	-	Epidermal growth factor receptor
EMA	-	European Medicines Agency
EMT	-	Epithelial-Mesenchymal Transition
ER	-	Estrogen Receptor
ERK	-	Extracellular signal-regulated Kinases
EtOH	-	Ethanol
FBS	-	Foetal Bovine Serum
FCS	-	Foetal Calf Serum
FDA	-	Food and Drug Administration
FGFR	-	Fibroblast growth factor receptor
FITC	-	Fluoroscein-Isocyanate
GAPDH	-	Glyceraldehyde-3-Phosphate Dehydrogenase
GEMMS	-	Genetically Engineered Mouse Models
H_2O_2	-	Hydrogen Peroxide
HATH	-	Homologous to the Amino Terminal of HDGF
HDGF	-	Hepatoma Derived Growth Factor
Her2	-	Human Epidermal Growth Factor Receptor 2
HRP	-	Horse Radish Peroxidase
IHC	-	Immunohistochemistry
IM	-	Immunomodulatory
IMS	-	Industrial Methylated Spirits
INA	-	Alpha-Internexin
IP	-	Immunoprecipitation
IQGAP1	-	GTPase-Activating Protein 1
kDa	-	Kilo Dalton
Kin	-	Kinesin
KRAS	-	Kirsten Rat Sarcoma viral oncogene homolog
LCLC	-	Large Cell Lung Carcinoma
LC-MS/MS	-	Liquid Chromatography-Mass Spectrometry/Mass Spectrometry
Lipo	-	Lipofectamine
L-NNA	-	Nω-Nitro-L-arginine
M	-	Mesenchymal
M	-	Molar
mA	-	Milliamps
mAb	-	Monoclonal Antibody

MEM	-	Minimun Essential Medium
MeOH	-	Methanol
MET	-	Mesenchymal to Epithelial Transition
Mitox	-	Mitoxantrone
mm	-	Millimeter
mM	-	Millimolar
MMP	-	Matrix Metalloproteinase
MOPS	-	3-(N-morpholino) propanesulfonic acid
MS	-	Mass Spectrometry
MS/MS	-	Tandem Mass Spectrometry
MSL	-	Mesenchymal stem-like
MW	-	Molecular weight
NaOH	-	Sodium Hydroxide
NCI	-	National Cancer Institute
NCRI	-	National Cancer Registry Ireland
NEG	-	Negative
NH_4HCO_3	-	Ammonium Bicarbonate
NICB	-	National Institute for Cellular Biotechnology
nm	-	nanometer
nM	-	nanoMolar
NO	-	Nitric Oxide
NOS	-	Nitric Oxide Synthase
NRK	-	Normal Rat Kidney
NSCLC	-	Non-Small Cell Lung Carcinoma
OCT	-	Optimum Cutting Temperature compound
ODC	-	Ornithine Decarboxylase
PANTER	-	Protein Analysis Through Evolutionary Relationships
PBS	-	Phosphate Buffered Saline
PCA	-	Principle Component Analysis
PDAC	-	Pancreatic Ductal Adenocarcinoma
PD-L1	-	Programmed death-ligand 1
PIK3CA	-	Phosphatidylinositol-4,5-Bisphosphate 3-Kinase, Catalytic Subunit Alpha
PNET	-	Pancreatic Neuroendocrine Tumours
PNPP	-	P-Nitrophenyl Phosphate

PTEN	-	Phosphatase and Tensin Homolog
PTM	-	Post Translation Modifications
PTPS	-	Pyruvoyl tetrahydrobiopterin
PVDF	-	Polyvinyl Difluoride
R.T.	-	Room Temperature
RIPA	-	Radio Immunoprecipitation Assay
ROBO2	-	Roundabout homolog 2
ROS	-	Reactive Oxygen Species
RPMI	-	Roswell Park Memorial Institute medium
SCC	-	Squamous cell carcinoma
SCID	-	Severe combined immune-deficient
SCLC	-	Small Cell Lung Carcinoma
SCR	-	Scrambled
SDS-PAGE	-	Sodium Dodecyl Sulfate - Polyacrylamide Gel Electrophoresis
SFM	-	Serum Free Medium
siRNA	-	Small Interfering Ribonucleic Acid
SOP	-	Standard Operating Procedure
SP	-	Sepiapterin
SPR/SR	-	Sepiapterin Reductase
Src	-	Sarcoma
TBS	-	Tris Buffered Saline
TFA	-	Trifluoroacetic Acid
TKI	-	Tyrosine Kinase Inhibitor
TMA	-	Tissue Microarray
TNBC	-	Triple Negative Breast Cancer
Tris	-	Tris (hydroxymethyl) aminomethane
UHP	-	Ultra-High Pure water
v/v	-	Volume to Volume Ratio
VDJ	-	Variable, Diversity, Joining
VEGF	-	Vascular Endothelial Growth Factor
w/v	-	Weight to Volume Ratio

ABSTRACT

Identification of Membrane Associated Proteins as Potential Markers for the DLKP Clonal Subpopulations

Andrew McCann

Lung cancer is one of the major causes of cancer death worldwide, it represents a heterogeneous group of tumours with distinct morphological, histological and molecular features reflected by varied clinical outcome and response to treatment. DLKP is a cell line originating from a lymph node metastasis of a primary lung tumour histologically described as a "poorly differentiated squamous cell carcinoma". DLKPSQ, DLKPI and DLKPM are three distinct subpopulations derived from DLKP, which are morphologically and phenotypically different from each other. The research outlined in this thesis aims to identify membrane associated proteins that could be used as potential markers for the DLKP clones, but also to identify potentially novel proteins associated with lung cancer.

Cell surface protein isolation and label-free mass spectrometry analysis were performed on proteins isolated from DLKP and the DLKP clones. Eight proteins were successfully validated in the DLKP clones; AHNAK, HDGF, ROBO2, SLIT2, ALCAM, IQGAP1, INA and SPR, using Western blot analysis, Immunofluorescence and Immunocytochemistry. Their expression was also investigated in various tumour types and representative cell lines. SPR is associated with poor survival of patients with Luminal A and basal-like breast cancers and also shows high expression across triple negative breast cancer subtypes. siRNA mediated knockdown studies of three candidate proteins. ALCAM, INA and SPR knockdown led to a significant reduction in the invasion and migration of DLKPM cells, indicating a potential functional role for these proteins in lung cancer invasion/migration.

A pilot *in vivo* study using severe combined immune-deficient (SCID) mice to investigate the growth of DLKP and its clones resulted in all four cell lines forming tumours following implantation. Tumours derived from DLKP and DLKPI were the fastest growing and largest tumours, DLKPM formed smaller solid tumours following an initial lag phase, while DLKPSQ formed large, highly vascularised tumours. Immunohistochemical analysis of the xenografts derived from all four cell lines revealed; strong Ki67 immunoreactivity, negligible CD31 immunoreactivity and strong N-cadherin immunoreactivity. Explant culture revealed a significant reduction in migratory capacity of DLKPSQ cells, but also a significant reduction in invasion/migration of DLKPM cells. Western blot analysis and immunohistochemical analysis indicated that expression of SLIT2, ALCAM, IQGAP1, INA and SPR were maintained *in vivo*.

The research presented demonstrates that proteomic analysis of cell surface isolates from the DLKP variants can lead to the identification of proteins with potential functional roles in cancer. AHNAK, SLIT2, ALCAM, and SPR were identified as potential markers capable of distinguishing between each of the DLKP clones. In addition, SPR may represent a novel target for triple negative breast cancer. The DLKP cell line model could also prove to be an invaluable model to study the effects of potential novel therapeutics in lung cancer, *in vivo.*

TABLE OF CONTENTS

Acknowledgements ..... **iii**
Abbreviations ..... **vii**
ABSTRACT ..... **xi**
List of Figures ..... **xviii**
List of Tables ..... **xx**

Chapter 1 Introduction **1**

1.1 Tumour Heterogeneity **2**
1.2 The Cancer stem cell model **3**
1.2.1 The clonal evolution model 3
1.2.2 Sources of heterogeneity 4
1.3 Lung Cancer **6**
1.3.1 Risk factors associated with Lung Cancer 7
1.3.2 Tobacco control initiatives 7
1.4 Lung Cancer Classification **8**
1.4.1 Non-Small Cell Lung Cancer 8
1.4.2 Small Cell Lung Cancer 11
1.5 Heterogeneity in Breast Cancer **14**
1.5.1 Luminal breast cancers 14
1.5.2 Her2+ Breast Cancer 16
1.5.3 Triple Negative Breast Cancer 16
1.6 Metastatic Process **17**
1.6.1 Epithelial to Mesenchymal Transition 17
1.7 Development of animal models to study heterogeneity **21**
1.7.1 $KRAS^{G12D}$ mouse model 22
1.8 Characteristics of DLKP and its clonal subpopulations **24**
1.8.1 History of DLKP 24
1.9 Aims of Thesis **28**

Chapter 2 Materials and Methods **29**

2.1 Cell lines and cell culture **30**
2.1.1 Sub-culturing of adherent cell lines 30
2.1.2 Sub-culturing of suspension/aggregate cell lines 32

2.1.3 Assessment of cell number....32
2.1.4 Cryopreservation of cells....32
2.1.5 Thawing of cryopreserved cells....32
2.1.6 Monitoring of sterility of cell culture solutions....33
2.1.7 Serum batch testing....33
2.1.8 *Indirect* mycoplasma analysis of cell lines....33
2.2 Proteomic analysis....34
2.2.1 Cell surface membrane protein Isolation....34
2.2.2 In-solution tryptic digestion....34
2.2.3 Label-Free Liquid chromatography mass spectrometry Analysis....35
2.2.4 Quantitative Profiling of Label-Free LC-MS/MS Analysis....36
2.3 Western blot analysis....37
2.3.1 Preparation of whole cell lysates....37
2.3.2 Preparation of membrane proteins....37
2.3.3 Preparation of conditioned medium....37
2.3.4 Protein Quantification....38
2.3.5 Gel Electrophoresis....38
2.3.6 Enhanced Chemiluminescence detection....39
2.3.7 Staining - Brilliant Blue G colloidal coomassie staining of gels....40
2.4 Functional analyses....41
2.4.1 *In vitro* invasion assays....41
2.4.2 *In vitro* migration assay....41
2.4.3 ROS assay....42
2.4.4 Anoikis assay....42
2.4.5 Statistical analysis....42
2.5 *In vitro* proliferation assays....44
2.5.1 Combination toxicity assays....44
2.5.2 Acid phosphatase assay....44
2.6 Immunohistochemistry....45
2.6.1 Immunofluorescence studies on fixed cells....45
2.6.2 Immunocytochemical analysis on fixed cells....45
2.6.3 Immunohistochemistry....45
2.7 RNA interference (RNAi)....47
2.7.1 Transfection optimisation....47
2.7.2 Analysis of the growth of siRNA transfected cells....48

2.7.3 Analysis of invasion and migration of siRNA transfected cells 48
2.7.4 Analysis of ROS generation of siRNA transfected cells 48
2.8 Development of cell line-derived tumours *in vivo* (xenografts) 49
2.8.1 Mice 49
2.8.2 Preparation of cell suspensions 49
2.8.3 Tumour development 50
2.8.4 Tumour removal and explant culture 50
2.8.5 Paraffin embedding of Xenograft tissues 50

Chapter 3 Results 51

3.1 Identification of membrane associated markers in DLKP 52
3.1.1 Cell surface protein isolation and protein identification 52
3.1.2 Principle component analysis of DLKP and the DLKP clones 54
3.1.3 Comparative proteomic analysis of DLKP and the DLKP clones 55
3.1.4 Summary of proteins selected for validation studies in DLKP 62
3.2 Validation of protein targets from proteomic analysis 63
3.2.1 Validation of AHNAK expression in DLKP 64
3.2.2 Validation of HDGF expression in DLKP 65
3.2.3 Validation of SLIT2 ligand and ROBO2 receptor expression in DLKP 67
3.2.4 Validation of ALCAM expression in DLKP 69
3.2.5 Validation of IQGAP1 expression in DLKP 71
3.2.6 Validation of INA expression in DLKP 73
3.2.7 Validation of SPR in DLKP 75
3.2.8 BreastMark Analysis 77
3.2.9 Summary of results from validation experiments 87
3.3 Expression of selected proteins in human cancer cell lines. 88
3.3.1 Expression of validated proteins in a representative panel of lung cancer cell lines 88
3.3.2 Expression of validated proteins in a representative panel of TNBC cell lines .. 95
3.3.3 Expression of validated proteins in a representative panel of pancreatic cancer cell lines 99
3.3.4 Expression of validated proteins in colon, glioma neuroblastoma and melanoma cell lines 103

3.3.5 Summary of immunoreactivity in DLKP Cell lines and Human cancer cell lines.. 106
3.4 Functional analysis of target proteins by siRNA knockdown 107
3.4.1 Investigation into the role of ALCAM in lung cancer 108
3.4.2 Investigation into the role of INA in lung cancer 117
3.4.3 Investigation into the role of SPR in DLKP clones 125
3.4.4 The investigation into the functional role of SPR in breast cancer and pancreatic cancer. 137
3.4.5 Summary of functional analyses 144
3.4.6 Immunohistochemical analysis of INA and SPR expression in lung cancer 145
3.4.7 Immunohistochemical analysis of SPR in Breast cancer 149
3.5 The investigation into the growth and tumour development of DLKP and its clonal subpopulations *in vivo*. 151
3.5.1 Background to DLKP clones 151
3.5.2 The *in vivo* investigation of DLKP 152
3.6 Characteristics of DLKP, DLKPSQ, DLKPI and DLKPM cell lines post tumour explant culture 167
3.6.1 Isolation of DLKP clones from Xenograft tumours by explant culture 167
3.6.2 Examination of the morphology of explanted tumour cells 168
3.6.3 Examination of growth of explanted tumour cells 170
3.6.4 Examination of invasive and migratory capacity of explanted tumour cells 172
3.7 Immunohistochemical analysis of xenograft tumours 175
3.7.1 Human mitochondrial protein 175
3.7.2 Ki-67 175
3.7.3 CD31 176
3.7.4 E-cadherin and N-cadherin 176
3.7.5 Summary of staining observed in cell line derived-xenografts 184
3.8 Immunohistochemical analysis of differentially expressed proteins in xenograft tumours derived from DLKP clones 185
3.8.1 Expression of SLIT2 and ROBO2 *in vivo*. 185
3.8.2 Expression of ALCAM *in vivo*. 189
3.8.3 Expression of IQGAP1 *in vivo* 192
3.8.4 Expression of INA *in vivo* 195
3.8.5 Expression SPR *in vivo* 197

Chapter 4 Discussion 200

4.1 DLKP and its clonal subpopulations 201
4.2 Proteomic analysis of DLKP and its subpopulations 204
4.2.1 Neuroblast differentiation-associated protein 205
4.2.2 Hepatoma-derived growth factor 207
4.2.3 SLIT2 and ROBO2 208
4.2.4 Ras-GTPase-activating-like protein 1 210
4.2.5 Activated Leukocyte Cell Adhesion Molecule 211
4.2.6 Alpha-Internexin 213
4.2.7 Sepiapterin Reductase 217
4.3 Investigation of the growth of DLKP and its clones, *in vivo* 226
4.3.1 Examination of DLKP and its clones *in vivo* 226
4.3.2 Investigation of the expression of validated proteins *in vivo* 230
4.3.3 Summary 233

Chapter 5 Conclusions and future work 234

5.1 Conclusions 235
5.2 Future work 237
Bibliography 239
Appendix 254
Appendix 1.1 Comparative proteomic analysis: DLKP vs. DLKPSQ ---------- 255
Appendix 1.2 Comparative proteomic analysis: DLKP *vs.* DLKPI ---------- 258
Appendix 1.3 Comparative proteomic analysis: DLKP *vs.* DLKPM ---------- 262
Appendix 1.4 Comparative proteomic analysis: DLKSQ *vs.* DLKPI ---------- 267
Appendix 1.5 Comparative proteomic analysis: DLKPSQ *vs.* DLKPM ---------- 271
Appendix 1.6 Comparative proteomic analysis: DLKPI *vs.* DLKPM ---------- 275

List of Figures

Figure 1.1-1:- Tumour heterogeneity in cancer. 2
Figure 1.2-1:- Suggested models of heterogeneity in cancer. 3
Figure 1.4-1:- Evolving genomic classification of NSCLC.....10
Figure 1.5-1:- Histological and molecular subtypes in breast cancer. 15
Figure 1.6-1:- Process of epithelial-mesenchymal transition. 18
Figure 1.6-2:- The main steps involved in the formation of metastases.....19
Figure 1.8-1:- Growth and invasion characteristics of the DLKP clones *in vitro*.....25
Figure 3.1-1:- Principle component analysis showing separation of DLKP and its clones. 54
Figure 3.2-1:- Validation of AHNAK expression in DLKP.....64
Figure 3.2-2:- Validation of HDGF expression in DLKP. 66
Figure 3.2-3:- Validation of SLIT2 and ROBO2 receptor expression in DLKP. 68
Figure 3.2-4:- Validation of ALCAM expression in DLKP.....70
Figure 3.2-5:- Validation of IQGAP1 expression in DLKP. 72
Figure 3.2-6:- Validation of INA expression in DLKP. 74
Figure 3.2-7:- Validation of SPR expression in DLKP. 76
Figure 3.2-8:- Survival analysis of AHNAK expression in breast cancer. 79
Figure 3.2-9:- Survival analysis of HDGF expression in breast cancer.....80
Figure 3.2-10:- Survival analysis of SLIT2 expression in breast cancer. 81
Figure 3.2-11:- Survival analysis of ROBO2 expression in breast cancer. 82
Figure 3.2-12:- Survival analysis of ALCAM expression in breast cancer 83
Figure 3.2-13:- Survival analysis of IQGAP1 expression in breast cancer. 84
Figure 3.2-14:- Survival analysis of INA expression in breast cancer.....85
Figure 3.2-15:- Survival analysis of SPR expression in breast cancer.....86
Figure 3.3-1:- Western blot analysis of HDGF expression in lung cancer cell lines. 90
Figure 3.3-2:- Western blot analysis of SLIT2 expression in lung cancer cell lines. 91
Figure 3.3-3:- Western blot analysis of ALCAM in lung cancer cell lines.....92
Figure 3.3-4:- Western blot analysis of INA in lung cancer cell lines. 93
Figure 3.3-5:- Western blot analysis of SPR in lung cancer cell lines. 94
Figure 3.3-6:- Western blot analysis of HDGF in TNBC cell lines.....96
Figure 3.3-7:- Western blot analysis of INA in TNBC cell lines.....97
Figure 3.3-8:- Western blot analysis of SPR in TNBC cell lines.....98
Figure 3.3-9:- Western blot analysis of HDGF in pancreatic cancer cell lines. 100
Figure 3.3-10:- Western blot analysis of ALCAM in pancreatic cancer cell lines. 101
Figure 3.3-11:- Western blot analysis of SPR in pancreatic cancer cell lines. 102
Figure 3.3-12:- Western blot analysis of HDGF in colon, glioma and melanoma cell lines.....104
Figure 3.3-13:- Western blot analysis of ALCAM in colon, glioma and melanoma cell lines. 104
Figure 3.3-14:- Western blot analysis of INA in neuroblastoma and glioma cell lines. 105
Figure 3.3-15:- Western blot analysis of SPR in neuroblastoma and glioma cell lines. 105
Figure 3.4-1:- ALCAM knockdown reduced cell growth of DLKPSQ-mitox-BCRP-6P. 109
Figure 3.4-2:- ALCAM increases the invasive capacity of DLKPSQ-mitox-BCRP-6P. 110
Figure 3.4-3:- ALCAM knockdown shows no effect on cell growth of DLKPM. 112
Figure 3.4-4:- ALCAM decreases the invasive capacity of DLKPM cells. 113
Figure 3.4-5:- ALCAM knockdown shows no effect of cell growth of DLKPI cells. 115
Figure 3.4-6:- ALCAM increases the invasive capacity of DLKPI cells.....116
Figure 3.4-7:- INA knockdown does not affect cell growth of DLKPSQ.....118
Figure 3.4-8:- INA knockdown does not affect invasion of DLKPSQ. 119
Figure 3.4-9:- INA knockdown does not affect migration of DLKPSQ. 119
Figure 3.4-10:- INA knockdown has does not affect cell growth of DLKPM.....121
Figure 3.4-11:- Morphology of DLKPM cells following siRNA knockdown of INA. 122
Figure 3.4-12:- INA knockdown decreases the invasive capacity of DLKPM cells. 123
Figure 3.4-13:- INA knockdown decreases the migratory capacity of DLKPM. 124
Figure 3.4-14:- SPR knockdown shows does not affect cell growth of DLKPSQ. 126
Figure 3.4-15:- SPR-6 siRNA potentially reduces the invasive capacity of DLKPSQ.....127

Figure 3.4-16:- SPR-6 siRNA potentially reduces the migratory capacity of DLKPSQ. 127
Figure 3.4-17:- SPR-6 siRNA reduces cell growth of DLKPM. 129
Figure 3.4-18:- SPR knockdown decreases the invasive capacity of DLKPM. 130
Figure 3.4-19:- SPR knockdown decreased the migratory capacity of DLKPM. 131
Figure 3.4-20:- DFMO treatment reduces the invasive capacity of DLKPM. 133
Figure 3.4-21:- L-NNA treatment reduces the invasive capacity of DLKPM. 135
Figure 3.4-22:- ROS generation is reduced in SPR transfected DLKPM cells. 136
Figure 3.4-23:- SPR knockdown reduces cell growth of MDA-MB-468. 138
Figure 3.4-24:- SPR knockdown reduces the invasive capacity of MDA-MB-468. 139
Figure 3.4-25:- SPR knockdown reduces the growth of MiaPaca2 clone 3. 141
Figure 3.4-26:- SPR knockdown reduces the invasive capacity of MiaPaCa2 Clone3 and AsPc-1. 142
Figure 3.4-27:- SPR knockdown reduces the migratory capacity of MiaPaCa2 clone 2. 143
Figure 3.4-28:- Immunohistochemical analysis of INA expression in human lung cancer. 147
Figure 3.4-29:- Immunohistochemical analysis of SPR expression in human lung cancer. 148
Figure 3.4-30:- Immunohistochemical analysis of SPR expression in human breast cancer. 149
Figure 3.4-31:- Immunohistochemical analysis of SPR in a panel of breast cancer tissues. 150
Figure 3.5-1:- Proposed model of interconversion between DLKPSQ, DLKPI and DLKPM. 151
Figure 3.5-2:- Schematic showing development of xenografts derived from DLKP and its clones. 153
Figure 3.5-3:- Growth of xenograft tumours from DLKP cells. 154
Figure 3.5-4:- Xenograft tumour growth curves for DLKP. 155
Figure 3.5-5:- Growth of xenograft tumours from DLKPSQ cells. 157
Figure 3.5-6:- Xenograft tumour growth curves for DLKPSQ. 158
Figure 3.5-7:- Growth of xenograft tumours from DLKPI cells. 160
Figure 3.5-8:- Xenograft tumour growth curves for DLKPI. 161
Figure 3.5-9:- Growth of xenograft tumours from DLKPM cells. 163
Figure 3.5-10:- Xenograft tumour growth curves for DLKPM. 164
Figure 3.5-11:- Summary growth curves of xenografts tumours developed by DLKP and its clones. 166
Figure 3.6-1:- Morphology of DLKP clones preimplantation *vs.* DLKP clones post explant culture. 169
Figure 3.6-2:- Growth and anoikis capabilities of the DLKP clones post tumour growth. 171
Figure 3.6-3:- The invasive capacity of DLKP and its clones post tumour growth. 173
Figure 3.6-4:- The invasive capacity of DLKP and its clones post tumour explant culture. 173
Figure 3.6-5:- Invasive and migratory capacity of DLKPSQ and DLKPM post tumour growth. 174
Figure 3.7-1:- Expression of human mitochondrial protein in xenograft tumours. 177
Figure 3.7-2:- Expression of Ki-67 in xenograft tumours. 178
Figure 3.7-3:- Representative images of xenograft tumours stained for the expression of CD31. 179
Figure 3.7-4:- Representative images of xenograft tumours stained for the expression of E-cadherin. 180
Figure 3.7-5:- Representative images of control cells *vs.* explanted cells stained for expression of E-cadherin. 181
Figure 3.7-6:- Expression of N-cadherin in xenograft tumours 182
Figure 3.7-7:- Expression of N-cadherin in cells derived from xenograft tumours. 183
Figure 3.8-1:- Expression of SLIT2 in the explanted DLKP tumour cells 186
Figure 3.8-2:- Expression of SLIT2 in the xenograft tumours. 187
Figure 3.8-3:- Expression of ROBO2 in the xenograft tumours. 188
Figure 3.8-4:- Expression of ALCAM in the explanted DLKP tumour cells. 190
Figure 3.8-5:- Expression of ALCAM in the xenograft tumours. 191
Figure 3.8-6:- Expression of IQGAP1 in the explanted DLKP tumour cells. 193
Figure 3.8-7:- Expression of IQGAP1 in the xenograft tumours. 194
Figure 3.8-8:- Expression of INA in the xenograft tumours. 196
Figure 3.8-9:- Expression of SPR in the explanted DLKP tumour cells. 198
Figure 3.8-10:- Expression of SPR in the xenograft tumours. 199
Figure 4.2-1:- Mechanisms of BH_4 biosynthesis. 218
Figure 4.2-2:- Proposed crosstalk between polyamine and nitric oxide (NO) pathways. 224

List of Tables

Table 1.4-1:- Current molecular targets and treatments for adenocarcinoma. 10
Table 1.4-2:- Examples of targeted therapies for SCLC in clinical trials. 13
Table 2.1-1:- Description of cell lines used in during this project. 31
Table 2.3-1:- List of antibodies and the dilutions used in Western blot analysis 40
Table 2.5-1:- Inhibitors used during this project. 44
Table 2.6-1:- Antibodies used in Immunofluorescence, Immunocytochemistry and Immunohistochemistry analysis. 46
Table 2.7-1:- Optimization of cell number for transfections siRNA. 48
Table 2.8-1:- Inoculation densities used for DLKP *in vivo* study. 50
Table 3.1-1:- Summary of six comparisons made using Progenesis LC-MS software and the number of proteins with increased expression in each cell line. 55
Table 3.1-2:- Comparison of DLKP *vs.* DLKPSQ. 56
Table 3.1-3:- Comparison of DLKP *vs.* DLKPI. 57
Table 3.1-4:- Comparison of DLKP *vs.* DLKPM. 58
Table 3.1-5:- Comparison of DLKPSQ *vs.* DLKPI. 59
Table 3.1-6:- Comparison of DLKPSQ *vs.* DLKPM. 60
Table 3.1-7:- Comparison of DLKPI *vs.* DLKPM. 61
Table 3.1-8:- Summary of all proteins selected for validation studies. 62
Table 3.2-1:- Summary of BreastMark survival analysis performed on validated proteins. 78
Table 3.2-2:- Summary table showing representative expression of the proteins validated in DLKP and its clones. 87
Table 3.3-1:- Lung cancer cell lines used to examine the expression of protein targets. 88
Table 3.3-2:- TNBC cell lines used to examine the expression of protein targets. 95
Table 3.3-3:- Colon, glioma, neuroblastoma and melanoma cell lines used for Western blot analysis. 103
Table 3.4-1:- Immunoreactivity of INA on lung cancer TMA. 146
Table 3.4-2:- Immunoreactivity of SPR on lung cancer TMA. 146
Table 3.4-3:- Immunoreactivity of SPR in invasive ductal breast cancer tissues with corresponding adjacent normal tissue. 149
Table 3.5-1:- DLKP xenograft tumour measurements. 155
Table 3.5-2:- DLKPSQ xenograft tumour measurements. 158
Table 3.5-3:- DLKPI xenograft tumour measurements. 161
Table 3.5-4:- DLKPM xenograft tumour measurements. 164
Table 3.6-1:- Nomenclature of DLKP and its clones in control culture *vs.* DLKP and its clones recovered from mouse xenografts. 167
Table 3.7-1:- Summary of Immunohistochemical analysis carried out on xenograft tumours. 184
Table 4.2-1:- Summary of all proteins selected for validation studies. 205
Table 4.3-1:- Expression of validated protein in xenograft tumours. 231
Table 4.3-2:- Expression of validated proteins was maintained in recovered cells from DLKP *in vivo* study. 231

Chapter 1 INTRODUCTION

1.1 Tumour Heterogeneity

Cancer is not one but many diseases and has traditionally been described as a disease attributed to a stepwise accumulation of mutations in key oncogenes and tumour suppressors. Tumours are now known to be dynamically evolving entities both genetically and epigenetically [1]. Primary and metastatic tumours are generally described as heterogeneous, meaning they contain distinct cell populations with differing heritable alterations. Cell populations within these heterogeneous tumours can display remarkable variability with distinct characteristics such as cellular morphology, metabolic activity, motility, proliferation rate, antigen expression, drug response and metastatic potential [2, 3]. Within the description of tumour heterogeneity exists; intra-tumour heterogeneity which specifically refers to heterogeneity within a tumour and inter-tumour heterogeneity which refers to heterogeneity in several different tumours [1], both types are illustrated in Figure 1.1-1 below.

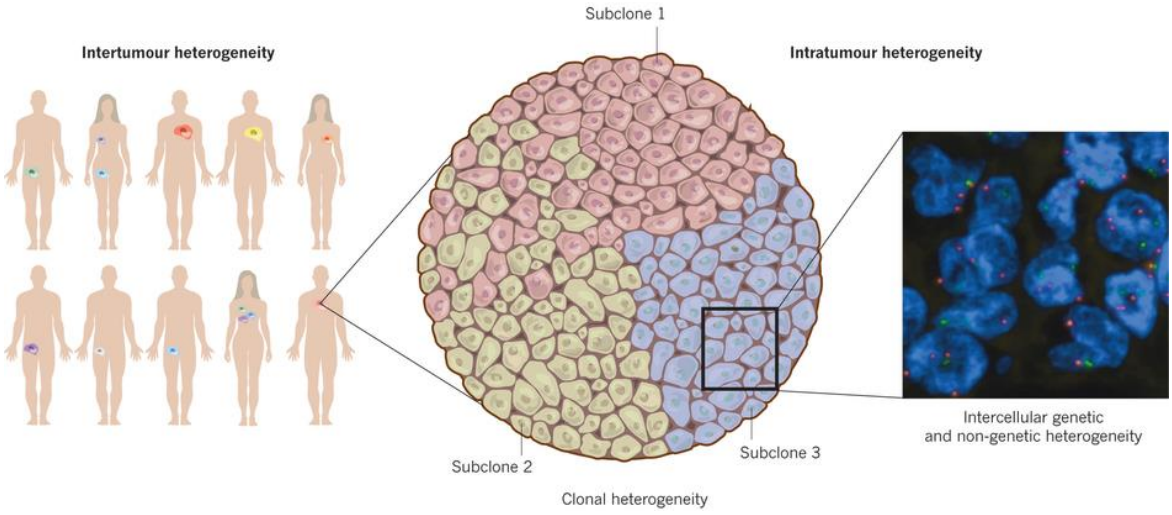

Figure 1.1-1:- Tumour heterogeneity in cancer.
Subclones may intermingle (as shown by subclones 1 and 2) or be spatially separated (as shown by subclone 3). Tumour subclones may show differential gene expression due to both genetic and epigenetic heterogeneity. Within a subclonal population of tumour cells - shown here as a tumour section, hybridized to two fluorescent probes for the centromeres of two chromosomes (chromosome 2, red; chromosome 18, green) with DNA (blue) there is intercellular genetic and non-genetic variation of, for example, chromosome copy number, somatic point mutations or epigenetic modifications that result in phenotypic diversity. Intercellular genetic heterogeneity is exacerbated by genomic instability, and may foster the emergence of tumour subclones. Genomic instability and tumour subclonal architecture may vary further over time if influenced by, for example, cancer treatment [4].

There are two known models lending to heterogeneity in cancer; the cancer stem cell model and the clonal evolution model. Both models are illustrated in Figure 1.2-1.

1.2 The Cancer stem cell model

The cancer stem cell model is not a new idea and generally, assumes hierarchical organisation within the tumour. It suggests that a subset of cells with stem cell properties drive tumour initiation and progression, cancer stem cells (CSCs). CSCs have been defined by the American association for cancer research (AACR) as "a cell within a tumour that possesses the capacity to self-renew and to cause heterogeneous lineages of cancer cells that comprise the tumour" [5-7]. A number of cell surface proteins have been designated as a marker of CSCs, some of which include CD166, CD133, CD44 (EpCAM) and CD271 [8].

1.2.1 The clonal evolution model

The Clonal Evolution model suggests that premalignant or malignant cell populations accumulate various hereditary changes over time that may confer certain advantages or disadvantages onto the cell. This model is subjected to natural selection. Carcinogenesis is initiated by the accumulation of several mutations in a single cell and is driven by the emergence of further genetic and epigenetic alterations that confer more aggressive, invasive and potentially drug resistant phenotypes [6].

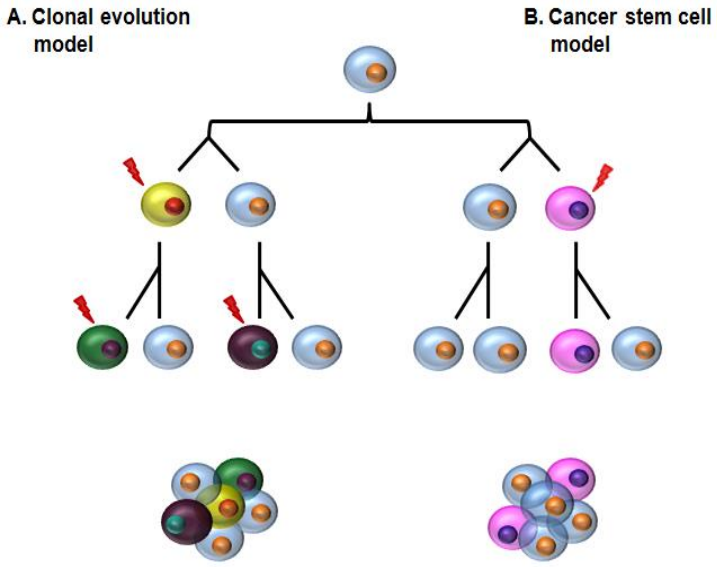

Figure 1.2-1:- Suggested models of heterogeneity in cancer.
(A) The clonal evolution model: cells are subjected to the Darwinian evolutional trajectory. (B) The Cancer stem cell model: cells have the ability of an unlimited number of divisions.

1.2.2 Sources of heterogeneity

Intratumour heterogeneity can be observed at many different levels and may be attributable to a number of different factors [9]. Varying degrees of clonal heterogeneity may arise as a result of selective outgrowth of any given clone. Subclones may continue to expand and evolve in a sequential linear fashion, or else they may continue to diverge, following a branched evolutionary trajectory [10, 11]. Diverse phenotypes can arise as a result of extrinsic factors such as pH, hypoxia and paracrine signalling interactions with stroma and other cells. These factors generate phenotypic diversity through modulation of cellular signalling, but also act as selection pressures supporting the clonal expansion of cells that proliferate efficiently in a particular micro-environment [12].

Genetic instability, a feature in a high proportion of solid tumours, generates a high level of intercellular genetic heterogeneity and has been linked with both drug resistance and poor prognosis in cancer. For normal cells in tissues, the goal is to accurately duplicate the genome and evenly divide up the duplicated genome into two daughter cells. If this does not happen, errors (such as amplifications, mutations, deletion, chromosome rearrangements etc.) will be passed on to the next generation of cells. This can have profound effects on the normal function of the cells (e.g. control of cell death). Normal cells control these errors, by preventing DNA replication until any genetic damage has been prepared. Certain genes are responsible for this, such as *TP53*, which encoded the checkpoint protein p53 and functions as a tumour suppressor. TP53 gene is mutated in approximately 70% lung tumours, 50% of these are NSCLC [1, 13, 14]. Regulation of such proteins helps protect the cell against tumorigenesis, which is effectively the accumulation of genetic alterations.

Epigenetic, transcriptomic and proteomic heterogeneity may arise due to underlying genotypic variation but can also reflect cell cycle stage and stochastic variation between cells or hierarchical organisation of cells according to the cancer stem theory [4]. There are a number of routes through which a tumour cell may acquire drug resistance: upregulation of drug efflux pumps, drugs may be inactivated or metabolised in the cell, or the drug may not be efficiently taken up by the cells. However, it is possible that resistance may be pre-existing in minor subpopulations of heterogeneous tumours. In the context of EGFR, mutations in its ATP binding sequence (T790M) have been reported [15].

However, the existence of genetic and epigenetic differences in different cancer cells within tumours may explain why some tumour cells remain present after cancer treatment.

Since genetic instability plays important roles in both cancer initiation and progression, it is hugely important to consider genetic instability during treatment regimens as it may ultimately be responsible for patient relapse. It is possible that the initial treatment may select out more aggressive or drug resistant cells which might be more difficult to treat, potentially resulting in a poorer patient prognosis [16].

Clonal heterogeneity of cells in tumours has the potential to produce many different types of tumours. Cells within the tumours may have certain characteristics which allow them to evolve down a number of different trajectories which may result varying genetic and phenotypic characteristics. Some of these characteristics may confer the ability of cells to evade therapeutic treatments leading to the development of tumours which are more resistant to therapy. Heterogeneity presents huge challenges for clinicians in classifying the disease and considering the most effective treatment for patients [17].

1.3 Lung Cancer

Lung cancer is a heterogeneous group of lesions with differences in clinical presentation, pathological features and biological behaviour. Lung cancer accounts for about 27% of all cancer related deaths and is by far the leading cause of cancer death in both men and women [18]. The American Cancer Society has estimated that there will be approximately 221,200 new cases of cancer in 201 of which 158,040 as a result of lung cancer (www.cancer.org). In Ireland, between 2011 and 2013 an average of 2,279 lung cancer cases was diagnosed, 1,005 were females and 1,274 were males (www.ncri.ie). Traditionally, lung cancer had been most common in men. However, it is nearly as common in women due to an increase in the number of women taking up smoking. Statistics for lung cancer in Europe for 2012 show that Hungary has the highest overall incidence in both men and women (51.6 cases per 100,000). For Ireland during the period between 1994 to 2013 lung cancer has been decreasing in men from 71 to 54 cases per 100,000, but increasing in women from 26 to 41 cases per 100,000. According to the National Cancer Registry Ireland (NCRI), these trends are comparable to those seen in other northern and western European countries [19]. While, according to the world health organisation, the lowest incidence of lung cancer is eastern, middle and western Africa (1.7 - 2.0 cases per 100,000).

Ireland is currently ranked 31st in the world for deaths related to lung cancer with 27.67 deaths per 100,000, irrespective of sex. The net 5-year survival of patients with lung cancer in Ireland has been steadily increasing from 9.3% between 1994 and 1999 to 15.3% between 2008 to 2012 (www.ncri.ie). Similarly, the rates in the UK have also been increasing from 4.6% between 1971 and 1972 to 9.7% in 2010 to 2011 (www.cancerresearchuk.org). However, data from the National Cancer Institute (NCI) also show that there is an increase in the number of people surviving to 5-year survival, for patients diagnosed between 1975-1977 the rate was 12.2% compared to 18.7% in 2006-2012 irrespective of sex and race. Overall, Ireland is performing well when it comes to patients with lung cancer with the increases in the 5-year survival rates potentially owing to improvements in lung cancer awareness, screening and treatments (www.hse.ie). However, survival is dependent on the relative staging and time of diagnosis. In England and Wales, statistics presented by cancer research UK indicate that the one-year survival rate for patients was 71% with stage I, 48% for stage II, 35% for stage III and 14% for stage IV. The survival rates drop dramatically after this period; 35%

for stage I, 21% for stage II and 6% for stage III. Therefore, further improvements in screening and treatment in order to improve patient outcome and survival.

1.3.1 Risk factors associated with Lung Cancer

There are a number of different risk factors associated with developing lung cancer. Smoking cigarettes are the main risk factor attributing to someone developing lung cancer over the course of their life. Smoking and exposure to second-hand smoke have long been accepted as the primary cause of lung cancer, accounting for 86- 95% of cases in the UK and Ireland each year (www.cancerresearchuk.org). With an estimated cost to the Irish public healthcare system of €506 million per year, lung cancer and indeed smoking is a major public health concern. Smoking is not the only risk factor, others include exposure to radiation (including radiation therapy, radon gas), exposure to asbestos, chromium, arsenic, soot or tar, exposure to environmental pollutants, possibly a genetic susceptibility and age is also considered a risk factor for many cancers, including lung cancer.

1.3.2 Tobacco control initiatives

It is well established that smoking is the major cause of lung cancer in Ireland and indeed worldwide and is, therefore, one of the most preventable cancers. Tobacco control measures are required to completely eliminate smoking from society and increase smoking cessation among smokers. Ireland has led the way with a number of initiatives with a view to Ireland being tobacco free by 2025. Some of those initiatives include; introducing standardised plain packaging of cigarettes, increasing the price of cigarettes through taxation, protecting people from second-hand smoke, making it illegal to smoke in cars where children are present, introduction of the workplace smoking ban, enforcing bans on advertising, promotion and sponsorship and helping people who want to quit (http://www.hse.ie/eng/about/Who/TobaccoControl/TCP/). Similar initiatives introduced in United states have markedly decreased smoking rates and the number of lung cancer occurrence [19] and it is hoped that through these programs that Ireland will see similar reductions in the uptake of smoking and lung cancer diagnosis.

1.4 Lung Cancer Classification

Lung cancer can be histologically classified into two main groups: non-small cell lung cancer (NSCLC) and small cell lung cancer (SCLC) [20, 21].

1.4.1 Non-Small Cell Lung Cancer

NSCLC accounts for approximately 80% of lung cancers and is subdivided into 3 main subtypes; (i) adenocarcinoma (AD), (ii) squamous cell carcinoma (SCC) and (iii) large cell carcinoma (LCC).

i. **Adenocarcinoma** is the most common form of lung cancer, accounting for approximately 40% of cases. It develops from mucus making cells in the lining of the airways and is often found in the outer, or peripheral, areas of the lungs. One of the subtypes of adenocarcinoma is bronchioloalveolar carcinoma (BAC) and have been associated with middle aged women. While smoking remains an important factor for most lung cancers, BAC is postulated to develop from previously scarred tissue such as inflammation or scar tissue as a result of tuberculosis [22, 23].

ii. **Squamous cell carcinoma** accounts for 25% to 30% of lung cancers. These cancers start in early versions of squamous cells, which are flat cells that line the inside of the airways in the lungs. They are often linked to a history of smoking and tend to be found in the middle of the lungs, near a bronchus.

iii. **Large cell carcinoma** accounts for 10-15% of lung cancer and can appear anywhere in the lung. Treatment of this type of lung cancer can be challenging as it tends to grow and spread quickly. Large cell neuroendocrine carcinoma is a subtype; it is similar to small cell lung cancer.

iv. **Mesothelioma** is also a subtype of NSCLC but is a much rarer type of cancer that affects the covering of the lung (the pleura). Diagnosis of mesothelioma can be difficult and caused by exposure to asbestos, which is an occupational risk in some professions [24, 25]

Genetic landscape of NSCLC

Lung cancer genomes and signalling pathways have further defined NSCLCs as a group of distinct diseases with genetic and cellular heterogeneity. Modern treatment strategies focus on the pathological classification of NSCLC, including the assessment of protein expression by immunohistochemistry to assess cell differentiation markers such as TIF1 and p63. A number of drugs have now been identified to specifically target molecular pathways that lead to lung cancer. Some of the most common genetic alterations targeted in NSCLC include *BRAF, EGFR, ALK, ROS1, RET, MET, FGFR1*, *PTEN* and *PIK*

oncogene and their prevalence, among others, in NSCLC are illustrated in Figure 1.4-1. Activating EGFR mutations were the first biomarkers to discriminate a molecular subpopulation in NSCLC patients. Patients with activating EGFR mutations then to show good prognostic value and benefit from treatment with EGFR tyrosine kinase inhibitors [26]

Small molecule inhibitors that target the tyrosine kinase activity of EGFR, include erlotinib and gefitinib, were the first to be made clinically available. Table 1.4-1 indicates the current number of targeted therapies available for treatment of lung adenocarcinoma [20] some of which may prove to be important as the genetic landscape of NSCLC evolves. A study indicated differences in mutations identified in never smokers (*EGFR* mutations and *ROS1* and *ALK* fusions) and smokers (*KRAS*, *TP53*, *BRAF*, *JAK2*, *JAK3*), indicating that the genomic landscape is markedly distinct in these two groups [27].

PD-L1 is a checkpoint protein in cells called T-cells. It's interaction with PD-1 and the B7.1 receptor on activated T cells plays an important role in tumour evasion of the host immune system [28]. PD-L1 was a significant poor prognostic factor in a 5 year follow up with patients with NSCLC, with PD-L1 positive patients having a poorer 5-year overall survival than PD-L1 negative patients. A number of MAb based immune therapies targeting either PD-1 or PD-L1 can boost the immune response against cancer cells and have shown great promise, Pembrolizumab and Nivolumab. There are other MAbs being used for the treatment of NSCLC; Bevacizumab (Avastin) and Ramucirumab (Cyramza), they are humanised monoclonal antibodies used to treat advanced NSCLC which both target vascular endothelial growth factor (VEGF) [29, 30].

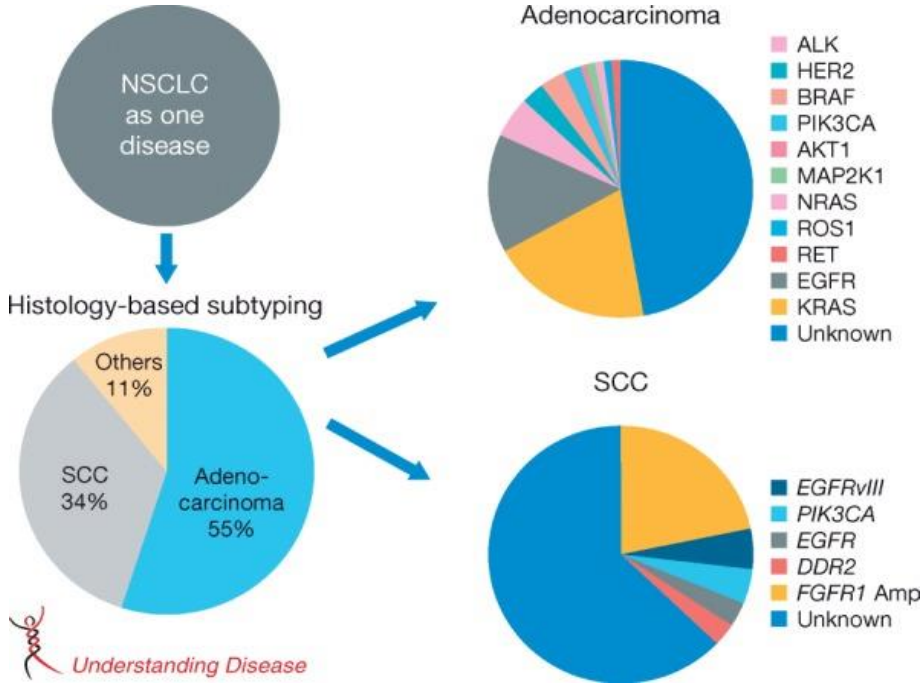

Figure 1.4-1:- Evolving genomic classification of NSCLC

Target	Prevalence (%)	Therapeutic agents
EGFR	Asians ~40%; Caucasians ~10	Erlotinib, Gefitinib, Afatinib
ALK	< 5	Crizotinib
Her2	< 3	Afatinib, Neratinib, Dacomitinib
PIK3CA	< 5	GDC-0941, XL-147, BKM120
BRAF	< 5	Vemurafenib, GSK2118436
MEK	< 1	AZD6244
ROS1	~1	Crizotinib
RET	~2	Sunitinib, Sorafenib, Vandetanib, Cabozantinib
MET	1-11	Onartuzumab, Rilotumumab, Cabozantinib, Tivantinib, Crizotinib
FGFR1	~3	AZD4547, S49076, Ponatinib, Brivanib
PTEN	< 10	Vandetanib
PD-1/PD-L1	~30	Nivolumab, MPDL3280A
NaPi2b	~70	DNIB0600A (early development)

Table 1.4-1:- Current molecular targets and treatments for adenocarcinoma.
Anaplastic lymphoma kinase (ALK); Epidermal Growth Factor Receptor (EGFR), Fibroblast Growth Factor Receptor 1 (FGFR1), Interaction of Programmed Death Ligand 1 (PD-L1), Phosphatidylinositol 3-kinase, catalytic subunit alpha (PIK3CA) [20].

1.4.2 Small Cell Lung Cancer

Small cell lung cancer (SCLC) is the lung neoplasia with the poorest outcome, due to its high metastatic potential and chemo-resistant phenotype upon relapse. It accounts for 15% to 20% of all lung cancers and exhibits rapid growth, aggressive behaviour and a tendency for early metastasis to distant sites [31]. SCLC occurs exclusively in smokers, especially heavy smokers but is also common in former smokers [32]. If left untreated, the aggressive nature of SCLC usually results in the death of patients within 2-4 months [20].

A feature of the cells in SCLC is the dense neurosecretory granules, which give this tumour type an endocrine/paraneoplastic syndrome association. These neurosecretory granules are believed to contain a variety of secretory products (including neuroendocrine hormones), cell surface antigens and enzymes [33]. Incidence rates have increased more rapidly in women than men. Depending on the presence of metastasis diagnosis of SCLC is described as limited stage or extensive stage disease. Sixty to seventy percent of patients have extensive disease (which cannot be targeted within a single radiation therapy field) at presentation. Late stage disease cannot usually be targeted with single field radiation therapy.

Although SCLC is a highly aggressive form of lung cancer it is responsive to chemotherapy and radiation, improving both quality of life and survival duration. Despite this good response to chemotherapy, patients with SCLC usually relapse within one to two years. Patients who experience a relapse tend to be more resistant to subsequent therapies, at which point different types of chemotherapies can be considered to help relieve symptoms and generally offer only a modest improvement of survival. A number of platinum based agents may be administered to patients at this point including; topotecan, cyclophosphamide and doxorubicin [34]. Combination therapies for the treatment of relapsed SCLC have been investigated involving platinum based agents and etoposide, vincristine, paclitaxel or irinotecan, their efficacies did not appear to be high enough compared to other standard topotecan therapy [35].

Alternative names for SCLC are oat cell cancer, oat cell carcinoma and small cell undifferentiated carcinoma [36]. SCLC is defined as a tumour with cells that are small in size, a round-to-fusiform shape, scant cytoplasm, finely granular nuclear chromatin and absent or inconspicuous nucleoli, nuclear moulding is frequent. Necrosis is frequent and often extensive [37].

There are two main types of SCLC;

i. **SCLC (pure-SCLC)** is primarily a neuroendocrine carcinoma. There are four main types of lung neuroendocrine tumours: typical carcinoid tumour (low grade malignancy), atypical carcinoid tumour (medium grade malignancy), large cell neuroendocrine carcinoma and small cell lung cancer (high grade malignancy) [38].
ii. **Combined small cell lung carcinoma (c-SCLC)** is currently the only recognised subtype of SCLC. It is small cell carcinoma combined with an additional component consisting of any non–small cell histologic type, including adeno-carcinoma, squamous cell carcinoma and large cell neuroendocrine carcinoma. Approximately 30% of small cell lung carcinoma contain a non–small cell lung carcinoma component. Patients with cSCLC have a better overall survival, however, they are believed to have a poorer response to chemotherapy [39].

Genetic landscape of SCLC

NSCLC has been widely researched to identify oncogenic drivers responsible for this type of lung cancers. However, researching oncogenic drivers in SCLC is lagging behind mainly due to the scarcity of patient material available for research use. Some genomic studies to date indicate high mutation rates in SCLC, possibly linked to mutagens in tobacco smoke. Loss of function of *TP53* and *RB1* tumour suppressors are the most striking alterations found in SCLC. The *TP53* gene encodes a transcription factor which is activated in response to several forms of cellular stress, including hypoxia and other anti-proliferative effects. The presence of *p53* and *HIF-1α* appears to be necessary for the hypoxia-induced cell death. The importance of *TP53* gene in SCLC is indicated by its reported mutation frequency of 75 and 90% [40, 41]. Implications for *MYC* and phosphatidylinositol-3-kinase (*PI3K*) proto-oncogene have also been identified in SCLC. *MYC* are transcriptional activators that contribute to cell cycle progression but have an association with control of pluripotency, self-renewal and Epithelial to mesenchymal transition (EMT). *PTEN* (phosphatase and tension homolog) an inhibitor of the *PI3K* pathway was found to be lost in SCLC. Other genetic alterations in SCLC include mutations in *CREBBP*, *EEP300* (histone acetyltransferases) and *MLL*, *MLL2* and *EZH2* (histone methyltransferases). There are a number of targeted therapies in clinical trials for the treatment of SCLC some of which are outlined in Table 1.4-2 below.

Mechanism of action	Targets	Agents
Inducers of apoptosis	BCL2, BCL-W, BCL-XL, cl-1	AT-101, Oblimersen
Kinase inhibitors	AURKA, CDK, EGFR, FGFR, IGF1R, KIT, PDGFR, FLT3, MET, mTOR, PI3K, PLK1	Alisertib, Roniciclib, Erlotinib, Gefitinib
NE targeting	GD2, GD3, NCAM, NTS1	BIW-8962, BEC2, Lorvotuzumab
Anti-angiogenesis	Matrix metalloproteinases, VEGF-A, VEGFB	BAY12-9566, Bevacuzumab, Afliberept
Immunotherapy	CTLA-4, PD-1, TLR	Ipilimumab, Nivolumab, Pembrolizumab, MGN1703

Table 1.4-2:- Examples of targeted therapies for SCLC in clinical trials.

1.5 Heterogeneity in Breast Cancer

Like lung cancer, breast cancer is also a complex and heterogeneous disease. Breast cancer is the second most common cause of cancer related death worldwide, after lung cancer and will account for approximately 72,330 deaths in the United States [42]. In Ireland, the Irish Cancer Society suggest that there are 2600 women diagnosed each year with breast cancer of which approx. 660 women die from the disease (www.irishcancersociety.ie).

Heterogeneity in cancer cell phenotypes and dynamic plasticity of the tumour microenvironment make tumour categorization demanding in relation to therapeutic responses and disease progression. Molecular profiling and immunohistochemical expression of ERα, progesterone receptor (PR) and HER2 led to further classification into at least five molecular subtypes Luminal A, Luminal B, HER2, basal and normal. Luminal A and Luminal B due to their expression of ER may be treated with hormone therapy [43]. The histological and the molecular subtypes identified in breast cancer are illustrated in Figure 1.5-1 below.

1.5.1 Luminal breast cancers

This group represents the majority of diagnosed breast cancers accounting for approximately 60% of breast cancer cases. They typically comprise of tumours expressing estrogen receptor (ERs) and are generally broken down into two main subtypes: Luminal A is ER positive, HER2 negative, Ki-67 low, and PR high. Luminal B (HER2 negative) - ER positive, HER2 negative, and either Ki-67 high or PR low; Luminal B-like (HER2 positive)- ER positive, HER2 overexpressed or amplified, any Ki-67, and any PR; HER2 positive - HER2 over-expressed or amplified, ER and PR absent; and triple negative - ER and PR absent and HER2 negative [44]. Two ERs are known to exist ERα and ERβ. More than 70% of breast cancers are ER positive, so the determination of ER status has proved to be successful therapeutic target for treatment [45]. Some of the standard hormone therapies used to treat luminal breast cancers include tamoxifen displays anti-oestrogen activity upon binding which ultimately inhibits the oestrogen receptor. Aromatase inhibitors (e.g. anastrozole) which prevent the conversion of androgens to oestrogens resulting in a reduction in the amount of estrogen available to the oestrogen receptor. Fulvestrant (also known as Faslodex) prevents dimerization and nuclear localization by binding to the oestrogen receptor [46].

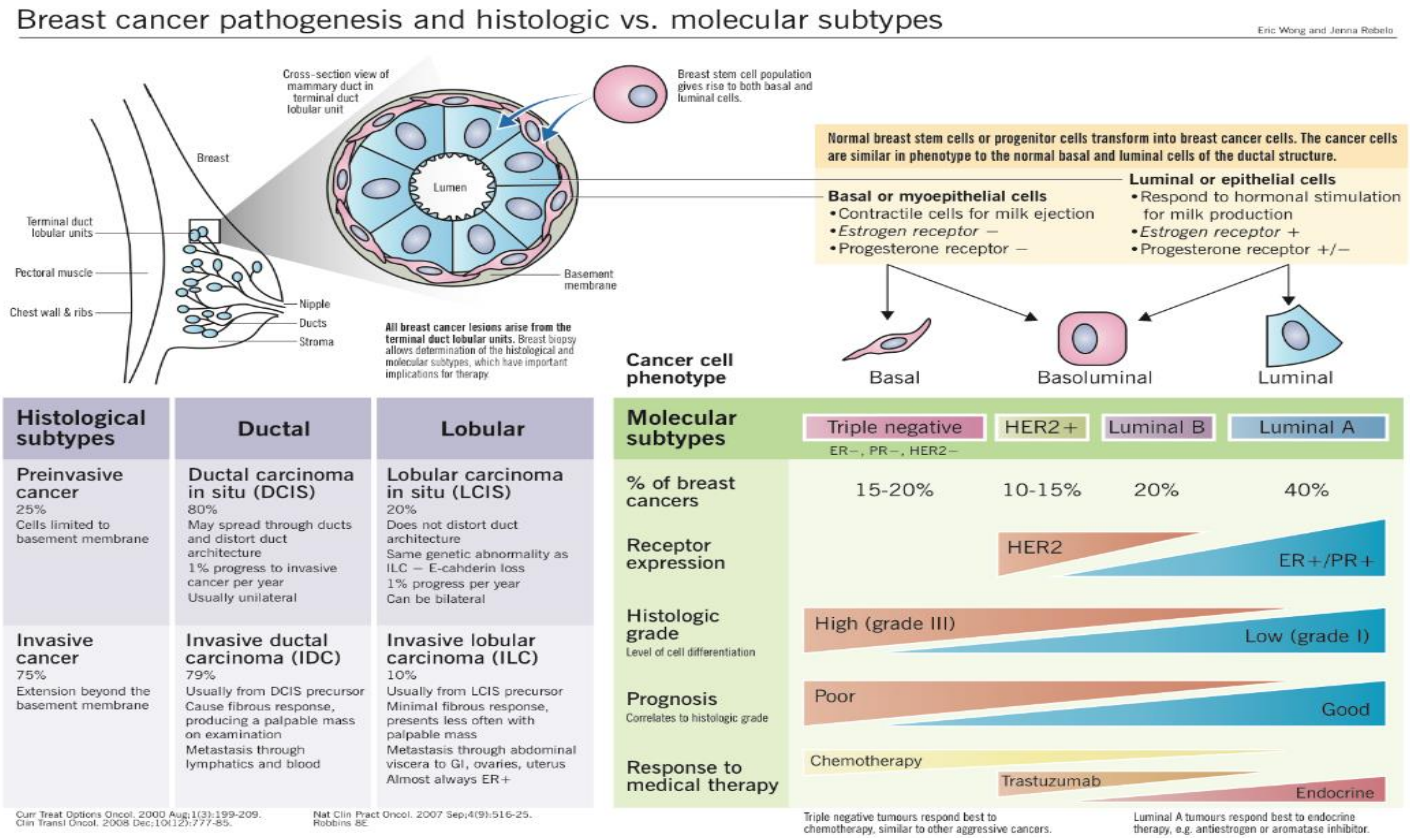

Figure 1.5-1:- Histological and molecular subtypes in breast cancer.

1.5.2 Her2+ Breast Cancer

Human epidermal growth factor receptor 2 (Her2) is a transmembrane protein that belongs to the ErbB/HER family of tyrosine kinases. The HER2 gene is amplified in up to 30% of breast cancers leading to an overexpression of HER2 receptor. This type of breast cancer is generally a more aggressive disease with higher recurrence rates and a poorer patient prognosis. Trastuzumab has become the standard treatment for patients with HER2 positive breast cancer. Patients receiving trastuzumab therapy have shown improved disease free and overall survival in a metastatic setting. However, resistance to therapy is a problem with the use of multiple anti-Her2 antibodies, dual tyrosine kinase inhibitors, and antibody-drug conjugates, alone or in combination as some of the methods used to overcome resistance [46, 47]. One of the newer treatments for HER2+ breast cancer is an antibody drug conjugate (ADC), T-DM1 which was approved by the European Medicines Agency and the Food and Drug Administration (FDA). It is a compound developed by conjugation of trastuzumab and a potent maytansine-derived cytotoxic drug (DM1), using a stable thiolinker [48]. T-DM1 was shown to have antitumor effects by inhibiting cell division and inducing cell death. It is also very specific as an ADC showing minimal effect on non-cancerous cells [49, 50].

1.5.3 Triple Negative Breast Cancer

Heterogeneity also exists in triple negative breast cancer (TNBC) one of the subtypes of breast cancer [51]. Within breast cancer, 15-20% are TNBC of which 85% are of the basal phenotype. TNBC are characterised as ER^{-ve}, PR^{-ve} & $HER2^{-ve}$ and are biologically aggressive and tend metastasize earlier [52]. Within TNBC, 6 additional molecular subtypes have been identified, 2 basal-like (BL1 and BL-2), an immunomodulatory (IM), a mesenchymal (M), a mesenchymal stem-like (MSL) and a luminal androgen receptor (LAR) [43]. Despite advances in treatment resistance to conventional therapy and metastasis remain the major causes of death in patients with TNBC. It is thought that the onset of metastasis may arise as a result of cells within a tumour with an ability to self-renewal and tumour initiating abilities. These cells are often referred to as CSCs [53]. *Currently, there is no targeted therapy available for the treatment of patients with TNBC.* Therefore, TNBC represents a challenge to patients and clinicians due to the poor prognosis and fewer treatment options. In terms of managing TNBC, there are several agents being developed including some associated with EGFR (Cetuximab (Erbitux)), FGFR2 (FGFR inhibitors) in addition to VEGF inhibition, and mTOR (combination of cisplatin and mTOR inhibitors) [54, 55].

1.6 Metastatic Process

Patients presenting with lung cancer generally do so at a late stage, when metastasis has already occurred and therefore beyond the realm of treatment by surgery or radiotherapy. Ninety percent of deaths from solid tumours can be attributed to the metastatic spread of cancer cells [56]. Invasion and migration, therefore, play crucial roles in lung cancer metastasis, which ultimately allow the majority of lung cancers to develop un-noticed. While progress has been made in understanding cancer biology and the process of how cancer spreads, our understanding of the molecular mechanisms remains poor. Metastasis is the spread of malignant tumour cells from their primary site to a distant site or secondary site, via a multistep process known as the metastatic cascade.

1.6.1 Epithelial to Mesenchymal Transition

In the 1980s, Elizabeth Hay made initial observations which described epithelial to mesenchymal phenotypic changes in primitive streaks of chick embryos. Epithelial to mesenchymal transition (EMT) was initially known as "epithelial to mesenchymal transformation" is a cellular mechanism recognised as a central feature of normal development [57, 58].

EMT is a biological process that allows a polarized epithelial cell, which normally interacts with its basement membrane via its basal surface, to undergo multiple biochemical changes that enable it to assume a mesenchymal cell phenotype [59]. Cells with a mesenchymal phenotype have distinctive characteristics including enhanced migratory and invasive capacity, elevated resistance to apoptosis, greatly increased production of ECM components and in some cases stem-like properties. A number of distinct molecular processes are engaged in order to initiate an EMT and enable it to reach completion. These include activation of transcription factors, over-expression of specific cell-surface proteins, reorganization and expression of cytoskeletal proteins and production of ECM-degrading enzymes. The plasticity of EMT is revealed by the occurrence of the reverse process called mesenchymal-epithelial transition (MET), which involves the conversion of mesenchymal cells to epithelial cells; but little is known about this process.

There are three classes of EMT: Type1 (associated with implantation, embryo formation, and organ development), Type2 (associated with wound healing, tissue regeneration, and organ fibrosis) and Type3 (associated with tumour growth and cancer progression) [59]. One hallmark of EMT is the downregulation or even loss of E-cadherin, which is an essential component of adherence junctions. E-cadherin binds with its extracellular

domain of an E-cadherin molecule of the neighbouring epithelial cell which stabilizes cell-to-cell contacts. Intracellularly, E-cadherin binds to β-catenin, α-catenin and p120-catenin which mediates intracellular signalling and links adherence junctions to the actin cytoskeleton. The beginning of the metastatic process is believed to start with EMT. The basic process of an EMT is illustrated in Figure 1.6-1 below.

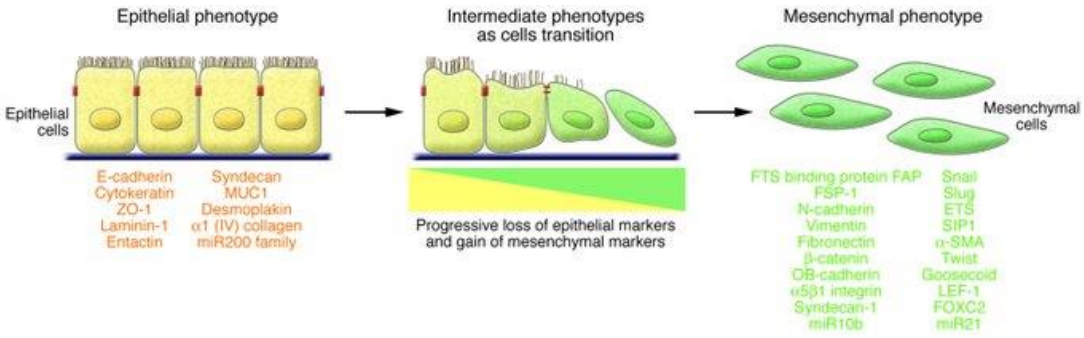

Figure 1.6-1:- Process of epithelial-mesenchymal transition.
An EMT involves a functional transition of polarized epithelial cells into mobile and ECM component–secreting mesenchymal cells. The epithelial and mesenchymal cell markers commonly used by EMT researchers are listed. Co-localization of these two sets of distinct markers defines an intermediate phenotype of EMT, indicating cells that have passed only partly through an EMT.

Primary and secondary microenvironments are known to promote metastasis by gene products of metastatic cells and/or by direct cell-cell and paracrine interactions between cancer cells and stromal cells. However, very few of the tumour cells released from a primary tumour lead to the development of metastasis, therefore the process of metastasis is said to be highly inefficient. The main steps involved in the development of metastasis are illustrated in Figure 1.6-2 [60]. However, these steps are briefly described below. To set up secondary tumours at a distant site, tumour initiating cells must;

1. Dissociate and leave the primary tumour, through loss of expression of cell-cell adhesion molecules such as cadherin's (e.g. E-cadherin/N-cadherin), selectins (e.g. PECAM, ALCAM, L1CAM) and integrin's (e.g. α3, α5, α6, αv).
2. Infiltrate the surrounding stroma, invade and migrate through the basement membrane of the endothelium of blood or lymphatic vessels using a plethora of proteases (e.g. MMPs, serine proteases, cathepsin D, cysteine cathepsin).
3. Enter into the bloodstream by a process of intravasation, cells survive in the bloodstream by evading apoptosis (and anoikis - detachment mediated apoptosis) and elements of the immune system (macrophages, neutrophils).

4. By a process of extravasation, cells must then leave the vasculature, invade local stroma and develop their own microenvironment. Newly formed tumours require an oxygen supply, so the development of new blood vessels is stimulated through angiogenesis (e.g. VEGF, FDGF) [61, 62].

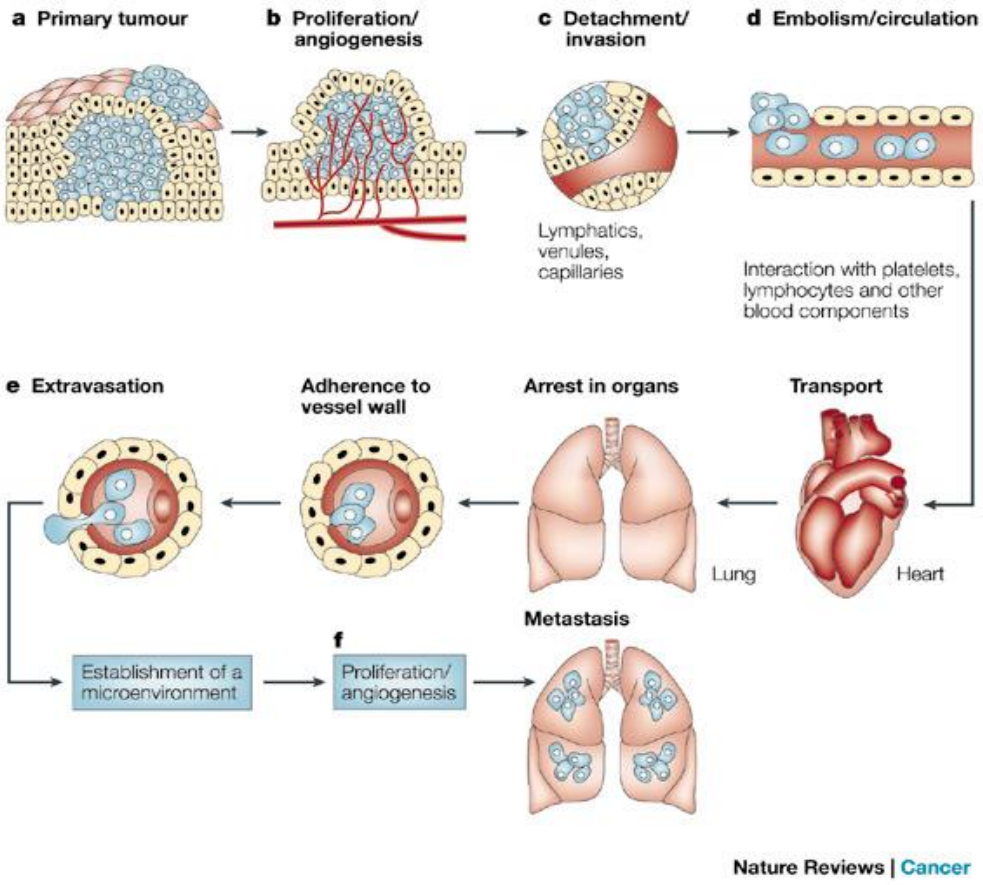

Figure 1.6-2:- The main steps involved in the formation of metastases

Disseminated metastatic tumour cells present in these organs often undergo a period of dormancy, whereby cells (and tumours) can remain asymptomatic for years. Dormancy is becoming a recognised step in cancer progression as it may lead to the formation of tumours years later. Clinical dormancy is frequently observed in many types of tumours such as B-cell lymphoma, melanoma, breast cancer and prostate cancer [63]. Tumours which are clinically dormant typically show no signs of active disease and are said to be asymptomatic tumours.

Dormant cells may be the source of disease recurrence. Cancer dormancy is poorly understood but there are mechanisms that can potentially explain this characteristic of tumours [64]. Tumour cells might exhibit a slowdown in the proliferation of the tumour cell population, this is known as tumour mass dormancy. In this mechanism, tumour cells are usually dividing but due to limitations in blood supply (or presence of an active

immune system), the tumour does not expand beyond a certain size. Other mechanisms of tumour dormancy result in the arrest of tumour cell growth, this is known as tumour cell dormancy or cellular dormancy. During this type of dormancy, tumour cells may enter a state of quiescence or senescence [65, 66]. Senescence is said to be an irreversible state of cellular growth arrest, while quiescent cells are in a state of 'rest' and can resume growth when more favourable environmental conditions arise [67].

Cellular dormancy appears to be an active process that can be activated through a variety of signalling mechanisms that ultimately downregulate the RAS/MAPK and PI(3)K/AKT pathways. Cancer cells rely on these pathways for their growth and survival [68]. These pathways are the subject of intensive research in human cancers [69, 70]. Other mechanisms may also play a role in tumour dormancy; including genetic and epigenetic changes, cancer stem cells, tumour microenvironment, epithelial-mesenchymal transition and non-coding RNA manipulation [63].

1.7 Development of animal models to study heterogeneity

Traditionally, the mechanisms of cancer invasion and metastasis have been investigated *in vitro,* through the use of human tumour derived cell lines. Invaluable information can be gained from cell line based studies however, it does not represent the tumour environment [71]. While animal models do not represent the ideal model to study human cancers, they do offer the best method to study the growth and behaviour of cancer cells *in vivo* [72], but also to study the effect of potential drug treatments on xenograft tumours. This is one of the main advantages animal studies have in comparison to cell line based studies.

Some examples of animal used for research include; mice, hamsters, rats, rabbits, zebrafish, Mouse models more than any other model system have revolutionised our ability to study gene function *in vivo* and to understand the molecular mechanisms driving cancer. There are several advantages when choosing mice as a model to study cancer, they are; (i) small in size (ii) inexpensive to maintain, (iii) produce rapidly and have large litters; and (v) are amenable to genetic manipulation [73]. Genetically engineered mouse models (GEMMs) have enabled numerous studies of non-small-cell-lung cancer that wouldn't normally be possible using patient material.

There are a number of criteria which should be considered when choosing genetically engineered mice (GEM) to study human tumours; (1) the mice must carry the same mutation that occurs in human tumours; (2) mutations should be engineered within the endogenous locus, and not expressed as a transgene (a transgene is a gene/genetic material that has been transferred from one organism to another either naturally or by any genetic engineering techniques); (3) mutated genes should be silent during embryogenesis and early postnatal development, (4) Mutations should be within the specific target tissues in selected cell types and (5) mutations must occur in a limited number of cells. Reproducing the tumour microenvironment is difficult to achieve in these mouse models, but should also be considered. This will help us to understand the interactions of tumour cells and cells of the tumour microenvironment, but also the impact of microenvironment has on tumour progression [74].

The discovery of the *Prkdc*^{scid} (protein kinase, DNA activated, catalytic polypeptide) mutation was one of the turning points for animal based research. This mutation was first identified by Bosma *et al.,* in BALB/c-lgh^{b} (CB-17/lcr) mice [75] and it results in the absence of *Prkdc* expression. Animal models are widely used to study cancer, and decades of breeding led to the identification and development of numerous strains for use by

researchers. Nude and SCID (Severe Combined Immune Deficient) mice are immune compromised, by their inability to generate enough T lymphocytes, in the case of nudes for the inability to produce any B or T lymphocytes, which are vital in mounting an immune response [76]. This is due to the absence of *Prkdc* expression that results in the failure of the VDJ (Variable, Diversity, Joining) rearrangement of lymphocyte antigen receptor genes. When considering Nude or SCID mice for animal studies, due to their immune deficient status they should be housed in sterile environments (environments free from pathogens). A phenomenon known as "leakiness", was observed in some mice bearing the SCID mutation which resulted in the development of functional T and B lymphocytes [75]. However, leakiness was mainly observed in aging mice that housed in non-sterile environments (www.thejax.org).

Genetically engineered mouse models (GEMMs) have enabled numerous studies of non-small-cell-lung cancer that wouldn't normally be possible using patient material. These immune alterations also allow foreign cancer cells to grow and develop in the xenograft models. Many studies have been carried out to investigate the factors involved in malignant transformation, invasion and metastasis, as well as to examine the response to therapy. GEMMs for the most common driver mutations in NSCLC have been generated e.g. *KRAS* and *EGFR* (epidermal growth factor receptor) [77]. Some of these mouse models have been developed to study various cancers including colon cancer [78], renal adenocarcinoma [79], Prostate cancer [80] and lung cancer [81, 82].

1.7.1 $KRAS^{G12D}$ mouse model

KRAS (also known as V-Ki-ras2 Kirsten rat sarcoma) is a guanine nucleotide transferase that can link cell surface receptors to intracellular signalling pathways including kinase cascades such as the MAPK pathway, lipid kinases such as phosphoinositide 3-kinase (PI3K), and other small molecular weight GTPases including Ral, Rac, and Rho. KRAS is known to regulate a number of processes such as cell proliferation, survival, differentiation, migration, and extracellular communication. It is an oncogene in approx. 30% of human cancers, including the majority of lung adenocarcinomas, but are uncommon in lung squamous carcinomas. Mutational activation of KRAS generally results in aggressive cancers, which confers poor prognosis on patients harbouring the mutation. Patients with the KRAS mutation generally show a poor response to current therapies [83]. A number of attempts to target KRAS activity, but all appear to have failed clinically, for this reason, KRAS has been considered undruggable [84].

Mouse models have been developed to investigate the growth of tumours harbouring the KRAS mutation. One example is the conditional oncogenic $KRAS^{G12D}$ mouse model has been used to elucidate the steps from early to late tumorigenesis, owing to the temporal controls it affords, and it is easy to combine with mice bearing conditional null alleles for other genes of interest. In these mice, $KRAS^{G12D}$ tumours only reach a full adenocarcinoma stage with a very long latency but $KRAS^{G12D}$-expression and transformation related protein 53 (Trp53)-null (p53) tumours are more advanced and show a decreased response to certain treatment strategies when compared to $KRAS^{G12D}$ tumours [85-87].

1.8 Characteristics of DLKP and its clonal subpopulations

It is well established that primary and metastatic tumours are heterogeneous in nature and are home to subpopulations of cancer cells that differ in their genetic, phenotypic and behaviour characteristics. Two theories have been described to explain the establishment and maintenance of tumour heterogeneity; the cancer stem cell (CSC) theory and the clonal evolution/selection model. Both had been thought to be exclusive from each other, however, the processes are now believed to be potentially complementary. Heterogeneity in tumours has its implications for the approach taken to personalised medicine as it can limit therapeutic efficacy, lead to resistance to therapies, impact the strategy taken for tumour biopsies and also interfere with the regimes associated with treatment planning [88-90].

1.8.1 History of DLKP

DLKP is a human lung cancer cell line which was established by Dr. Geraldine Grant. The DLKP cell line was established from lymph node metastasis of a primary lung tumour which was initially described as a 'poorly differentiated squamous cell carcinoma'. This tumour was taken from a 52-year old patient who was believed to have smoked 40 cigarettes per day for most of his adult life. The karyotype of DLKP was previously determined [91] to consist of a hyperdiploid subpopulation (65% of cells with 56 chromosomes) and hypertetraploid subpopulation (35% of cells with 95-115 chromosomes).

DLKP was found to contain at least three morphologically distinct subpopulations, DLKPSQ, DLKPI and DLKPM. DLKPSQ resembled a squamous like morphology, with distinct cell boundaries and a cobble stone appearance. DLKPM resembled mesenchymal appearance with a fibroblast-like morphology, while DLKPI grew in tightly packed colonies with indistinct cell boundaries (Figure 1.8-1). The karyotype of the DLKP clones was also established; examination of the chromosome distribution found that DLKPM was near diploid having between 50-59 chromosomes in 60% of its population and was, therefore, the most homogenous. DLKPI was near tetraploid with 36% of its population containing 90-99 chromosomes and the remaining population containing 40-110 chromosomes. DLKPSQ was found to contain 3 large chromosomal populations with 90-99, 100-110, and 80-89 chromosomes. The morphological diversity seemed to be reflected in their respective chromosome numbers, however, the chromosomal distribution of the clones was not substantially found in the parental population [92, 93].

The ratio of clones present within the DLKP parental cell line seems to be tightly controlled through a model of interconversion proposed in previous studies performed by McBride, 1995. The model proposed that DLKPSQ may interconvert with DLKPI and DLKPI may interconvert with DLKPM. However, interconversion was not observed between DLKPSQ and DLKPM. It was therefore suggested that DLKPI resembled a potential stem cell-like population in DLKP with its ability to interconvert and give rise to both DLKPSQ and DLKPM-like cells.

A core property of a stem cell is one with a self-renewal capacity. These initial studies also indicated that DLKP should be classified as either a variant small cell lung carcinoma or non-small cell lung carcinoma with neuroendocrine differentiation. Keratins are the first intermediate filament proteins detectable during foetal development and are among the most differentiation-specific proteins synthesised in epithelial cells. DLKP contains neurofilament and vimentin markers, but no keratin proteins were detected during early Immunohistochemical analysis. BrdU is a thymidine analogue capable of inducing epitheloid morphology and altering expression of neuroendocrine markers in SCC. Upon treatment with BrdU keratin 8 and keratin 18 appeared to be synthesised, and it was postulated that a posttranslational block on keratin can be reversed using agents such as BrdU [94].

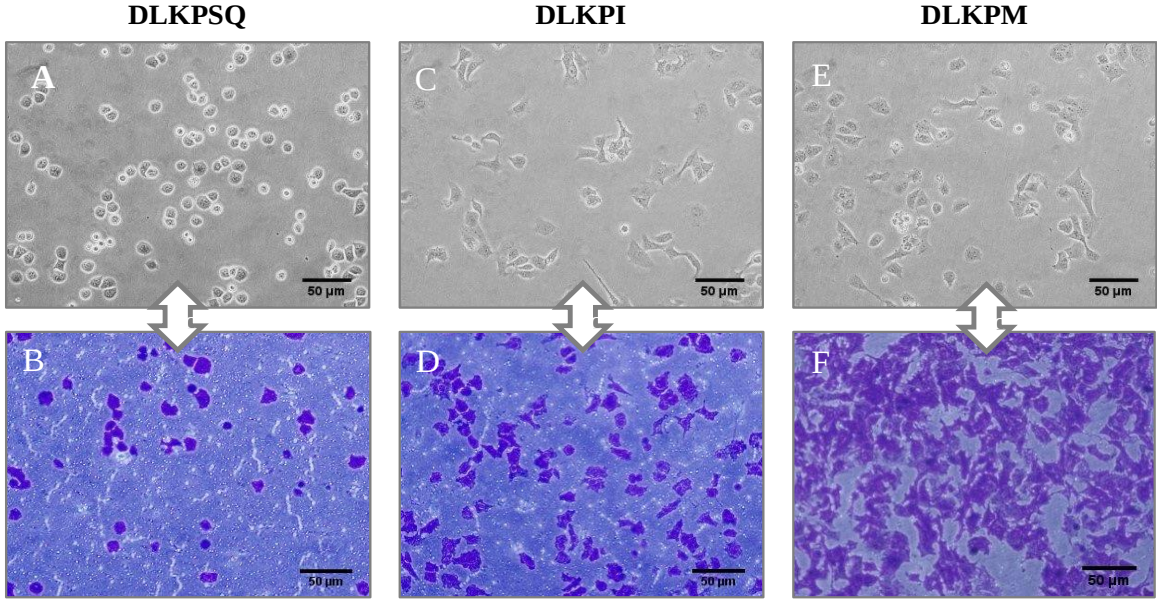

Figure 1.8-1:- Growth and invasion characteristics of the DLKP clones in vitro.
Morphology of DLKP clones on plastic (A, C and E) and visual analysis of the level of invasion of the DLKP clones (B, D and F) (original magnification = 100×, scale bar 50µm).

In addition, later studies carried out on DLKP and its clones indicated that they displayed differences in the levels of *in vitro* invasion (Figure 1.8-1), migration and anoikis resistance. The DLKPSQ clone displays a poor invasive and migratory capacity, is anoikis resistant and displays low level expression of integrin-αv. The DLKPM clone displays a high invasive and migratory capacity but is anoikis sensitive. DLKPI clone displays an intermediate level of invasive and migratory capacity, with an intermediate ability to resist anoikis [95]. Both DLKPI and DLKPM display high adherence capacity to bind fibronectin and vitronectin, potentially explained by its increased expression of integrin-αv. There was also differences in expression of matrix-metalloproteinases (MMPs) which appear to correlate the invasive profile of the clones (Figure 1.8-1). DLKPSQ was previously found to express MMP2 and MMP10 at low levels, while MMP2 is expressed in DLKPI and MMP2 is expressed in DLKPM [95, 96].

The DLKP parental cell line was previously used as a model to investigate the mechanism of resistance to adriamycin *in vitro*. Adriamycin is a drug commonly used to treat a variety of malignancies including lung and breast cancer. A proteomic comparison between DLKP parental *vs.* DLKPA (adriamycin resistant variant) identified 80 differentially regulated proteins including NDPK, RPA2, CCT2, HSP70 and Annexin. Many of the other proteins identified correlated with known targets of adriamycin resistance including DNA damage repair, apoptosis and ROS [97].

Previous attempts were made to identify specific markers for the DLKP clones, for which immunocytochemical methods were employed. These methods were qualitative and therefore did not allow for the quantitative analysis of expressed proteins. To date, no markers have emerged that can allow for the differentiation of individual DLKP clones in DLKP. Ideally, a good marker would be one that is expressed in 1 or 2 of the clones, but not in all 3 clones. Quantitative proteomic analysis could allow for the identification of proteins that are differentially expressed between the clonal variants and could potentially act as markers for the clones. Also, identification of such protein markers could provide the means to study the model of interconversion between the clones, as well as their potential involvement in cell invasion and migration. Identification of markers specific to the DLKP clones is also hugely important in the context of tumour heterogeneity because if cells within a given tumour have the ability to regenerate through a model of interconversion this could have implications for the effectiveness of treatments, (i.e. leading to renewed tumour growth after cessation of therapy). Therefore, any markers identified to differentiate each of the clonal subpopulations in DLKP, with

further investigation, could have the potential to be used in the development of more targeted or combination therapies allowing for more personalised treatment of patients with lung cancer. The phenotypic differences displayed within the DLKP cell line model presents an opportunity to explore both differences in expression of potentially biologically relevant proteins but also is a unique model to investigate tumour heterogeneity in lung cancer.

1.9 Aims of Thesis

The aims of this thesis are as follows:

1. To isolate and identify membrane associated proteins from DLKP, DLKPSQ, DLKPI and DLKPM and to carry out proteomic profiling to identify differentially expressed proteins that could be used as potential markers of the individual clones, but also to identify potentially novel proteins associated with lung cancer.

2. To investigate the functional roles (*in vitro*) of selected proteins in lung cancer, using siRNA silencing.

3. To examine the expression of selected proteins in human tumours and in representative cell lines (lung, pancreatic and breast cancers), using Western blot analysis and immunohistochemistry.

4. To investigate the growth and potential tumour development of DLKP, DLKPSQ, DLKPI and DLKPM *in vivo,* using SCID mice.

5. To investigate the expression of established markers associated with cancer progression (including; Ki-67, CD31, E-cadherin and N-cadherin) and the expression of the candidate protein markers in explanted tumour cells and xenograft tissues, from the *in vivo* study.

Chapter 2 MATERIALS AND METHODS

2.1 Cell lines and cell culture

All cell culture work was carried out in class II laminar air-flow cabinets (NuAIR). Before and after use the laminar flow cabinet was cleaned with 70% industrial methylated spirits (IMS). Any items brought into the cabinet were also swabbed down with IMS. At any time only one cell line was used in the laminar flow cabinet and upon completion of work with any given cell line, 15 mins clearance was given to eliminate any possibilities of cross-contamination between the various cell lines. The cabinet was cleaned routinely with Virkon (Antech International, P0550) and IMS. Details pertaining to the cell lines used for the experiments are provided in Table 2.1-1. All cells were incubated at 37ºC and where required, in an atmosphere of 5% CO_2. Cell lines were maintained in their appropriate complete medium (Table 2.1-1) and subcultured, as per section 2.1.1, every 2-3 days or as required in order to maintain active cell growth.

2.1.1 Sub-culturing of adherent cell lines

Waste cell culture medium was removed from the tissue culture flask and discarded into a sterile glass bottle. The flask was then rinsed out with 2-5mls trypsin/EDTA solution (0.25% trypsin (Gibco, 043-05090), 0.01% w/v EDTA (Sigma, E9884) solution in PBS (Oxoid, BRI4a)) to ensure the removal of any residual media. Depending on the size of the flask, 2-5ml of trypsin was then added to the flask, which was then incubated at 37ºC, for approximately 5 mins until all of the cells detached from the inside surface of the flask monitored by microscopic observation. Adding an equal volume of complete media (described in Table 2.1-1) to the flask deactivated the trypsin. The cell suspension was removed from the flask and placed in a sterile universal container (Sterilin, 128A) and centrifuged (Beckman, Allegra™, 6KR centrifuge) at 1000rpm for 5 mins. The supernatant was then discarded from the universal and the pellet was suspended gently in complete medium. A cell count was performed and an aliquot of cells was used to seed a flask at the required density. All cell waste and media exposed to cells were autoclaved before disposal.

Cell line	Details	Source	Complete Media
DLKP parent	Human poorly differentiated lung carcinoma	NICB	DMEM-HAMS-F12, 5% FCS
DLKPSQ (McBride *et al.*, 1998)	Squamous-like subpopulation clone of DLKP	NICB	DMEM-HAMS-F12, 5% FCS
DLKPI	Intermediate sub-Population cloned from DLKP	NICB	DMEM-HAMS-F12, 5% FCS
DLKPM	Mesenchymal-like clone of DLKP	NICB	DMEM-HAMS-F12, 5% FCS
SQ-Mitox-BCRP-6P	Mitoxantrone selected variant of DLKPSQ	NICB	DMEM-HAMS-F12, 5% FCS
DLRP (Law *et al.*, 1992)	Human poorly differentiated lung carcinoma	NICB	DMEM-HAMS-F12, 5% FCS
NCI-H69	Small cell lung carcinoma	NICB	RPMI 1640, 10% FCS
NCI-H82	Small cell lung carcinoma	NICB	RPMI 1640, 10% FCS
DMS-53	Small cell lung carcinoma	NICB	RPMI 1640, 10% FCS
NCI-H460	Lung large cell carcinoma	NICB	RPMI 1640, 10% FCS
NCI-H1229	Lung large cell carcinoma	NICB	RPMI 1640, 5% FCS, 1mM Na Pyruvate
A549	Lung adenocarcinoma	NICB	DMEM-HAMS- F12, % FCS
SK-LU-1	Lung adenocarcinoma	NICB	MEM, 5% FCS, 1% NEAA, 1mM Na Pyruvate
SK-MES-1	Squamous cell lung carcinoma	NICB	DMEM-HAMS-F12, 5% FCS
HCC-1937	Triple Negative Breast Cancer	ATCC	RPMI 1640, 10% FCS
HCC1143	Triple Negative Breast Cancer	ATCC	RPMI 1640, 5-10% FCS
MDA-MB-468	Triple Negative Breast Cancer	ATCC	RPMI 1640, 10% FCS
CAL-85-1	Triple Negative Breast Cancer	ATCC	DMEM, 10% FCS, 2mM L-Glut, 1mM Na pyruvate
HDQP-1	Triple Negative Breast Cancer	ATCC	DMEM, 10% FCS
CAL-51	Triple Negative Breast Cancer	ATCC	DMEM, 5-10% FCS, 1% Na pyruvate, 2mM L-Glut
Hs-578-T	Triple Negative Breast Cancer	ATCC	DMEM, 10% FCS, 0.01mg/ml insulin
MDA-MB-231	Triple Negative Breast Cancer	ATCC	RPMI 1640, 10% FCS
MDA-MB-157	Triple Negative Breast Cancer	ATCC	RPMI 1640, 10% FCS
BxPc-1	Pancreas adenocarcinoma	ATCC	RPMI 1640, 5% FCS, 1mM Na pyruvate
HPAC	Pancreas adenocarcinoma	ATCC	RPMI 1640, 10% FCS
Panc-1	Pancreas adenocarcinoma	ATCC	DMEM, 10% FCS, 2mM L-Glut
MiaPaca2	Pancreas adenocarcinoma	ECACC	DMEM, 5% FCS
MiaPaca2 clone3	Pancreas adenocarcinoma clone of MiaPaca2	NICB	DMEM, 5% FCS
AsPc-1	Pancreatic adenocarcinoma from metastatic ascites	ATCC	RPMI 1640, 10% FCS
Capan-1	Liver metastasis of pancreas adenocarcinoma	ATCC	DMEM, 20% FCS, 2mM L-Glut
SW480	Dukes' type B colorectal adenocarcinoma	ATCC	RPMI 1640, 10% FCS
SW620	Dukes' type C colorectal adenocarcinoma	ATCC	RPMI 1640, 10% FCS
SNB-19	Glioma	DSMZ	DMEM, 5% FCS
Lox IVMI	Human melanoma	NICB	RPMI 1640, 10% FCS
SK-N-SH	Neuroblastoma	NICB	DMEM-HAMS-F12, 5% FCS

Table 2.1-1:- Description of cell lines used in during this project.

ATCC: - American Type Culture Collection, Rockville, MD, USA.
DSMZ: - Deutsche Sammlung von Mikroorganismen und Zellkulturen GmbH (German Collection of Microorganisms and Cell Cultures).
ECACC: - European Collection of Animal Cell Cultures, Salisbury, Wiltshire, UK.
NICB: - National Institute for Cellular Biotechnology, DCU, Dublin, Ireland.

2.1.2 Sub-culturing of suspension/aggregate cell lines

The cell suspension was removed from the flask and placed in a sterile universal container and centrifuged at 1000rpm for 5 mins. The supernatant was then discarded from the universal container and the pellet was re-suspended in complete medium. The aggregates were broken up by gently pipetting the suspension up and down using a 10ml pipette. An aliquot of the cell suspension was used to seed a flask.

2.1.3 Assessment of cell number

Prior to cell counts, cells were prepared for sub-culturing as detailed in section 2.1.1 and section 2.1.2. An aliquot was then applied to the chamber of a glass coverslip-enclosed haemocytometer. For each of the four grids, cells in the 16 squares were counted. The average of the four grids was multiplied by a factor of 10^4 (volume of the grid) and the relevant dilution factor to determine the average cell number per ml in the original cell suspension. On this basis, the cell number per ml could be calculated. The cell pellet was then resuspended in an appropriate volume to obtain a cell suspension of $1x10^6$cells/ml.

2.1.4 Cryopreservation of cells

Cells for cryopreservation were harvested in the log phase of growth as described in section 2.1.1 and section 2.1.2. Cell pellets were re-suspended in a suitable volume of serum. An equal volume of a 10 - 20 % DMSO (Sigma, D2438)/serum solution was added dropwise with mixing, to the cell suspension. The cell suspension was then aliquoted in 1ml volumes to cryovials (Greiner, 122278) and immediately placed at -20^{o}C for up to four hours. After four hours, the cryovials were transferred to -80^{o}C for short term storage, after which the vials were gradually transferred to the liquid phase of liquid nitrogen for long term storage (-196^{o}C).

2.1.5 Thawing of cryopreserved cells

A volume of 5ml of fresh growth medium containing serum was added to a sterile universal. The cryopreserved cells were removed from the liquid nitrogen and thawed at 37^{o}C quickly. The cells were removed from the vials and transferred to the aliquoted media (also at 37^{o}C). The resulting cell suspension was centrifuged at 1000rpm for 5 mins. The supernatant was removed and the pellet re-suspended in fresh culture medium. Cell viability of thawed cells was noted. Thawed cells were then added to an appropriately sized tissue culture flask with a suitable volume of growth medium and allowed to attach overnight. The following day, flasks were re-fed with fresh media to remove any remaining DMSO and non-viable cells.

2.1.6 Monitoring of sterility of cell culture solutions

Sterility testing was performed in the case of all cell culture media and cell culture related solutions. Samples of prepared basal media were incubated at 37^{o}C for a period of seven days. This ensured that no bacterial or fungal contamination was present in the media or the solutions.

2.1.7 Serum batch testing

To prevent batch to batch variation in foetal calf serum (FCS) which is a common problem in cell culture, a range of FCS batches were screened and the most suitable were chosen for a block of work (HyClone®, ThermoFisher Scientific, SV30143.03). Screening involved growing cells in 96-well plates and growth was recorded as a percentage of growth of a serum with known acceptable growth rate.

More specific screening involved performing invasion assays to determine the effects of different batches of serum on the ability of particular cell lines to invade through an extracellular matrix, *in vitro*. Invasion assays were performed and evaluated as per section 2.4.1.

2.1.8 *Indirect* mycoplasma analysis of cell lines

Mycoplasma testing was carried out quarterly, using the *indirect* method. Mycoplasma-negative NRK (normal rat kidney fibroblast) cells were used as indicator cells for this analysis. NRK cells were seeded onto 35mm petri dishes (Sigma) in DMEM supplemented with 10% FCS. A 1ml volume of conditioned medium (from test cell lines) was inoculated onto the petri-dishes containing NRK cells and incubated for 4 days at 37^{o}C in a 5% CO_2 atmosphere. Prior to inoculation, test cell lines must be in log phase of growth, passaged a minimum of 3 times, free from antibiotics and the conditioned medium collected from cell lines must be at least 3 days old. Cells were fixed in Carnoys Fixative (1 part of glacial acetic acid to 3 parts of methanol at -20^{o}C) at a ratio of 50:50 Carnoys: PBS. A fluorescent Hoechst stain was used in for analysis. The stain binds specifically to DNA and so stains the nucleus of the cells in addition to any mycoplasma present. Mycoplasma infection was indicated by fluorescent bodies in the cytoplasm of the NRK cells. The analysis was performed by Michael O'Donohoe or Michael Henry. Cell lines used throughout this thesis were mycoplasma negative.

2.2 Proteomic analysis

Proteomic analysis detailed in this thesis was carried out with the help and guidance of Dr. Paul Dowling and Mr. Michael Henry.

2.2.1 Cell surface membrane protein Isolation

Isolation of cell surface proteins was carried using the Cell Surface Isolation kit (ThermoFisher Scientific, 89881). This kit used a biotinylation approach to efficiently label proteins with accessible lysine residues and sufficient extracellular exposure. The process uses a cell impermeable, cleavable biotinylation reagent to label exposed primary amines of proteins on the cell surface of intact cells. Biotinylation is a rapid and specific process of covalently attaching biotin to a protein. Biotin has a high affinity to streptavidin and avidin so proteins can be easily recovered for examination.

DLKP, DLKPSQ, DLKPI and DLKPM cell lines were obtained from NICB culture collection. Cell lines were maintained in $75cm^2$ flasks in DMEM/Hams-F12 supplemented with 5% FCS at 37^oC in an atmosphere of 5% CO_2. Cells were cultured until they were approximately 90-95% confluency before treated and processed as per manufacturer's instructions. Triplicate biological replicates of cell surface proteins were isolated from all four cell lines. Briefly, for labelling and lysis, cells were treated using Sulfo-NHS-SS-Biotin on a rocking platform for 30 mins at 4^oC, followed by lysis and multiple sonication steps. To isolate labelled proteins, the clarified supernatant was added to washed NeutrAvidin agarose slurry and incubated for 60 mins at room temperature with end over end mixing on a rotator, after which agarose beads were washed using wash buffers. Protein elution was performed during a 60 min incubation at room temperature with end over end mixing using 50 mM DTT in PBS.

2.2.2 In-solution tryptic digestion

Initial preparation of individual protein fractions for LC-MC/MS analysis was carried out by buffer exchange overnight by acetone precipitation. Protein pellets were resuspended in Label-Free buffer solubilisation buffer containing 6 M urea, 2 M thiourea, 10 mM Tris, pH 8.0 in LC-MS grade water. Re-suspended protein samples were then carefully vortexed, sonicated and centrifuged to ensure pellets were fully resuspended. For label-free MS analysis, volumes were initially equalised with label free buffer and kept to a minimum. Protein was re-quantified using the Quick Start Bradford assay kit (Bio-Rad, 5000201) and 5 µg of each sample were reduced for 30 mins at 56^oC with 10 mM DTT in 50 mM ammonium bicarbonate. The samples were then alkylated for 20 mins in the

dark with 25 mM iodoacetamide in 50 mM ammonium bicarbonate. A final volume of 0.1% ProteaseMAX (v/v) was added to each fraction and protein digestion was carried out using sequencing-grade trypsin at a ratio of 1:20 (protease: protein) overnight at 37^{o}C. Ahead of mass spectrometry, digestion was stopped by adding Trifluoroacetic Acid (TFA) to a final concentration of 0.5% (v/v). Peptide suspensions were purified using Pierce C18 Spin Columns (ThermoFisher Scientific, 89870) and the resulting peptide samples were dried through vacuum centrifugation and suspended in 25µl of loading buffer consisting of 2% acetonitrile (ACN) and 0.05% TFA in LC-MS grade water. Protein suspensions were vortexed and sonicated again to ensure an even suspension.

2.2.3 Label-Free Liquid chromatography mass spectrometry Analysis

An Ultimate 3000 nanoLC system (Dionex Corporation, Sunnyvale, CA, USA) coupled to an LTQ Orbitrap XL mass spectrometer from ThermoFisher Scientific (Dublin, Ireland) was used for the nano LC-MS/MS analysis of differentially expressed proteins from cell surface protein preparations of DLKP, SQ, I and M, as previously described. Digested peptide mixtures (5 µl volume) were loaded onto a C18 trap column (C18 PepMap, 300 µm id × 5 mm, 5 µm particle size, 100 Å pore size; Dionex). Desalting was carried out at a flow rate of 25 µl/min in 0.1% TFA and 2% ACN for 5 min. The trap column was switched on-line with an analytical PepMap C18 column (75 µm id × 500 mm, 3 µm particle, and 100 Å pore size; Dionex). Peptides generated from skeletal muscle proteins were eluted with the following binary gradients: solvent A (2% ACN and 0.1% formic acid in LC-MS grade water) and 0%–25% solvent B (80% ACN and 0.08% formic acid in LC-MS grade water) for 240 min and 25%–50% solvent B for a further 60 min. The column flow rate was set to 350 nL/min. Data was acquired with Xcalibur software, version 2.0.7 (ThermoFisher Scientific). The MS apparatus was operated in data-dependent mode and externally calibrated. Survey MS scans were acquired in the Orbitrap in the 400–1800 m/z range with the resolution set to a value of 30,000 at m/z 400 and lock mass set to 445.120025 u. CID fragmentation was carried out in the linear ion trap with up to three of the most intense ions (1+, 2+ and 3+) per scan. Within 40 s, a dynamic exclusion window was applied. A normalised collision energy of 35%, an isolation window of 3 m/z, and one microscan were used to collect suitable tandem mass spectra.

2.2.4 Quantitative Profiling of Label-Free LC-MS/MS Analysis

Progenesis label-free LC-MS software version 3.1 from Non-Linear Dynamics (Newcastle upon Tyne, UK) was used to process the raw data generated from LC-MS/MS analysis. Data alignment was based on the LC retention time of each sample, allowing for any drift in retention time given and adjusted retention time for all runs in the analysis. A reference run was established with the sample run that yielded most features (i.e., peptide ions). The retention times of all of the other runs were aligned to this reference run and peak intensities were then normalized. Prior to exporting the MS/MS output files to MASCOT (www.matrixscience.com) for protein identification, a number of criteria were employed to filter the data. This included (i) peptide features with ANOVA ≤ 0.05 between experimental groups, (ii) mass peaks (features with charge states of +1, +2 and +3, and (iii) greater than one isotope per peptide. A MASCOT generic file was used for peptide identification using proteome discoverer 2.0 (ThermoFisher Scientific) against MASCOT (version 2.2) and Sequest HT (SEQUEST HT algorithm, licence ThermoScientific, registered trademark University of Washington, USA) and was searched against the UniProtKB-SwissProt database (downloaded January 2015, taxonomy: Homo Sapiens). The following search parameters were used for protein identification. (i) peptide mass tolerance set to 20ppm, (ii) fragment mass tolerance set to 0.02 Da, (iv) up to two missed cleavages were allowed, (v) carboxymethylation set as a fixed modification, (vi) methionine oxidation set as a variable modification. For re-importation back into Progenesis LC-MS software, further analysis on only peptides with ion score set to minimum of 40.00 of more (from Mascot) and Sequest HT XCorr set to minimum of >1.9 for singly charged ions, >2.2 for doubly charged ions and >3.75 for triply charged ions or more (from SEQUEST HT) were selected. Target FDR for PSMs and peptide validation, peptide and protein filtering, protein scoring, protein FDR validation, protein grouping and ProteinCenter annotation was carried out. The ProteinCenter annotation node retrieves from the ProteinCenter information from Gene Ontology (GO) database, protein annotations from the Ensembl database and PTM modifications from the UniProt database. All protein identifications for each sample were exported to Microsoft Excel [98, 99].

2.3 Western blot analysis

2.3.1 Preparation of whole cell lysates

Cells were grown to 80 - 90% confluency in culture flasks (T75cm2 flask), media was removed, cells were washed 3 x in ice cold PBS and then removed. 500 µl (per T75cm^2 flask) or 1 ml (per T175cm^2 flask) of RIPA lysis buffer (Sigma, R0278) containing 1X Halt protease/phosphatase inhibitor cocktail (ThermoScientific, 78440) and incubated on ice for 30 mins with regular agitation. Following centrifugation at 16,000 g (Eppendorf) for 5 mins at 4°C, the resulting lysate was stored at -80°C.

2.3.2 Preparation of membrane proteins

Membrane proteins were isolated from cells using the ProteoExtract Native Membrane Protein Extraction Kit (Calbiochem, 444810) and used according to the manufacturer's instructions. Samples were stored at -80^{o}C.

2.3.3 Preparation of conditioned medium

Cells were seeded (1x10^{6}cells: DLKP and DLKPM, 1.25x10^{6}cells: DLKPI-and 1.5x10^{6}cells: for DLKPSQ) in three biological replicates in T175cm^2 flasks and cultured for 72 hrs or until 50-60% confluent. Cells were washed x 3 in serum-free media (SFM, DMEM/Hams-F12) and incubated in SFM (10 ml/T175cm^2 flask) for 60 mins. After this time, cells were washed again x 3 in SFM, 30 mls of SFM was added to the cells and incubated for a further 72 hrs. After such time, conditioned media was collected, centrifuged for 5 min at 1000 rpm and filtered through 0.22µm filter. CM samples were kept on ice until required or stored at 4^{o}C for no longer than 24hrs prior to concentration.

To concentrate conditioned media, 20mls was added to a Vivaspin20 concentrator with a 5kDa molecular weight cut off (Sartorius, *VS*.0112) and centrifuged at 4^{o}C at 4000rpm (ThermoFisher Scientific, 11175774) until the final volume 10 times the original volume (e.g. 10 mls to 1 ml). The sample was removed and then stored in aliquots at -80^{o}C.

2.3.4 Protein Quantification

Protein levels were determined using the Pierce™ BCA Protein assay kit (ThermoFisher Scientific, 23225) or the QuickStart Bradford protein Assay Kit (Bio-Rad, 5000201) as follows:

2.3.4.1 BCA protein assay

Protein in whole cell preparations (prepared in RIPA buffer), Membrane enriched samples and CM was quantified using the Pierce BCA Protein Assay Kit (Thermo-Fisher Scientific, 23227) as per the manufacturer's instructions.

2.3.4.2 Bio-Rad protein assay

The Quick Start Bradford assay kit (Bio-Rad, 5000201) was used for protein samples prepared in 2D lysis buffer (20 mM Tris, 7 M Urea, 2 M Thiourea, 4% CHAPS, pH 8.5). A protein standard curve (0, 0.2, 0.4, 0.6, 0.8, 1.0 and 1.5mg/ml) was prepared from the BSA stock with dilutions made in UHP and stored at -20^{o}C. A 20 µl volume of protein standard dilution or sample (diluted 1:4 to 1:8) was added to appropriate wells of a 96-well plate. A 250 µl of the Bradford reagent dye was then added to each well and incubated at room temperature for 5 mins. All samples were assayed in triplicate. Absorbance was assessed at 570nm. The concentration of the protein samples was determined from the plot of absorbance at 570nm versus the concentrations of the standard curve.

Protein concentrations obtained using both protein quantifications were adjusted relative to the dilutions (e.g. If a 1:4 dilution was used to obtain a concentration of X µg/ml, then the value for X was multiplied by 4).

2.3.5 Gel Electrophoresis

Protein samples for Western blotting were separated by SDS-PAGE gel electrophoresis, using 4-12% gradient gels (ThermoFisher Scientific, NP0335, NP0321). Approximately 15µg (for whole cell lysates), 8µg (for membrane proteins) and 30ug (for conditioned medium) of protein in 4x sample buffer (ThermoFisher Scientific, NP0007) was applied to each well of the polyacrylamide gel. Pre-stained molecular weight markers (ThermoFisher Scientific, LC5800) were also loaded onto the gel for the determination of the molecular weight of the protein samples. Gels were run at 200 volts and 250 milliamps for 1 hour with 1× MOPS, Tris/ Glycine/ SDS running buffer (ThermoFisher Scientific, NP0001). 500 µl of antioxidant (NP0005) was then added to the inner chamber of the Xcell SureLock® minicell (EI0001) electrophoresis gel-rig. When the dye front of

the samples and the molecular weight markers had reached the end of the gel, electrophoresis was stopped.

2.3.6 Enhanced Chemiluminescence detection

Proteins were transferred to Polyvinylidene fluoride (PVDF) membranes (ThermoFisher Scientific, IB4010-01) using the iBlot transfer system (ThermoFisher Scientific, IB1001). The membrane was blocked with 5% milk powder (Biorad, 170-6404) in TBS/Tween (1x TBS (Sigma, T5912) and 0.1% Tween20 (Sigma, P1379-500ml)) at room temperature for 2 hours, then incubated overnight at 4°C in primary antibody (Table 2.3-1) diluted with 0.1 % TBS-Tween in 5 % milk powder. The membrane was washed three times with 0.5 % TBS-Tween and then incubated at room temperature with secondary antibody (Table 2.3-1) in 5 % milk powder with 0.5 % TBS-Tween for 1 hour. The membrane was washed three times with 0.5 % TBS-Tween followed by one wash with TBS alone. Following the final wash, membranes were incubated for 5mins with 3 ml (for a full membrane) of a 50:50 mixture of ECL reagent A and ECL reagent B (Amersham, ECL, RPN 2105 or Clarity, BioRad, 170506). Immunoblots were developed using ECL reagents which facilitated the detection of bound peroxidase conjugated secondary antibody. While developments have made in the way which Western blots are developed such as the use of Chemiluminescence imaging systems (e.g. BioRad Chemidoc imaging system or ThermoFisher Scientific, MyECL imager), darkroom facilities were used for the duration of this thesis. In the darkroom, the PVDF membranes were exposed to Amersham Hyperfilm^{TM}, Chemiluminescence film (GE Healthcare, 28906837) for various times (from 10 seconds to 30 mins depending on the signal). The exposed auto-radiographic film was developed for between 45 seconds to 1 mins in the developer (Kodak, LX-24). The film was then transferred to a fixative (Kodak, FX-40) for 2 mins. The film was rinsed with water for 2 mins and left to dry at room temperature. Once dry, the blots were then converted into a digital format using Epson Perfection photo scanner 4990 and Epson Scan software version 3.04a.

	Antibody	Concentration/Dilution	Company
Primary Antibodies	**ALCAM**	1:1000	Abcam (ab109215)
	HDGF	1:1000	Abcam (ab128921)
	INA	1:7500	Abcam (ab40758)
	IQGAP1	1:1500	Abcam (ab86064)
	SLIT2	1:1000	Abcam (ab134166)
	SPR	1:6000	Abcam (ab157194)
	GAPDH	1:2000	R&D Systems
	α-tubulin	1:40000	Sigma Aldrich (T9026)
Secondary Antibodies	**Swine Anti-Rabbit HRP**	1/2000	Dako (P0399)
	Goat Anti-Mouse HRP	1/2000	Dako (P0477)
	Goat Anti-Rabbit HRP	1/2000	Dako (P0448)

Table 2.3-1:- List of antibodies and the dilutions used in Western blot analysis

To control for protein loading, blots were probed with an antibody specific to α-Tubulin or GAPDH for whole cell lysates (Table 2.3-1). It was more difficult obtain an appropriate housekeeping antibody against specific proteins in membrane enriched samples and conditioned medium samples, in this case, a coomassie stain was used to control for equal loading (see section 2.3.7).

2.3.7 Staining - Brilliant Blue G colloidal coomassie staining of gels

After electrophoresis, the gels containing membrane enriched samples and conditioned medium samples were placed into a square petri dish (Sigma, Z617679) containing a solution of Brilliant Blue G colloidal Coomassie. A working solution of 50mls prepared (32mls of UHP, 8mls of Brilliant Blue G colloidal Coomassie and 10mls of methanol) and then applied to the gels for at least 2 hours at room temperature on a rotating platform. After this time the coomassie stain was removed and gels were destained in UHP overnight with regular changes of UHP. Coomassie stained gels when required were used to ensure equal protein loading in these sample types.

2.4 Functional analyses

2.4.1 *In vitro* invasion assays

Matrigel (BD Biosciences, 354234) was diluted to a working stock of 1mg/ml in serum-free DMEM. Aliquoted stocks were stored at -20^{o}C for up to 1 year. Invasion assays were performed using the method modified from [100].

Matrigel was removed from the freezer and allowed to thaw overnight on ice at 4^{o}C. A volume of 100 µl of matrigel was placed into each insert (BD Biosciences, 353097) (8.0µm pore size, 24-well format) and kept at 4^{o}C for 24 hours. The insert and the plate were then incubated for one hour at 37^{o}C to allow the proteins to polymerise. To remove excess matrigel/media, each well was rinsed by gently by adding 150 µl of warm SFM to each insert containing matrigel. This media was then gently removed, all the time trying not to disturb the thin layer of matrigel. Cells were harvested and re-suspended in culture media containing 5% FCS at 1×10^{6} cells/ml. 100 µl of media (or test solution) was then added to each insert followed by 100 µl of the cell suspension (at the optimised cell number) to each insert. Finally, 500 µl of culture media containing 5% FCS was added to the well underneath the insert and cells were incubated for 24 hours.

To investigate the effect of the inhibitors DFMO (Sigma, D193) and L-NNA (Sigma N5501) on cell invasion, cells were seeded in culture media containing 5% FCS and DFMO (2.5 mM and 5 mM) or L-NNA (150µM), see Table 2.5-1. Appropriate concentrations of inhibitor were added to the underneath of the insert in 500 µl of media containing 5% FCS.

After a 24-hour incubation, the media was removed from the inside of the insert and the insert was wiped with a cotton swab dampened with PBS. The outer side of the insert was stained with 0.25% crystal violet for 10 mins and then rinsed in Ultrapure water (UHP) and allowed to dry. The inserts were viewed and photographed under the microscope. The invasion assays were quantified by counting cells in 10 random fields within a grid at 20x objective and graphed as the total number of cells invading at 200× magnification (section 2.4.2.1). A minimum of 2 inserts was used per sample tested.

2.4.2 *In vitro* migration assay

Migration assays were carried out as described in section 2.4.1, without the addition of extracellular matrix proteins.

2.4.2.1 Determination of total number of invading or migrating cells

To determine the total number of invading or migrating cells within an assay, the average number of invading or migrating cells (of 10 random fields) per insert was multiplied by a factor of 140 (growth area of the membrane divided by the area of the field viewed at 200x magnification), giving the total number of invading cells per insert. The total number of invading or migrating cells were then imported into excel and displayed on a histogram chart.

2.4.3 ROS assay

Cells were set up at $4x10^4$ cells/well in duplicate wells of a 24-well plate. After overnight incubation, the cells were washed with Hanks Balanced Salts solution (HBSS) and one well was exposed to HBSS and the other to the dye DCFDA at 10uM for 10 mins at 37ºC. After the incubation, each well was washed twice with HBSS and exposed to fresh medium (ATCC + 5% FCS) or to fresh medium containing 100µM H_2O_2 for 2hrs at 37ºC. The wells were then washed with HBSS and 1 ml of fresh HBSS added to each well. The fluorescence was measured with an excitation of 485nm and emission at 525nm. Cell counts were then made to compare the ROS generated per cell.

2.4.4 Anoikis assay

Cells were set up at $1x10^5$ cells/well in duplicate wells of a 24-well plate and a 24-well ultra-low attachment plate (Sigma, CLS3473-24EA) to a final volume of 1ml of DMEM/Hams-F12 with 5% FCS. Cells were allowed to incubated for a total of 24 hours. At 21 hours, 100µl of Alamar blue (ThermoFisher Scientific, DAL1100) was added to each well and allowed to incubate for the remaining 3 hours. Plates were read in a dual beam plate reader at 570 nm with a reference wavelength of 600nm. Percent anoikis was determined using following equation:

% Anoikis = (1-(delta OD of unattached cells/delta OD of attached cells)) *100

2.4.5 Statistical analysis

A minimum of two replicates was used per sample and three separate biological replicates were performed. Triplicate biological replicates refer to a single experiment that was carried out in duplicate on three separate occasions e.g. three different passage numbers of a particular cell line. For each experiment, assays were performed weekly or bi-weekly until triplicate assays displayed agreement. Histograms were plotted using mean (average

between triplicate assays) values from triplicate experiments. Error bars were applied to each graph indicating plus and minus standard deviations.

All assays were then subjected to statistical analysis using student's t-test (two-tailed, equal variance, unpaired) in Microsoft Excel 2016. Using Microsoft Excels t-test function with mean figures calculated between replicates, a *p* value was obtained. The *p* value measures the probability that the differences between the control and test samples would be observed by chance.

A *p* value of ≤ 0.05 was considered significant and assigned *

A *p* value of ≤ 0.01 was considered more significant and assigned **

A *p* value of ≤ 0.005 was considered highly significant and assigned ***

In siRNA experiments, scrambled siRNA or negative control siRNA transfected cells were used as controls and were compared to test siRNA treated cells. This was to ensure that no off target effects were occurring within the transfection process. Non-treated controls (cells only and transfection reagent) were also used within each experiment to ensure that the scrambled or negative control siRNA was having no effect and to normalise the data.

In transfection experiments where an effect of less than 20% was observed, the siRNA was considered to have "little or no effect". However, results from these experiments may still indicate statistical significance. It is, therefore, important to carry out statistical analyses of all results obtained from experiments.

2.5 *In vitro* proliferation assays

2.5.1 Combination toxicity assays

Cells in the exponential phase of growth were harvested by trypsinisation. Cell suspensions containing 1×10^4 cells/ml (for 96-well plates, Costar, 3599) or $1x10^6$ cells/ml (for 6-well plates, Costar, 3516) were prepared in cell culture medium. To each well 100µl (of $1x10^4$ cells/ml, for 96-well plates) or 1 ml (of $1x10^6$cells/ml for 6-well plates) of the cell suspension was added. Plates were agitated gently in order to ensure even dispersion of cells over the surface of the wells and cells were incubated overnight at 37ºC. Stock L-NNA and DFMO inhibitors (N5501 and D193) were diluted in UHP as per manufacturer's instructions and stored at -20ºC (Table 2.5-1) Subsequent dilutions were made in cell culture medium to the desired concentrations. Inhibitor diluent (UHP) was used as a control and also prepared in cell culture medium. A volume of 100 µl of the inhibitor dilutions was added to each well and mixed gently. Cells were incubated for 48 hours. Assessment of cell survival in the presence of the inhibitors was determined by the acid phosphatase assay (section 2.5).

Inhibitor	Storage	Source
D, L-a-difluoromethylornithine (DFMO)	-20ºC	Sigma Aldrich
Nω-Nitro-L-arginine (L-NNA)	-20ºC	Sigma Aldrich

Table 2.5-1:- Inhibitors used during this project.

2.5.2 Acid phosphatase assay

Following the incubation period, media was removed from each plate/well. Each well on a plate was washed with 100 µl (for 96-well plates) or 500ul (for 6-well plates) of PBS. This was removed and 100 µl (for 96-well plates) or 1 ml (for 6-well plates) of freshly prepared phosphatase substrate (1.5µg/ml p-nitrophenol phosphate (ThermoScientific, 34045) in 0.1 M sodium acetate (Sigma, S8625), 0.1% triton X-100 (BDH, 30632), pH 5.5) was added to each well. The plates were wrapped in tinfoil and incubated in the dark at 37°C for 30mins to 2 hours. The enzymatic reaction was stopped by the addition of 50 µl (96-well plate) or 500 µl (6-well plate) of 1 M NaOH to each well. Plates were read in a dual beam plate reader at 405 nm with a reference wavelength of 620nm.

2.6 Immunohistochemistry

2.6.1 Immunofluorescence studies on fixed cells

Aliquots of 30 µl of 1×10^6 cells/ml cell suspension from actively growing cultures were plated directly onto 10 well 7 mm microscope slides (Erie Scientific Company, 465-68X). Cells were allowed to attach overnight. After such time, slides were washed 3 x in PBS and allowed to air dry. Slides were carefully foil wrapped and stored at -80^{o}C until required. When required, slides were allowed to come to room temperature, cells were then fixed in 4% paraformaldehyde for 5 mins. Slides were washed 3 x in PBS and in between the wells were then dried using a cotton bud wrapped in lint free tissue, to prevent the primary antibody from running into neighbouring wells. The primary antibody (Table 2.6-1) was applied to appropriate wells and incubated overnight at 4^{o}C. After 24 hours, the slides were washed 3 x in PBS and appropriate secondary antibody was applied. Either, Alexa Fluor488 goat anti-mouse IgG (ThermoFisher Scientific, A11029) or goat anti-rabbit (Thermofisher Scientific, A11034) which was diluted 1:2000 was added for 1hr at room temperature in the dark. The secondary antibody was removed and cells washed as outlined. Slides were mounted with ProLong Gold mounting medium (ThermoFisher Scientific, P36930) and covered using a glass cover slip. Cells were viewed and photographed using a Nikon phase contrast microscope fitted with an FITC filter.

2.6.2 Immunocytochemical analysis on fixed cells

A 30µl volume of the appropriate cell suspension was added to slides and incubation is as described in section 2.6.1). After 24hrs, the excess supernatant was tapped off, and the microscope slides were rinsed gently with PBS. Slides were then air dried overnight, wrapped in tin foil, and stored at -80°C. Slides are then removed from -80°C freezers, and left for 15 mins prior to immunostaining. Cells were fixed in ice-cold paraformaldehyde for 2-4 mins. Immunostaining was carried out as per section 2.6.3, without the initial antigen retrieval step.

2.6.3 Immunohistochemistry

All Immunohistochemical (IHC) staining was performed using the Dako Autostainer (Dako, S3800). Deparaffinisation and antigen retrieval was performed using Epitope Retrieval 3-in-1 Solution (pH 6) (Dako, S1699) or the Epitope Retrieval 3-in-1 Solution (pH 9) (Dako, S2375) and the PT Link system (Dako, PT101). For epitope retrieval, slides were heated to 97°C for 20 mins and then cooled to 65°C. The slides were then immersed

in wash buffer (Dako, S3006). On the Autostainer slides were blocked for 10 mins with 200 µl HRP Block (Dako, S2023). Cells were washed with 1 x wash buffer and 200 µl of antibody added to the slides at the optimised concentration/dilution for a minimum of 20 mins (Table 2.6-1). Slides were washed again with 1 x wash buffer and then incubated with 200 µl Real EnVision (Dako, K4065) for 30 mins. A positive control slide was included in each staining run. Each slide was also run with Negative Control Reagent (1× TBS/0.05% Tween 20), to allow evaluation of non-specific staining and allow better interpretation of specific staining at the antigen site. All slides were counterstained with haematoxylin (Dako, CS700) for 5 mins, and rinsed with deionised water, followed by wash buffer. All slides were then dehydrated in graded alcohols (2 x 3 mins each in 70% IMS, 90% IMS and 100% IMS), and cleared in xylene (2 x 5 mins), and mounted with coverslips using DPX mounting medium (Sigma, 44581). Mounted slides were allowed to stand overnight before examination under the microscope. Slides were viewed and photographed using Olympus microscope and imaging system.

Antibody	Concentration used for:			Company
	I/F	ICC	IHC	
AHNAK	1:250	---	---	Abcam (Ab168149/Ab68556)
ALCAM	1:150	1:150	1:150	Abcam
CD31	---	---	1:50	Dako
E-cadherin	---	---	2.5 µl	Abcam (Ab40772)
HDGF	1:250	1:500	1:500	Abcam
Human Mitochondrial Protein	---	---	1:1000	Abcam (Ab92824)
INA	1:210	1:210	1:210	Abcam
IQGAP1	1µg/ml	1µg/ml	1:100	Abcam
Ki67	---	---	1:75	Dako (M7240)
N-cadherin	---	---	3µg/ml	Thermofisher Scientific (333900), Abcam (ab19348)
ROBO2	1:100	1µg/ml	1µg/ml	Abcam (ab75014)
SLIT2	1:500	1:500	1:500	Abcam
SPR	1:2000	---	1:2500	Abcam

Table 2.6-1:- Antibodies used in Immunofluorescence, Immunocytochemistry and Immunohistochemistry analysis.

2.7 RNA interference (RNAi)

RNAi using small interfering RNA's (siRNAs) was carried out to silence specific genes. The siRNAs used were chemically synthesised and were purchased from Ambion^{Inc} or Qiagen. These siRNAs were 21-23 bps in length and were introduced to the cells via reverse transfection with the transfection agents siPORT NeoFX^{TM} (Ambion Inc., 4511) or Lipofectamine 2000 (ThermoFisher Scientific, 11668019).

2.7.1 Transfection optimisation

RNA interference knockdown of genes is a well-established method and is used routinely to investigate the effect a certain gene has on a cell line of choice. In order to determine the optimal conditions for siRNA transfection, optimisation with kinesin siRNA (Ambion Inc., 16704) or AllStars Cell Death siRNA (Qiagen, S104381048) was carried out for each cell line. There were a number of different parameters that had to be determined to establish an optimised protocol for the siRNA transfection of the DLKP clones. Cell suspensions were prepared at 1×10^5, 2×10^5 and 3×10^5 cells per ml. Solutions of the negative control and positive control siRNA (kinesin or AllStars Cell Death siRNAs) at a final concentration of 10 and 30nM were prepared in optiMEM (Gibco^{TM}, 31985047). Solutions containing 1.2 µl NeoFX or 2 µl lipofectamine were prepared in 50µl optiMEM in duplicate and incubated at room temperature for 10 mins. After incubation, either negative control or positive control (kinesin siRNA or AllStars Cell Death siRNA) solution was added to each NeoFX or lipofectamine solution. These solutions were mixed well and incubated for a further 10 mins at room temperature. To each well of a 6-well plate, 100 µl of the siRNA/NeoFX or lipofectamine solutions was added. A volume of 1 ml of the relevant cell concentrations was added to each well and the plates were mixed gently and incubated at 37°C for 24 hours. After 24 hours, the transfection mixture was removed from the cells and the plates were fed with fresh medium. The plates were assayed for changes in proliferation at 72 hours using the acid phosphatase assay (section 2.5). Optimal conditions for siRNA transfection were determined, as the combination of conditions gave the greatest reduction in cell number after positive control transfection and also the least cell kill in the presence of transfection reagent. The optimised conditions were 1.2 µl NeoFx or 2 µl of Lipofectamine to transfect 30nM siRNA (for ALCAM) and 10nM (for both SPR and INA) siRNA respectively, optimised cell densities are shown in Table 2.7-1 below.

Cell line	Cell density (per well in 6-well plates)
DLKPSQ	1.5 x10^5 cells
DLKPI	1.25x10^5 cells
DLKPM	1x10^5 cells
DLKPSQ-Mitox-BCRP-6P	1.5x10^5 cells
MDA-MD-468	2x10^5 cells
MiaPacC2 Clone3	2x10^5 cells
AsPC-1	2x10^5 cells

Table 2.7-1:- Optimization of cell number for transfections siRNA.

2.7.2 Analysis of the growth of siRNA transfected cells

Cells were seeded using 1.2 µl NeoFX to transfect 30nM siRNA (for ALCAM) or 10mM siRNA (for INA and SPR) to optimised cell numbers (shown in Table 2.7-1) per well of a 6-well plate. After 24 hrs, the medium was replaced with fresh medium and cells were allowed to grow until they reached 80 - 90% confluency over a total of 4 days. Cell number was assessed using the acid phosphatase assay (section 2.5).

2.7.3 Analysis of invasion and migration of siRNA transfected cells

To assay for changes in invasive capacity using ALCAM, INA and SPR siRNAs, siRNA experiments were set up as described in section 2.7.1 in 6-well plates. Transfection medium was removed after 24hr and replaced with fresh growth medium. The transfected cells were assayed at 72hrs post transfection for changes in invasive capacity using the *in vitro* invasion assay as described in section 2.4.1 and migration assay described in section 2.4.2.

2.7.4 Analysis of ROS generation of siRNA transfected cells

DLKP-M cells with siRNA knock-down of SPR, lipofectamine transfected, or negative siRNA transfected cells or untreated cells were set up at 4x10^4 cells/well in a 24-well plate with two wells per condition. Seventy-two hours post transfection, ROS generation in DLKPM cells was analysed as described in section 2.4.3.

2.8 Development of cell line-derived tumours *in vivo* (xenografts)

This *in vivo* study was carried out in collaboration with Prof. Robert Straubinger (University of Buffalo, USA), Ms Ninfa Straubinger (University of Buffalo, USA), Dr. Sandra Roche (NICB, DCU, Ireland) and Dr. Fiona O'Neill (NICB, DCU, Ireland) at the BioResource Unit (BRU) in the School of Biotechnology, Dublin City University.

2.8.1 Mice

For this study, 28-35 day old CB17/lcr-*Prkdc*^{scid}/Crl mice were chosen based on the extensive experience and publishing history our collaborator has using SCID mice for *in vivo* modelling [101, 102]. Mice were used under the guidelines of the Irish Department of Health and procedures approved by the research ethics committee of Dublin City University, Dublin 9. CB17/lcr-Prkdcscid/Crl mice were purchased from Charles River (Charles River International Inc., Wilmington, MA). The immunodeficiency of these animals is as a result of the inhibition to produce B and T lymphocytes. This deficiency provides the mice with a wide tolerance to implanted foreign tissues and tumours, which makes them an ideal model for research.

2.8.2 Preparation of cell suspensions

DLKP, DLKPSQ, DLKPI and DLKPM were cultured in vented T75cm^2 flasks until approximately 70% confluent. Cell counts were completed as per section 2.1.3. Cell suspensions were prepared in SF-DMEM as follows: 5x10^6 cells in 500 µl, 1.5x10^7 cells in 250 µl and 5x10^7 cells in 250 µl. Matrigel Matrix High concentration (BD, Franklin Lakes, NJ, USA, 354262) at a ratio of 1:1 was added to the cell suspensions. This matrigel is suited for *in vivo* studies where a high concentration augments the growth of tumours. The high protein concentration (18-22mg/ml) also allows the Corning Matrigel Matrix plug to maintain its integrity after subcutaneous injection into mice. This keeps the injected cells and/or angiogenic compounds localized for *in situ* analysis and/or future excision. Cell and matrigel suspensions were stored on ice until required. For tumour growth, the cells and matrigel mixture was then inoculated into the mice at a final cell density shown in Table 2.8-1.

	Right Flank	Left Flank
Mouse 1	1 x 10^6 cells	5 x 10^6 cells
Mouse 2	1 x 10^6 cells	5 x 10^6 cells
Mouse 3	1 x 10^6 cells	1 x 10^7 cells
Mouse 4	1 x 10^6 cells	1 x 10^7 cells

Table 2.8-1:- Inoculation densities used for DLKP *in vivo* study.

2.8.3 Tumour development

An appropriate needle was selected for injection of cell suspensions; this prevents the destruction of the cells within the matrigel plug. Using the cell suspensions in prepared in section 2.8.2, 200 µl of the appropriate cell lines and matrigel suspension was subcutaneously injected into the appropriate flank of each mouse as indicated in Table 2.8-1 above. Mice were monitored daily and once tumours were observed they were measured using a digital calliper. The equation used to evaluate the tumour volume was;

H(height of tumour) x W(width of tumour) x D (depth of tumour)/2 = volume of tumour (mm^3)

2.8.4 Tumour removal and explant culture

Explant culture was performed to examine any changes in the *in vitro* characteristics of DLKP, DLKPSQ, DLKPI and DLKPM cells after a period of growth in tumours. Tumours were developed in mice as per section 2.8.1, 2.8.2 and 0, once tumours were removed from mice, they were kept cool by placing the specimen into ice-cold serum free DMEM-HAMS-F12 until required. Tumours were diced into small pieces and placed onto 0.4 µm inserts (Falcon, 353090), then placed into 6-well plates. Cells were allowed to migrate out of the tumour for 3 days without being disturbed. Once cells were seen to be attached to the insert, cells were trypsinised and moved to 12.5cm^2 flasks and cultured as per section 2.1.1. DLKPSQ, DLKPSQ, DLKPI and DLKPM cells were examined for changes in morphology, proliferation (as described in section 2.5), invasion (as described in section 2.4.1), migration (as described in section 2.4.2) and anoikis (as per section 2.4.4) capacities post tumour explantation.

2.8.5 Paraffin embedding of Xenograft tissues

Preparation of tumours for Immunohistochemical analysis was carried out by Mr Damian Tiernan (Royal Victoria Eye and Ear Hospital, Ireland) and Mr. Colin Barr (NICB, DCU). Pathological examination of tissues was performed by Prof. Susan Kennedy (Royal Victoria Eye and Ear Hospital, Dublin).

Chapter 3 RESULTS

3.1 Identification of membrane associated markers in DLKP

Lung Cancer is a leading cause of cancer related death worldwide. Cell surface proteins are an important subset of proteins in the cell. They play an important role in signal transduction, cell adhesion and in cancer invasion and migration. The accessible location of cell surface proteins makes them ideal candidates for use as targets for cancer therapy. While membrane proteins constitute 20-30% of the human they represent over 60% of all drug targets [103]. With the evolution of patient specific therapy in other cancers, there is a continuing need to identify new targets for lung cancer therapy. In this thesis, the Pierce cell surface protein isolation kit (ThermoFisher Scientific, 89881) was used to identify potential markers in the poorly differentiated squamous cell carcinoma cell line, DLKP and also potentially novel proteins associated with lung cancer. Sulfo-NHS-SS-Biotin, a cleavable biotinylation reagent that is cell-impermeable was used to label exposed primary amines on the surface of intact cells from the parental DLKP and its clones, DLKPSQ, DLKPI and DLKPM.

3.1.1 Cell surface protein isolation and protein identification

DLKP contains at least 3 clonal subpopulations with distinct morphological and phenotypical differences (e.g. invasion and anoikis). To identify potential markers for each of the clones, cell surface protein isolation was carried out using cell surface isolation kit (see section 2.2.1). Reduction and alkylation steps were used to prepare proteins for label-free LC-MS/MS analysis. Proteins were eluted in DTT, precipitated in acetone (buffer exchange), reduced and alkylated in DTT, iodoacetamide (IAA) (breaks di-sulphide bonds and prevents refolding). The proteins were then broken up into peptides by a trypsin digestion step. Samples containing peptides were applied to the mass spectrometer. Proteome Discoverer Software 2.0 allows for peptides to be assigned to proteins using the Mascot and SEQUEST HT (see section 2.2.3 and 2.2.4). Each cell line will have a list of proteins that was identified. Progenesis software was used to analyse these proteins and identify proteins that were differentially expressed between DLKP and its clones. To do this a number of criteria was applied to the software; (i) to ensure proteins are statistically significant an ANOVA score of ≤ 0.05 as used, (ii) to ensure increased expression between cell lines a minimum fold change of ≥ 1.5-fold was applied and (iii) to ensure correct proteins are identified, proteins with greater than 2 unique peptides matched to a particular protein were considered. Data analysis was carried out by Michael Henry using the standard criteria outlined above. The criteria used in the data analysis

gives strong confidence that the proteins identified are potentially expressed in the cell lines, validation needs to be carried out to confirm expression in the cell lines.

To evaluate the differentially expressed proteins in the cell lines DLKP, DLKPSQ, DLKPI and DLKPM, six comparative protein lists were generated and exported to excel from Progenesis. The analysis was designed to identify biologically relevant differentially expressed proteins that correlated with increased expression, that is, from highest to lowest fold changes (DLKP *vs.* DLKPSQ, DLKP *vs.* DLKPI, DLKP *vs.* DLKPM, DLKPSQ *vs.* DLKPI, DLKPSQ *vs.* DLKPM, DLKPI *vs.* DLKPM). Unique and common proteins, as well as proteins with a novel aspect, were chosen. To further strengthen the choice of proteins selected, their expression was also examined in a combination of analyses previously performed in our laboratory (i) microarray analysis performed by Dr. Helena Joyce (ii) unpublished proteomic analysis (on conditioned medium (CM) from DLKP clones) performed by Dr. Joanne Keenan and (iii) unpublished proteomic analysis (of whole cell lysates) performed by Mr. Shane Kelly. The analysis presented in this thesis was performed using a protein isolation protocol. The kit may potentially allow for isolation and subsequent identification (through LC-MS/MS analysis) of novel proteins associated with cell membrane using a biotin labelling approach. Validation of selected proteins was performed to confirm their expression in DLKP and its clones by Immunofluorescence staining, Western blot analysis and immunocytochemical analysis.

3.1.2 Principle component analysis of DLKP and the DLKP clones

Principle component analysis (PCA) is a statistical analysis used to visualise variation and strong patterns between data sets. To show differences in protein expression between DLKP and DLKP clones a global analysis was carried out on all four cell lines, using Progenesis LC-MS software. To identify proteins that are differentially expressed between the DLKP and its clones, it was important to ensure good separation between all four cell lines and that each of the replicate samples clustered together. The PCA analysis shown in Figure 3.1-1, indicates a clear separation between all four cell lines but also the individual replicates are clustering together. The analysis also indicates that DLKP (Green) and DLKPSQ (blue) cluster close together, this is not surprising due to the fact that DLKP is made up of approx. 70% DLKPSQ cells [93]. The PCA analysis indicates that the isolation of cell membrane associated protein and subsequent proteomic analysis in DLKP and its clones was robust and reproducible.

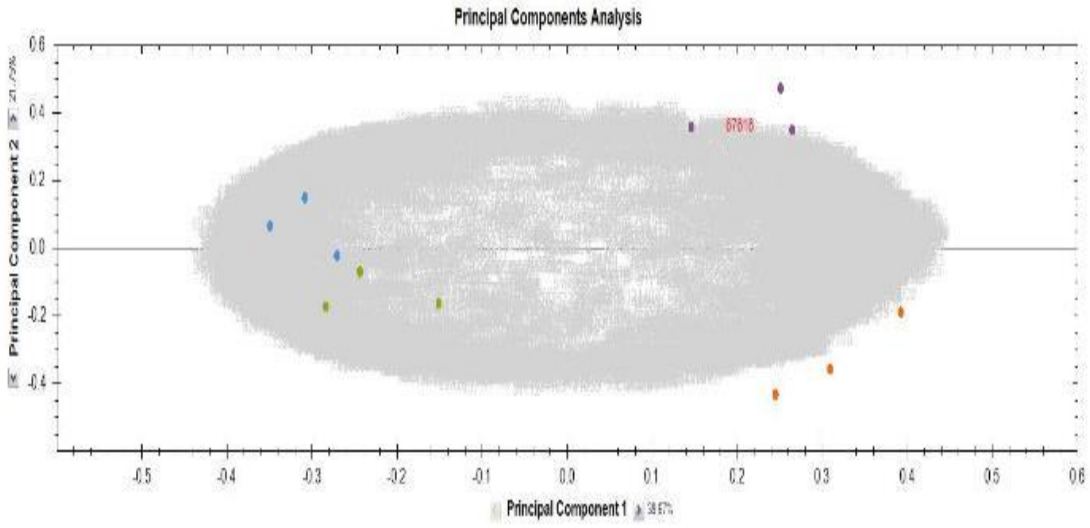

Figure 3.1-1:- Principle component analysis showing separation of DLKP and its clones.
Label free proteomic analysis was carried out on triplicate cell surface preparations of DLKP (Green), DLKPSQ (Blue), DLKPI (Orange) and DLKPM (purple), using the cell surface isolation kit.

3.1.3 Comparative proteomic analysis of DLKP and the DLKP clones

Following principle component analysis of the four cell lines, six comparative protein lists were generated. The analysis was designed to identify biologically relevant differentially expressed proteins that correlated with increased expression, that is, from highest to lowest fold changes. The six comparisons were: DLKP *vs.* DLKPSQ, DLKP *vs.* DLKPI, DLKP *vs.* DLKPM, DLKPSQ *vs.* DLKPI, DLKPSQ *vs.* DLKPM, DLKPI *vs.* DLKPM. Table 3.1-1 summarises the total number of proteins that were identified from each comparison and the number of proteins that showed increased expression. The subsequent tables (Table 3.1-2 - Table 3.1-7) shows the first 14 - 18 proteins in each comparison and are organised by maximum fold change (see appendix I for full differentially expressed protein lists). The proteins which were identified in these comparisons represent a number of different cellular processes, however, to elucidate the molecular function, biological processes and pathways which control these proteins further analysis using PANTHER classification system should be carried out.

Experimental comparison	No. of identified differentially expressed proteins
DLKP *vs.* DLKPSQ	**49 proteins in total** 35 were increased in DLKP 14 were increased in DLKPSQ (See Table 3.1-2)
DLKP *vs.* DLKPI	**114 proteins in total** 74 were increased in DLKP 40 were increased in DLKPI (See Table 3.1-3)
DLKP *vs.* DLKPM	**144 proteins in total** 86 were increased in DLKP 58 were increased in DLKPM (see Table 3.1-4)
DLKPSQ *vs.* DLKPI	**94 proteins in total** 55 were increased in DLKPSQ 39 were increased in DLKPI (see Table 3.1-5)
DLKPSQ *vs.* DLKPM	**110 proteins in total** 59 were increased in DLKPSQ 51 were increased in DLKPM (see Table 3.1-6)
DLKPI *vs.* DLKPM	**58 proteins in total** 26 were increased in DLKPSQ 32 were increased in DLKPM (see Table 3.1-7)

Table 3.1-1:- Summary of six comparisons made using Progenesis LC-MS software and the number of proteins with increased expression in each cell line.

DLKP *vs.* DLKPSQ							
Highest in DLKP				**Highest in DLKPSQ**			
Accession Number	**Protein Name**	**Gene symbol**	**Fold Change**	**Accession Number**	**Protein Name**	**Gene symbol**	**Fold Change**
Q9HCK4	**Roundabout homolog 2**	**ROBO2**	**56.88**	P16930	Fumarylacetoacetase	FAH	19.87
P05362	Intercellular adhesion molecule 1	ICAM1	56.16	O43175	D-3-phosphoglycerate dehydrogenase	PHGDH	4.52
P35221	Catenin alpha-1	CTNNA1	30.84	A0MZ66	Shootin-1	KIAA1598	3.87
Q16658	Fascin	FSCN1	14.08	P43358	Melanoma-associated antigen 4	MAGEA4	2.44
P35222	Catenin beta-1	CTNNB1	12.58	P11137	Microtubule-associated protein 2	MAP2	2.24
Q9UBR2	Cathepsin Z	CTSZ	6.85	O75531	Barrier-to-autointegration factor	BANF1	2.15
Q6PIU2	Neutral cholesterol ester hydrolase 1	NCEH1	6.39	Q9BUF5	Tubulin beta-6 chain	TUBB6	2.01
Q09666	**Neuroblast differentiation-associated protein**	**AHNAK**	**5.00**	P13010	X-ray repair cross-complementing protein 5	XRCC5	1.97
P50454	Serpin H1	SERPINH1	4.21	Q06830	Peroxiredoxin-1	PRDX1	1.75
Q8NBJ5	Procollagen galactosyltransferase 1	COLGALT1	3.31	**P46940**	**Ras GTPase-activating-like protein**	**IQGAP1**	**1.73**
Q01581	Hydroxymethylglutaryl-CoA synthase, cytoplasmic	HMGCS1	3.10	Q15417	Calponin-3	CNN3	1.65
O60888	Protein CutA	CUTA	2.59	Q96AE4	Far upstream element-binding protein 1	FUBP1	1.58
Q96PK6	RNA-binding protein 14	RBM14	2.40	O00264	Membrane-associated progesterone receptor component 1	PGRMC1	1.54
P35579	Myosin-9	MYH9	2.33	P30041	Peroxiredoxin-6	PRDX6	1.54

Table 3.1-2:- Comparison of DLKP *vs.* DLKPSQ.
List of top 14 statistically significant, differentially expressed proteins in DLKP and DLKPSQ. The following criteria were applied; (i) ANOVA score ≤ 0.05, (ii) max-fold change of ≥ 1.5 and (iii) a minimum of 2 peptides leading to the identification of proteins.

DLKP *vs.* DLKPI							
Highest in DLKP				**Highest in DLKPI**			
Accession Number	**Protein Name**	**Gene symbol**	**Fold Change**	**Accession Number**	**Protein Name**	**Gene symbol**	**Fold Change**
Q6UVK1	Chondroitin sulfate proteoglycan 4	CSPG4	82.94	P08575	Receptor-type tyrosine-protein phosphatase C	PTPRC	37.62
P05362	Intercellular adhesion molecule 1	ICAM1	55.65	**Q13740**	**CD166 antigen**	**ALCAM**	**18.80**
P32119	Peroxiredoxin-2	PRDX2	31.26	Q05707	Collagen alpha-1(XIV) chain	COL14A1	15.61
Q9UBR2	Cathepsin Z	CTSZ	9.26	P35232	Prohibitin	PHB	7.71
O75347	Tubulin-specific chaperone A	TBCA	5.34	Q99623	Prohibitin-2	PHB2	7.64
P43487	Ran-specific GTPase-activating protein	RANBP1	5.21	**P46940**	**Ras GTPase-activating-like protein**	**IQGAP1**	**7.61**
P12277	Creatine kinase B-type	CKB	4.63	O75369	Filamin-B	FLNB	7.44
P55060	Exportin-2	CSE1L	4.48	P11233	Ras-related protein Ral-A	RALA	6.55
Q99798	Aconitate hydratase, mitochondrial	ACO2	4.00	P02545	Prelamin-A/C	LMNA	5.75
P07602	Prosaposin	PSAP	3.63	**Q09666**	**Neuroblast differentiation-associated protein**	**AHNAK**	**5.55**
P00441	Superoxide dismutase [Cu-Zn]	SOD1	3.57	Q9BSJ8	Extended synaptotagmin-1	ESYT1	4.61
Q14240	Eukaryotic initiation factor 4A-II	EIF4A2	3.53	P21333	Filamin-A	FLNA	4.59
P49419	Alpha-aminoadipic semialdehyde dehydrogenase	ALDH7A1	3.48	Q96HC4	PDZ and LIM domain protein 5	PDLIM5	4.55
P09211	Glutathione S-transferase P	GSTP1	3.43	O75947	ATP synthase subunit d, mitochondrial	ATP5H	3.81

Table 3.1-3:- Comparison of DLKP *vs.* DLKPI.
List of top 14 statistically significant, differentially expressed proteins in DLKP and DLKPI. The following criteria were applied; (i) ANOVA score ≤ 0.05, (ii) max-fold change of ≥ 1.5 and (iii) a minimum of 2 peptides leading to the identification of proteins.

DLKP *vs.* DLKPM							
Highest in DLKP				**Highest in DLKPM**			
Accession Number	**Protein Name**	**Gene symbol**	**Fold Change**	**Accession Number**	**Protein Name**	**Gene symbol**	**Fold Change**
P10586	Receptor-type tyrosine-protein phosphatase F	PTPRF	89.23	Q96HC4	PDZ and LIM domain protein 5	PDLIM5	13.80
P05362	Intercellular adhesion molecule 1	ICAM1	61.31	Q05707	Collagen alpha-1(XIV) chain	COL14A1	12.64
Q9HCK4	**Roundabout homolog 2**	**ROBO2**	**60.59**	**P46940**	**Ras GTPase-activating-like protein**	**IQGAP1**	**8.99**
Q6UVK1	Chondroitin sulfate proteoglycan 4	CSPG4	45.49	P02538	Keratin, type II cytoskeletal 6A	KRT6A	8.81
O15031	Plexin-B2	PLXNB2	27.33	P11233	Ras-related protein	RALA	8.81
Q92692	Nectin-2	PVRL2	25.06	Q99623	Prohibitin-2	PHB2	8.35
P28906	Hematopoietic progenitor cell antigen CD34	CD34	24.97	P46087	Probable 28S rRNA (cytosine (4447)-C (5))-methyltransferase	NOP2	8.25
Q13308	Inactive tyrosine-protein kinase 7	PTK7	10.40	O75643	U5 small nuclear ribonucleoprotein 200kDa helicase	SNRNP200	8.00
Q9UBR2	Cathepsin Z	CTSZ	10.01	P35232	Prohibitin	PHB	7.83
O00410	Importin-5	IPO5	7.44	Q14008	Cytoskeleton-associated protein 5	CKAP5	7.80
P30533	Alpha-2-macroglobulin receptor-associated protein	LRPAP1	6.68	O75369	Filamin-B	FLNB	7.75
Q15084	Protein disulfide-isomerase A6	PDIA6	6.05	P62805	Histone H4	HIST1H4A	6.86
Q13740	**CD166 antigen**	**ALCAM**	**5.97**	Q8WXF1	Paraspeckle component 1	PSPC1	5.90
Q9Y4L1	Hypoxia up-regulated protein 1	HYOU1	5.83	P23246	Splicing factor, proline- and glutamine-rich	SFPQ	5.65

Table 3.1-4:- Comparison of DLKP *vs.* DLKPM.
List of top 14 statistically significant, differentially expressed proteins in DLKP and DLKPM. The following criteria were applied; (i) ANOVA score ≤ 0.05, (ii) max-fold change of ≥ 1.5 and (iii) a minimum of 2 peptides leading to the identification of proteins.

DLKPSQ *vs.* DLKPI							
Highest in DLKPSQ				**Highest in DLKPI**			
Accession Number	**Protein Name**	**Gene symbol**	**Fold Change**	**Accession Number**	**Protein Name**	**Gene symbol**	**Fold Change**
P55957	BH3-interacting domain death agonist	BID	18.07	P08575	Receptor-type tyrosine-protein phosphatase C	PTPRC	42.10
O43175	D-3-phosphoglycerate dehydrogenase	PHGDH	7.36	P19022	Cadherin-2	CDH2	29.00
O00625	Pirin	PIR	6.45	P23246	Splicing factor, proline- and glutamine-rich	SFPQ	28.92
Q9UBB4	Ataxin-10	ATXN10	6.23	P35222	Catenin beta-1	CTNNB1	26.80
P12277	Creatine kinase B-type	CKB	6.08	**Q13740**	**CD166 antigen**	**ALCAM**	**24.30**
P43487	Ran-specific GTPase-activating protein	RANBP1	5.89	**Q9HCK4**	**Roundabout homolog 2**	**ROBO2**	**21.85**
P31937	3-hydroxyisobutyrate dehydrogenase, mitochondrial	HIBADH	5.12	Q96PK6	RNA-binding protein 14	RBM14	17.52
P00441	Superoxide dismutase [Cu-Zn]	SOD1	5.07	Q14126	Desmoglein-2	DSG2	17.34
P04792	Heat shock protein beta-1	HSPB1	4.76	Q15233	Non-POU domain-containing octamer-binding protein	NONO	14.81
P34897	Serine hydroxymethyltransferase, mitochondrial	SHMT2	4.68	Q16658	Fascin	FSCN1	14.34
O75347	Tubulin-specific chaperone A	TBCA	4.44	P35221	Catenin alpha-1	CTNNA1	10.81
P09211	Glutathione S-transferase P	GSTP1	4.41	Q99623	Prohibitin-2	PHB2	10.26
P00390	Glutathione reductase, mitochondrial	GSR	4.31	P35232	Prohibitin	PHB	10.06
P07602	Prosaposin	PSAP	4.14	**Q09666**	**Neuroblast differentiation-associated protein**	**AHNAK**	**9.29**
P00558	Phosphoglycerate kinase 1	PGK1	4.13	Q86UP2	Kinectin	KTN1	8.37
P12004	Proliferating cell nuclear antigen	PCNA	3.86	P02545	Prelamin-A/C	LMNA	7.38
O43399	Tumor protein D54	TPD52L2	3.72	P21333	Filamin-A	FLNA	7.07
P35270	**Sepiapterin reductase**	**SPR**	**3.64**	Q9BSJ8	Extended synaptotagmin-1	ESYT1	6.23

Table 3.1-5:- Comparison of DLKPSQ *vs.* DLKPI.
List of top 18 statistically significant differentially expressed proteins in DLKP and DLKPI. The following criteria were applied; (i) ANOVA score ≤ 0.05, (ii) max-fold change of ≥ 1.5 and (iii) a minimum of 2 peptides leading to the identification of proteins.

DLKPSQ *vs.* DLKPM							
Highest in DLKPSQ				**Highest in DLKPM**			
Accession Number	**Protein Name**	**Gene symbol**	**Fold Change**	**Accession Number**	**Protein Name**	**Gene symbol**	**Fold Change**
A0MZ66	Shootin-1	KIAA1598	7.02	P46087	Probable 28S rRNA (cytosine (4447)-C (5))-methyltransferase	NOP2	12.26
O43175	D-3-phosphoglycerate dehydrogenase	PHGDH	6.70	O75643	U5 small nuclear ribonucleoprotein 200 kDa helicase	SNRNP200	11.69
Q9Y2Q3	Glutathione S-transferase kappa 1	GSTK1	5.22	Q99623	Prohibitin-2	PHB2	11.52
O00625	Pirin	PIR	4.95	P23246	Splicing factor, proline- and glutamine-rich	SFPQ	10.66
P08107	Heat shock 70 kDa protein 1A/1B	HSPA1A	4.84	Q15233	Non-POU domain-containing octamer-binding protein	NONO	10.17
O43399	Tumor protein D54	TPD52L2	4.31	Q96HC4	PDZ and LIM domain protein 5	PDLIM5	9.67
P27797	Calreticulin	CALR	4.12	P35232	Prohibitin	PHB	9.45
P34931	Heat shock 70 kDa protein 1-like	HSPA1L	3.98	**Q09666**	**Neuroblast differentiation-associated protein**	**AHNAK**	**8.04**
O14980	Exportin-1	XPO1	3.96	P62805	Histone H4	HIST1H4A	7.84
P23526	Adenosylhomocysteinase	AHCY	3.86	Q96PK6	RNA-binding protein 14	RBM14	7.59
O00410	Importin-5	IPO5	3.65	P11233	Ras-related protein Ral-A	RALA	7.46
Q58FF7; Q58FF8	Putative heat shock protein HSP 90-beta-3	HSP90AB3P	3.58	Q14444	Caprin-1	CAPRIN1	6.91
P04792	Heat shock protein beta-1	HSPB1	3.52	**P46940**	**Ras GTPase-activating-like protein**	**IQGAP1**	**6.17**
P27824	Calnexin	CANX	3.48	P35222	Catenin beta-1	CTNNB1	5.71

Table 3.1-6:- Comparison of DLKPSQ *vs.* DLKPM.
List of top 14 statistically significant differentially expressed proteins in DLKPSQ and DLKPM. The following criteria were applied; (i) ANOVA score ≤ 0.05, (ii) max-fold change of ≥ 1.5 and (iii) a minimum of 2 peptides leading to the identification of proteins.

DLKPI *vs.* DLKPM							
Highest in DLKPI				**Highest in DLKPM**			
Accession Number	**Protein Name**	**Gene symbol**	**Fold Change**	**Accession Number**	**Protein Name**	**Gene symbol**	**Fold Change**
P08575	Receptor-type tyrosine-protein phosphatase C	PTPRC	41.79	P31937	3-hydroxyisobutyrate dehydrogenase, mitochondrial	HIBADH	7.32
Q13740	**CD166 antigen**	**ALCAM**	**30.15**	P12277	Creatine kinase B-type	CKB	7.28
Q9HCK4	**Roundabout homolog 2**	**ROBO2**	**26.95**	O75347	Tubulin-specific chaperone A	TBCA	4.52
P10586	Receptor-type tyrosine-protein phosphatase F	PTPRF	25.10	P49419	Alpha-aminoadipic semialdehyde dehydrogenase	ALDH7A1	4.11
Q14126	Desmoglein-2	DSG2	24.70	P07195	L-lactate dehydrogenase B chain	LDHB	3.47
P60709	Actin, cytoplasmic 1	ACTB	22.32	P07741	Adenine phosphoribosyltransferase	APRT	3.45
P19022	Cadherin-2	CDH2	20.86	P08758	Annexin A5	ANXA5	3.45
P30533	Alpha-2-macroglobulin receptor-associated protein	LRPAP1	9.17	P43487	Ran-specific GTPase-activating protein	RANBP1	3.43
Q92692	Nectin-2	PVRL2	7.93	P09211	Glutathione S-transferase P	GSTP1	3.32
P35222	Catenin beta-1	CTNNB1	7.92	P16152	Carbonyl reductase [NADPH] 1	CBR1	3.22
Q15067	Peroxisomal acyl-coenzyme A oxidase 1	ACOX1	4.47	P50454	Serpin H1	SERPINH1	3.18
Q01581	Hydroxymethylglutaryl-CoA synthase, cytoplasmic	HMGCS1	4.25	Q96HC4	PDZ and LIM domain protein 5	PDLIM5	3.03
Q9Y2Q3	Glutathione S-transferase kappa 1	GSTK1	4.05	P62937	Peptidyl-prolyl cis-trans isomerase A	PPIA	3.02
P21333	Filamin-A	FLNA	3.89	P00441	Superoxide dismutase [Cu-Zn]	SOD1	2.87

Table 3.1-7:- Comparison of DLKPI *vs.* DLKPM.
List of top 14 statistically significant differentially expressed proteins in DLKPSQ and DLKPM. The following criteria were applied; (i) ANOVA score ≤ 0.05, (ii) max-fold change of ≥ 1.5 and (iii) a minimum of 2 peptides leading to the identification of proteins.

3.1.4 Summary of proteins selected for validation studies in DLKP

Table 3.1-8 below summarises the proteins that were selected as potential protein markers for DLKP clones and possibly novel proteins associated with lung cancer. Two proteins that did not appear on the comparative proteomic lists (i) Alpha-Internexin (INA) and (ii) SLIT2 were also selected for validation. On further examination, less stringent criteria revealed HDGF as differentially expressed in DLKP *vs.* DLKPI (fold change 2.19), criteria applied was (i) an ANOVA of ≤0.05, (ii) ≥1.5 fold and (ii) proteins with ≥1 unique peptide matched to identify HDGF. Little is known about HDGF and its receptor and was, therefore, an interesting protein for follow up analysis. INA was chosen for validation in DLKP and its clones based on novelty, on its association with pancreatic neuroendocrine cancer tumour aggressiveness [104]. On further examination of INA, unpublished proteomic analysis on whole cell lysates of DLKP and its clones revealed its expression was increased in DLKPSQ *vs.* DLKPM. Early studies performed on DLKP indicated that DLKP should be characterised as either variant small cell lung carcinoma (SCLC-V) or non-small cell lung carcinoma with neuroendocrine differentiation [93], further strengthening our reasons for selecting INA. Microarray analysis carried out by Dr. Helena Joyce found that SLIT2 was expressed in DLKP. In this proteomic study, ROBO2 (the receptor for SLIT2 and probably SLIT1) was found to be expressed within the DLKP cell line model, therefore both proteins were chosen for validation studies. Surprisingly, a number of the proteins selected for validation appear to have a neuronal association, which may further indicate the borderline nature of DLKP towards a neuroendocrine tumour.

No	Protein Name	Gene Symbol	Accession number	Molecular function
1.	Neuroblast differentiation-associated protein	AHNAK	Q09666	Structural molecule conferring elasticity
2.	Hepatoma Derived Growth Factor	HDGF	P51858	Transcription co-factor activity, Growth factor activity
3.	SLIT2 Homolog	SLIT2	O94813	Receptor activity
4.	Roundabout 2 Homolog	ROBO2	Q9HCK4	Receptor activity, Phosphoprotein phosphatase activity
5.	Activated Leukocyte cell adhesion molecule	ALCAM	Q13740	Receptor activity
6.	Ras-GTPase-activating-like protein 1	IQGAP-1	P46940	Catalytic activity, small GTPase activity
7.	Alpha-Internexin	INA	Q16352	Structural constituent of Cytoskeleton
8.	Sepiapterin Reductase	SPR	P35270	Oxidoreductase activity

Table 3.1-8:- Summary of all proteins selected for validation studies.

3.2 Validation of protein targets from proteomic analysis

A number of proteins were identified as differentially expressed following comparative proteomic analysis of DLKP and its clonal variants (DLKPSQ, DLKPI and DLKPM). Six comparisons were performed to identify statistically significant proteins that were differentially expressed: DLKP *vs.* DLKPSQ, DLKP *vs.* DLKPI, DLKP *vs.* DLPKPM, DLKPSQ, *vs.* DLKPI, DLKPSQ *vs.* DLKPM and DLKPI *vs.* DLKPM. Presented in section 3.1.3 were tables of statistically significant differentially expressed proteins of each comparison from which proteins were selected. Selection of proteins from these comparisons was based on (i) ANOVA score of ≤ 0.05, (ii) max-fold change of ≥ 1.5 and a minimum of 1-2 peptides matched in order to identify each protein. The aim was to identify differentially expressed proteins that could act as potential markers for individual clones and to potentially identify novel proteins associated with lung cancer. Table 3.1-8 shows a summary of all of the proteins that were selected for validation studies.

Western blot analysis was used to validate the expression of the selected proteins in whole cell lysates, membrane enriched fractions and conditioned medium samples of DLKP, DLKPSQ, DLKPI and DLKPM cells (section 2.3). Validation of selected proteins in whole cell lysate and membrane enriched fractions would indicate the expression of particular proteins in the cells, while validating in conditioned medium (CM) samples would suggest if the protein was secreted. With further investigation, this information could be useful for determining whether a particular protein could be used as a cancer biomarker. Biomarkers are proteins or factors produced by cancer cells and secreted into bodily fluids such as blood and urine. Immunofluorescence (section 2.6.1) and/or Immunocytochemical analysis (see sections 2.6.2) was performed to confirm localisation of expression in the cells. Commercially available antibodies described in Table 2.3-1 and Table 2.6-1.

3.2.1 Validation of AHNAK expression in DLKP

Originally identified as a nuclear phosphoprotein in human neuroblastomas and skin epithelial cells, AHNAK is an exceptionally large protein of ~629kDa protein. Lee *et al.*, reported that AHNAK functions as a tumour suppressor by mediating TGFβ signalling, leading to cell cycle arrest. AHNAK expression was found to be increased in differentially expressed protein comparisons: DLKP *vs.* DLKPSQ, DLKPI *vs.* DLKPSQ, DLKPI *vs.* DLKPSQ and DLKPM *vs.* DLKPSQ, following comparative proteomic analysis of membrane preparations, Tables of proteins showing expression of AHNAK are presented in section 3.1.3. Immunofluorescence staining was performed to validate the expression of AHNAK in DLKP and its clonal subpopulations, see Figure 3.2-1 below. Immunoreactivity was observed in all of the cell lines with the DLKPI and DLKPM cells showing the strongest immunoreactivity, membrane reactivity was observed in a small population (< 10%) of DLKPSQ cells.

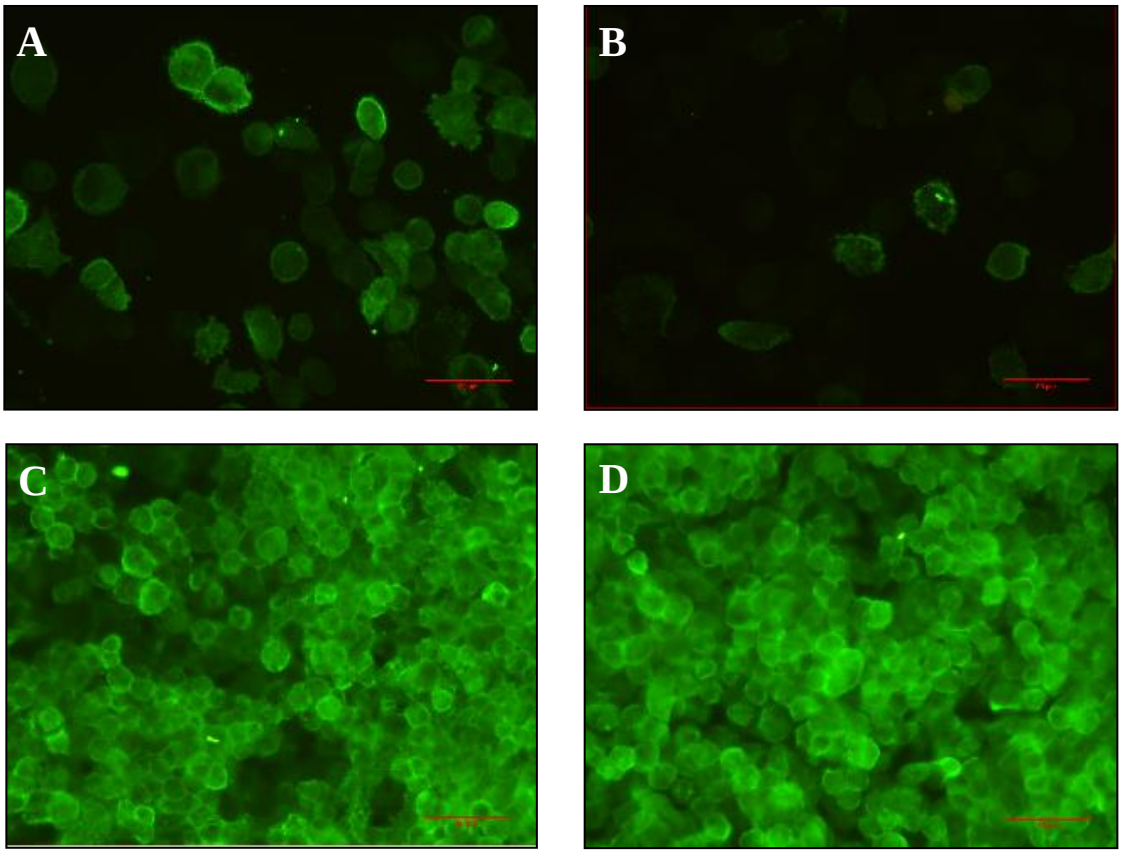

Figure 3.2-1:- Validation of AHNAK expression in DLKP.
Representative immunofluorescence staining of AHNAK, (A) DLKP parental cells, (B) DLKPSQ, (C) DLKPI and (D) DLKPM cells stained with an AHNAK specific antibody. Immunoreactivity was observed in all cell lines. (Original magnification of all photomicrographs, ×400, *scale-bar* = 50μm (n=1).

3.2.2 Validation of HDGF expression in DLKP

While little is known about the receptors of hepatoma derived growth factors (HDGFs), it is thought that HDGF contains a peptide region responsible for binding to the cell surface. Subsequent binding of HDGF at the cell surface is also thought to activate ERK1/2 in fibroblasts [105]. The ERK pathway is thought to play a key role in the invasion of DLKP [96]. Hepatoma derived growth factor (HDGF) was found to be increased in comparative proteomics analysis of DLKP *vs.* DLKPI (2.19 fold), however, less stringent criteria were applied (i) ANOVA score of ≤ 0.05, (ii) a max-fold change of ≥ 1.5, with 1 peptide matched to identify HDGF. Refer to appendix 1, which shows expression of HDGF in DLKP.

HDGF is thought to be localised mainly to the nucleus, but localisation to the cytosol has also been reported [106]. In DLKP, no membrane immunoreactivity was observed but there was strong nuclear and some cytoplasmic immunoreactivity observed. Immunoreactivity was strongest in DLKP with lower levels in DLKPSQ, DLKPI and DLKPM (see Figure 3.2-2 (A)).

Western blot analysis of whole cell lysates, membrane enriched fractions and conditioned media (CM) preparations of DLKP, DLKPSQ, DLKPI and DLKPM cells was performed to investigate the expression of HDGF. Western blot analysis of membrane enriched fractions clearly shows expression of HDGF is highest in DLKP compared to the clones (SQ, I and M). Analysis of whole cell lysates and CM samples showed expression of HDGF across the four cell lines. Immunoblots show the migration of HDGF at approximately 37kDa, however, non-specific bands were observed in the whole cell and CM samples above 37kDa which may represent potential HDGF-related proteins [106] of HDGF (see Figure 3.2-2 (B)). Immunocytochemical analysis of HDGF in DLKP, DLKPSQ, DLKPI and DLKPM cells displayed strong immunoreactivity in all cell lines, however, DLKP showed the strongest membrane reactivity (see Figure 3.2-2 (C)).

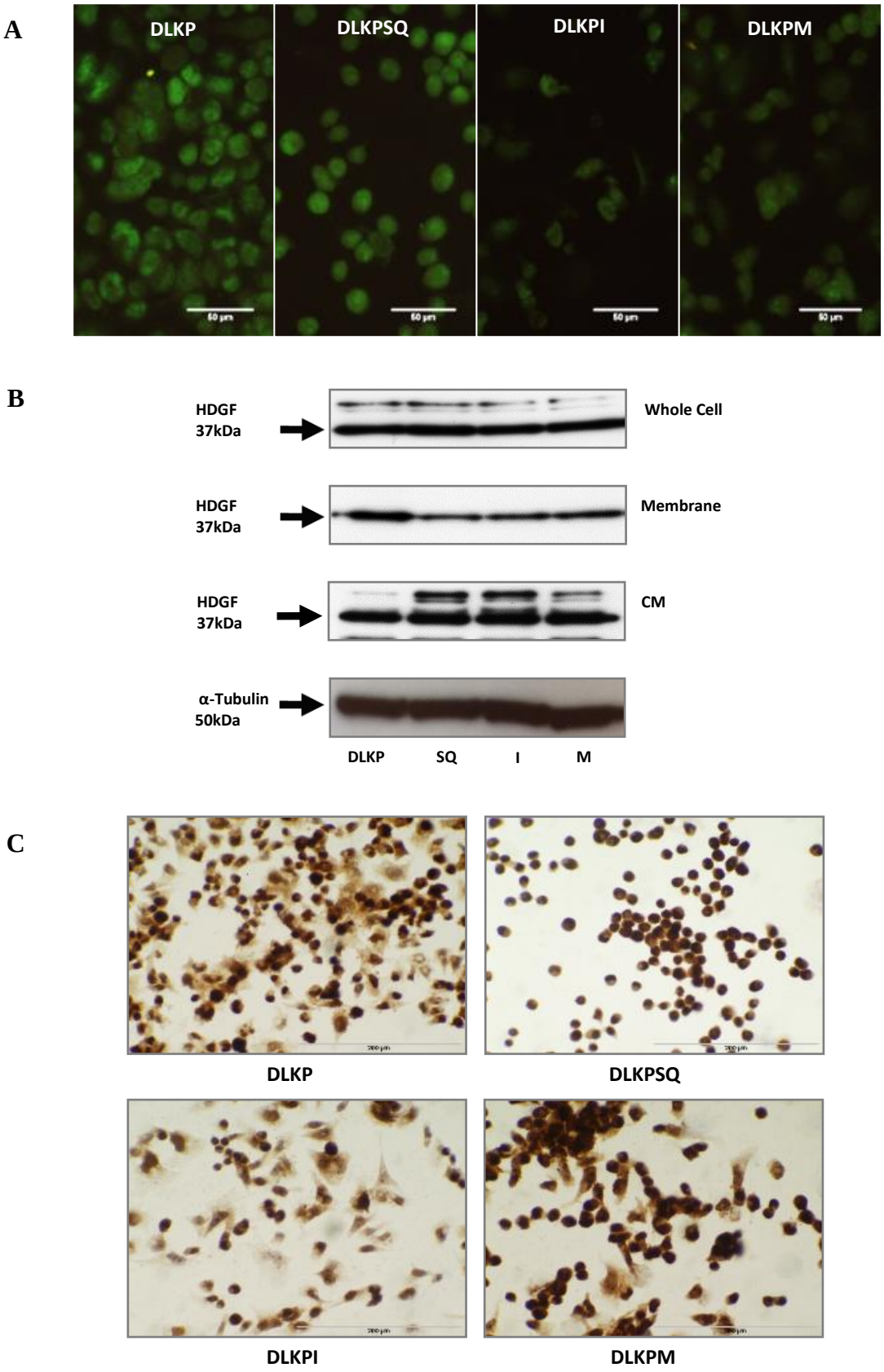

Figure 3.2-2:- Validation of HDGF expression in DLKP.
(A) Immunofluorescence staining of HDGF (n=1) **(B)** Representative immunoblot showing expression of HDGF in the DLKP clones (α-tubulin served as loading control (n=3), and **(C)** Immunocytochemical staining of HDGF in DLKP and its clones (n=1). Immunoreactivity was observed in all cell lines with the DLKP cells showing the strongest immunoreactivity (Original magnification of all photomicrographs, ×400, scale-bar = 50μm (A) and 200μm (C)).

3.2.3 Validation of SLIT2 ligand and ROBO2 receptor expression in DLKP

Roundabout-2 Homolog (ROBO2) expression was found to be increased in differentially expressed protein comparisons: DLKP *vs.* DLKPSQ (~57-fold), DLKP *vs.* M (~60-fold), DLKPI *vs.* DLKPSQ (~21-fold) and DLKPI *vs.* DLKPM (27~fold), Tables of proteins showing expression of ROBO2 in DLKP are presented in section 3.1.3.. In addition, microarray analysis previously carried out on DLKP and its clones had revealed that ROBO2 was overexpressed in DLKPI only, while proteomic analysis on CM also indicated its expression in DLKP and its clones. Interestingly, ROBO2 expression in CM was highest in DLKPSQ, this may indicate that DLKPSQ may shed ROBO2 into the CM. ROBO2 acts as the receptor for SLIT2 (and probably SLIT1) guide to cellular migration during neuronal development [107]. Recently, it has been shown that ROBO1 expression in breast cancer cells coupled with SLIT2 expression from stromal fibroblasts has been associated with inhibition of tumour progression [108]. This indicates the influence the expression of proteins from cells within the tumour microenvironment may have on cancer progression. Both ROBO2 and SLIT2 proteins were selected for validation studies.

Both Immunofluorescence and Immunocytochemical analysis of SLIT2 show immunoreactivity in all cell lines, DLKPM showing an overall the highest expression with DLKPSQ showing lower expression, this cell line appears to display membrane reactivity. Extracellular immunoreactivity can be observed in all cell lines (see Figure 3.2-3 (A) & (D)), indicating potential secretion of SLIT2 into the surrounding media. Immunofluorescence staining for ROBO2 (Figure 3.2-3 (C)) revealed immunoreactivity in all of the cells with the DLKP-M cells showing the strongest immunoreactivity and DLKP showing weakest expression. SLIT2 expression appears to correlate with ROBO2 expression in DLKP and its subpopulations, by immunofluorescence.

Western blot analysis (Figure 3.2-3 (B)) was carried out to investigate the expression of SLIT2 in whole cell lysates, membrane enriched fractions and CM of DLKP, DLKPSQ, DLKPI and DLKPM cells. DLKPM and DLKP showed the highest level of expression while DLKPSQ and DLKPI showed the lowest level of expression in all samples. Western blot analysis of SLIT2 does not appear to correlate with Immunofluorescence analysis, however, there does appear to be similar expression trends between both techniques. ROBO2 expression was only validated by Immunofluorescence staining as the antibody did not work for Western blot analysis or Immunocytochemical analysis.

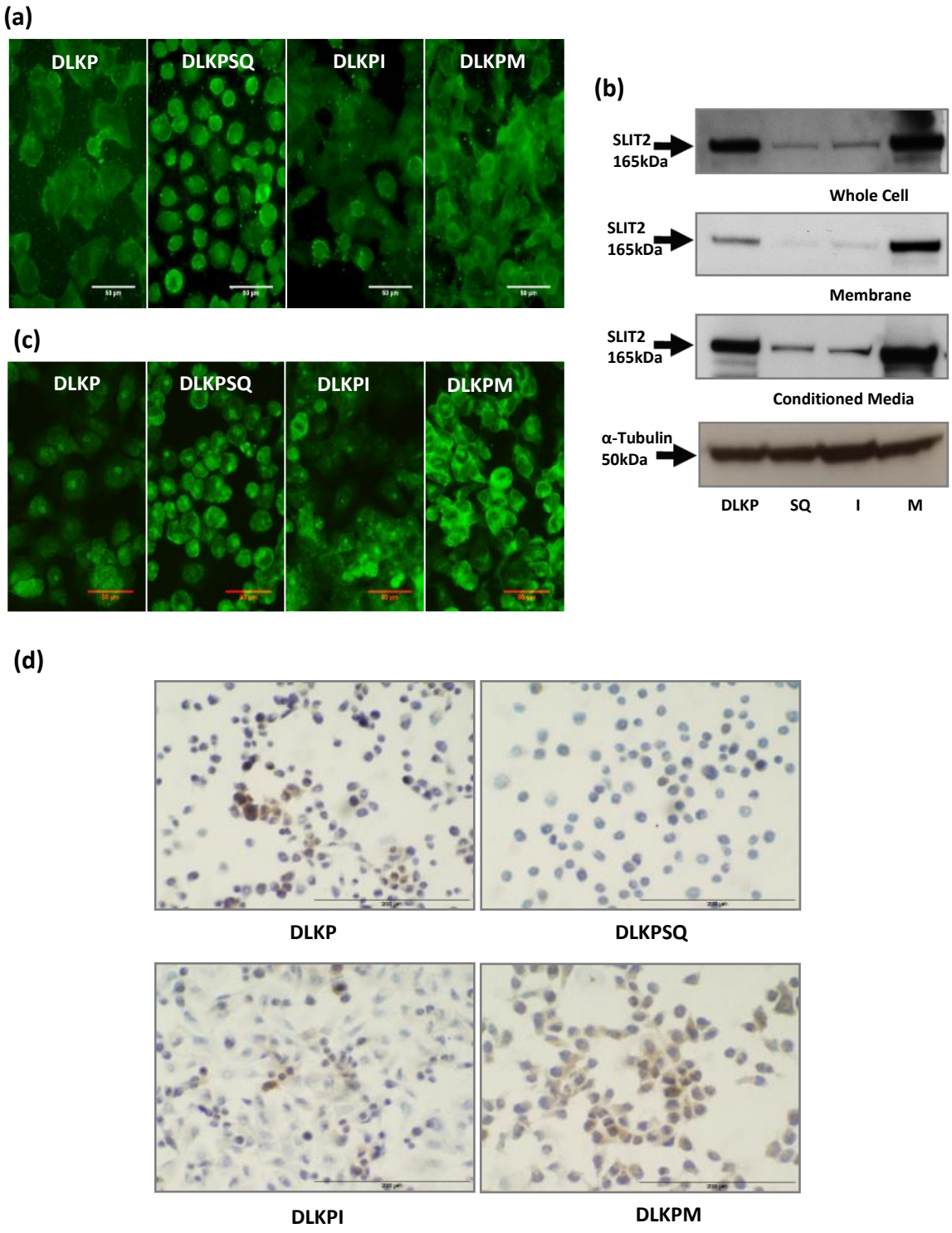

Figure 3.2-3:- Validation of SLIT2 and ROBO2 receptor expression in DLKP.
(A) Immunofluorescence staining of SLIT2 in the DLKP clones (n=1). **(B)** Representative Immunoblot showing expression of SLIT2 in the DLKP clones (α-tubulin was used as an equal loading control (n=3)). **(C)** Immunofluorescence staining showing cell surface staining of ROBO2 (n=1). **(D)** Immunocytochemical staining of SLIT2 in the DLKP clones (n=1). DLKP parental cells, DLKPSQ, DLKPI and DLKPM cells stained with both an antibody specific to SLIT2 and ROBO2. Immunoreactivity was observed in all cells (Original magnification of all photomicrographs, ×400, *scalebar* = 50μm (A and C) and 200μm (D)).

3.2.4 Validation of ALCAM expression in DLKP

Activated Leukocyte Cell Adhesion molecule (ALCAM), also known as CD166 antigen, is a highly conserved 110kDa multi-domain, transmembrane type-1 glycoprotein of the immunoglobulin superfamily. ALCAM was first described as a CD6 ligand but is capable of homophilic and heterophilic interactions [109]. ALCAM expression was found to be increased in a number of comparisons of differentially expressed proteins; DLKP *vs.* DLKPM (~5.97-fold), DLKPI *vs.* DLKPSQ (~24.3-fold) and DLKPI *vs.* DLKPM (~30.15-fold), Tables of proteins showing expression of ALCAM in DLKP are presented in section 3.1.3. In addition, microarray analysis previously carried out on DLKP and its clones revealed that ALCAM was overexpressed in DLKPI only relative to DLKPSQ, while proteomic analysis on CM also indicated expression in DLKP cell lines. Interestingly, ALCAM expression in CM was highest in DLKPSQ and DLKPM. Potentially indicating that DLKPSQ sheds ALCAM into the conditioned medium. A number of studies have identified ALCAM as a potential lung cancer stem cell marker [110]. Since DLKPI may show a potential ability to interconvert to DLKPSQ and DLKPM, it was proposed that DLKPI may resemble a possible stem cell population in DLKP and was therefore chosen for validation studies.

Immunofluorescence (Figure 3.2-4 (A)) and Immunocytochemical analysis of ALCAM (Figure 3.2-4 C)) indicated strong membrane reactivity in DLKPI compared to DLKP and DLKPM. ALCAM appeared to be almost absent in DLKPSQ. Western blot analysis (Figure 3.2-4 (B)) confirms that the expression level of ALCAM was highest in DLKPI compared to DLKP, DLKPSQ and DLKPM. Immunofluorescence, Western blot analysis and immunocytochemical analysis confirmed proteomics analysis by showing strongest expression of ALCAM in DLKPI. ALCAM, due to its strong expression could potentially be a good candidate for use as a marker for DLKPI.

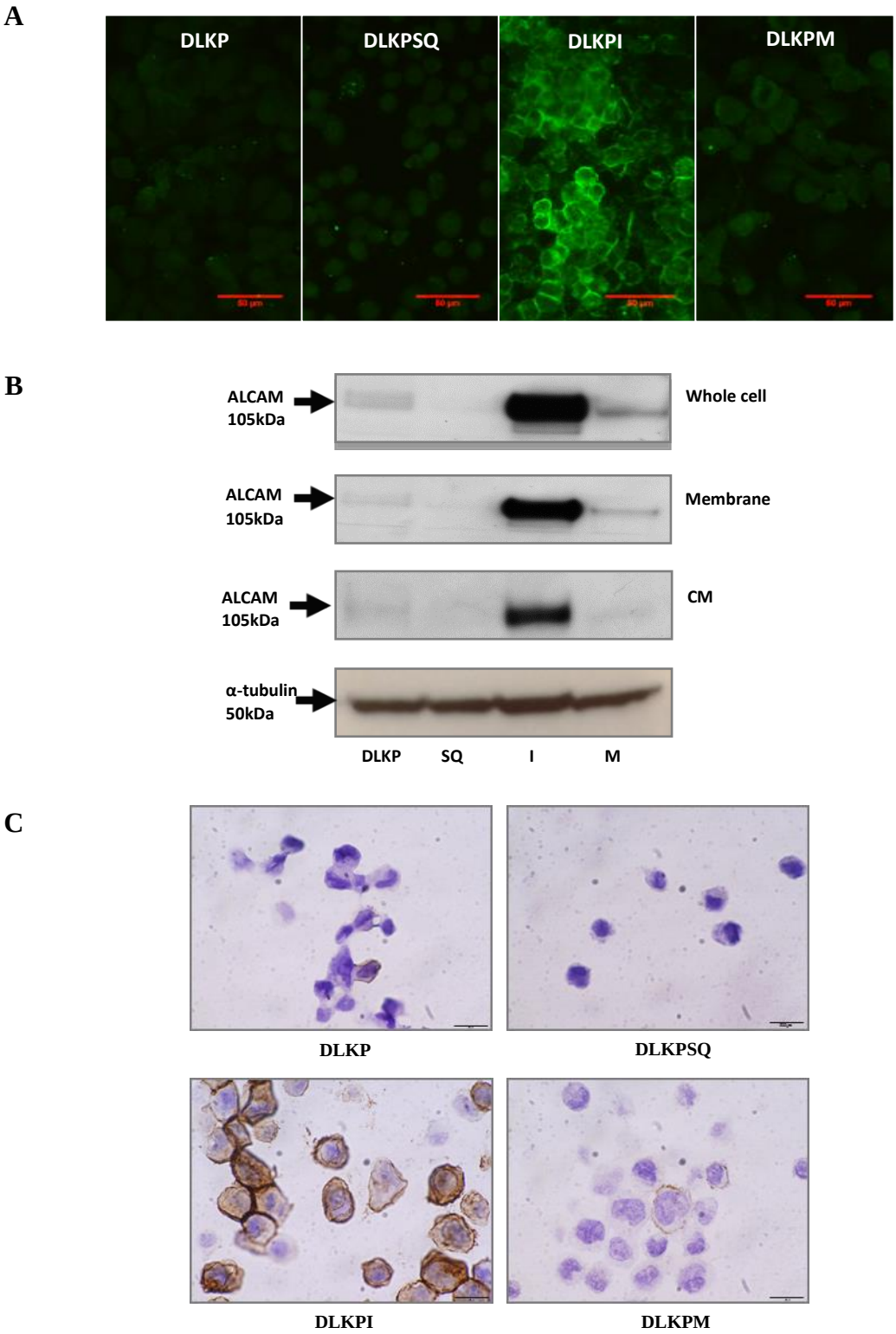

Figure 3.2-4:- Validation of ALCAM expression in DLKP.
(A) Immunofluorescence staining of ALCAM in the DLKP clones (n=1). **(B)** Representative Immunoblot showing expression of ALCAM in the DLKP clones (α-tubulin was used as an equal loading control (n=3)). **(C)** Immunocytochemical staining of ALCAM in formalin fixed paraffin embedded cells from DLKP and its clones (1000x magnification (n=1). Strongest immunoreactivity is observed in DLKPI. (Original magnification of all photomicrographs, ×400, *scalebar* = 50µm (A) and 200µm (C)).

3.2.5 Validation of IQGAP1 expression in DLKP

Ras-GTPase-activating-like protein-1 (IQGAP1) is a member of the IQGAP family of proteins with a molecular weight of approximately 189kDa. IQGAP1 regulates cell morphology and motility by its interaction with cell adhesion molecules, signalling molecules and components of the cytoskeleton [111]. IQGAP1 expression was found to be increased in a number of comparisons of differentially expressed proteins: DLKPSQ *vs.* DLKP (~2-fold), DLKPI *vs.* DLKP (~8-fold), DLKPM *vs.* DLKP (~9-fold) and DLKPM *vs.* DLKPSQ (~6-fold) obtained from comparative proteomic analysis of DLKP, Tables presented in section 3.1.3 show expression of IQDAP. In addition, microarray analysis previously carried out on DLKP and its clones revealed that IQGAP1 was overexpressed in DLKPI relative to DLKPSQ. IQGAP1 is thought to interact with over 90 proteins including β-catenin, E-cadherin and N-cadherin, which are well established in cancer. In addition, IQGAP1 has also been reported to be a potential interacting protein of ALCAM [112] which we found to be almost uniquely expressed in DLKPI (see section 3.2.4).

Immunofluorescence (Figure 3.2-5 (A)) and Immunocytochemical analysis (Figure 3.2-5 (C)) of IQGAP1 indicated that immunoreactivity was observed in all four cell lines. Expression appears to be strongest in DLKPM relative to DLKP, DLKPSQ and DLKPI. Western blot analysis Figure 3.2-5 (B)) also confirms expression levels of IQGAP1 is highest in DLKPM compared to DLKP, DLKPSQ and DLKPI.

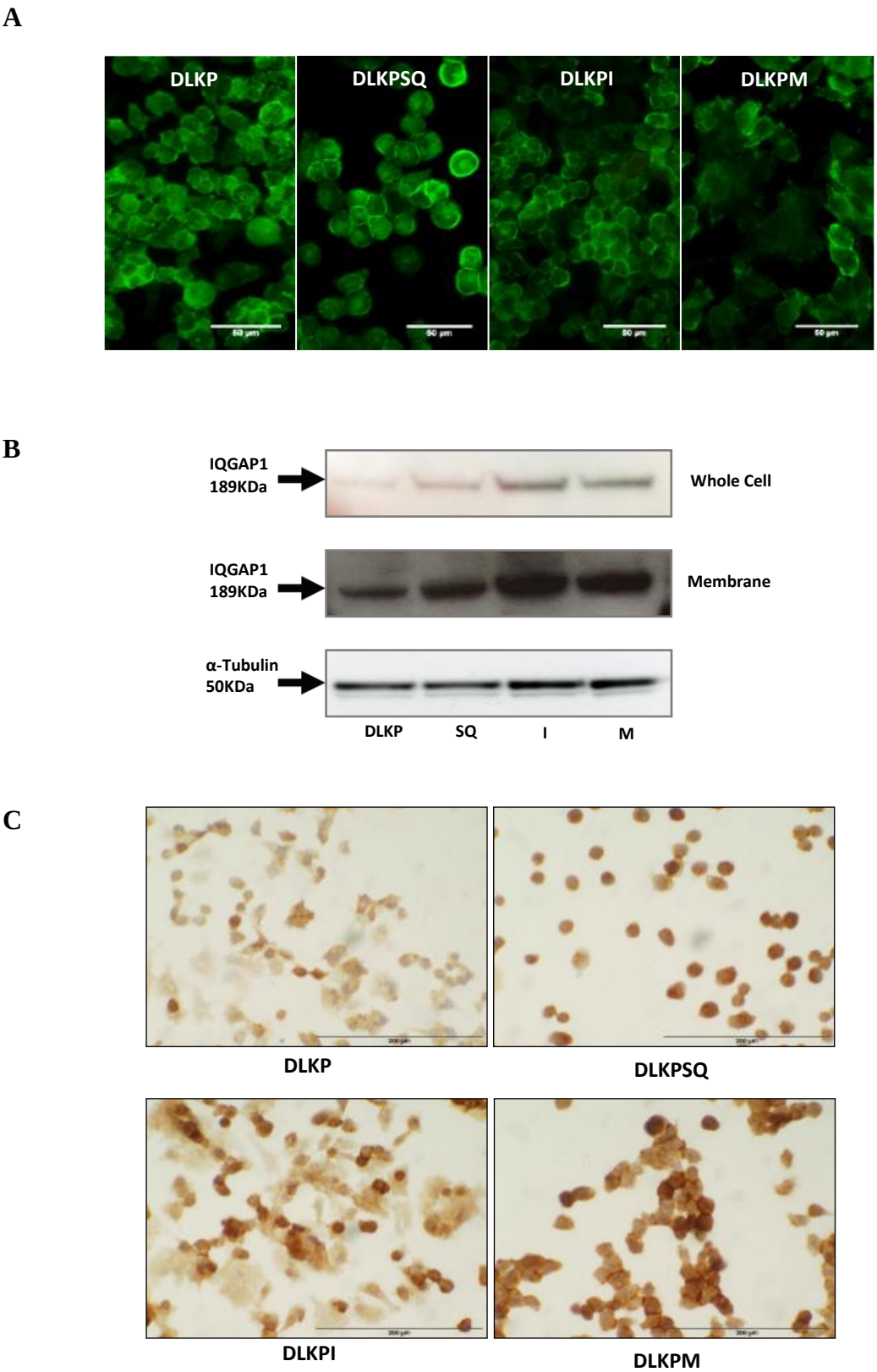

Figure 3.2-5:- Validation of IQGAP1 expression in DLKP.
(A) Immunofluorescence staining of IQGAP1 in the DLKP clones. **(B)** Representative Immunoblot showing expression of IQGAP1 in the DLKP clones (α-tubulin was used as an equal loading control). **(C)** Immunocytochemical staining of IQGAP1, strongest immunoreactivity was observed in DLKPM (Original magnification of all photomicrographs, ×400, *scalebar* = 50μm (A) and 200μm (C)).

3.2.6 Validation of INA expression in DLKP

Alpha-Internexin (INA) is a 66kDa neuronal intermediate filament that is abundantly expressed in the peripheral nervous system. Overexpression of INA in oligodendroglial phenotype gliomas has been related to the 1p/19q co-deletion and been reported as a favourable prognostic marker [113]. Increased expression of INA was identified as a biomarker for neuroendocrine pancreatic cancer tumour aggressiveness and prognosis [104]. However, unpublished proteomic analysis performed on whole cell lysates of DLKP and its clones also indicated that INA expression was increased in DLKPSQ *vs.* DLKPM (~2.4-fold). Initial studies performed on DLKP indicated that DLKP should be characterised as either variant small cell lung carcinoma (SCLC-V) or non-small cell lung carcinoma with neuroendocrine differentiation. INA was therefore chosen for validation in DLKP based on novelty, relating to lung cancer and on its association with pancreatic neuroendocrine cancer.

Immunofluorescence (Figure 3.2-6 (A)) and immunocytochemical (Figure 3.2-6 (C)) analysis of INA indicated that immunoreactivity was observed in DLKP, DLKPSQ and DLKPM. Expression appears to be strongest in DLKPSQ and weak immunoreactivity observed in DLKPI. Western blot analysis (Figure 3.2-6 (B)) confirmed expression of INA in whole cell lysates and membrane enriched samples of DLKP and its clones. INA appears to show association with the membrane of DLKPSQ and not for DLKP.

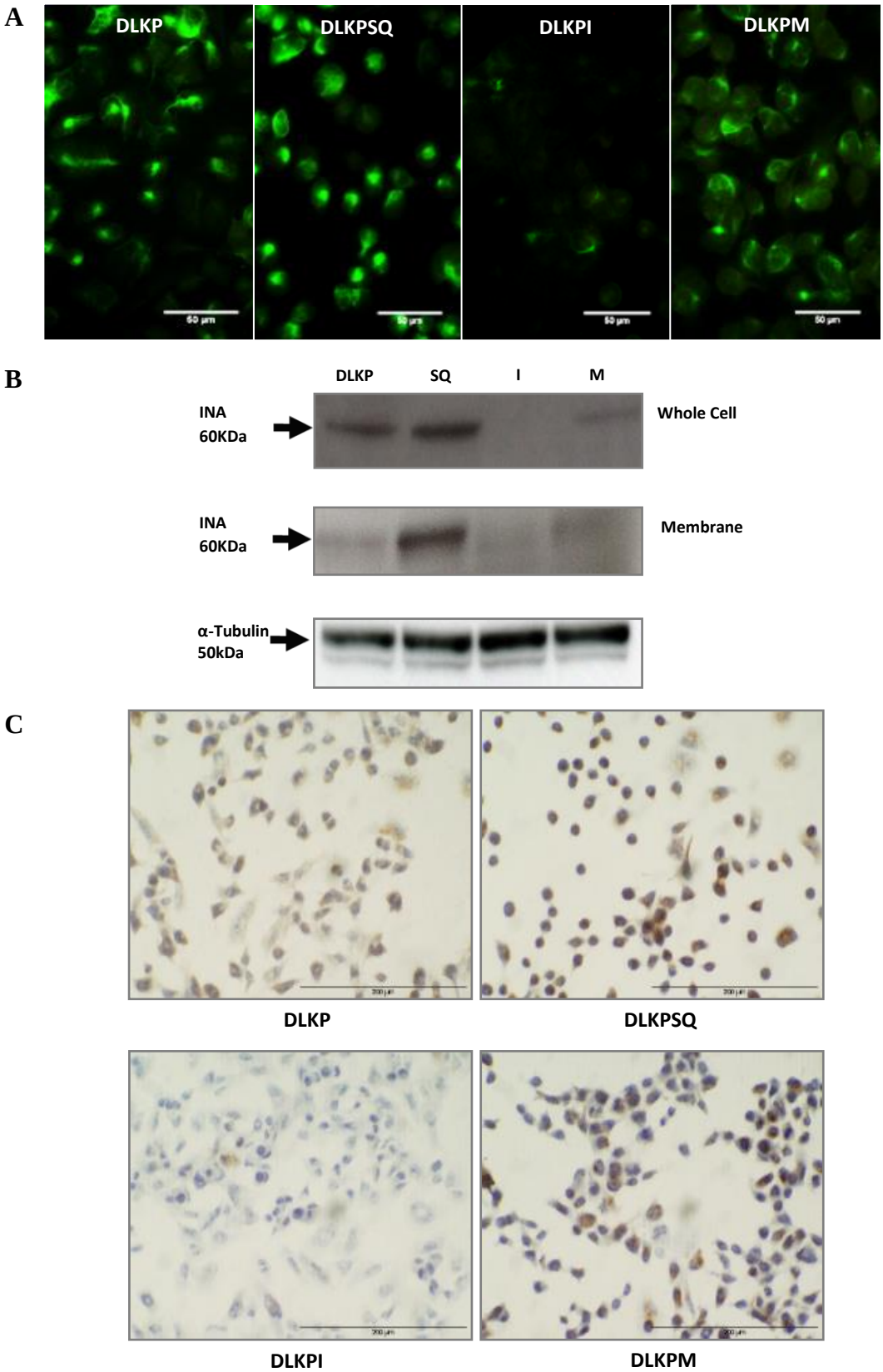

Figure 3.2-6:- Validation of INA expression in DLKP.
(A) Immunofluorescence staining of INA in DLKP and the clones (n=1). **(B)** Representative Immunoblot showing expression of INA in the DLKP clones (α-tubulin was used as an equal loading control (n=3)). **(C)** Immunocytochemical staining of INA, strongest immunoreactivity was observed in DLKPSQ (Original magnification of all photomicrographs, ×400, *scalebar* = 50μm (A) and 200μm (C)).

3.2.7 Validation of SPR in DLKP

Sepiapterin Reductase (SPR) is a 27-kDa enzyme localised to the cytoplasm. It is involved in the final two steps in the conversion of 6-pyruvol-tetrahydrobiopterin to tetrahydrobiopterin (BH_4), an essential co-factor of nitric oxide synthase. Nitric oxide synthase (NOS) is required for the conversion of L-Arginine to Citrulline or nitric oxide. Comparative proteomics analysis found increased expression of SPR in DLKPSQ *vs.* DLKPI (3.64 fold) (see Table 3.1-5). In addition, microarray analysis previously carried out on DLKP and its clones indicated that SPR was overexpressed in DLKPSQ and DLKPM relative to DLKPI.

Immunofluorescence analysis of SPR (Figure 3.2-7 (A)) shows that immunoreactivity was observed DLKP, DLKPSQ and DLKPM. Expression appears to be strongest in DLKPSQ, with weak immunoreactivity observed in DLKPI. In DLKPSQ, immunoreactivity appears to be nuclear or sub-cytoplasmic. Western blot analysis (Figure 3.2-7 (B)) confirmed expression of SPR in whole cell lysates and membrane enriched samples of DLKP and its clones.

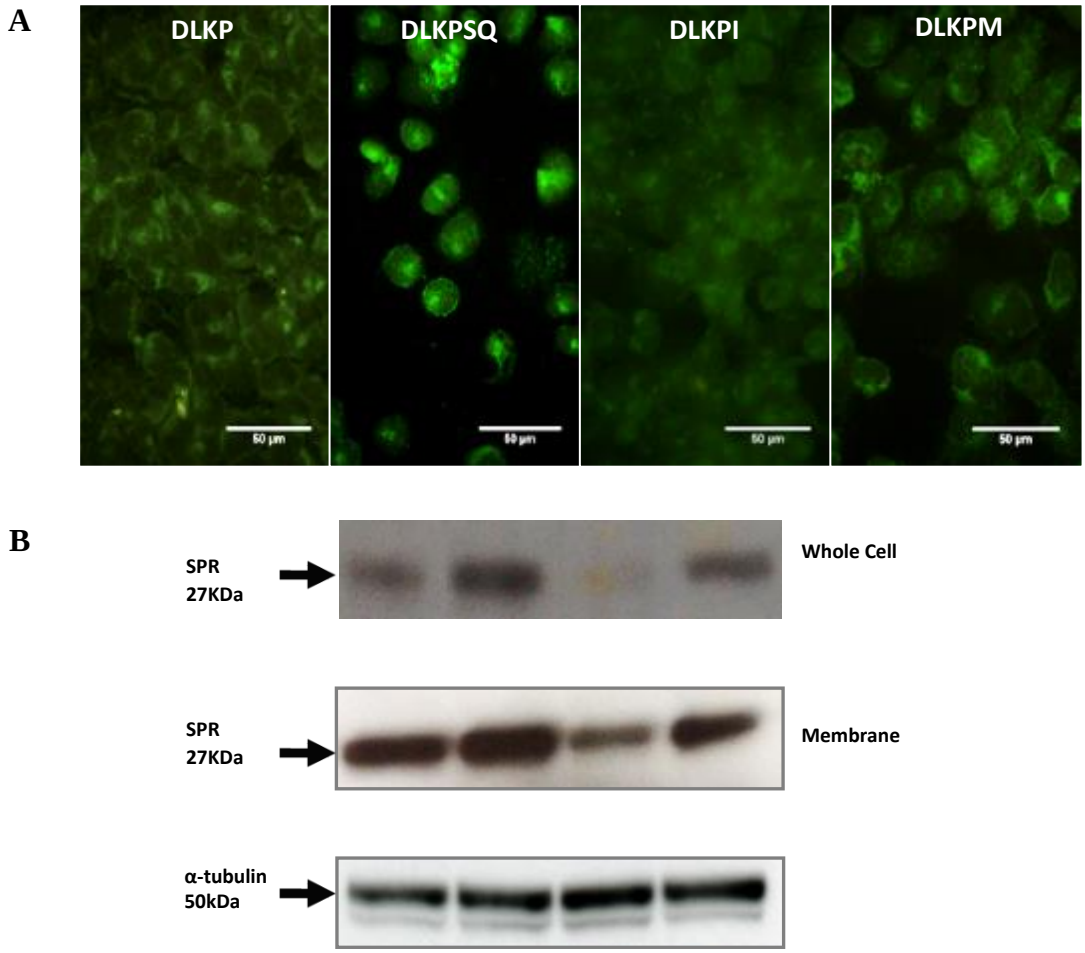

Figure 3.2-7:- Validation of SPR expression in DLKP.
(A) Immunofluorescence staining of SPR in DLKP and its clones, n=1. **(B)** Representative Immunoblot showing expression of SPR in the DLKP clones (α-tubulin was used as an equal loading control (n=3)). Strongest Immunoreactivity was observed in DLKPSQ (Original magnification of all photomicrographs, ×400, *scalebar* = 50µm).

3.2.8 BreastMark Analysis

Breast cancer is a heterogeneous disease of which the majority of cases develop resistance to drugs despite advances in early detection and the progress made in the treatment of patients using systemic agents. This becomes a challenge for clinicians who are involved in the treatment of patients. It is, therefore, critical in the effective treatment of breast cancer (and other cancers) to identify and target the pathways that promote or sustain growth and invasion of cancer cells. There is a greater understanding of the molecular mechanisms underlying carcinogenesis which has led to the identification of novel molecular targets and development of targeted therapies [114, 115]. Targeted therapies for breast cancer include the use of tyrosine kinase inhibitors (TKIs) that target HER1, HER2, HER3, IGF receptor, C-MET and FGF receptor, but also inhibitors of intracellular signalling pathways such as PI3K, AKT, mTOR and ERK [116]. We used BreastMark to evaluate the significance of the markers identified in this thesis in relation to survival of patients with breast cancer. BreastMark is an algorithm developed to allow for the identifications of genes that are associated with disease progression in various breast cancer subtypes. It integrates gene expression and survival data from 26 datasets on 12 different microarray platforms corresponding to ~17,000 genes in up to 4,738 clinical samples. [117].

The prognostic significance of each of the proteins validated in section 3.2.8 was determined for each breast cancer molecular subtype (i) Luminal A (ii) Luminal B (iii) Her2+ and (iv) Basal-like. Validated proteins were analysed using the combined survival option in BreastMark, where he outcome is overall survival. The Kaplan Meir survival curves are presented in Figure 3.2-8 to Figure 3.2-15 for each of the validated proteins, results are summarised in Table 3.2-1. Of the eight proteins chosen for validation studies, BreastMark analysis indicated that six of those were statistically significant and potentially worthy of further investigation in breast cancer.

Target	Significance in Molecular subtypes	Patient outcome	Hazard Ratio	*p*-value
AHNAK	**High expression in Luminal B**	**Better**	**0.88**	**0.0330**
ALCAM	Not significant in Luminal A, Luminal B, Her2+ or Basal subtypes			
HDGF	**Low expression Luminal A**	**Better**	**1.27**	**0.0094**
INA	**High expression in Luminal B**	**Better**	**0.27**	**0.0009**
IQGAP1	**High expression in Luminal A**	**Better**	**0.72**	**0.0006**
ROBO2	Expression not significant in Luminal A, Luminal B, Her2+ or Basal subtypes			
SLIT2	Expression not significant in Luminal A, Luminal B, Her2+ or Basal subtypes			
SPR	**Low expression in Luminal A**	**Poor**	**1.36**	**0.0019**
	Low expression in Basal	**Poor**	**1.33**	**0.0228**

Table 3.2-1:- Summary of BreastMark survival analysis performed on validated proteins.

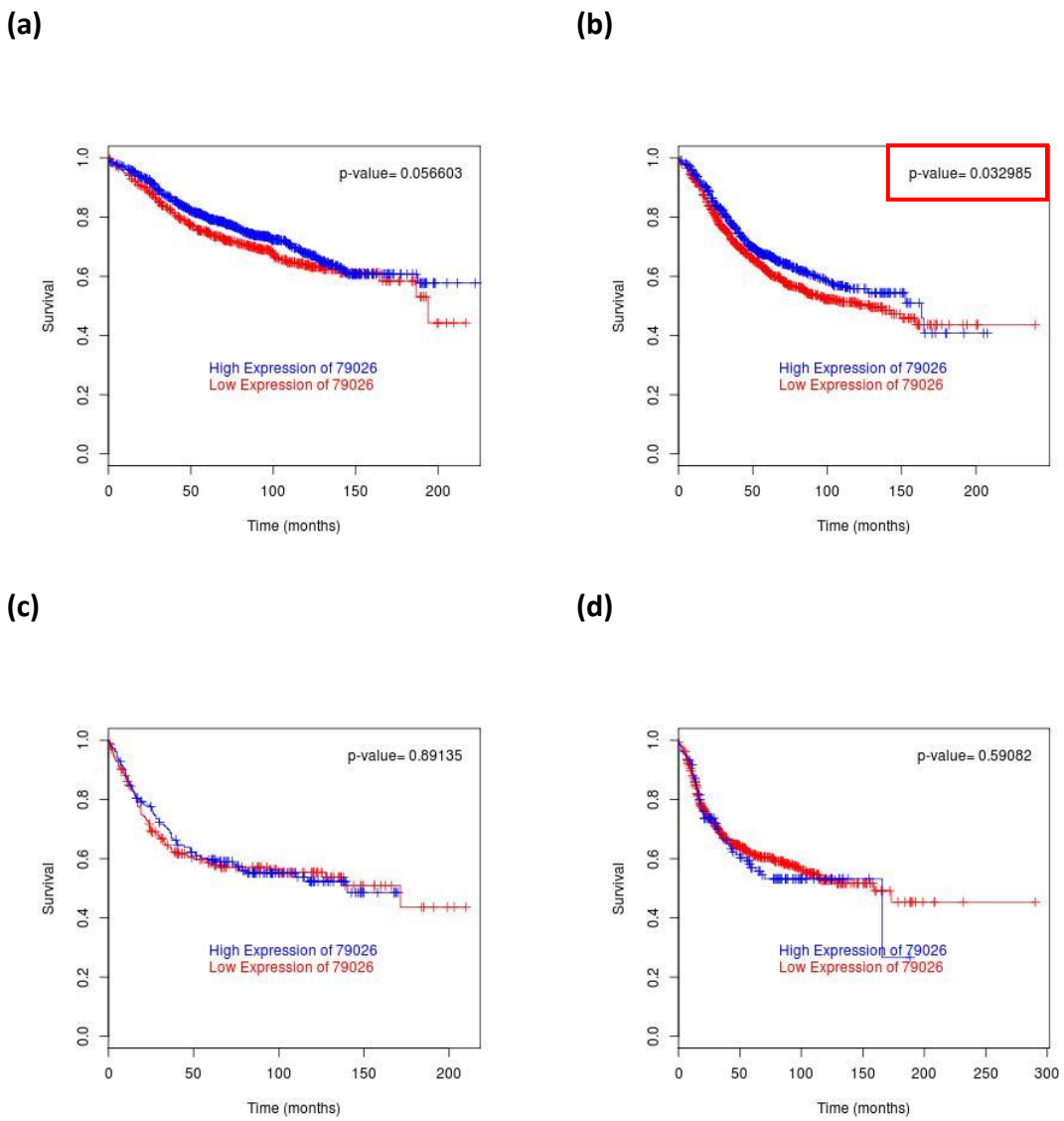

Figure 3.2-8:- Survival analysis of AHNAK expression in breast cancer.
Kaplan-Meier estimates of prognostic significance of AHNAK expression in molecular subtypes of breast cancer; **(a)** Luminal A (n= 1544, HR = 0.8314 (0.6875 - 1.005), *p*=0.05663), **(b)** Luminal B (n= 1473, HR = 0.8344 (0.7063 - 0.9858), *p*=0.03305), **(c)** Her2+ (n= 377, HR = 0.9786 (0.719 - 1.332), *p*=0.8907) and **(d)** Basal-like (n= 674, HR = 1.085 (0.8064 - 1.459), *p*=0.5907). Kaplan-Meier graph representing survival prognosis in patients based on high or low expression of AHNAK in their tumour. Data generated using BreastMark at http://glados.ucd.ie/BreastMark/index.html.

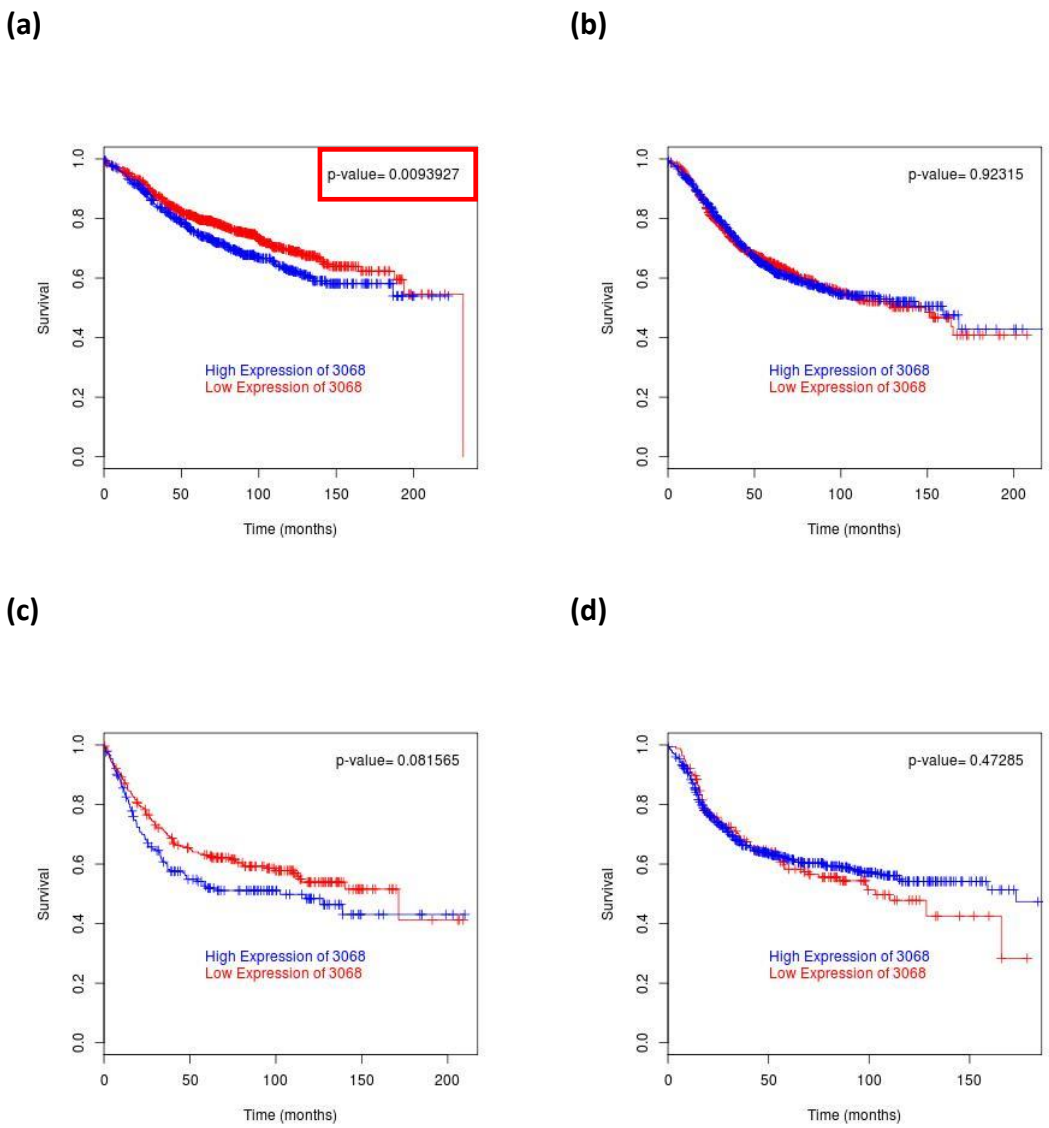

Figure 3.2-9:- Survival analysis of HDGF expression in breast cancer.
Kaplan-Meier estimates of prognostic significance of HDGF expression in molecular subtypes of breast cancer; **(a)** Luminal A (n= 1650, HR = 1.271 (1.06 - 1.523), *p*=0.0094), **(b)** Luminal B (n= 1499, HR = 0.992 (0.8436 - 1.166), *p*=0.9224), **(c)** Her2+ (n= 417, HR = 1.293 (0.9678 - 1.728), *p*=0.0813) and **(d)** Basal-like (n= 710, HR = 0.9072 (0.6951 - 1.184), *p*=0.4732). Kaplan-Meier graph representing survival prognosis in patients based on high or low expression of HDGF in their tumour. Data generated using BreastMark at http://glados.ucd.ie/BreastMark/index.html.

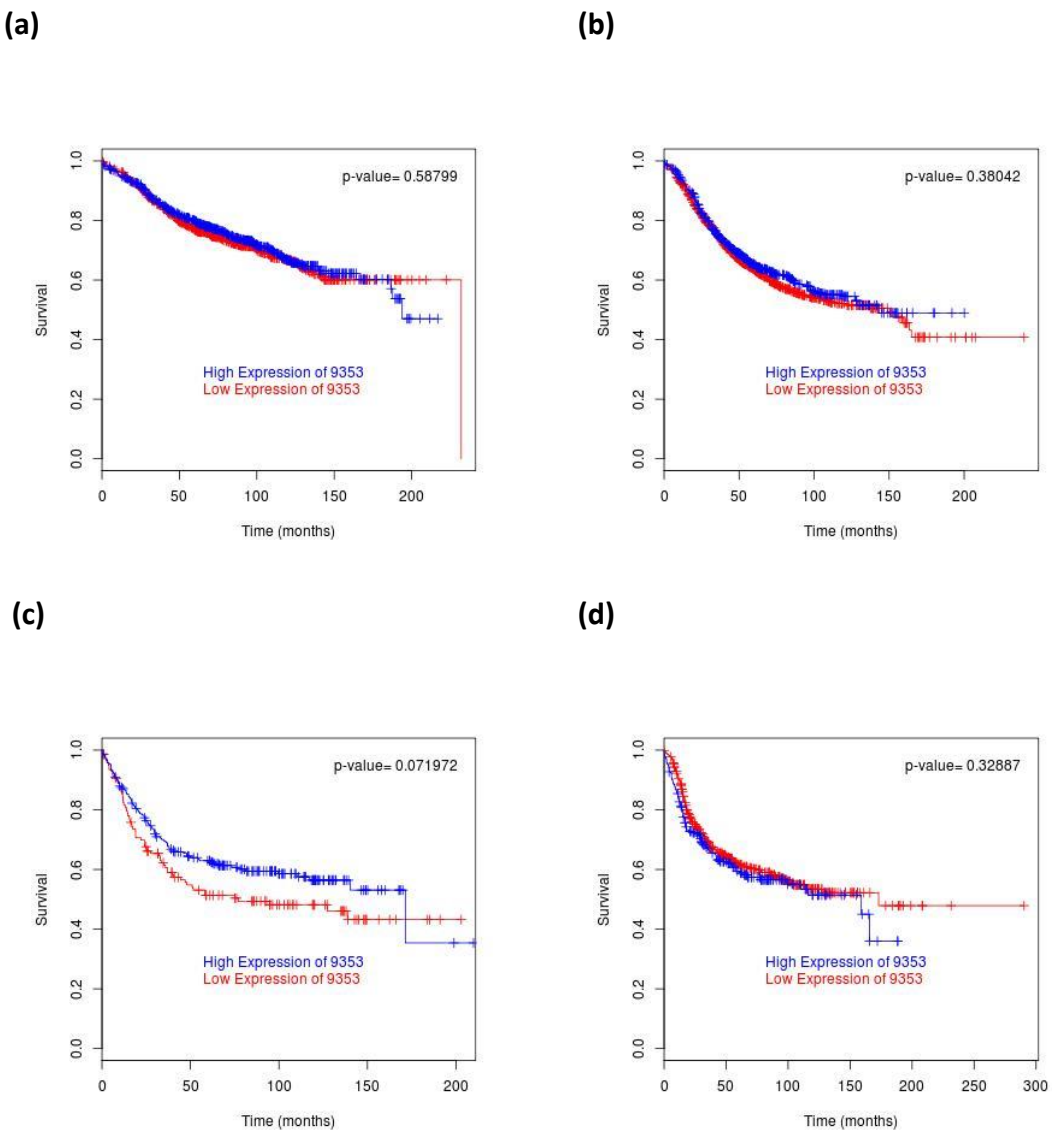

Figure 3.2-10:- Survival analysis of SLIT2 expression in breast cancer.
Kaplan-Meier estimates of prognostic significance of SLIT2 expression in molecular subtypes of breast cancer; **(a)** Luminal A (n= 1523, HR = 0.9492 (0.7858 - 1.147), *p*=0.5883), **(b)** Luminal B (n= 1464, HR = 0.928 (0.7851 - 1.097), *p*=0.3809), **(c)** Her2+ (n= 371, HR = 0.752 (0.5509 - 1.026), *p*=0.07161) and **(d)** Basal-like (n= 662, HR = 1.134 (0.8808 - 1.46), *p*=0.3288). Kaplan-Meier graph representing survival prognosis in patients based on high or low expression of SLIT2 in their tumour. Data generated using BreastMark at http://glados.ucd.ie/BreastMark/index.html.

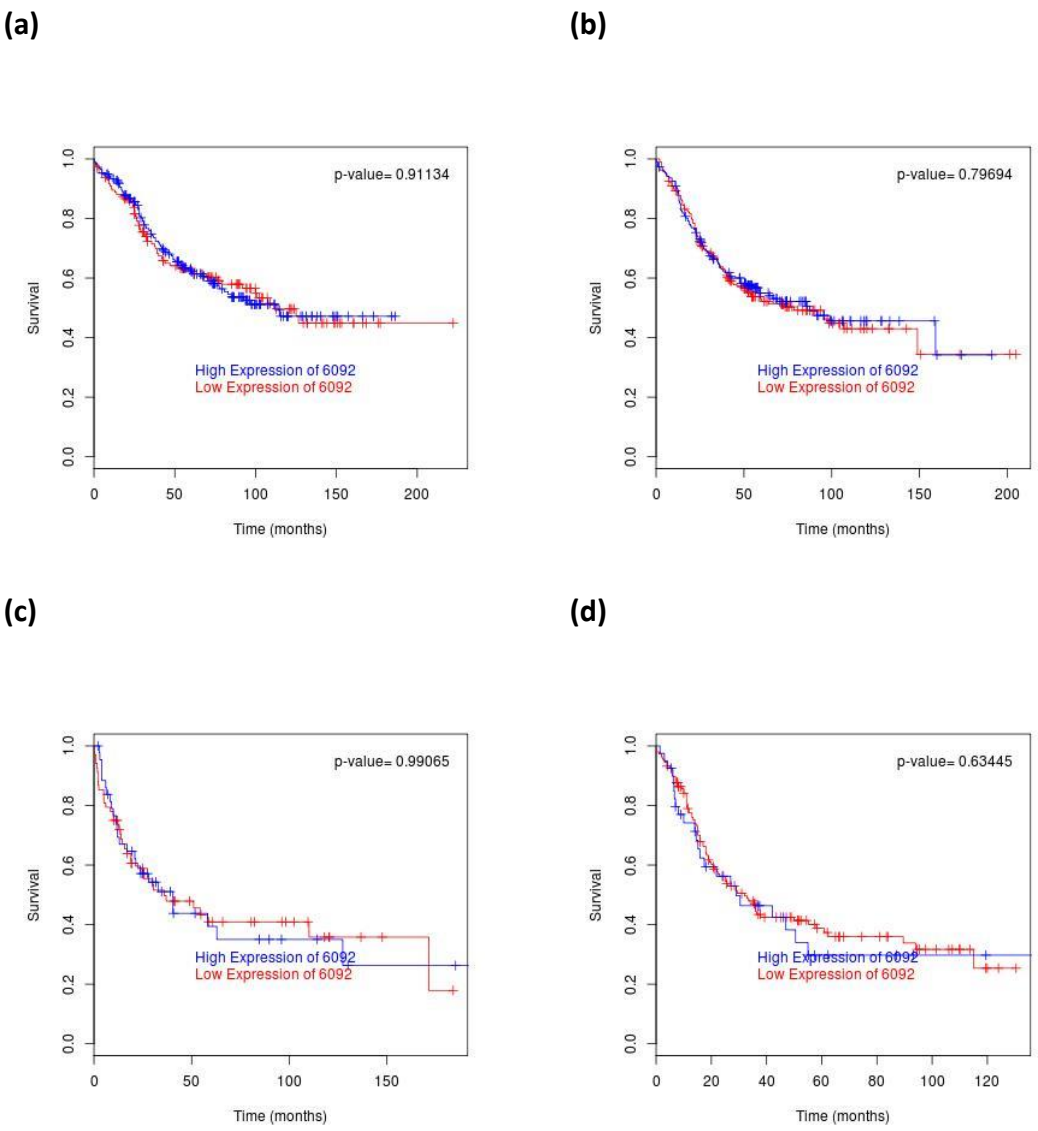

Figure 3.2-11:- Survival analysis of ROBO2 expression in breast cancer.
Kaplan-Meier estimates of prognostic significance of ROBO2 expression in molecular subtypes of breast cancer; **(a)** Luminal A (n= 338, HR = 0.9812 (0.7023 - 1.371), *p*=0.9112), **(b)** Luminal B (n= 376, HR = 0.9626 (0.7186 - 1.29), *p*=0.7984), **(c)** Her2+ (n= 112, HR = 1.005 (0.6062 - 1.666), *p*=0.9842) and **(d)** Basal-like (n= 187, HR = 1.116 (0.7032 - 1.771), *p*=0.6415). Kaplan-Meier graph representing survival prognosis in patients based on high or low expression of ROBO2 in their tumour. Data generated using BreastMark at http://glados.ucd.ie/BreastMark/index.html.

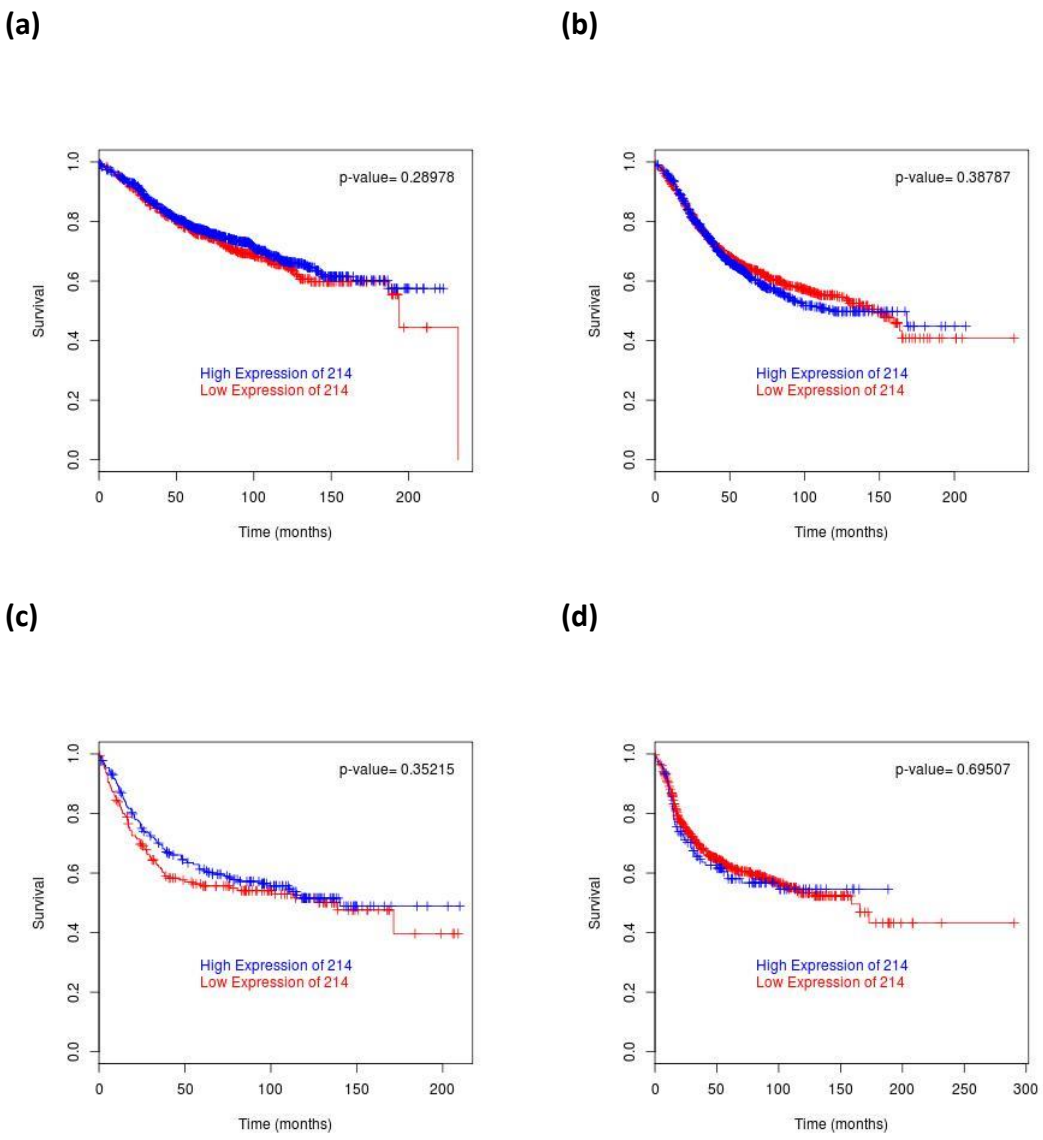

Figure 3.2-12:- Survival analysis of ALCAM expression in breast cancer
Kaplan-Meier estimates of prognostic significance of ALCAM expression in molecular subtypes of breast cancer; **(a)** Luminal A (n= 1630, HR = 0.9045 (0.7509 - 1.089), *p*=0.2902), **(b)** Luminal B (n= 1474, HR = 1.075 (0.9124 - 1.266), *p*=0.3879), **(c)** Her2+ (n= 399, HR = 0.8696 (0.6478 - 1.167), *p*=0.3521) and **(d)** Basal-like (n= 704, HR = 1.064 (0.7813 - 1.449), *p*=0.6938). Kaplan-Meier graph representing survival prognosis in patients based on high or low expression of ALCAM in their tumour. Data generated using BreastMark at http://glados.ucd.ie/BreastMark/index.html.

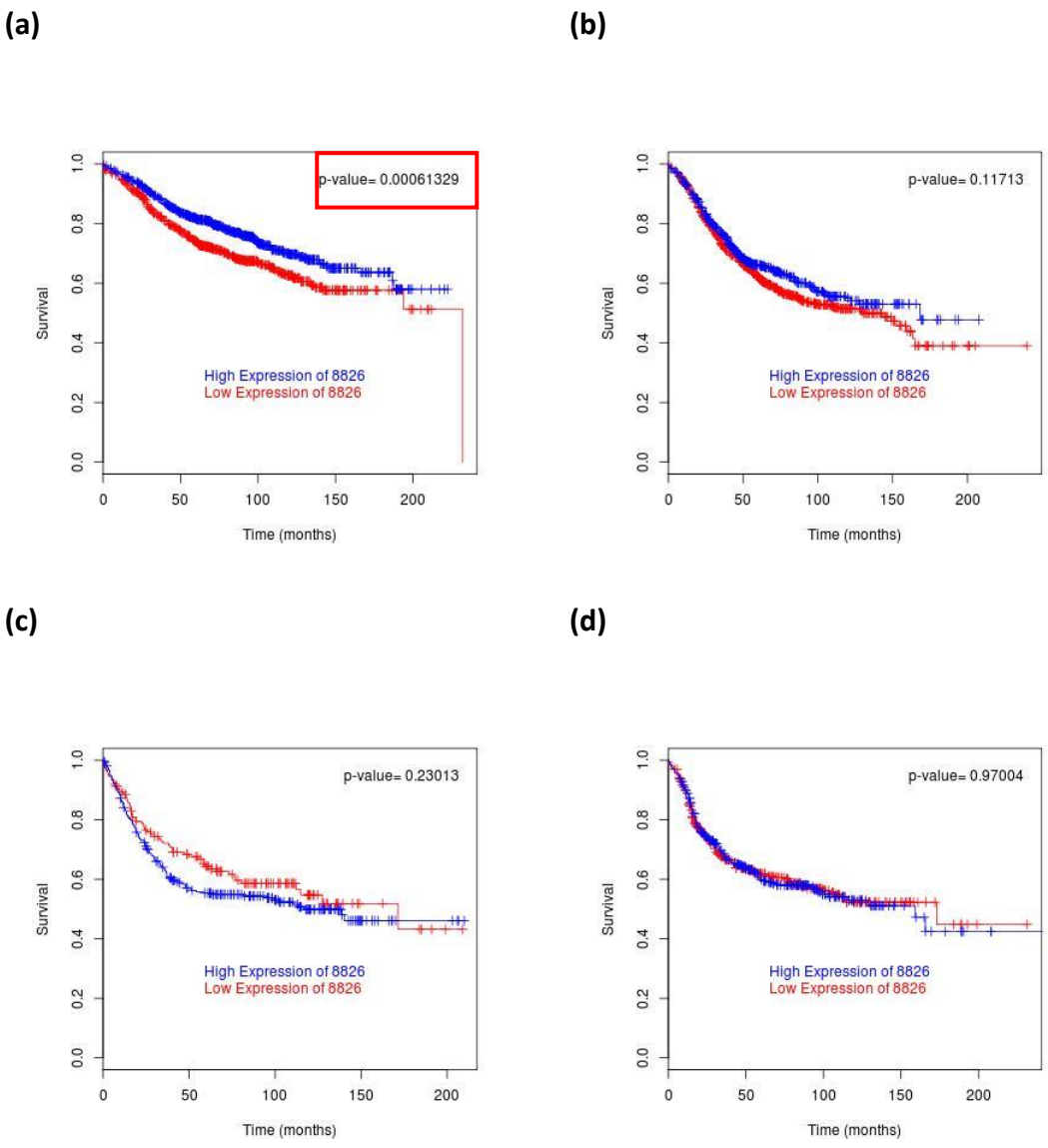

Figure 3.2-13:- Survival analysis of IQGAP1 expression in breast cancer.
Kaplan-Meier estimates of prognostic significance of IQGAP1 expression in molecular subtypes of breast cancer; **(a)** Luminal A (n= 1650, HR = 0.729 (0.6079 - 0.8741), *p*=0.0006124), **(b)** Luminal B (n= 1499, HR = 0.8769 (0.7438 - 1.034), *p*=0.1174), **(c)** Her2+ (n= 417, HR = 1.207 (0.8871 - 1.643), *p*=0.2301) and **(d)** Basal-like (n= 710, HR = 1.004 (0.7958 - 1.267), *p*=0.9711). Kaplan-Meier graph representing survival prognosis in patients based on high or low expression of IQGAP1 in their tumour. Data generated using BreastMark at http://glados.ucd.ie/BreastMark/index.html.

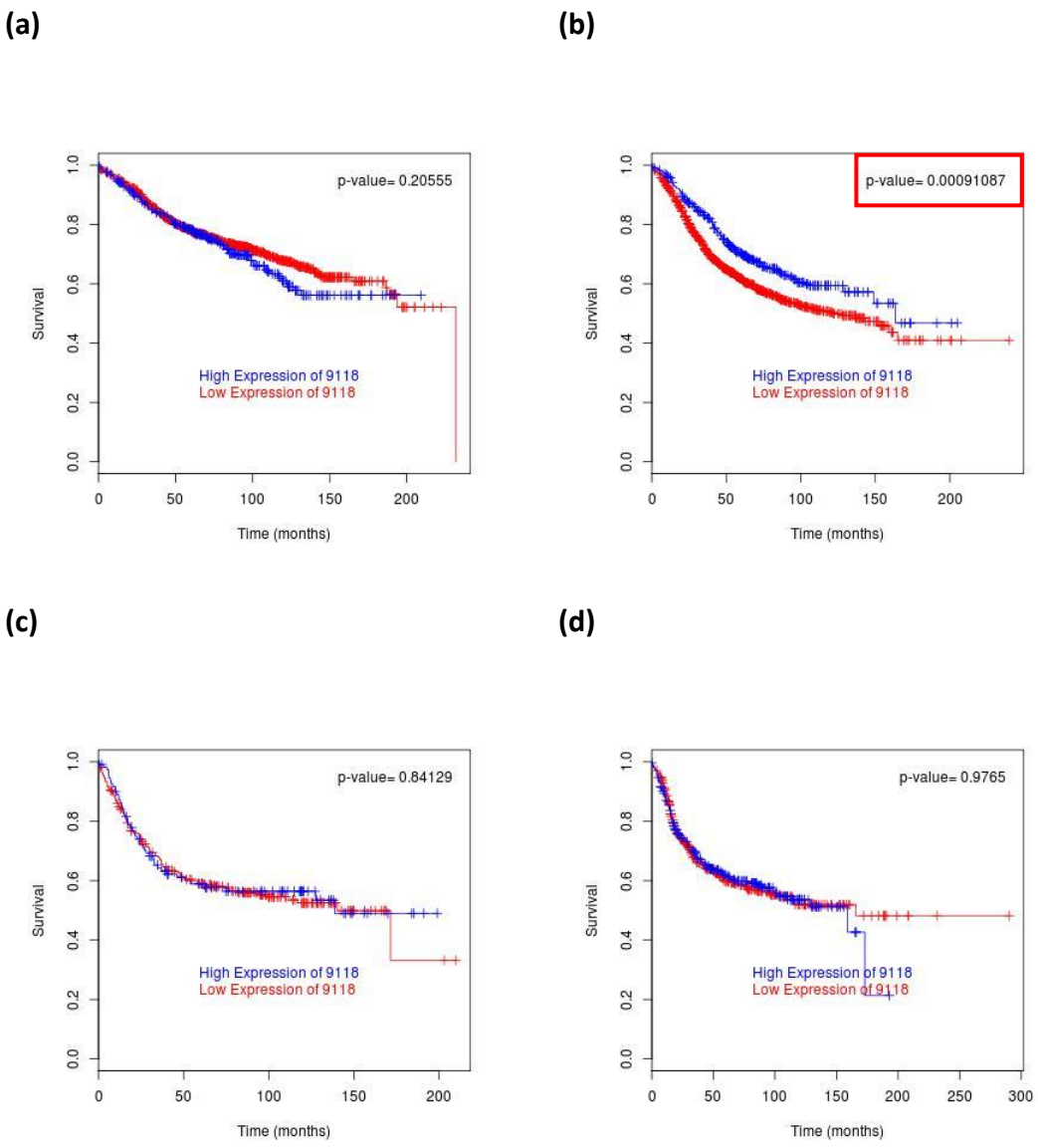

Figure 3.2-14:- Survival analysis of INA expression in breast cancer.
Kaplan-Meier estimates of prognostic significance of INA expression in molecular subtypes of breast cancer; **(a)** Luminal A (n= 1544, HR = 1.15 (0.9259 - 1.428), p=0.2061), **(b)** Luminal B (n= 1473, HR = 0.7271 (0.6018 - 0.8783), p=0.000904), **(c)** Her2+ (n= 377, HR = 0.9656 (0.6877 - 1.356), p=0.84) and **(d)** Basal-like (n= 674, HR = 1.004 (0.7862 - 1.281), p=0.9772). Kaplan-Meier graph representing survival prognosis in patients based on high or low expression of INA in their tumour. Data generated using BreastMark at http://glados.ucd.ie/BreastMark/index.html.

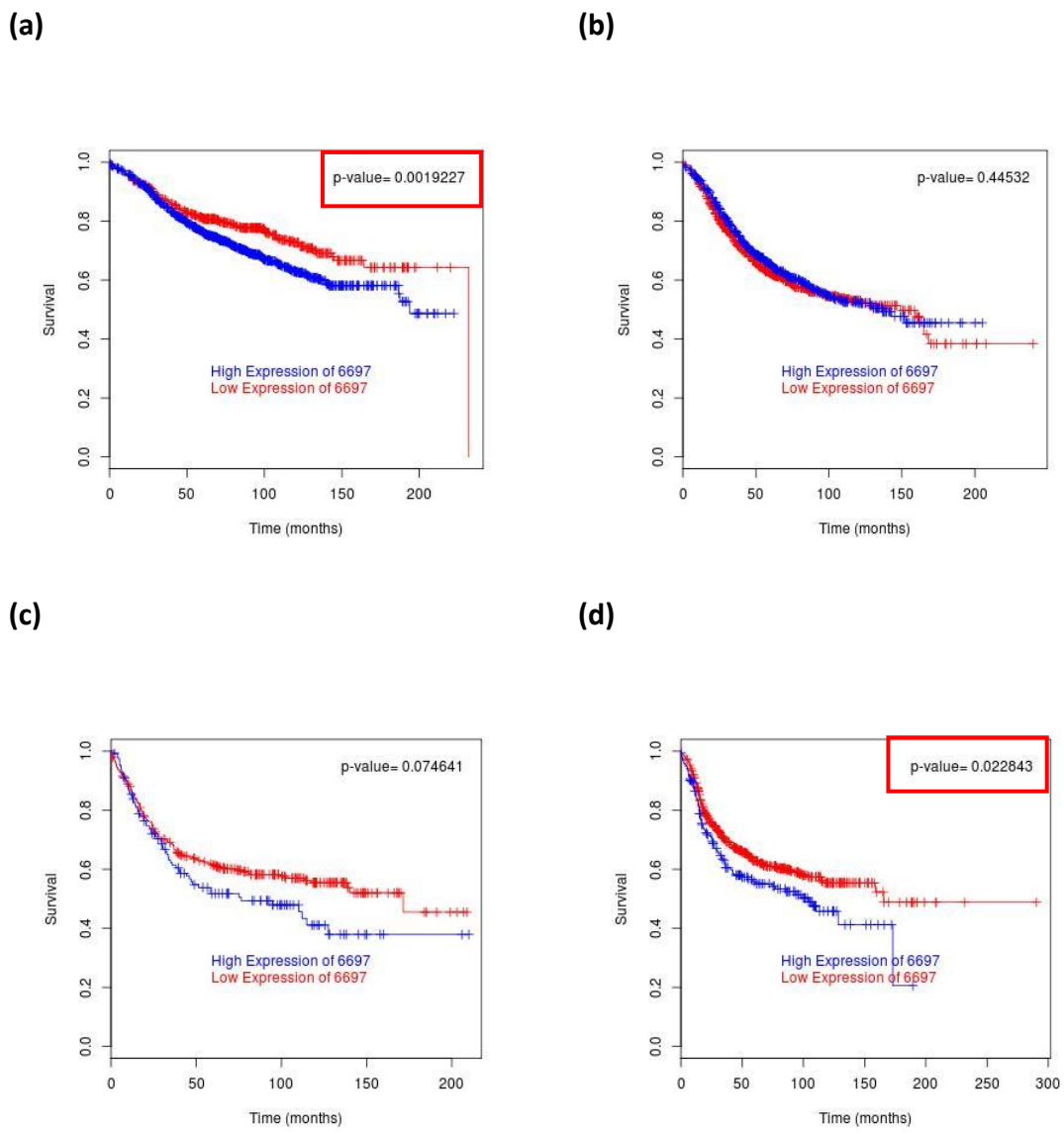

Figure 3.2-15:- Survival analysis of SPR expression in breast cancer.
Kaplan-Meier estimates of prognostic significance of SPR expression in molecular subtypes of breast cancer; **(a)** Luminal A (n= 1678, HR = 1.366 (1.121 - 1.664), *p*=0.001923), **(b)** Luminal B (n= 1519, HR = 0.9395 (0.8002 - 1.103), *p*=0.4459), **(c)** Her2+ (n= 423, HR = 1.317 (0.9721 - 1.783), *p*=0.07463) and **(d)** Basal-like (n= 714, HR = 1.335 (1.04 - 1.714), *p*=0.02289). Kaplan-Meier graph representing survival prognosis in patients based on high or low expression of SPR in their tumour. Data generated using BreastMark at http://glados.ucd.ie/BreastMark/index.html.

3.2.9 Summary of results from validation experiments

Proteins identified through comparative proteomic analysis performed on DLKP, DLKPSQ, DLKPI and DLKPM cell lines revealed a number of differentially expressed proteins between within DLKP cell line model. Six proteins (AHNAK, ALCAM, HDGF, IQGAP1, ROBO2 and SPR) were selected directly from this analysis. INA was selected based on its association with neuroendocrine pancreatic cancer and its novelty. SLIT2 was selected due to its association with its receptor ROBO2, identified in the proteomic analysis presented in. All of the selected proteins were examined in DLKP, DLKPSQ, DLKPI and DLKPM cells and their expression was presented in section 3.2. Some differences in the expression levels of the proteins were observed between each of the techniques used for validation, however, overall the expression patterns of individual proteins showed similar trends. Table 3.2-2 presents a representative indication of the expression of each of the protein validated by Western blot analysis (of the whole cell, membrane enriched and/or conditioned medium samples), Immunofluorescence, and/or Immunocytochemical analysis of the cell lines.

	DLKP	DLKPSQ	DLKPI	DLKPM
AHNAK	+	+	++++	++++
ALCAM	+	-/+	++++	+
HDGF	++	+	+	+
INA	++	++	-/+	+
IQGAP1	++	+	++	+++
ROBO2	+	++	+	++
SLIT2	++	+	+	++
SPR	+	++	+	++

Table 3.2-2:- Summary table showing representative expression of the proteins validated in DLKP and its clones.

-/+ absent or weak expression
\+ weak expression
++ moderate expression
+++ strong expression
++++ very strong expression

3.3 Expression of selected proteins in human cancer cell lines.

Comparative proteomics analysis was used to select differentially expressed proteins as potential markers for DLKP clones. A number of proteins were selected and validated by Western blot analysis, Immunofluorescence and Immunohistochemistry. AHNAK, ROBO2, ALCAM, IQGAP1, and SPR were selected following membrane proteomics. SLIT2 was selected from microarray analysis, through its association with the ROBO2 receptor. HDGF was selected from membrane proteomics, however, less stringent criteria were applied. These proteins were examined further for their expression across panels of representative tumour cell lines including lung cancer, pancreatic cancer, TNBC, colon, glioma, melanoma and neuroblastoma.

3.3.1 Expression of validated proteins in a representative panel of lung cancer cell lines

Preliminary investigations were carried out to examine the expression of HDGF, SLIT2, ALCAM, INA and SPR in a representative panel of lung cancer cell lines. The full panel of cell lines including their subtypes are shown in Table 3.3-1 below:

Subtype	Abbreviation	Cell lines
Small Cell Lung Cancer	SCLC	NCI-H69, NCI-H82, DMS-53
Large Cell Lung Cancer	LCLC	NCI-H460, H1229
Adenocarcinoma	AC	A549, SK-LU-1
Squamous Cell Carcinoma	SCC	DLRP, SKMES-1

Table 3.3-1:- Lung cancer cell lines used to examine the expression of protein targets.

HDGF expression appears to be strongest in the SCLC and AC cell lines, while lower expression levels were observed in the remaining subtypes (Figure 3.3-1), SLIT2 (Figure 3.3-2) and ALCAM (Figure 3.3-3) expression appears to be strongest in NCI-H69 (SCLC) and lower expression levels were observed in the remaining subtypes. SCC cell lines were not available at the time of carrying out western blot analysis of HDGF, SLIT2, ALCAM and INA, but their expression should be examined in this lung cancer subtype. Expression of INA in the whole cell preparations displayed strongest expression in all SCLC cell lines, in one LCLC (H1229) and in one SCC (SKMES-1), while low to an absence of expression was observed in AC and in the remaining cell lines. Analysis of the panel for membrane expression appears to associate INA to SCLC cell lines since no

detectable levels of INA was observed in LCLC and AC cell lines (Figure 3.3-4). Expression of SPR in whole cell preparations and membrane preparations appears to be strongest in DMS-53 (SCLC), A549 (AC) and DLRP and SKMES-1 (SCC) cell lines, strong expression was also observed in LCLC and AC cell lines, while low level expression was observed in two SCLC cell lines (Figure 3.3-5). Western blot analysis of the markers in cell lines representing various lung cancer subtypes appears to show strong expression in the SCLC subtype. The expression of these markers in DLKP could suggest a potential SCLC component in DLKP, which was originally proposed by McBride, 1995 [93]. To confirm this suggestion, further analysis should be carried out using these markers.

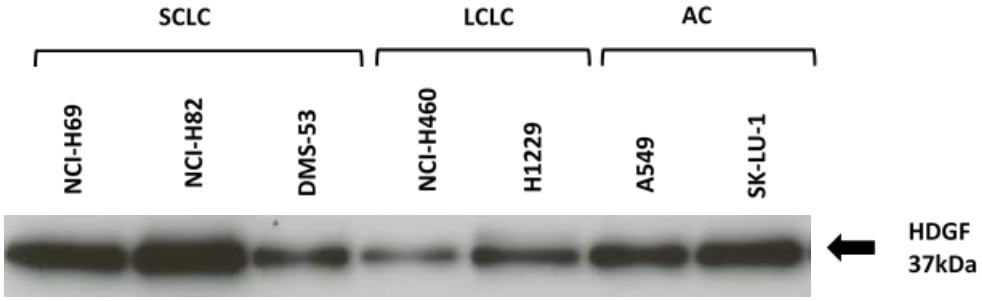

Figure 3.3-1:- Western blot analysis of HDGF expression in lung cancer cell lines.
Representative immunoblot showing expression of HDGF in; (i) SCLC: NCI-H69, NCI-H82 and DMS-53, (ii) LCLC: NCI-H460 and H1229 and (iii) AC: A549 and SK-LU-1. Membrane enriched samples were separated by SDS-PAGE and probed with an antibody specific to HDGF. SCLC cell lines appear to show the strongest expression of HDGF (n=1).

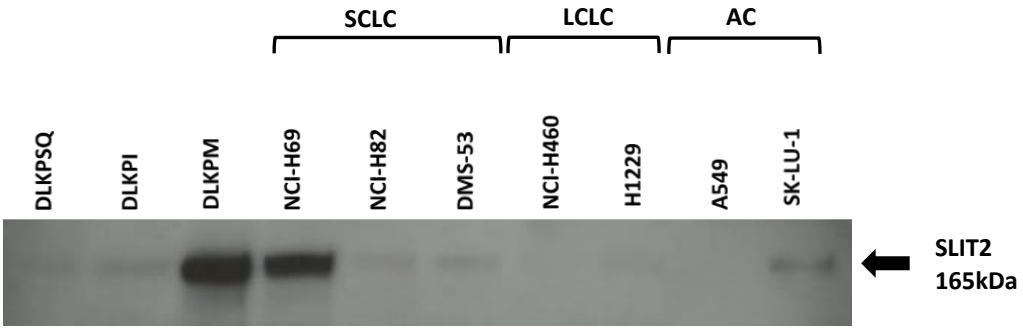

Figure 3.3-2:- Western blot analysis of SLIT2 expression in lung cancer cell lines.
Representative immunoblot showing expression of SLIT2 in; (i) SCLC: NCI-H69, NCI-H82 and DMS-53, (ii) LCLC: NCI-H460 and H1229 and (iii) AC: A549 and SK-LU-1. Membrane enriched samples were separated by SDS-PAGE and probed with an antibody specific to SLIT2. NCI-H82 appears to show the strongest expression of SLIT2 (DLKPM served as a positive control) (n=1).

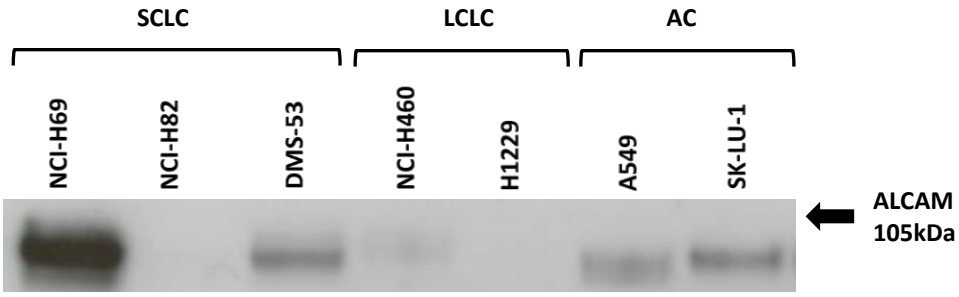

Figure 3.3-3:- Western blot analysis of ALCAM in lung cancer cell lines
Representative immunoblot showing expression of ALCAM in; (i) SCLC: NCI-H69, NCI-H82 and DMS-53, (ii) LCLC: NCI-H460 and H1229 and (iii) AC: A549 and SK-LU-1. Membrane enriched samples were separated by SDS-PAGE and probed with an antibody specific of ALCAM. NCI-H69 appears to show the strongest expression of ALCAM. (n=1).

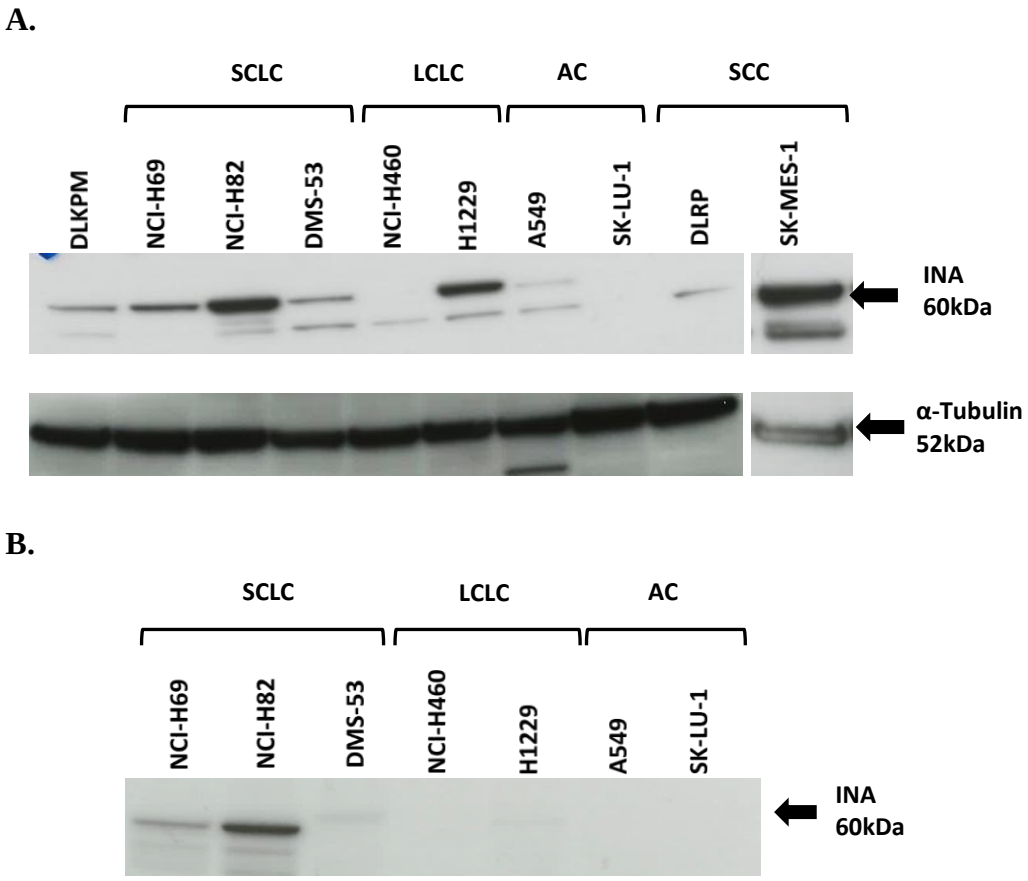

Figure 3.3-4:- Western blot analysis of INA in lung cancer cell lines.
Representative immunoblot showing expression of INA in; (i) SCLC: NCI-H69, NCI-H82 and DMS-53, (ii) LCLC: NCI-H460 and H1229, (iii) AC: A549 and SK-LU-1 and (iv) SCC: DLRP and SKMES-1. Expression of INA was examined in; (a) whole cell lysates (α-tubulin served as loading control) and (b) membrane enriched samples were separated by SDS-PAGE and probed with an antibody specific to INA. NCI-H69 and NCI-H82 appear to show the strongest expression of INA (n=1).

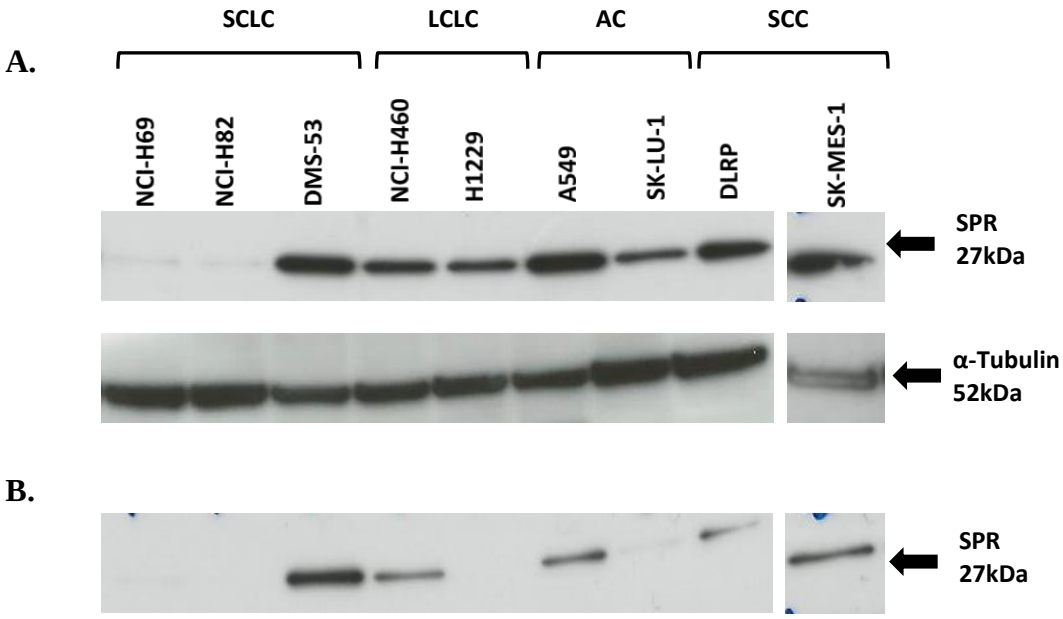

Figure 3.3-5:- Western blot analysis of SPR in lung cancer cell lines.
Representative immunoblot showing expression of SPR in, (i) SCLC: NCI-H69, NCI-H82 and DMS-53, (ii) LCLC: NCI-H460 and H1229, (iii) AC: A549 and SK-LU-1 and (iv) SCC: DLRP and SKMES-1. Expression of SPR was examined in; (a) whole cell lysates (α-tubulin served as loading control), (b) membrane enriched fractions samples were separated by SDS-PAGE and probed with an antibody specific to SPR (n=1).

3.3.2 Expression of validated proteins in a representative panel of TNBC cell lines

Preliminary investigations were carried out to examine the expression of HDGF, INA and SPR in a representative panel of triple negative breast cancer (TNBC) cell lines. Survival analysis using the BreastMark algorithm did not find the expression of SLIT2 and ALCAM to be statistically significant in patients with breast cancer and were therefore excluded from this analysis. The full panel of cell lines including their subtypes are shown in Table 3.3-2 below:

Molecular subtype	Abbreviation	Cell lines
Basal-like-1	BL-1	HCC-1143, MDA-MB-468.
Basal-like-2	BL-2	HCC1937, CAL-851, HDQP-1.
Mesenchymal	M	CAL-51
Mesenchymal-like	MSL	Hs-578-T, MDA-MB-231, MDA-MB-157.

Table 3.3-2:- TNBC cell lines used to examine the expression of protein targets.

Whole cell lysates were used to examine the expression of HDGF, INA and SPR in this cell line panel. Western blot analysis revealed strong expression of HDGF across the TNBC subtypes (Figure 3.3-6). INA appeared to show strongest expression in HCC-1937 and HCC-1143 (BL-1), with strong expression was also observed in HDQP-1 (M) and MDA-MB-157 (MSL) cell lines. Low level to an absence of expression was observed in the remaining cell lines on the panel (Figure 3.3-7). Expression of SPR appeared to be strongest in MDA-MB-468 (BL-1), CAL-51 (M) and MDA-MB-231 and MDA-MB-157 (MSL) cell lines, while lower expression levels were observed in BL-2 (CAL-851 and HDQP-1) and in the remaining cell lines on the panel (Figure 3.3-8). There are clear differences in the expression of these targets across the panel of TNBC cell lines, but SPR and INA appear to be strongly expressed in BL-1 breast cancer.

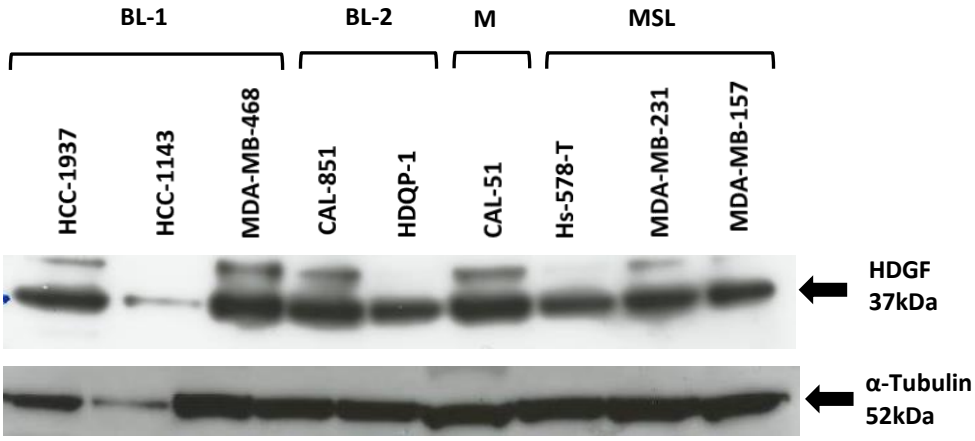

Figure 3.3-6:- Western blot analysis of HDGF in TNBC cell lines.
Representative immunoblot showing expression of HDGF in; (i) BL-1: HCC1937, HCC-1143 and MDA-MD-468, (ii) BL-2: CAL-851 and HDQP-1, (iii) M: CAL-51 and (iv) MSL: Hs-578-T, MDA-MB-231 and MDA-MB-157. Samples were separated by SDS-PAGE and probed with an antibody specific to HDGF. Strong expression is observed across TNBC (α-tubulin served as loading control (n=1)).

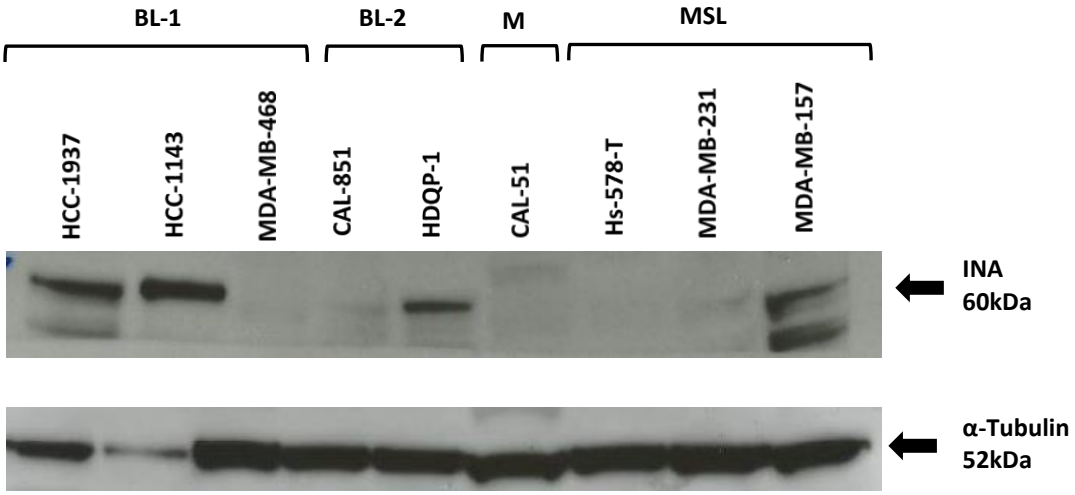

Figure 3.3-7:- Western blot analysis of INA in TNBC cell lines.
Representative immunoblot showing expression of INA in; (i) BL-1: HCC1937, HCC-1143 and MDA-MD-468, (ii) BL-2: CAL-851 and HDQP-1, (iii) M: CAL-51 and (iv) MSL: Hs-578-T, MDA-MB-231 and MDA-MB-157. Samples were separated by SDS-PAGE and probed with an antibody specific to INA. Expression of INA appears to be strongest in the BL-1 subtype. (α-tubulin served as loading control) n=1.

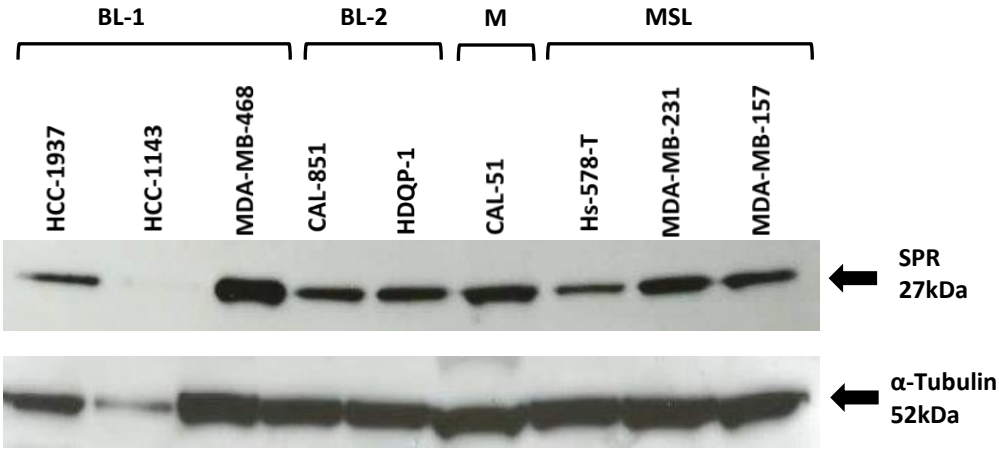

Figure 3.3-8:- Western blot analysis of SPR in TNBC cell lines.
Representative immunoblot showing expression of SPR in; (i) BL-1: HCC1937, HCC-1143 and MDA-MD-468, (ii) BL-2: CAL-851 and HDQP-1, (iii) M: CAL-51 and (iv) MSL: Hs-578-T, MDA-MB-231 and MDA-MB-157. Samples were separated by SDS-PAGE and probed with an antibody specific to SPR. SPR expression is observed across TNBC cell lines (α-tubulin served as loading control (n=1)).

3.3.3 Expression of validated proteins in a representative panel of pancreatic cancer cell lines

Preliminary investigations were carried out to examine the expression of HDGF, ALCAM, INA and SPR in a representative panel of pancreatic cancer cell lines. SLIT2 was not included in this analysis. INA was included in this analysis, however, extremely low level of expression to the absence of expression was observed (data not shown). The panel of cell lines was BxPc-3, HPAC, Panc-1, MiaPaca2, MiaPaca2 clone3, AsPc-1 and Capan-1 (all cell lines are pancreatic ductal adenocarcinoma).

Western blot analysis was used to examine the expression of HDGF, ALCAM and SPR in (a) Whole cell lysates and/or (b) membrane-enriched fractions of the cell lines. HDGF showed strong expression across all pancreatic cancer cell lines, with Panc-1 showing lowest expression levels. Strong expression of HDGF was also observed in whole cell lysates obtained from explanted human pancreatic cancer tumour cells. An increased membrane expression of HDGF was observed in MiaPaca2 clone3 (invasive clone of MiaPaca2) compared to its parental cell line. Figure 3.3-9 shows expression of HDGF in (a) Whole cell lysates (b) membrane enriched fractions and (c) cells recovered via explant culture from two human pancreatic cancer tumours (explant culture was performed by Dr. Fiona O'Neill and Dr. Sandra Roche, whole cell and membrane samples were prepared by Edel McAuley).

ALCAM appeared to show strong expression in BxPc-3, with low level to no expression observed in the remaining cell lines on the panel (Figure 3.3-10)**.** Strong expression of SPR was observed in whole cell lysates across the panel of pancreatic cancer cell lines, with exception of BxPc-3 showing weakest SPR expression. Expression in membrane enriched preparations appear to be much lower, with AsPc-1 displaying strongest expression (Figure 3.3-11). Both whole cell lysate and membrane samples appear to show increased expression in the invasive MiaPaca2 clone3 cell line compared to its parental.

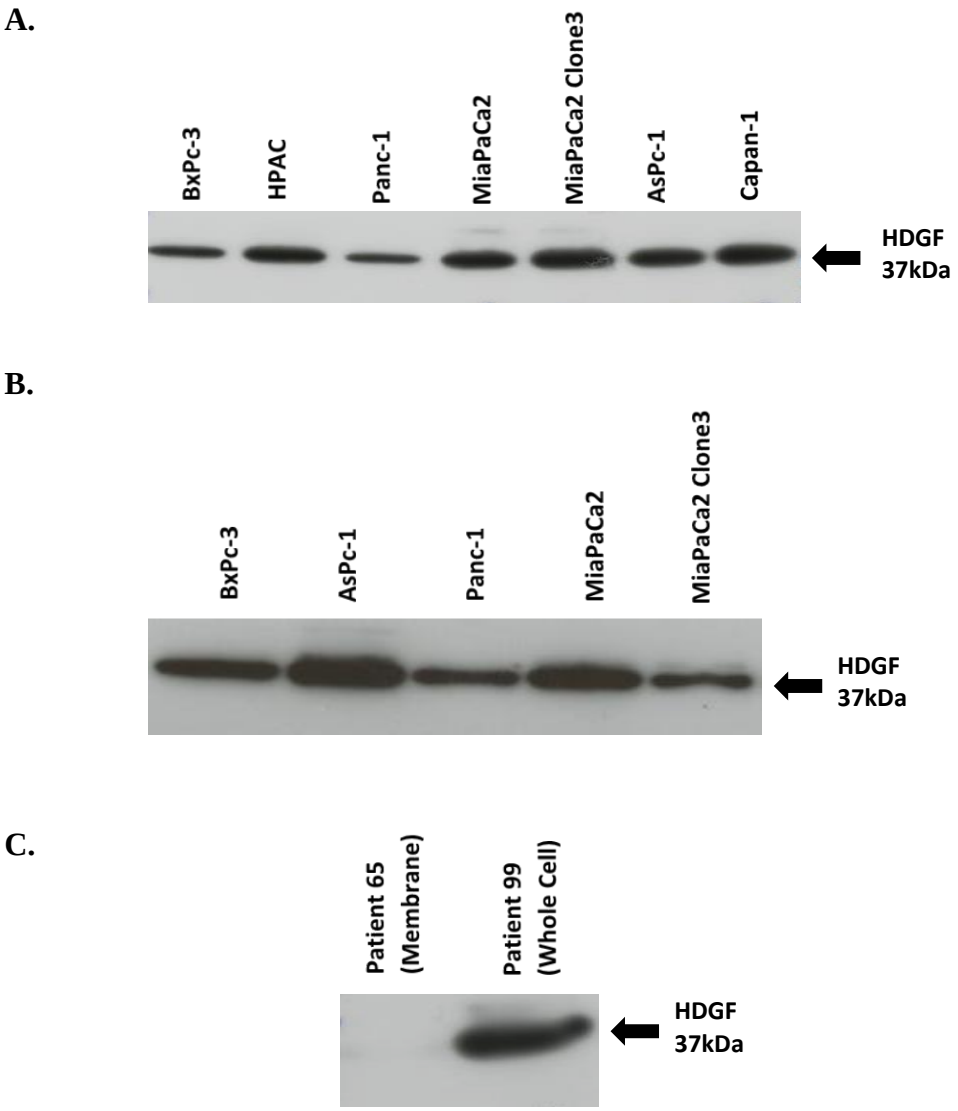

Figure 3.3-9:- Western blot analysis of HDGF in pancreatic cancer cell lines.
Representative immunoblot showing expression of HDGF in; (a) whole cell Lysates of BxPc-3, HPAC, Panc-1, MiaPaca2, MiaPaca2 clone3, AsPc-1 and Capan-1 (α-tubulin served as loading control). (b) membrane enriched fractions of BxPc-3, AsPc-1, Panc-1, MiaPaca2 and MiaPaca2 clone2 and (c) membrane samples and whole cell lysates from explanted human patient tumour cells. Samples separated by SDS-PAGE and probed with an antibody specific to HDGF (n=1).

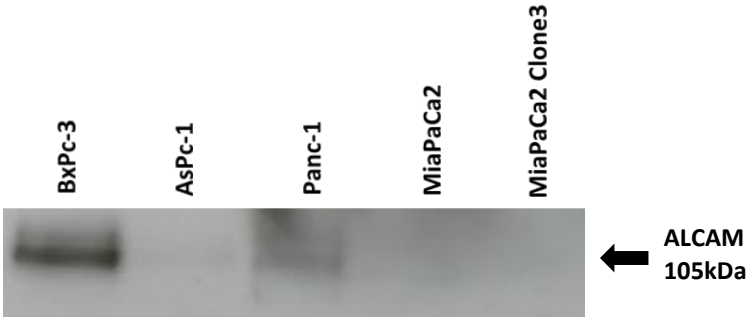

Figure 3.3-10:- Western blot analysis of ALCAM in pancreatic cancer cell lines.
Representative immunoblot showing expression of ALCAM in membrane enriched samples of BxPc-3, AsPc-1, Panc-1, MiaPaCa2 and MiaPaCa2 clone3 invasive. Samples were separated by SDS-PAGE and probed with an antibody specific to ALCAM. Expression of ALCAM appears strongest in the membrane fractions of BxPc-3 (n=1).

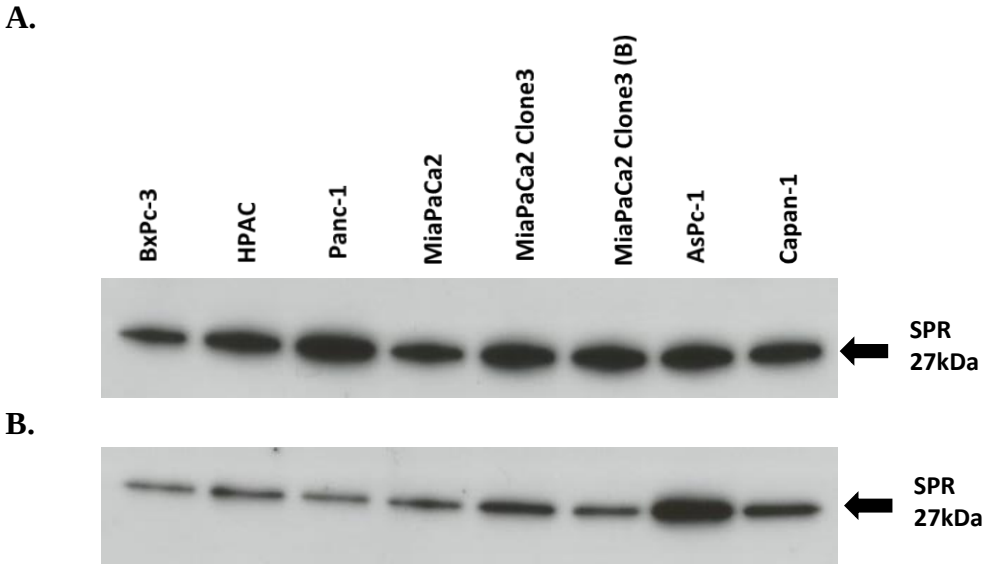

Figure 3.3-11:- Western blot analysis of SPR in pancreatic cancer cell lines.
Representative immunoblot showing expression of SPR in; BxPc-3, HPAC, Panc-1, MiaPaCa2, MiaPaCa2 clone3, and clone3 (B), AsPc-1 and Capan-1. SPR expression was examined in (a) whole cell lysates and (b) membrane enriched fractions, samples were separated by SDS-PAGE and probed with an antibody specific to SPR (n=1).

3.3.4 Expression of validated proteins in colon, glioma neuroblastoma and melanoma cell lines

Preliminary investigations were carried out to examine expression HDGF, ALCAM, INA and SPR in representative cell lines from colon, glioma, neuroblastoma and melanoma tumour types. The cell lines used are presented in Table 3.3-3 below.

Tumour type	Cell line
SW480	Primary colon
SW620	Metastatic colon
SNB-19	Glioma
SK-N-SH	Neuroblastoma
LOX IVMI	Melanoma

Table 3.3-3:- Colon, glioma, neuroblastoma and melanoma cell lines used for Western blot analysis.

Western blot analysis was used to examine the expression of HDGF, ALCAM, INA and SPR in whole cell lysates and/or membrane enriched fractions of the cell lines. Strong expression of HDGF was observed in the metastatic colon cancer cell line (SW620) versus the isogenic primary cell line (SW480) from the same patient, strong expression was also observed in glioma and melanoma cell lines (Figure 3.3-12). ALCAM expression was increased in glioma and melanoma, while expression of ALCAM appeared to be undetectable in both colon cancer cell lines (Figure 3.3-13).

Increased expression of INA was also observed in membrane enriched fractions of neuroblastoma compared to glioma (Figure 3.3-14), while whole cell lysates indicate increased expression of SPR in glioma compared to neuroblastoma (Figure 3.3-15).

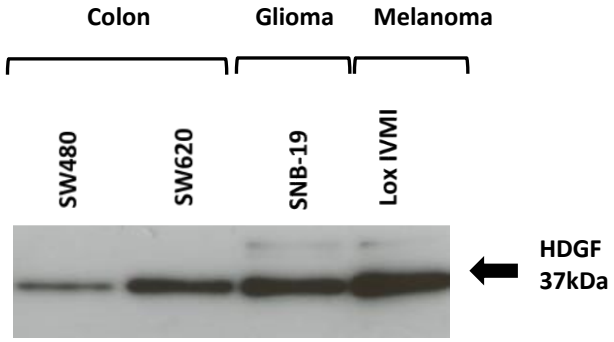

Figure 3.3-12:- Western blot analysis of HDGF in colon, glioma and melanoma cell lines. Representative immunoblot showing expression of HDGF in; colon (SW480 and SW620), glioma (SNB-19) and melanoma (Lox) cell lines. HDGF expression appears to be increased in the metastatic colon cell line (SW620) compared the primary colon (SW480), samples were separated by SDS-PAGE and probed with an antibody specific to HDGF (n=1).

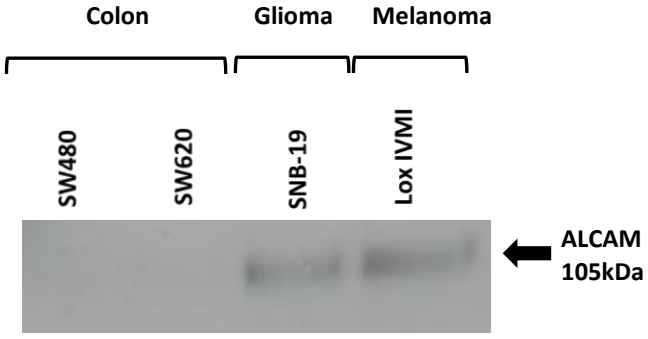

Figure 3.3-13:- Western blot analysis of ALCAM in colon, glioma and melanoma cell lines. Representative immunoblot showing expression of ALCAM in; colon (SW480 and SW620), glioma (SNB-19) and melanoma (Lox) cell lines. Low expression of ALCAM was observed in glioma and melanoma cell lines, samples were separated by SDS-PAGE and probed with an antibody specific to ALCAM (n=1).

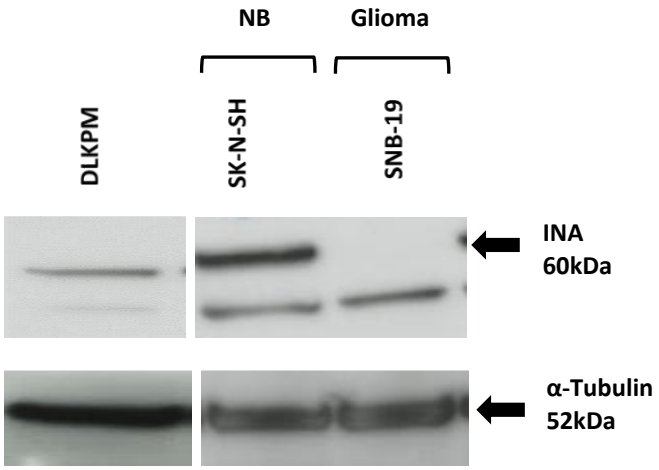

Figure 3.3-14:- Western blot analysis of INA in neuroblastoma and glioma cell lines.
Representative immunoblot showing expression of INA in neuroblastoma (SK-N-SH) and glioma (SNB-19). Increased expression of INA is observed in the neuroblastoma cell line *vs.* glioma, samples were separated by SDS-PAGE and probed with an antibody specific to INA. Increased expression of INA is observed in SK-N-SH (n=1).

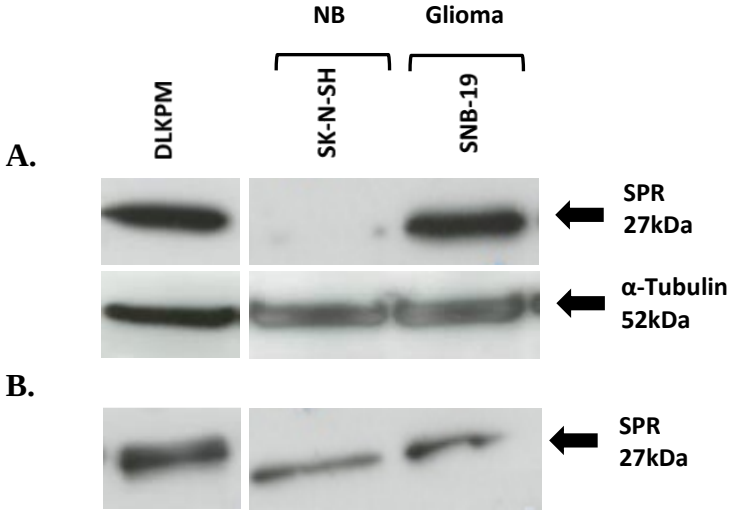

Figure 3.3-15:- Western blot analysis of SPR in neuroblastoma and glioma cell lines.
Representative immunoblot showing expression of SPR in neuroblastoma (SK-N-SH) and glioma (SNB-19). SPR expression was examined in; (a) whole cell lysates and (b) membrane enriched fractions, samples were separated by SDS-PAGE and probed with an antibody specific to INA. Increased expression of SPR was observed in SNB-19 *vs.* SK-N-SH cell line (n=1).

3.3.5 Summary of immunoreactivity in DLKP Cell lines and Human cancer cell lines

- HDGF, SLIT2, ALCAM, INA and SPR were examined for their expression in a representative panel of lung cancer cell lines. Expression of all proteins was found in all subtypes, the SCLC subtype displayed the strongest expression of each protein target.
- HDGF, INA and SPR were examined for their expression in a representative panel of TNBC cell lines. Expression of these protein targets was found in all of the cell lines used in this panel. However, INA appeared to show strong expression in a small number of the TNBC cell lines used, but absent in the remaining cell lines on the panel.
- Strong expression of HDGF and SPR was observed in a representative panel of pancreatic cancer cell lines. HDGF expression was decreased in the invasive MiaPaCa2 clone 3 *vs.* MiaPaCa2 parent, but also in the metastatic colon cell line (SW480) compared to the primary (SW620). SPR expression was increased in MiaPaCa2 clone3 *vs.* MiaPaCa2 parent but was highest in the AsPc-1 (a cell line established from an ascites). Both proteins should be investigated further as having a potential association with cancer invasion.

3.4 Functional analysis of target proteins by siRNA knockdown

Differentially expressed protein targets were chosen based on comparative proteomic analysis of DLKP, DLKPSQ, DLKPI and DLKPM cell lines. Conditions were optimised in 6-well plates (see section 2.7.1) using a positive control (Kinesin (Ambion) or Cell Death (Qiagen) and a negative control (scrambled-2 siRNA (Ambion) or negative control siRNA (Qiagen)). Un-transfected cells (Control) and NeoFX or lipofectamine (Lipo) were also included in all sets of transfections as further controls.

Three protein targets were chosen to investigate their functional roles in DLKP; (i) Activated leukocyte cell adhesion molecule (ALCAM), (ii) α-Internexin (INA) and (ii) Sepiapterin Reductase (SPR) and were all shown to be expressed in DLKP and its clones (see section 3.2). These three proteins were considered for follow up functional studies based on their expression profile in the DLKP cell line model and whether they could be used as potential markers for any of the clones. Other considerations included the availability of commercially produced siRNAs (ALCAM (Ambion^{Inc}, 4392420), INA (Qiagen, GC9118) and SPR (Qiagen, GS6697), a suitable antibody for evaluation by Western blot analysis and on their novelty.

Seventy-two hours post transfection:

- Western blot analysis (see section 2.3) was performed to confirm knockdown of each protein, whole cell lysates were prepared and separated by SDS-PAGE and analysed using specific antibodies targeted at each protein.
- Acid-phosphatase assays (see section 2.5) were carried out on transfected cells to assess the impact of a specific protein knockdown on growth.
- Invasion assays (see section 2.4.1) were carried out on transfected cells to investigate if the proteins play a functional role in invasion.
- Migration assays (see section 2.4.2) were carried out on transfected cells to investigate if the proteins play a functional role in migration.

3.4.1 Investigation into the role of ALCAM in lung cancer

The comparative proteomic analysis identified ALCAM to be differentially expressed between DLKPSQ, DLKPI and DLKPM, highest ALCAM expression was observed in DLKPI. The analysis showed that ALCAM was increased by ~30-fold when compared to DLKP, DLKPSQ and DLKPM. Expression of ALCAM was confirmed by Immunofluorescence, Western blot analysis and Immunocytochemistry in section 3.2.4. Three cell lines were chosen to investigate a functional role for ALCAM in lung cancer (i) DLKPSQ-Mitox-BCRP-6P, (ii) DLKPM and (iii) DLKPI.

3.4.1.1 Effect of siRNA knockdown of ALCAM on DLKPSQ-Mitox-BCRP-6P

DLKPSQ-Mitox-BCRP-6P is an invasive drug resistant variant of DLKPSQ. DLKPSQ-Mitox-BCRP-6P was chosen for ALCAM knockdown studies because this cell line was previously shown to exhibit an increased invasive capacity and increased expression of ALCAM compared to the parental DLKPSQ cell line [96]. Figure 3.4-1 (a) shows by Western blot analysis, the efficient knockdown of ALCAM in one of two siRNAs used to transfect DLKPSQ-Mitox-BCRP-6P cells compared to negative control and un-transfected cells.

Seventy-two hours post-transfection with ALCAM siRNAs, invasion assays were performed. The total number of cells invading was increased in DLKPSQ-Mitox-BCRP-6P cells transfected with ALCAM siRNAs. Figure 3.4-2 (a) shows representative images of invading cells and (b) the total number of invading cells post siRNA transfection. ALCAM siRNA transfection increased the invasion capabilities of the cells. Invasion was increased by 55% (p=0.0563) with ALCAM-1 and a significant increase 111% (p=0.0040) for ALCAM-2, when compared to negative control. This significant increase in the invasive ability was a surprising result as a reduction was expected following ALCAM knockdown.

(a)

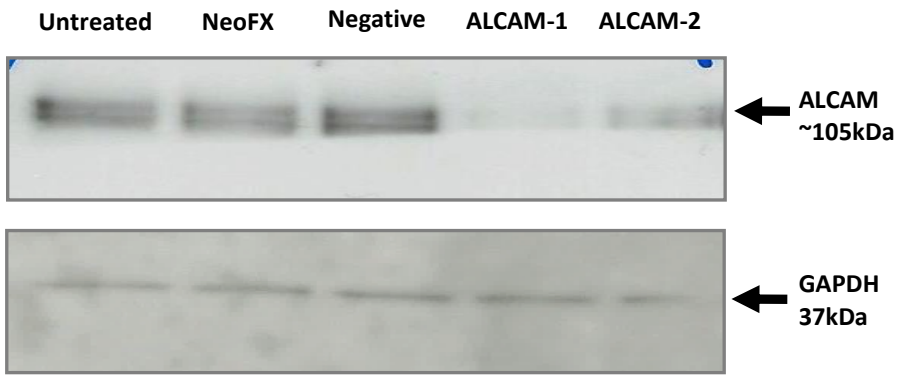

(b)

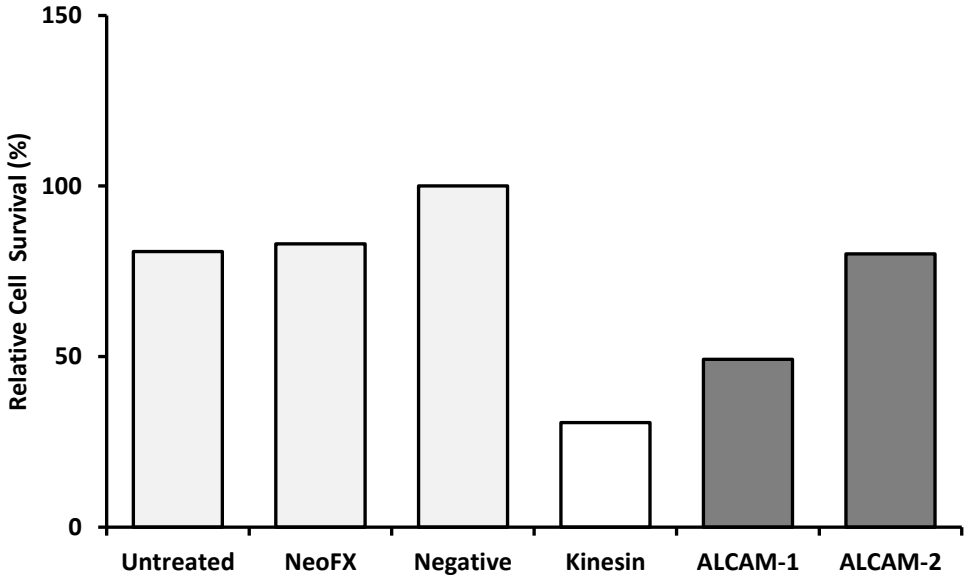

Figure 3.4-1:- ALCAM knockdown reduced cell growth of DLKPSQ-mitox-BCRP-6P.
(a) Representative immunoblot showing efficient knockdown of ALCAM 72hrs post-transfection in DLKPSQ-Mitox-BCRP-6P cells transfected with two independent siRNAs targeting ALCAM relative to negative control siRNA transfected cells (GAPDH served as a loading control). **(b)** Proliferation assays on siRNA transfected DLKPSQ-mitox-BCRP-6P cells targeting ALCAM. Results graphed as % cell survival relative to negative control siRNA in a single experiment (n=1).

(a)

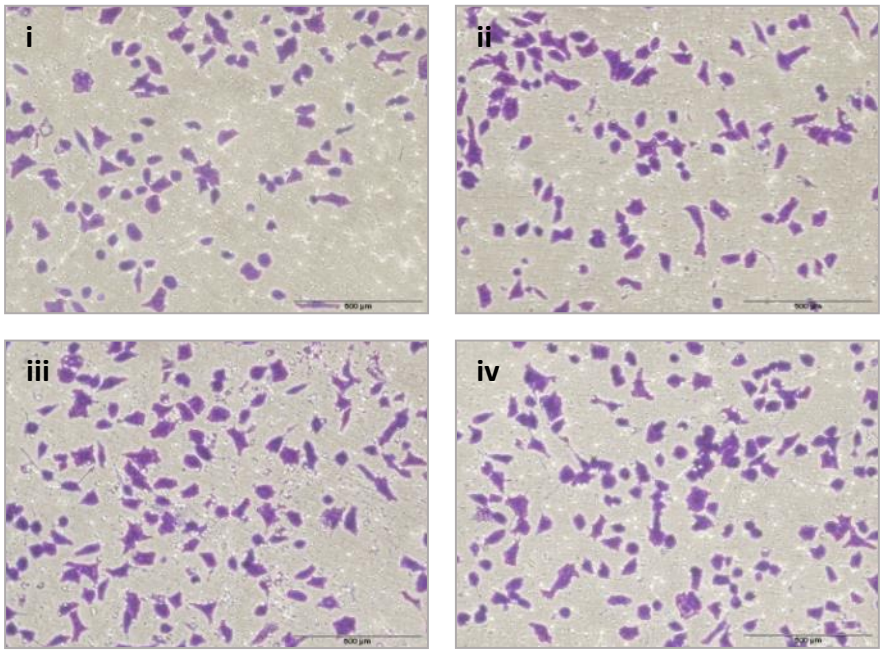

(b)

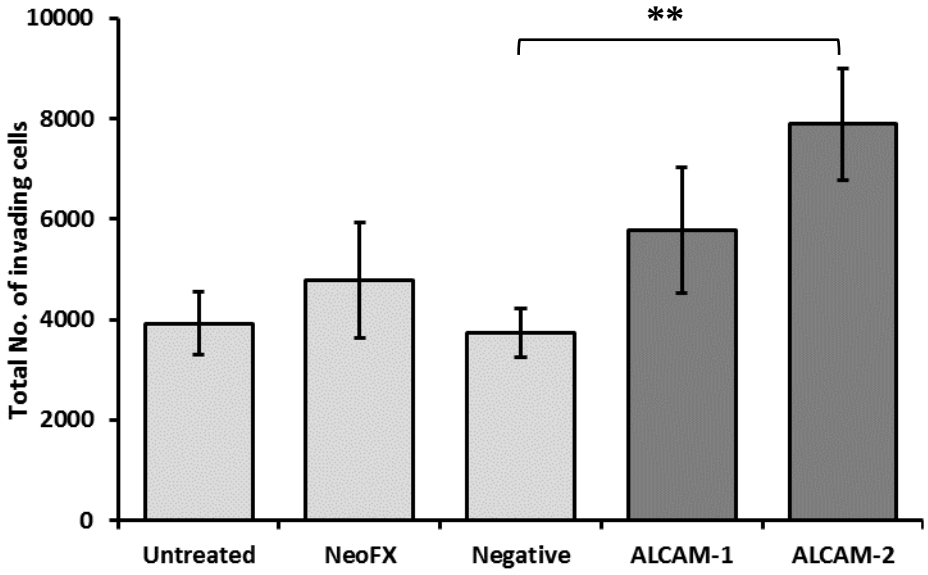

Figure 3.4-2:- ALCAM increases the invasive capacity of DLKPSQ-mitox-BCRP-6P.
(a) Invasion assays of DLKPSQ-Mitox-BCRP-6P cells (i) Untreated control (ii) Negative control (iii) ALCAM-1 siRNA and (iv) ALCAM-2 siRNA (Magnification, x100; *scale bar* = 500µm) **(b)** Histogram showing an increase in the total number of invading DLKPSQ-mitox-BCRP-6P cells post siRNA transfection targeting ALCAM. Data plotted represents the mean ± standard deviation of duplicate trans-well inserts from triplicate biological assays. Statistics $^{**}p \leq 0.01$ and compared with negative control siRNA. Student's *t* test (two-tailed with equal variance, unpaired (n=3)).

3.4.1.2 Effect of siRNA knockdown of ALCAM on DLKPM

Western blot analysis (Figure 3.4-3 (a)) shows the efficient knockdown of ALCAM in DLKPM cells transfected with two siRNAs, compared to negative control and un-transfected cells. Proliferation assays (Figure 3.4-3 (b)) showed a slight reduction in growth in ALCAM-1 siRNA (p= 0.023) and no effect using ALCAM-2. The effect seen on growth using ALCAM-1 could be as a result of an off target effect.

Seventy-two hours post-transfection with ALCAM siRNAs; Western blot analysis and invasion assays were performed. The total number of cells invading was reduced in DLKPM cells transfected with ALCAM siRNAs. Figure 3.4-4 (a) shows representative images of invading cells and (b) shows the total number of invading cells following siRNA knockdown. ALCAM siRNA transfection reduced the invasion capabilities of the cells. Invasion was significantly decreased using ALCAM-1 (p=0.05) by 19% and 51% (p=0.004) for ALCAM-2, when compared to negative control.

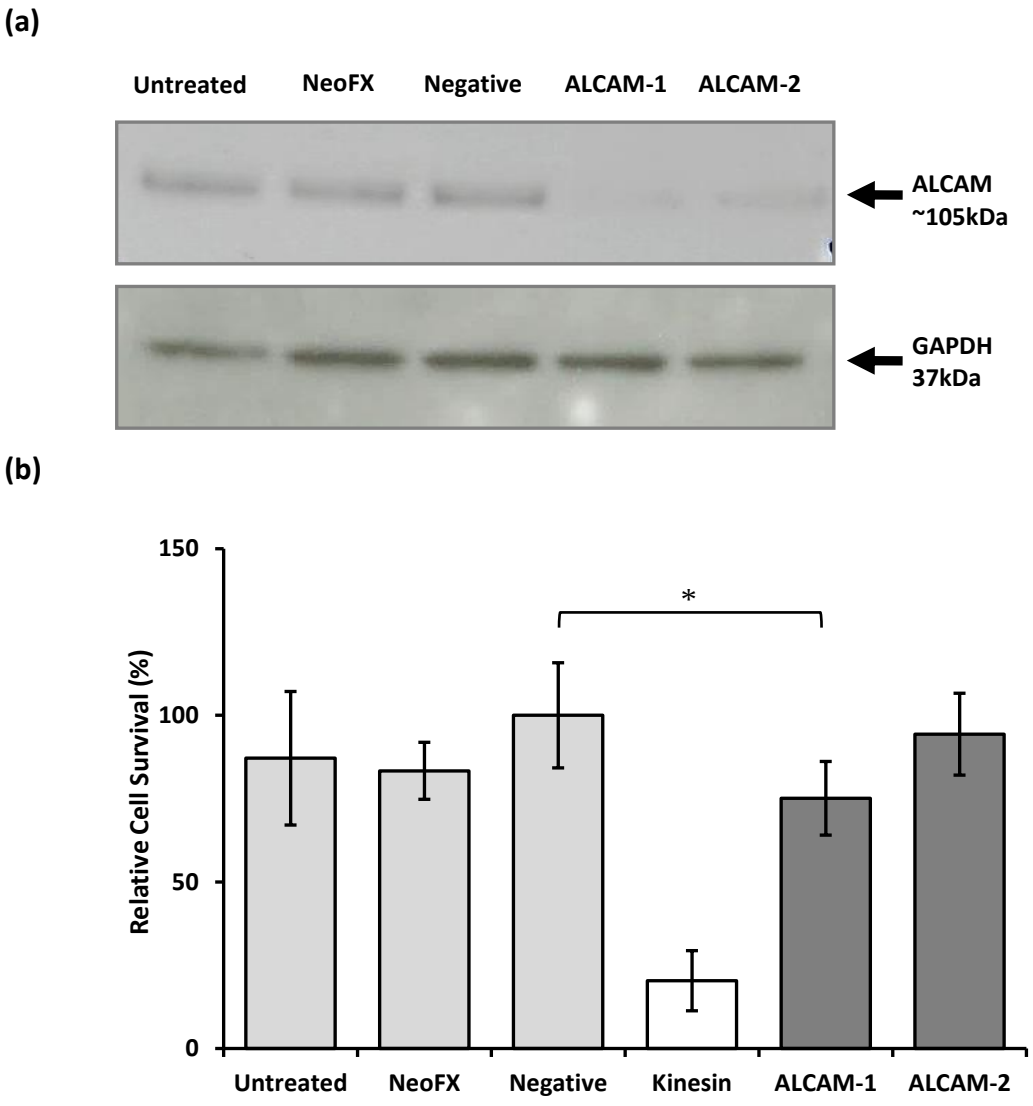

Figure 3.4-3:- ALCAM knockdown shows no effect on cell growth of DLKPM.
(a) Representative immunoblot showing knockdown of ALCAM 72hrs post-transfection in DLKPM cells transfected with two independent siRNAs targeting ALCAM relative to negative control siRNA transfected cells (GAPDH served as a loading control). **(b)** Proliferation assays showing the effect of ALCAM on DLKPM cells targeting ALCAM. Results graphed as % cell survival relative to negative control siRNA. Data plotted represents the mean ± standard deviation of from triplicate biological assays. Statistics *$p \leq 0.05$ compared with negative control siRNA. Student's *t* test (two-tailed with equal variance, unpaired (n=3)).

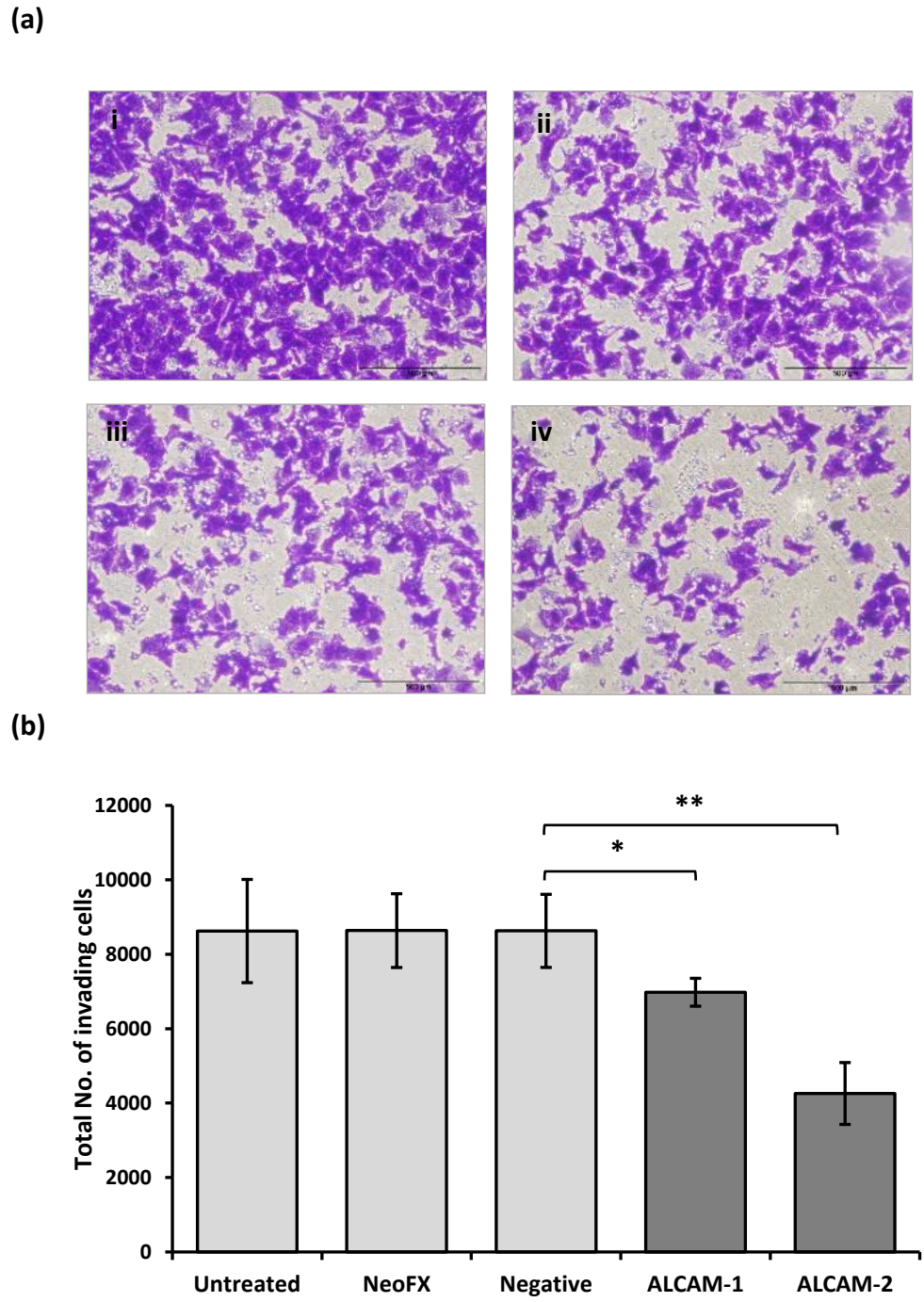

Figure 3.4-4:- ALCAM decreases the invasive capacity of DLKPM cells.
(a) Invasion assays of DLKPM cells (i) Untreated control (ii) Negative control (iii) ALCAM-1 siRNA and (iv) ALCAM-2 siRNA, (Magnification, x100; *scale bar* = 500µm). **(b)** Histogram showing a reduction in the total number of invading DLKPM cells following transfection targeting ALCAM. Data plotted represent the mean ± standard deviation of duplicate transwell inserts from triplicate biological assays. Statistics *$p \leq 0.05$ and **$p \leq 0.01$ compared with negative control siRNA. Student's *t* test (two-tailed with equal variance, unpaired (n=3)).

3.4.1.3 Effect of siRNA knockdown of ALCAM on DLKPI

Western blot analysis (Figure 3.4-5 (a)) shows a partial knockdown of ALCAM in DLKPI cells transfected with two siRNAs, compared to negative control and un-transfected cells. The partial knockdown achieved as a result of transfection of ALCAM in DLKPI may be due to the extremely high levels of ALCAM these cells. Proliferation assays (Figure 3.4-5(b)) shows a slight decrease in growth for DLKPI cells.

Seventy-two hours post-transfection with ALCAM siRNAs, invasion assays were performed. The total number of cells invading was increased slightly in DLKPI cells transfected with both ALCAM siRNAs. Figure 3.4-6 (a) shows representative images of invading cells and (b) shows the total number of invading cells following siRNA knockdown. No significant increase was observed for ALCAM transfected DLKPI cells using ALCAM-1 (p=0.079) and ALCAM-2 (p=0.057) siRNAs.

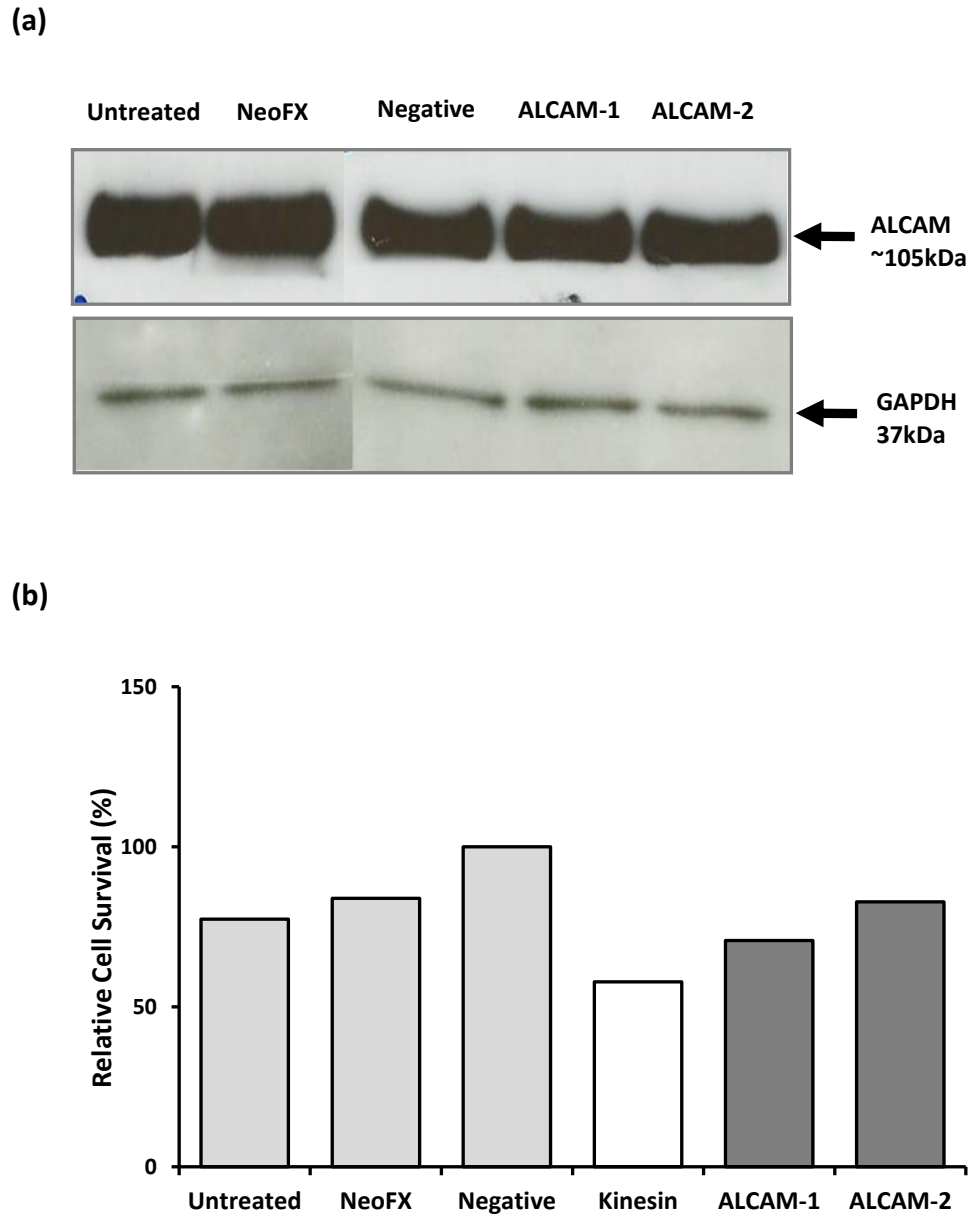

Figure 3.4-5:- ALCAM knockdown shows no effect of cell growth of DLKPI cells.
(a) Representative immunoblot showing a partial knockdown of ALCAM at 72hrs post-transfection in DLKPI cells transfected with two independent siRNAs targeting ALCAM (GAPDH served as a loading control). **(b)** Proliferation assays on siRNA transfected DLKPI cells indicate a slight reduction in monolayer cell growth. Results graphed as % cell survival relative to negative control siRNA in one experiment (n=1).

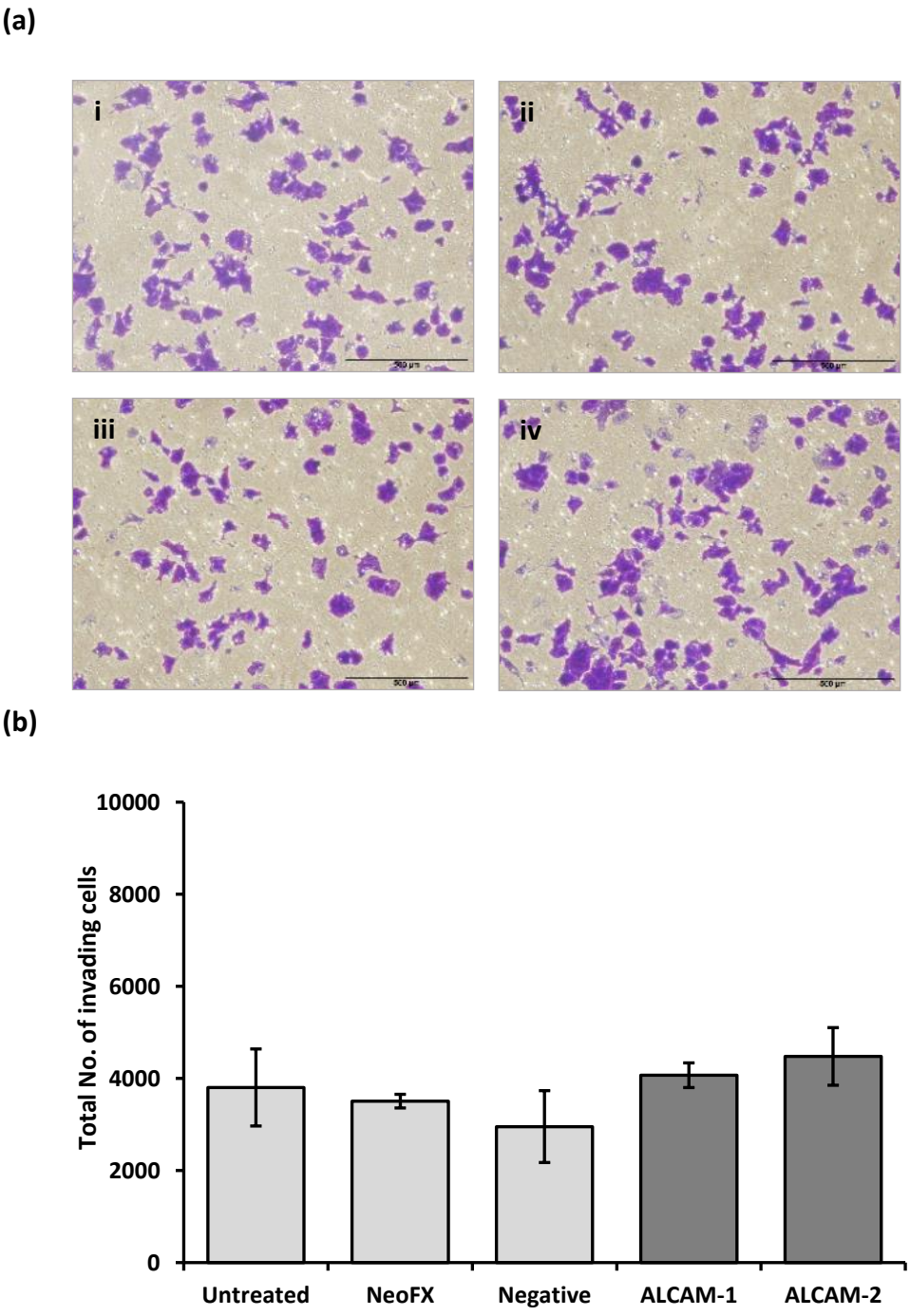

Figure 3.4-6:- ALCAM increases the invasive capacity of DLKPI cells.
(a) Invasion assays of DLKPI cells (i) Untreated control (ii) Negative control (iii) ALCAM-1 siRNA and (iv) ALCAM-2 siRNA, (Magnification, x100; *scale bar* = 500µm). **(b)** Histogram showing a slight increase in the total number of invading DLKPI cells following transfection. Data plotted represent the mean ± standard deviation of duplicate trans-well inserts from triplicate biological assays. Statistics *$p \leq 0.05$, **$p \leq 0.01$ and ***$p \leq 0.005$ compared with negative control siRNA. Student's *t* test (two-tailed with equal variance, unpaired (n=3)).

3.4.2 Investigation into the role of INA in lung cancer

As previously mentioned, DLKP was proposed to be classified as a variant small cell lung carcinoma (SCLC-V) or a non-small cell lung carcinoma with neuroendocrine differentiation (NSCLC-NE) [93]. Recently, α-Internexin (INA) was reported to have a novel association with pancreatic neuroendocrine tumour aggressiveness and prognosis. Unpublished work performed in our laboratory indicated expression of INA was increased in the lowly invasive DLKPSQ (~2.3-fold) compared to highly invasive DLKPM. INA expression was not previously reported in lung cancer but a novel association with pancreatic neuroendocrine cancer (PNETs) was previously reported [104]. INA was selected for follow up functional investigations into its role in the invasion process of DLKPSQ and DLKPM.

3.4.2.1 Effect of siRNA knockdown of INA on DLKPSQ

Figure 3.4-7 (a) shows by Western blot analysis, the efficient knockdown of INA in two siRNA transfected DLKPSQ cells compared to negative control and un-transfected cell. Negligible effect on growth was observed for DLKPSQ cells (Figure 3.4-7 (b)).

Seventy-two hours post-transfection with INA siRNAs, invasion and migration assays were performed. There was no change in the total number of invading and migrating DLKPSQ cells transfected with INA siRNAs. Figure 3.4-8 (a) shows representative images of invading cells and Figure 3.4-9 (a) shows representative images of migrating cells. Knockdown of INA using two siRNAs, INA-6 and INA-8, did not affect the invasive or migratory capacities of DLKPSQ cells when compared to negative control (Figure Figure 3.4-8 (b) and Figure 3.4-9 (b)). DLKPSQ is a lowly invasive cell line,

(a)

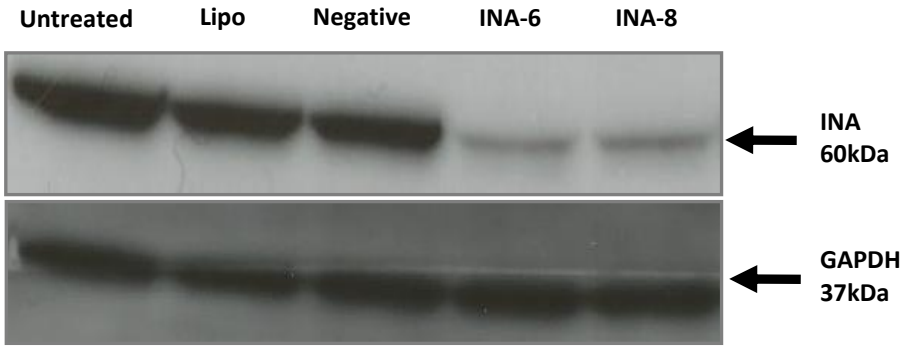

(b)

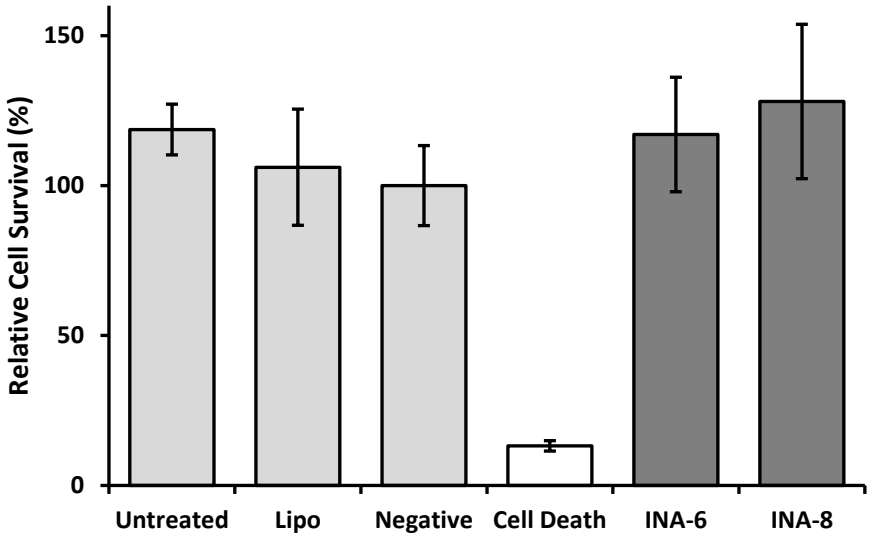

Figure 3.4-7:- INA knockdown does not affect cell growth of DLKPSQ.
(a) Representative immunoblot showing efficient knockdown of INA 72hrs post-transfection in DLKPSQ cells transfected with two independent siRNAs targeting INA relative to negative control siRNA transfected cells (GAPDH served as a loading control). **(b)** Proliferation assays on siRNA transfected DLKPSQ cells transfected targeting INA. Results graphed as % cell survival relative to negative control. Data plotted represents the mean ± standard deviation of duplicate biological assays (n=2).

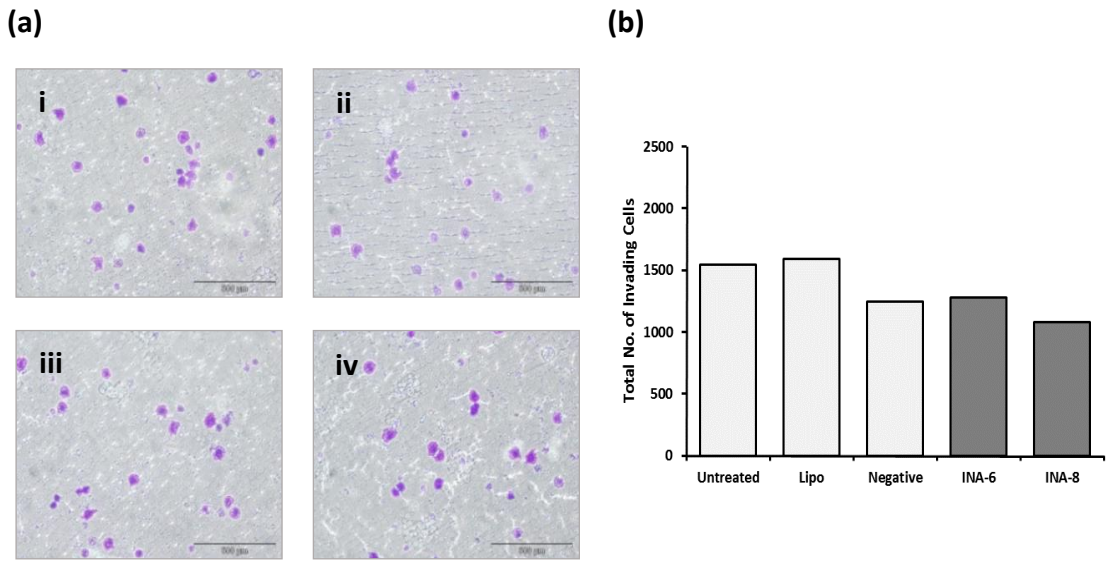

Figure 3.4-8:- INA knockdown does not affect invasion of DLKPSQ.
(a) Invasion assays of DLKPSQ cells (i) Untreated control, (ii) Negative control siRNA, (iii) INA-6 siRNA and (iv) INA-8 siRNA. (Magnification, x100; *scale bar* = 500µm). **(b)** Histogram showing the total number of invading DLKPSQ cells following transfection with siRNAs targeting INA. Data plotted represents the mean between two inserts from one single experiment (n=1).

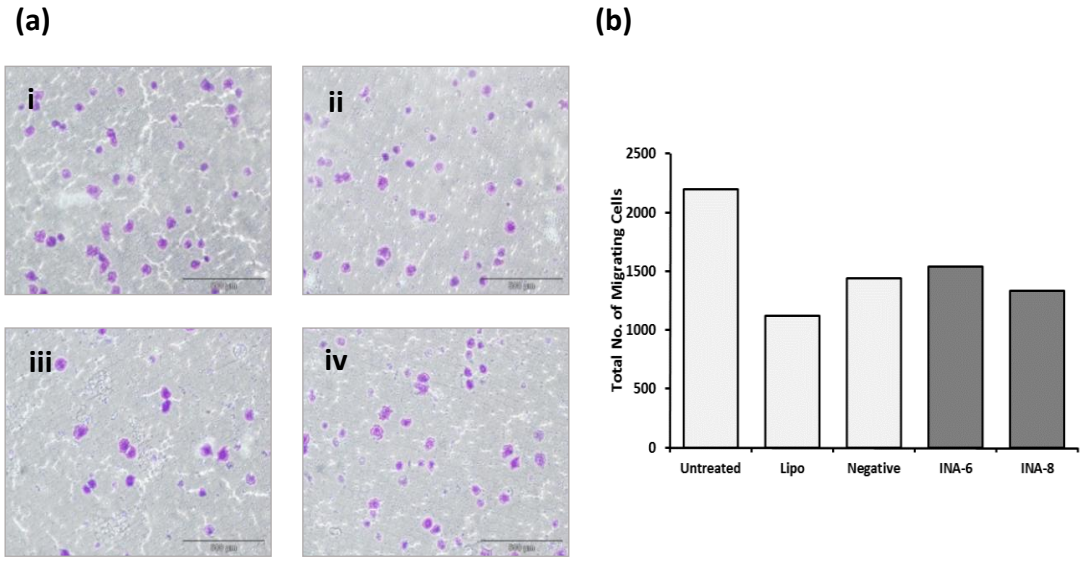

Figure 3.4-9:- INA knockdown does not affect migration of DLKPSQ.
(a) Migration assays of DLKPSQ cells (i) Untreated control, (ii) Negative control siRNA, (iii) INA-6 siRNA and (iv) INA-8 siRNA. (Magnification, x100; *scale bar* = 500µm). **(b)** Histogram showing the total number of migrating DLKPSQ cells following transfection with siRNAs targeting INA. Data plotted represents the mean between two inserts from one single experiment (n=1).

3.4.2.2 Effect of siRNA knockdown of INA on DLKPM

INA expression was shown to be expressed in DLKPM cells compared to DLKP and DLKPI. Its expression in DLKPM was marginally lower than DLKPSQ. Seventy-two hours' post-transfection with INA siRNAs, invasion and migration assays were performed using four siRNAs targeting INA.

The efficient knockdown of INA is shown in Figure 3.4-10, by Western blot analysis, with negligible effect on growth was observed for DLKPM cells (Figure 3.4-10). The morphology of DLKPM cells was also monitored and is shown in Figure 3.4-11, under control conditions (i) un-transfected, (ii) lipofectamine control and post transfection with four independent siRNAs targeting INA; (iii) INA-6, (iv) INA-7, (v) INA-8 and (vi) INA-9. The morphology of the cells after transfection using two siRNAs is obviously different. The cells are more elongated using INA-7 (iv), while using INA-9 (vi) the cells are notably shorter, in both cases cells were growing in a more isolated pattern, compared to the control (ii).

Invasion and migration assays were performed on INA transfected cells. Figure 3.4-12 (b) shows significantly reduced invasion capability of DLKPM cells following transfection with INA-7 (p=0.0021) and INA-9 (p=0.0015) siRNAs. A reduction in invasion was noted with INA-6 but did not show statistical significance (p=0.0662), while an increase was observed using INA-8 (p=0.07286). Figure 3.4-13 shows reduced migratory ability of DLKPM cells following transfection with INA-6 (n=3), INA7 (n=2), INA8 (n=3) and INA9 (n=2) siRNAs, however, the reduction did not prove significant. To investigate if reduction observed with INA7 and INA 9 was significant further biological replicates would need to be carried out.

(a)

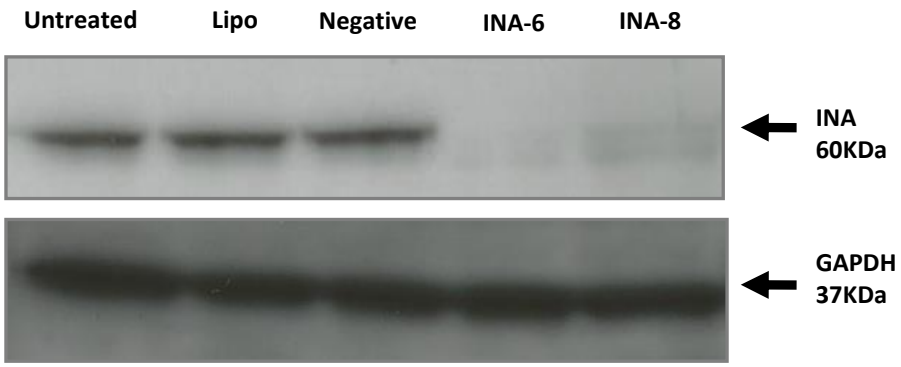

(b)

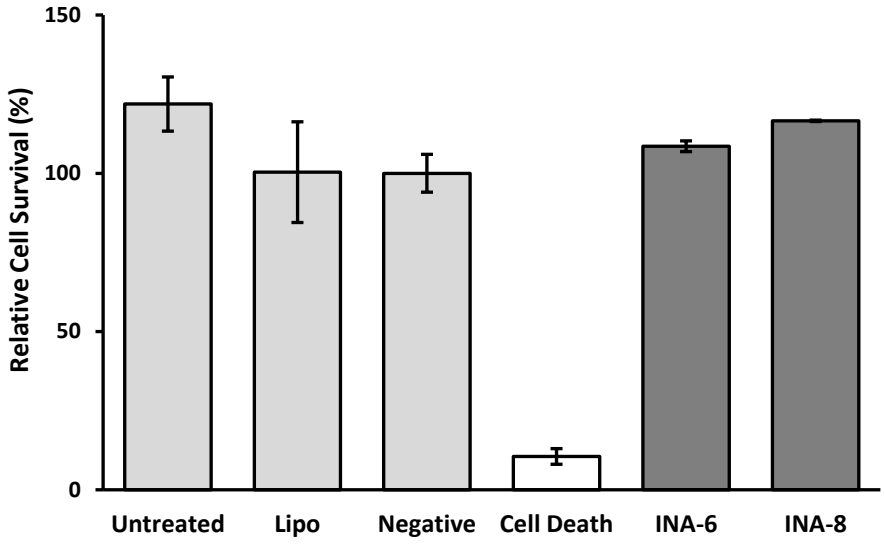

Figure 3.4-10:- INA knockdown has does not affect cell growth of DLKPM.
(a) Representative immunoblot showing efficient knockdown of INA in DLKPM 72hrs post-transfection with two independent siRNAs targeting INA (GAPDH served as a loading control). **(b)** Proliferation assays on siRNA transfected DLKPM cells targeting INA. Results graphed as % cell survival relative to negative control. Data plotted represents the mean ± standard deviation of duplicate biological assays (n=2).

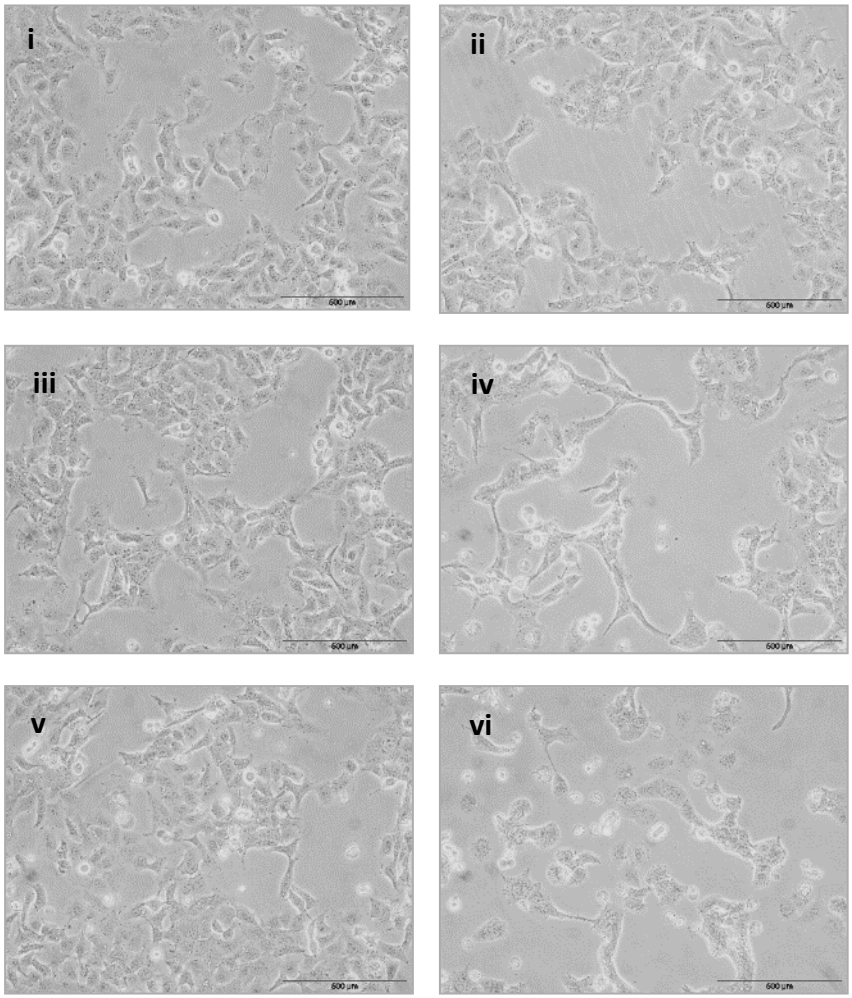

Figure 3.4-11:- Morphology of DLKPM cells following siRNA knockdown of INA.
(i) Untreated control, (ii) Negative control siRNA, (iii) INA-6 siRNA (iv) INA-7 siRNA (v) INA-8 siRNA and (vi) INA-9 siRNA, compared to negative control. (Magnification, x100; *scale bar* = 500µm).

(a)

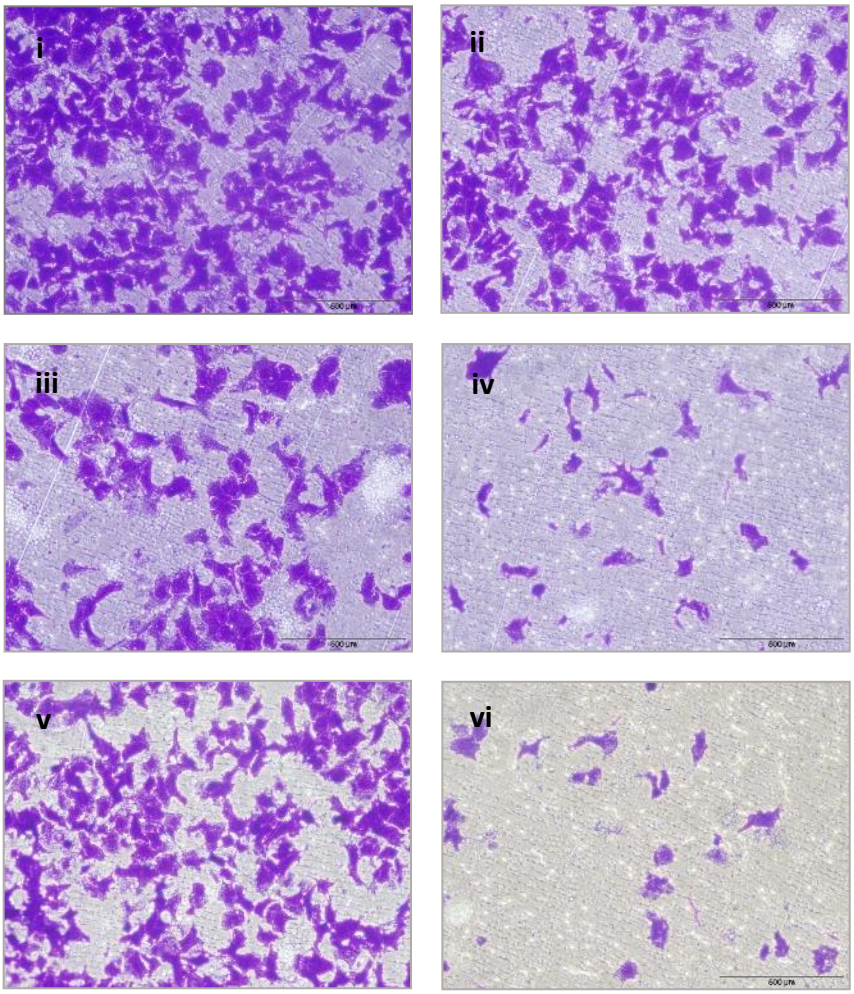

(b)

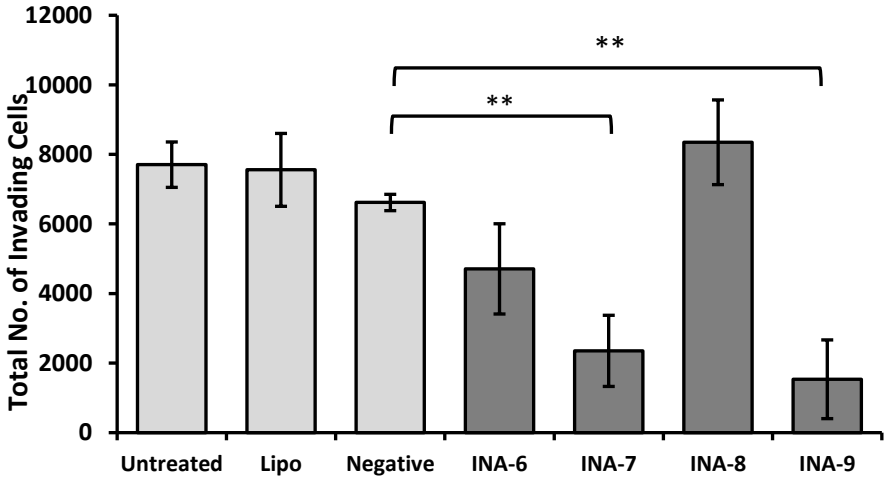

Figure 3.4-12:- INA knockdown decreases the invasive capacity of DLKPM cells.
(a) Invasion assays of DLKPM cells (i) Untreated control, (ii) Negative control siRNA, (iii) INA-6 siRNA (iv) INA-7 siRNA (v) INA-8 siRNA and (vi) INA-9 siRNA. (Magnification, x100; *scale bar* = 500µm). **(b)** Histogram showing a reduction in the total number of invading DLKPM cells following transfection with INA-6, INA-7 siRNA and INA-9 siRNAs, while an increase for INA-9. Data plotted represent the mean ± standard deviation of duplicate transwell inserts from triplicate biological assays. Statistics $^{**}p \leq 0.01$ and $^{***}p \leq 0.005$ compared with negative control siRNA. Student's *t* test (two-tailed with equal variance, unpaired, n=3).

(a)

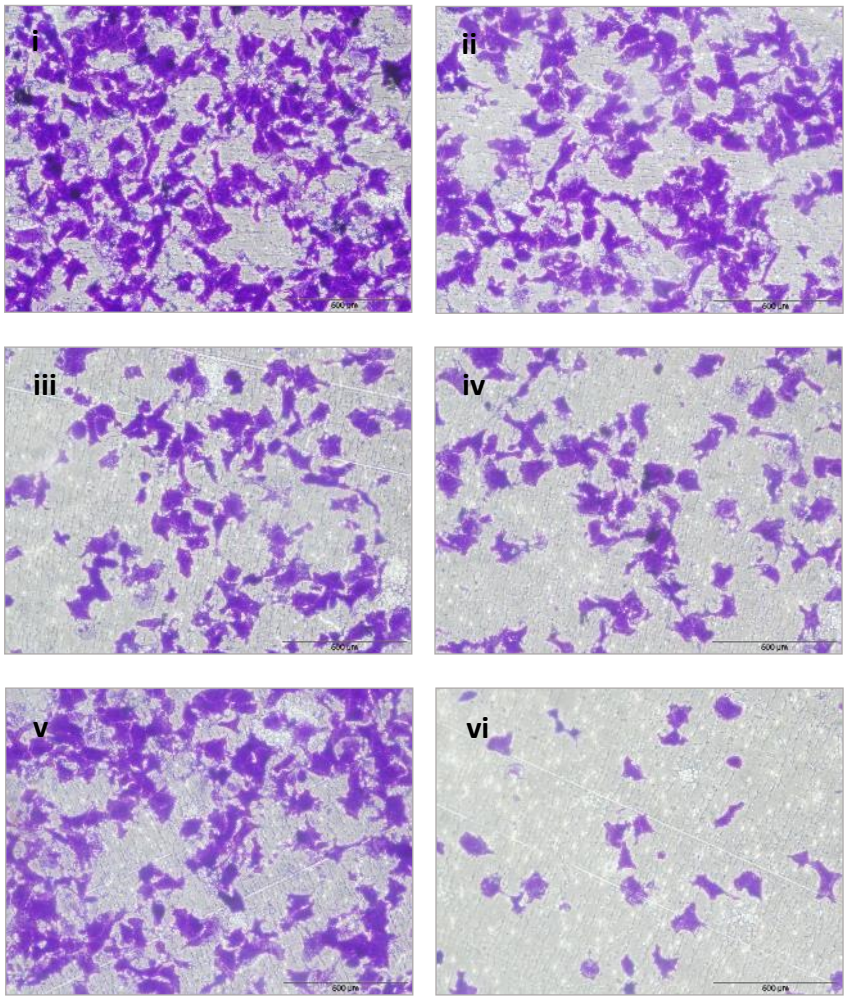

(b)

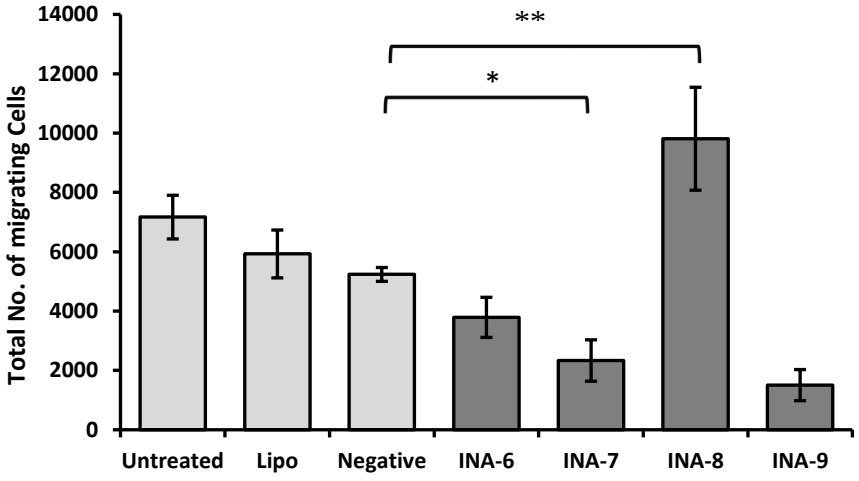

Figure 3.4-13:- INA knockdown decreases the migratory capacity of DLKPM.
(a) Migration assays of DLKPM cells (i) Untreated control, (ii) Negative control siRNA, (iii) INA-6 siRNA (iv) INA-7 siRNA (v) INA-8 siRNA and (vi) INA-9 siRNA. (Magnification, x100; *scale bar* = 500µm). **(b)** Histogram showing a reduction in the total number of migrating DLKPM cells following transfection with INA-6 siRNA, INA-7 and INA-9, an increase for INA-8 siRNA. Data plotted represent the mean ± standard deviation of duplicate transwell inserts from triplicate biological assays. Statistics *$p \leq 0.05$ compared with negative control siRNA. Student's *t* test (two-tailed with equal variance, unpaired, n=3).

3.4.3 Investigation into the role of SPR in DLKP clones

The comparative proteomic analysis identified sepiapterin reductase (SPR) to be differentially expressed in DLKPSQ compared to DLKPI. The analysis showed that expression of SPR was 4-fold highest in DLKPSQ compared to DLKPI (section 3.2.7). To date, there are no reports associating SPR and cancer invasion, so SPR was investigated further for potential functional roles in the invasion and migration processes of DLKPSQ and DLKPM.

3.4.3.1 Effect of siRNA knockdown of SPR in DLKPSQ

The efficient knockdown of SPR in two siRNA transfected DLKPSQ cells is shown in Figure 3.4-14, by Western blot analysis. A negligible effect was observed for cell growth compared to negative control and un-transfected cells. Seventy-two post-transfection with SPR siRNAs, invasion and migration assays were performed. There was a reduction in the total number of cells invading and migrating DLKPSQ cells transfected with SPR-6 siRNAs. Figure 3.4-15 (a) shows representative images of invading cells and Figure 3.4-16 (a) shows representative images of migrating cells. Knockdown of SPR using two siRNAs shows a reduction of invasion (Figure 3.4-15 (b) and migration (Figure 3.4-16 (b) using SPR-6 siRNA but not SPR-1, compared to the negative control siRNA. DLKPSQ is a lowly invasive cell line and it was unclear if this result represented an off target effect, it was decided to continue transfections in DLKPM cells.

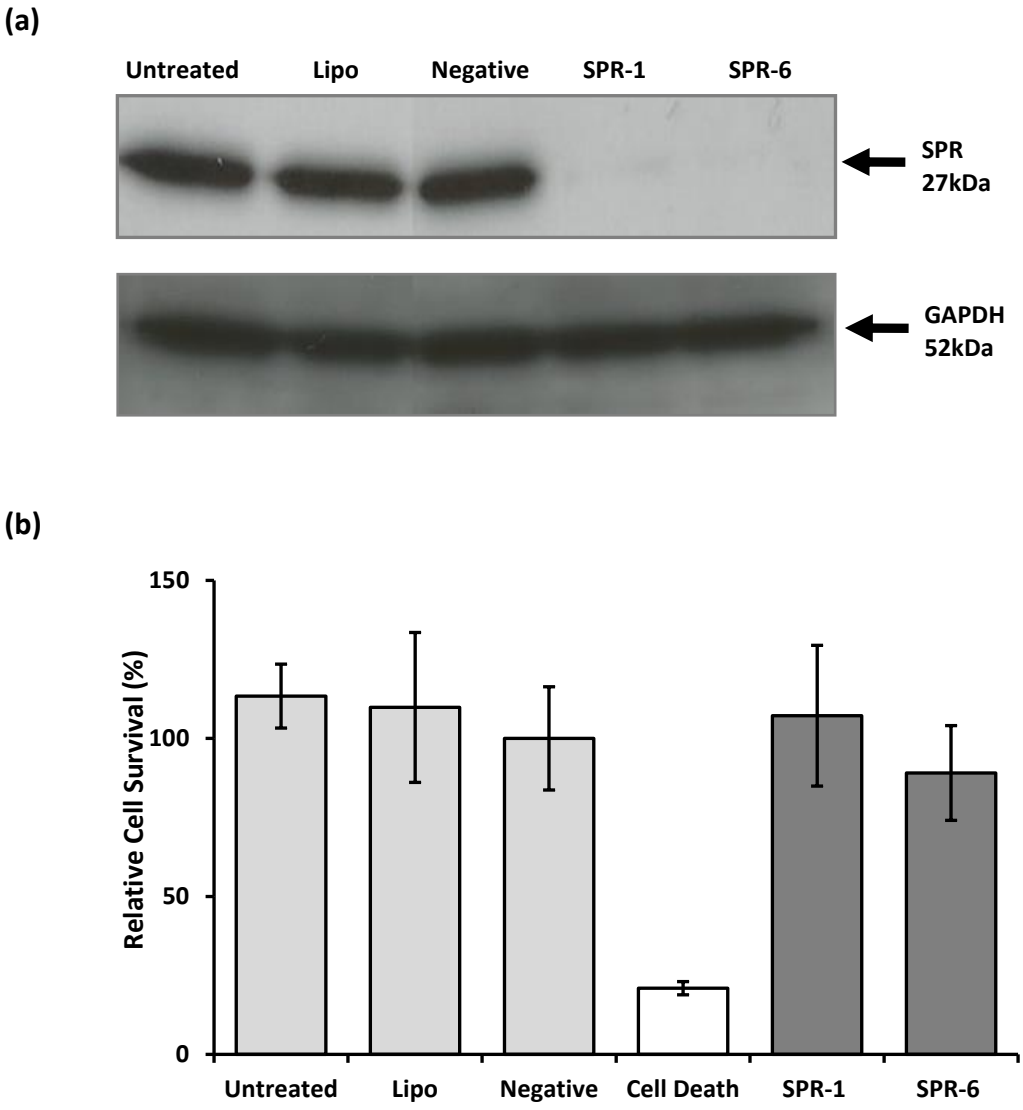

Figure 3.4-14:- SPR knockdown shows does not affect cell growth of DLKPSQ.
(a) Representative immunoblot showing efficient knowdown of SPR 72 hrs post-transfection in DLKPSQ cells transfected with two independent siRNAs targeting SPR, relative to negative control siRNA transfected cells (GAPDH served as a loading control). **(b)** Proliferation assays on siRNA transfected DLKPSQ cells targeting SPR. Results graphed as % cell survival relative to negative control in two independent biological experiments (n=2).

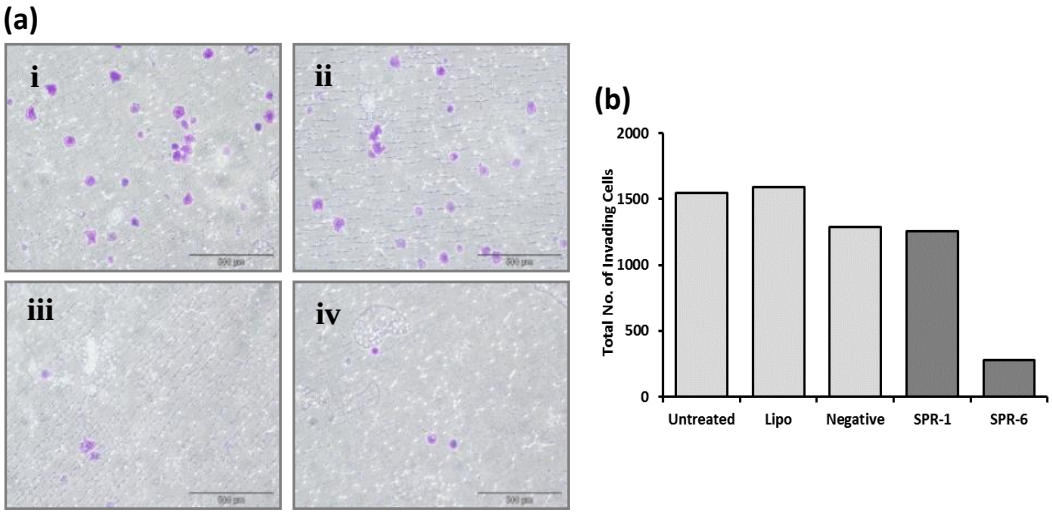

Figure 3.4-15:- SPR-6 siRNA potentially reduces the invasive capacity of DLKPSQ.
(a) Invasion assays of DLKPSQ cells (i) Untreated control, (ii) Negative control siRNA, (iii) SPR-1 siRNA, and (iv) SPR-6 siRNA (magnification, x100; *scale bar* = 500µm). **(b)** Histogram showing a reduction in the total number of invading DLKPSQ cells following transfection with SPR-6 siRNA. Data plotted represents the mean of duplicate trans-well inserts from two biological experiments (n=2).

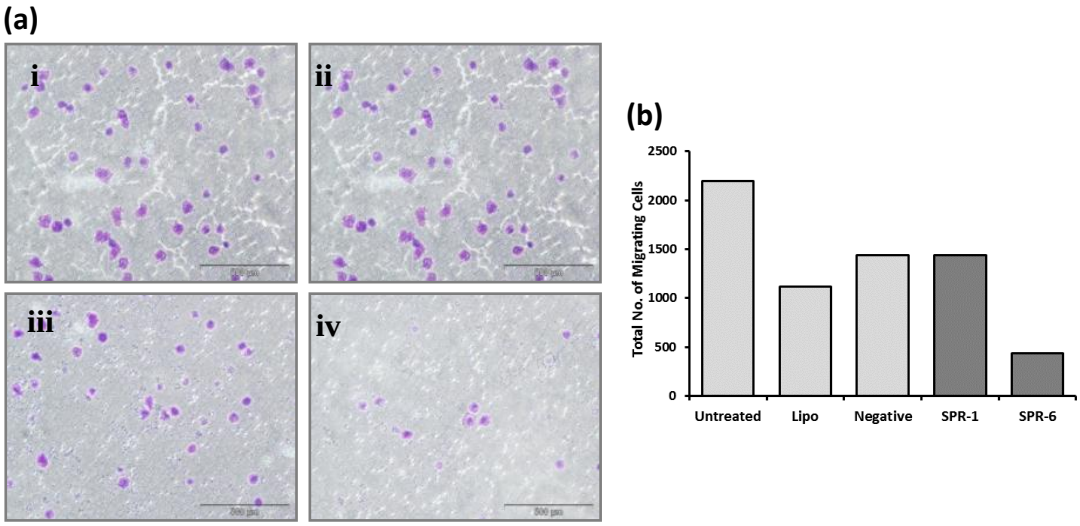

Figure 3.4-16:- SPR-6 siRNA potentially reduces the migratory capacity of DLKPSQ.
(a) Migration assays of DLKPSQ cells (i) Untreated control, (ii) Negative control siRNA, (iii) SPR-1 siRNA, and (iv) SPR-6 siRNA (magnification, x100; *scale bar* = 500µm). **(b)** Histogram showing a reduction in the total number of migrating DLKPSQ cells following transfection with SPR-6 siRNA. Data plotted represents the mean of duplicate trans-well inserts from two biological experiments (n=2).

3.4.3.2 Effect of siRNA knockdown of SPR in DLKPM

The efficient knockdown of SPR in DLKPM is shown in Figure 3.4-17 by Western blot analysis using four independent siRNAs (SPR-1, SPR-2, SPR-5 and SPR-6). The effect on proliferation (b) using SPR-1, SPR-2, SPR-5 was negligible, however, a significant effect on proliferation was observed using SPR-6 (p=0.0158) when compared to negative control.

Seventy-two hours post-transfection with SPR siRNAs, invasion and migration assays were performed. SPR siRNA transfection reduced invasive and migratory abilities of DLKPM cells. Figure 3.4-18, shows (a) representative images of invading cells and (b) shows highlights the total number of invading cells. Invasion was significantly reduced by 71% with SPR-1 (p=0.0031) and 81% with SPR-6 (p=0.0014) siRNAs. Figure 3.4-19 shows (a) representative images of migrating cells and (b) shows highlights the total number of migrating cells. Migration was reduced by 78% with SPR-1 (p=0.0054) and 80% with SPR-6 (p=0.0048) siRNAs when compared to the negative control siRNA. Huge variability was observed using SPR-2 and SPR-5 siRNAs.

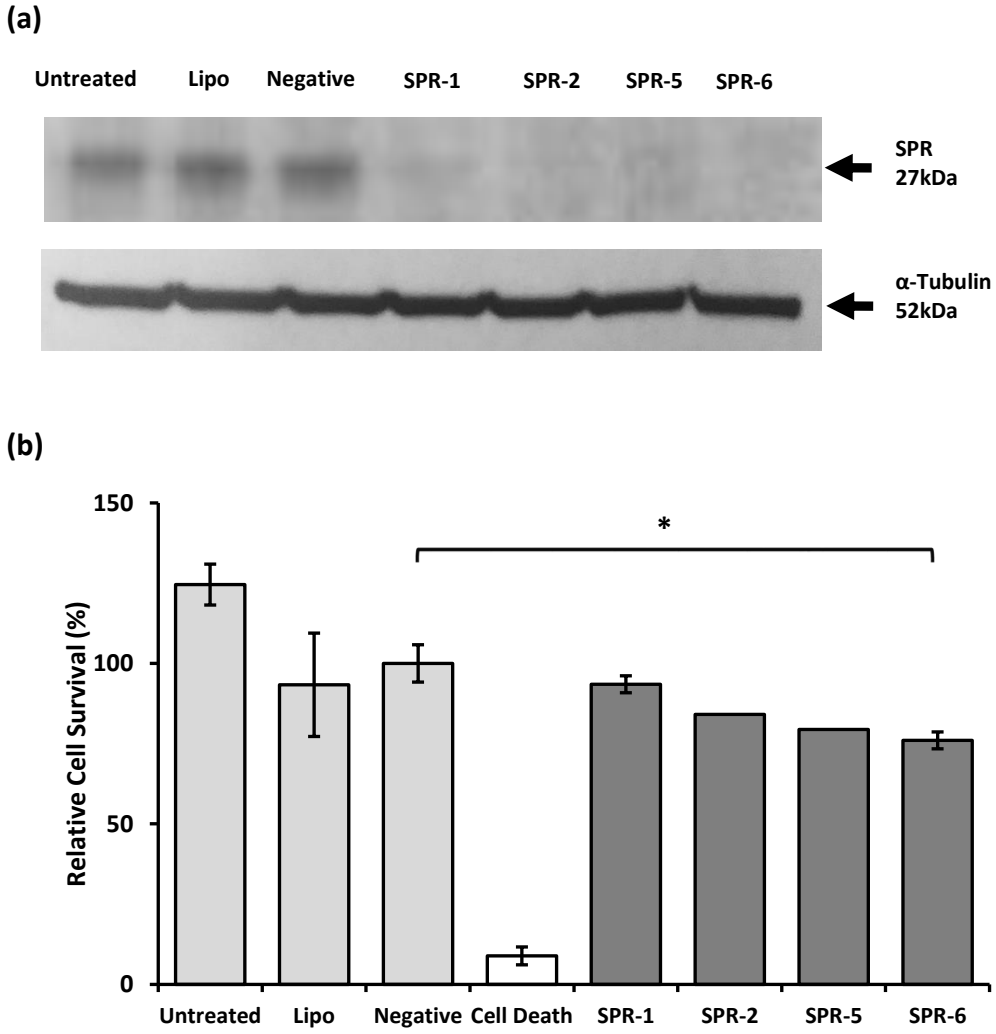

Figure 3.4-17:- SPR-6 siRNA reduces cell growth of DLKPM.
(a) Representative Immunoblot showing efficient knockdown of SPR 72hrs post-transfection in DLKPM cells transfected with four independent siRNAs targeting SPR relative to negative control siRNA transfected cells (α-Tubulin served as a loading control). **(b)** Proliferation assays carried out on siRNA transfected DLKPM cells indicates a significant reduction in cell growth with SPR-6 siRNA (*p*-value 0.015859). Results graphed as % cell survival relative to negative control. Data plotted represents the mean +/- standard deviation of triplicate biological assays. Statistics *$p \leq 0.05$ compared with negative control siRNA. Student's *t* test (two tailed with equal variance, unpaired, n=3).

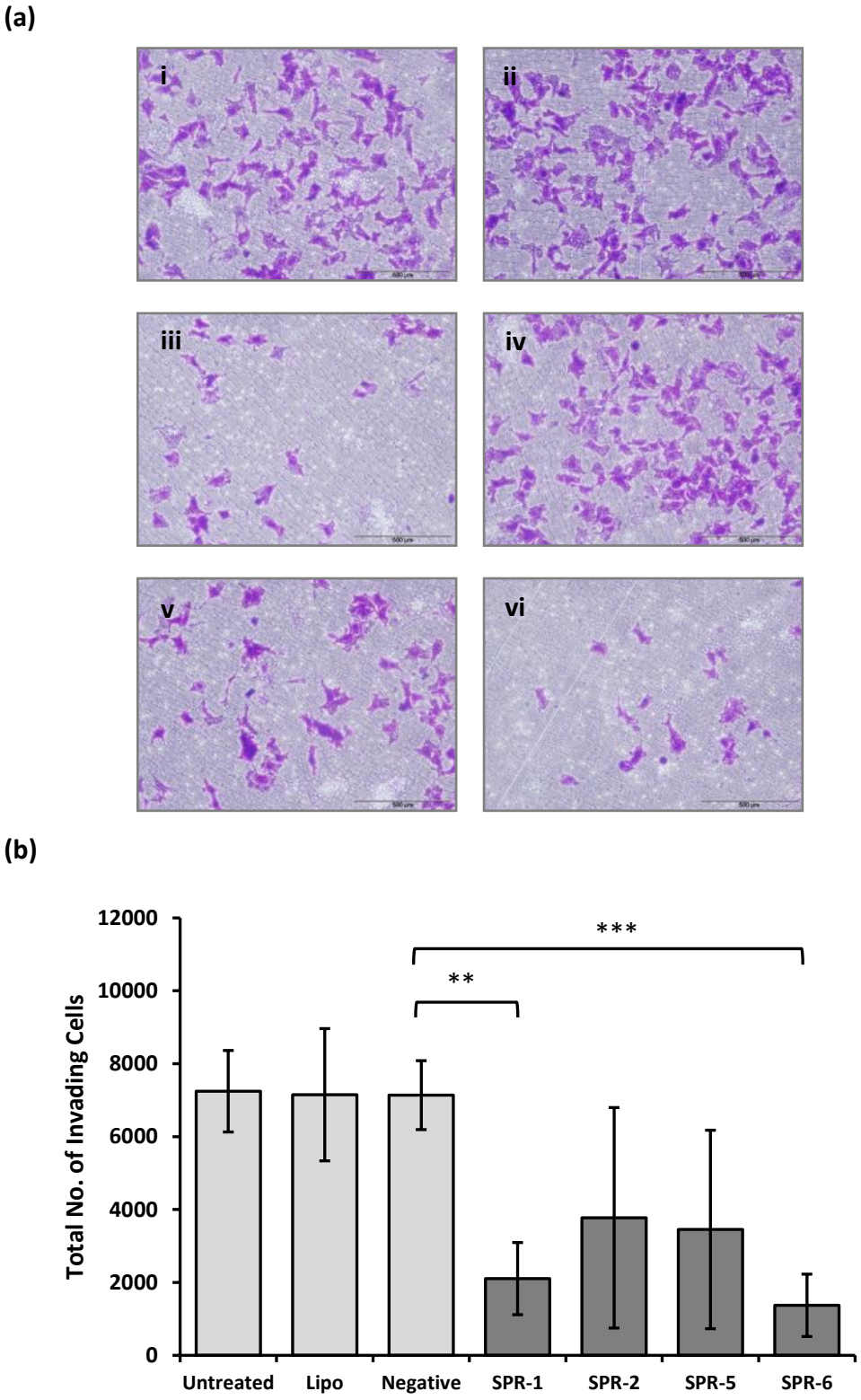

Figure 3.4-18:- SPR knockdown decreases the invasive capacity of DLKPM.
(a) Invasion assays of DLKPM cells (i) Untreated, (ii) Negative control siRNA, (iii) SPR-1 siRNA, (iv) SPR-2 siRNA, (v) SPR-5 siRNA and (vi) SPR-6 siRNA (magnification, x100; *scale bar* = 500µm). **(b)** Histogram showing a reduction in the total number of invading DLKPM cells following transfection with SPR-1 and SPR-6 siRNAs. Data plotted represents the mean ± standard deviation of duplicate trans-well inserts from triplicate biological assays. Statistics $^{**}p \leq 0.01$ and *** $p \leq 0.005$ compared with negative control siRNA. Student's *t* test (two tailed with equal variance, unpaired (n=3)).

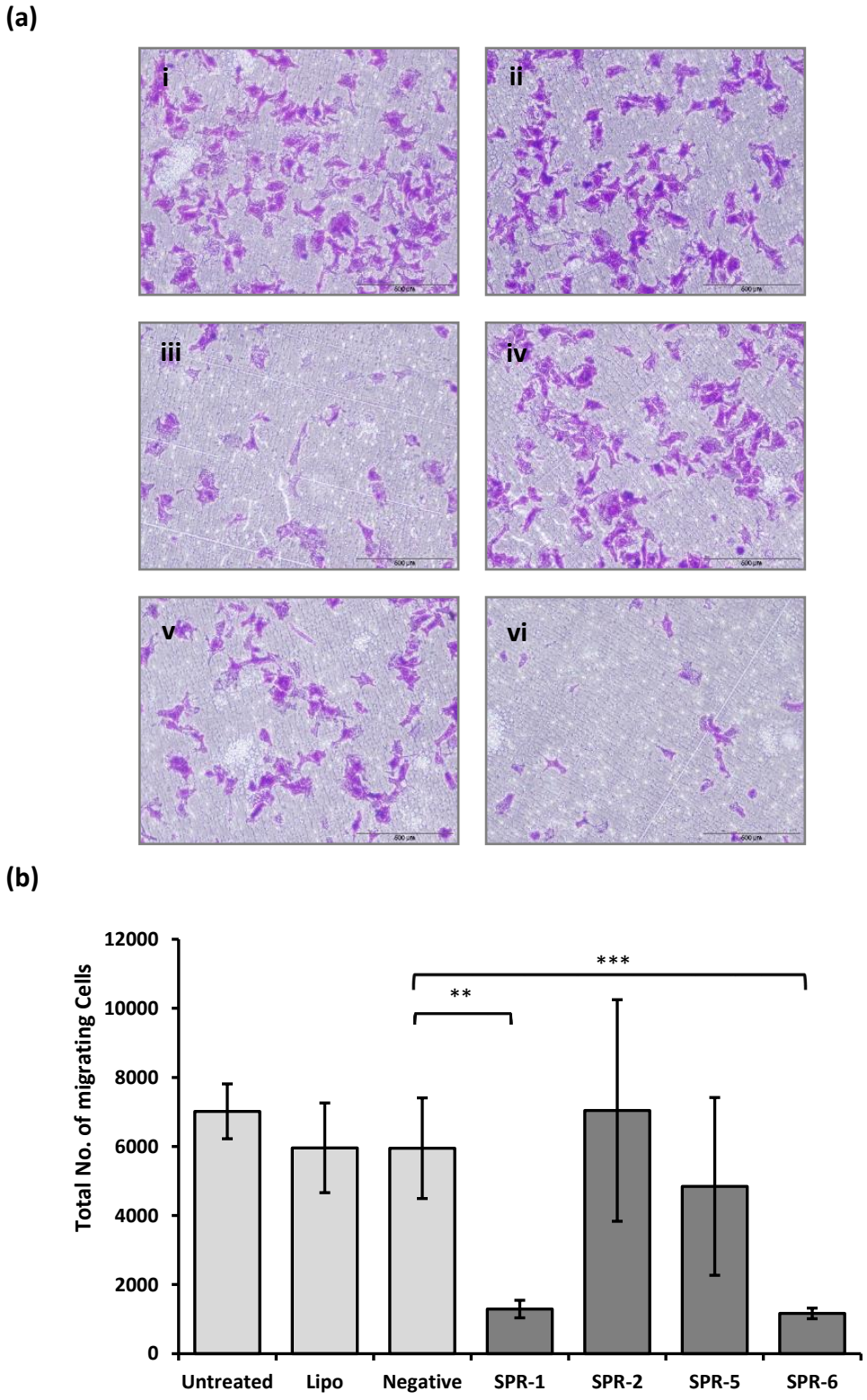

Figure 3.4-19:- SPR knockdown decreased the migratory capacity of DLKPM.
(a) Migration assays of DLKPM cells (i) Untreated, (ii) Negative control siRNA, (iii) SPR-1 siRNA, (iv) SPR-2 siRNA, (v) SPR-5 siRNA and (vi) SPR-6 siRNA (magnification, x100; *scale bar* = 500µm). **(b)** Histogram showing a reduction in the total number of migrating DLKPM cells following transfection with SPR-1 and SPR-6 siRNAs. Data plotted represents the mean ± standard deviation of duplicate trans-well inserts from triplicate biological assays. Statistics $**p \leq 0.01$ and $*** p \leq 0.005$ compared with negative control siRNA. Student's *t* test (two tailed with equal variance, unpaired (n=3)).

3.4.3.3 Investigation into the effect of ornithine decarboxylase on DLKPM

Polyamines are often elevated in cancer cells and tissues, compared to normal cells and tissues. D,L-α-difluoromethylornithine (DFMO) is an irreversible inhibitor of ornithine decarboxylase (ODC) which can be used to induce depletion of polyamines. In 2013, Lange *et al* identified SPR as a regulator of ODC enzyme activity and described a model in which SPR drives ODC-mediated malignant progression in Neuroblastoma (NB). In section 3.4.3, siRNA interference knockdown was used to investigate SPR in lung cancer cell lines. SPR was found to play a potential role in the invasion and migration processes of DLKPM. To investigate a role for ODC in the invasion process in DLKPM, the DFMO inhibitor was used to treat DLKPM cells prior to their addition to invasion assays. Various concentrations of DFMO were used to optimise conditions in 6-well plates, final concentrations of 2.5mM and 5mM of DFMO were used. Untreated cells were also included as controls.

Prior to testing the effects of the DFMO, the appropriate concentration range for each inhibitor was established with the aim of finding a concentration which caused approximately 10% cytotoxicity. Proliferation assays were carried out over 5 days to assess the impact of the various concentrations (1mM, 2.5mM and 5mM) of the DFMO inhibitor on DLKPM cells. In preliminary investigations, a reduction in cell growth of 47% and 40% was observed for DFMO at concentrations of 1mM and 2.5mM respectively, while a negligible effect was observed using 5mM DFMO, compared to untreated control cells. Therefore, an optimum concentration of between 2.5mM to 5mM of DFMO could be used for further assays (Figure 3.4-20 (a)); for the purpose of this investigation 2.5mM and 5mM was used.

To assess the impact of DFMO on DLKPM, cells were treated with 2.5mM and 5mM DFMO 30mins (co-treat) and 24hrs (pre-treat) prior to setting up invasion assays. In a preliminary investigation, co-treatment with 2.5mM DFMO resulted in a significant reduction of 27% (p=0.0412) in the invasion of DLKPM cells, a reduction was also observed following 24hr pre-treatment. A modest reduction in invasion was observed for 5mM DFMO when compared to untreated control (Figure 3.4-20 (b)).

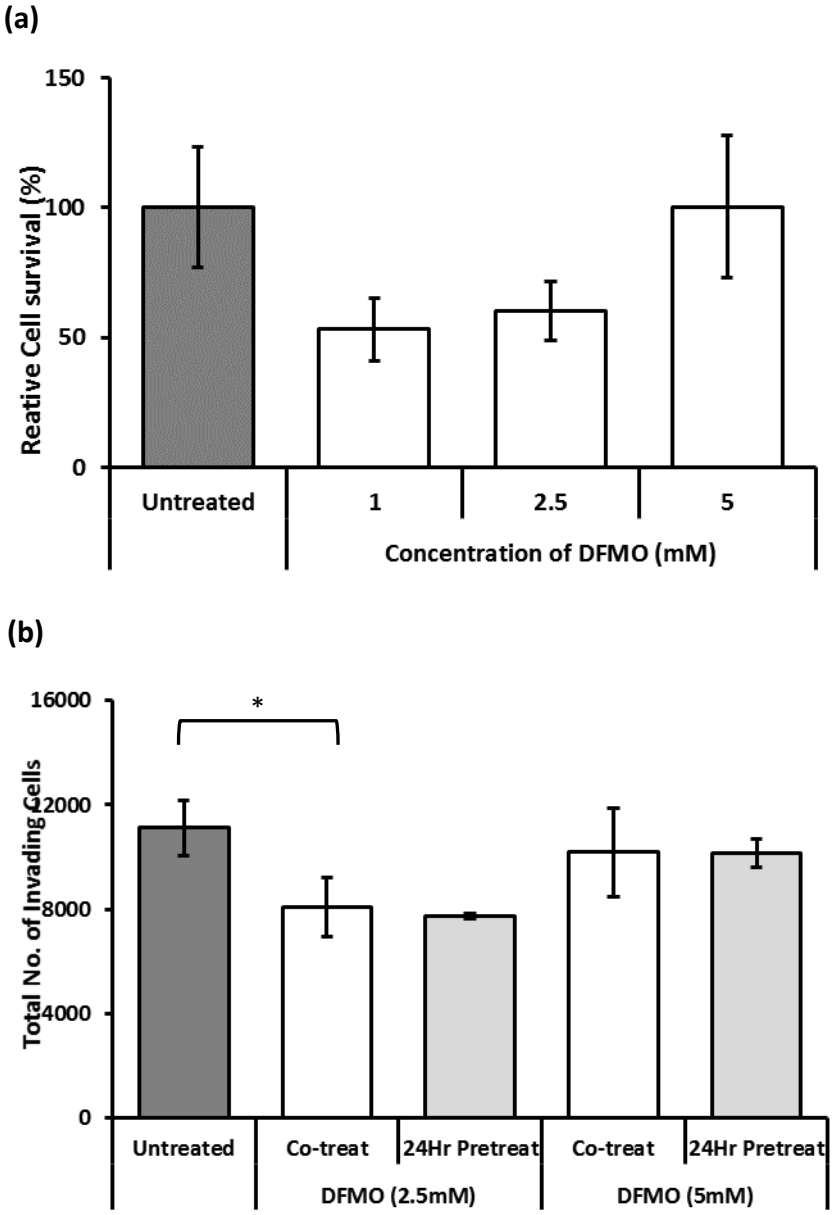

Figure 3.4-20:- DFMO treatment reduces the invasive capacity of DLKPM.
(a) Histogram showing proliferation assays carried out on DLKPM cells treated with 1mM, 2.5mM and 5mM DFMO over 5 days' (n=2). **(b)** Histogram showing a reduction in the total number of invading DLKPM cells following co-treatment (30mins) and pre-treatment (24hrs). Data plotted represents the mean ± standard deviation of duplicate trans-well inserts from duplicate biological assays. Statistics *$p \leq 0.05$, compared with negative control siRNA (n=3). Student's *t* test (two tailed with equal variance, unpaired).

3.4.3.4 Investigation into the effect of Nω-Nitro-L-arginine on DLKPM

SPR is an enzyme that converts 6-pyruvoyl-tetrahydropterin to tetrahydrobiopterin (BH_4), which acts as a co-factor for Nitric-Oxide-Synthase (NOS) in the conversion of Arginine to Citrulline. This reaction results in the production of Nitric Oxide (NO). We have shown the involvement of SPR-1 and SPR-6 in the invasion and migration processes in DLKPM. To investigate the potential role of NO in the invasive and migratory process we aimed to inhibit the action of NOS using an arginase inhibitor. The N_ω-Nitro-L-arginine (L-NNA) inhibitor was used to treat DLKPM cells prior to their inclusion in invasion assays.

Prior to testing the effects of the L-NNA, the appropriate concentration range for each inhibitor was established with the aim of finding a concentration which caused approximately 10% cytotoxicity. Proliferation assays were carried out over 5 days to assess the impact of the L-NNA inhibitor on DLKPM cells. In a preliminary investigation, an increase in growth of 33% and 85% was observed for L-NNA at concentrations of 50µM and 150µM respectively, while a negligible effect was observed using 100µM L-NNA, compared to untreated control cells. Therefore, an optimum concentration of between 100µM to 150µM of L-NNA could be used for further assays (Figure 3.4-21 (a)); for the purpose of this investigation, 150µM L-NNA was used.

To assess the impact of L-NNA on DLKPM, cells were treated with 150µM of L-NNA for 30mins (co-treatment) and 24hrs (pre-treatment) prior to setting up invasion assays. In a preliminary investigation, pre-treatment with L-NNA resulted in 37% reduction in the invasive capacity of DLKPM cells. However, the addition of L-NNA directly (co-treatment) into invasion assay at a concentration of 150µM, did not result in any change in invasion (Figure 3.4-21 (b)).

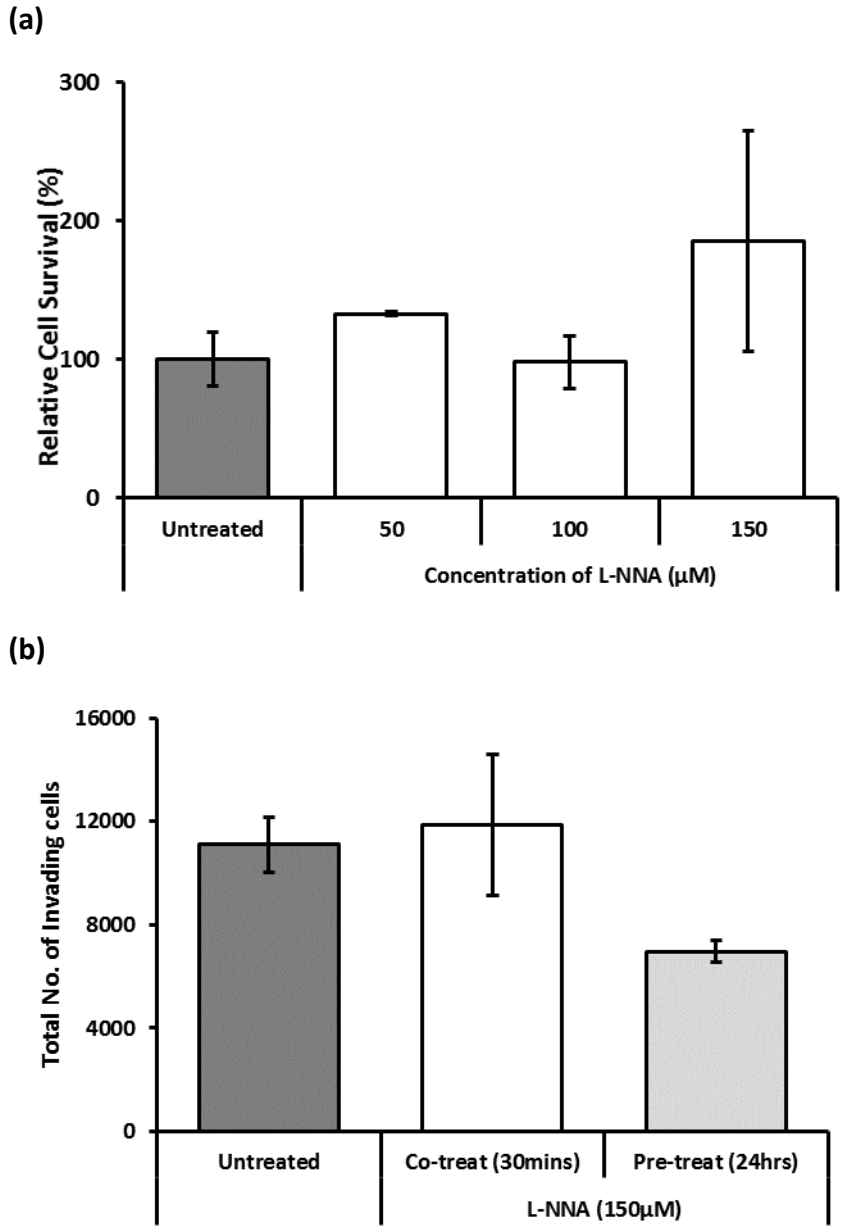

Figure 3.4-21:- L-NNA treatment reduces the invasive capacity of DLKPM.
(a) Histogram showing proliferation assays carried out on DLKPM cells treated with 50µM, 100µM and 150µM L-NNA over 5 days'. Data plotted represents the mean +/- standard deviation of duplicate biological assays (n=2). **(b)** Histogram showing the invasive capacity of DLKPM cells following L-NNA treatment for 30mins (co-treat) and 24hrs (pre-treat), in a Boyden chamber assay. The total number of invading cells through the matrigel is shown. Data plotted represents the mean ± standard deviation of duplicate trans-well inserts from duplicate biological assays (n=1).

3.4.3.5 Investigation into the effect of SPR knockdown on the generation of ROS

To investigate the role of reactive oxygen species (ROS) on SPR transfected in DLKPM cells, siRNA knockdown on DLKPM was performed and cells were tested for ROS generation. There was a reduction in ROS generation in SPR transfected cells using four independent siRNAs when compared to negative control cells. A significant reduction of ROS generation was observed in three out of four siRNAs targeting SPR; SPR-1 (22%, $p = 0.04$), SPR-5 (32%, $p = 0.006$) and SPR-6 (31%, $p = 0.009$), see Figure 3.4-22 below. The reduction in ROS generation as a result of SPR transfection may indicate that (with further investigation) that reactive oxygen species may be associated with SPR in DLKPM cells.

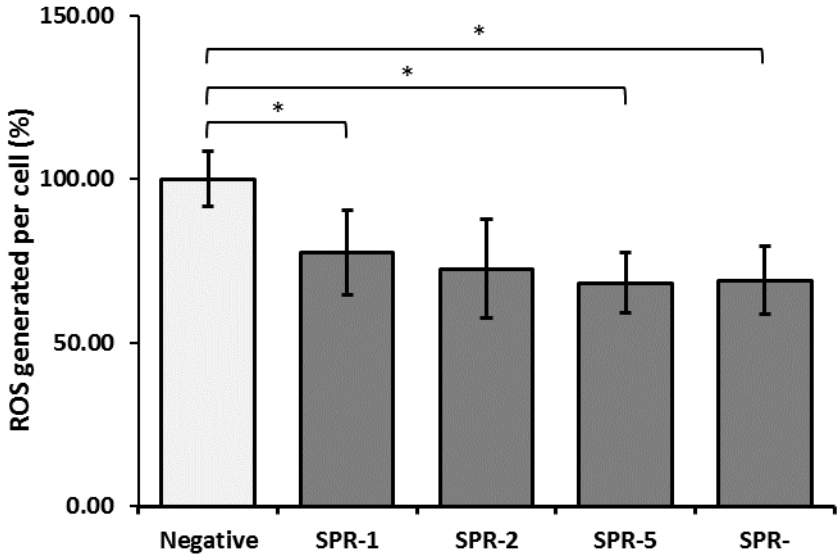

Figure 3.4-22:- ROS generation is reduced in SPR transfected DLKPM cells.
ROS assays on transfected DLKPM cells 72 hrs post-transfection using four independent siRNAs targeting SPR, relative to negative control siRNA transfected cells. Results graphed as % ROS generated per cell relative to negative control. Data plotted represents the mean ± standard deviation of duplicate wells from triplicate biological assays. Statistics *$p \leq 0.05$, compared with negative control siRNA. Student's *t* test (two tailed with unequal variance, unpaired, n=3).

3.4.4 The investigation into the functional role of SPR in breast cancer and pancreatic cancer.

BreastMark survival analysis indicated that low expression of SPR was associated with poor survival ability of patients with Luminal A and basal molecular subtypes of breast cancer. To investigate the functional role for SPR in breast cancer and pancreatic cancer, three cell lines were chosen for preliminary siRNA knockdown studies; (i) MDA-MB-468 (TNBC), (ii) MiaPaCa2 clone3 (PDAC) and (iii) AsPc1 (PDAC).

3.4.4.1 Effect of siRNA knockdown of SPR on MDA-MB-468

In the panel of TNBC breast cancer cell lines, MDA-MD-468 showed highest expression of SPR (Figure 3.3-8). To represent TNBC, the MDA-MB-468 cell line was chosen to perform siRNA knockdown of SPR. Figure 3.4-23 (a), shows the efficient knockdown of SPR by Western blot analysis using four independent siRNAs, compared to negative control and un-transfected cells. There was approximately a 15 and 52% reduction in growth with SPR-1 and SPR-2 respectively (see Figure 3.4-23 (b)). This significant reduction in growth which was observed with SPR-2 (p=0.00945576) may be as a result of toxicity to the siRNA.

Seventy-two hours post-transfection with SPR siRNAs, invasion assays were performed. There was a significant reduction in the total number of invading MDA-MB-468 cells transfected with SPR-6 siRNA (p=0.000908). Figure 3.4-24 (a) shows representative images of invading cells post transfection with SPR-1, SPR-5 and SPR-6 siRNAs, images for the SPR-2 siRNA could not be acquired due to the toxic effect of this siRNA. The total number of invading cells is presented in Figure 3.4-24 (b). These experiments indicate that SPR may potentially be involved in growth and invasion of the MDA-MB-468 cell line. In order to establish a potential role of SPR in breast cancer further investigations would need to be completed on another breast cancer cell line.

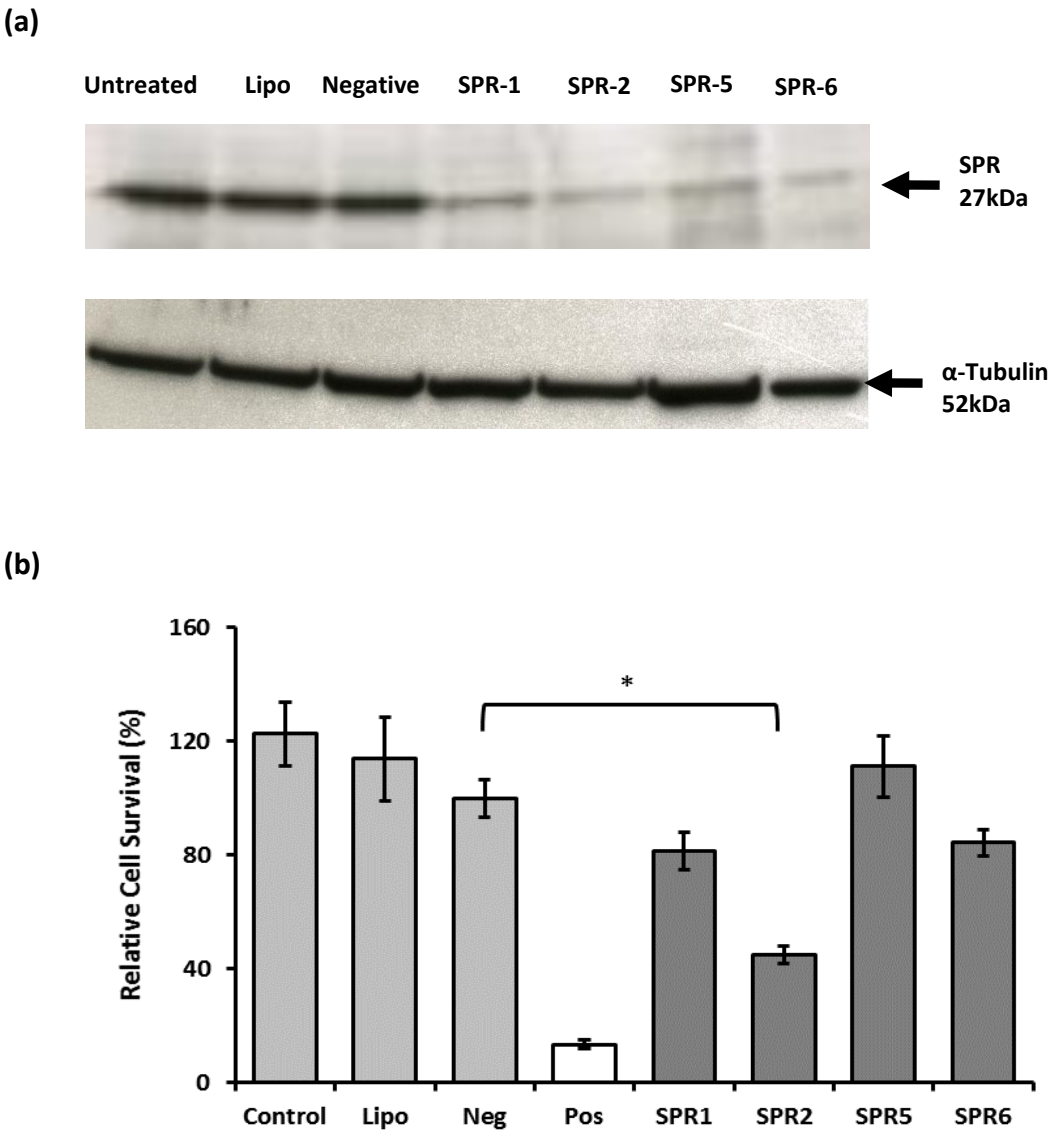

Figure 3.4-23:- SPR knockdown reduces cell growth of MDA-MB-468.
(a) Representative immunoblot showing knockdown of SPR 72 hrs post-transfection, in MDA-MB-468 cells transfected with four independent siRNAs targeting SPR, relative to negative control siRNA transfected cells (α-Tubulin served as the loading control). **(b)** Proliferation assays on siRNA transfected MDA-MB-468 cells uing SPR-1, SPR-2 and SPR-6 siRNAs. Results graphed as % cell survival relative to negative control. Data plotted represents the mean ± standard deviation of triplicate biological experiments. Statistics *$p \leq 0.05$ compared with negative control siRNA. Student's *t* test (two tailed with equal variance, unpaired (n=3)).

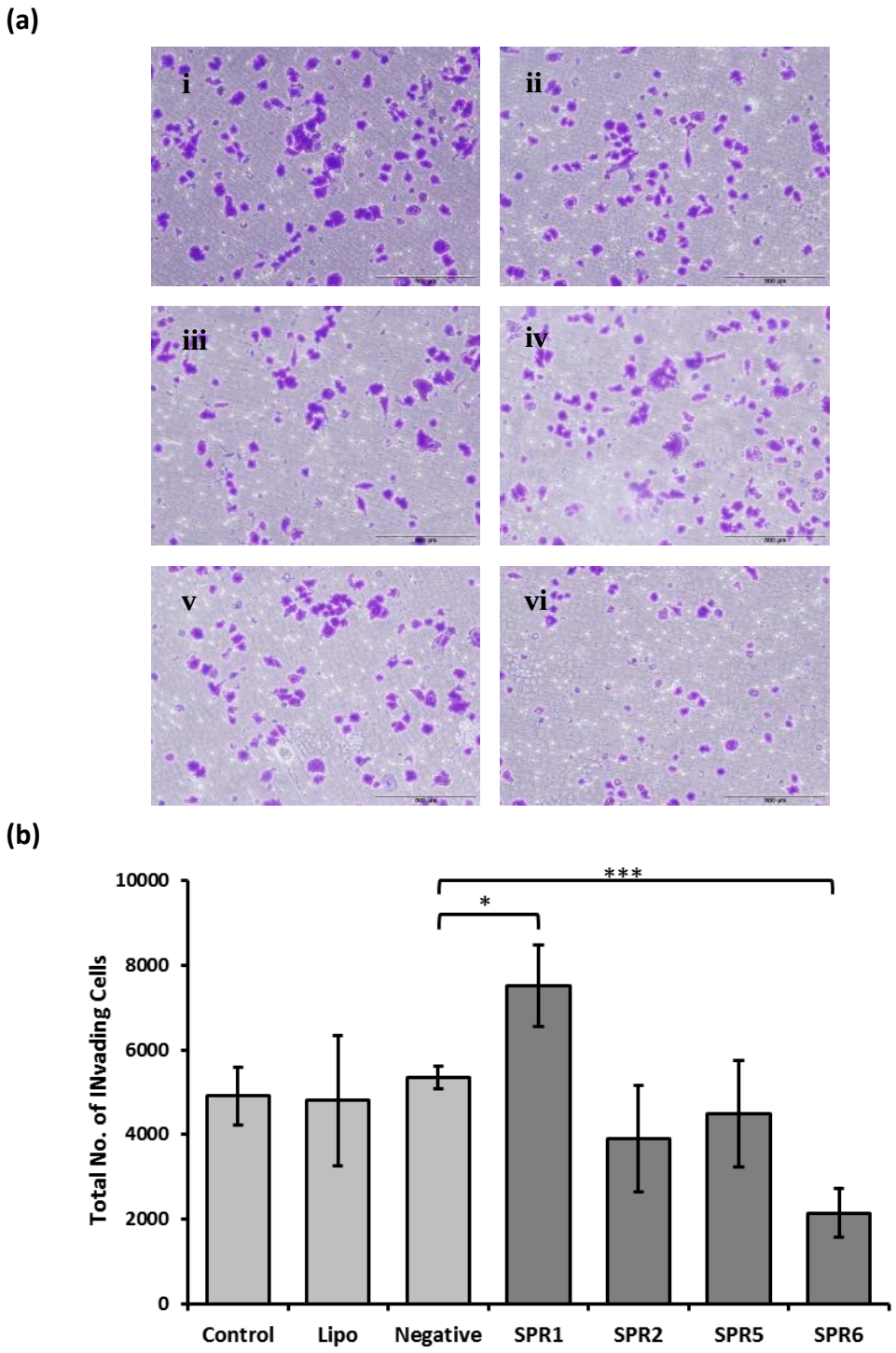

Figure 3.4-24:- SPR knockdown reduces the invasive capacity of MDA-MB-468.
(a) Invasion assays of MDA-MB-468 cells (i) Untreated Control, (ii) Lipofectamine Control, (iii) Negative control, (iv) SPR-1 siRNA, (v) SPR-5 siRNA and (iv) SPR-6 siRNA (Magnification, x100; *scale bar* = 500µm). (b) Histogram showing a reduction in the total number of invading MDA-MB-468 cells following transfection with SPR-6 siRNA. Data plotted represents the mean ± standard deviation between duplicate inserts from triplicate biological experiments. Statistics *$p \leq 0.05$ and *** $p \leq 0.005$ compared with negative control siRNA. Student's *t* test (two tailed with equal variance, unpaired (n=3)).

3.4.4.2 Effect of SPR knockdown in pancreatic cell lines MiaPaCa2 Clone3 and AsPc-1

Expression of SPR in MiaPaCa2 Clone3 and AsPc-1 was established in a previous investigation (see section 3.3.3), where a panel of pancreatic cancer cell lines was examined for SPR expression. Expression of SPR was shown to be increased in MiaPaca2 clone3 compared to the parental MiaPaca2, while AsPc1 also showed increased expression of SPR. Preliminary siRNA transfections were performed on both cell lines, to investigate a potential functional role for SPR in pancreatic cancer.

Figure 3.4-25 shows by Western blot analysis, the efficient knockdown of SPR using four independent siRNAs transfected into (a)(i) MiaPaca2 clone 2 and (b) (i) AsPc-1 cell, compared to negative control and un-transfected cells. A reduction in growth is shown for MiaPaca2 clone3 (a)(ii), with negligible effect on growth for (b)(ii) AsPc-1 cells.

Invasion and migration assays were performed on SPR transfected cells. Figure 3.4-26 shows reduced invasion capability of (a)(i) MiaPaca2 clone3 and (b)(i) AsPc-1 cells following transfection with SPR-6 (n=1), a negligible effect was observed for SPR-1, SPR-2 and SPR-5 siRNAs for both cell lines. Figure 3.4-26 (a)(ii) and (b)(ii) shows the total number of cells invading for MiaPaca2 Clone3 and AsPc-1 respectively. Figure 3.4-27 shows reduced migratory capability of (a)(i) MiaPaca2 clone3 and (b)(i) AsPc-1 cells following transfection with SPR-6 (n=1), A negligible effect was observed for SPR-1, SPR-2 and SPR-5 siRNAs for both cell lines. The total number of migrating cells is shown in Figure 3.4-27 (b)(ii) MiaPaca2 Clone3 and (b)(ii) AsPc-1 cell lines. These transfections were preliminary investigations, further invasion and migration assays would need to be performed on MiaPaca2 clone 3 and AsPc-1 to establish a functional role for SPR in these cell lines.

(a) MiaPaCa2 Clone3

(i)

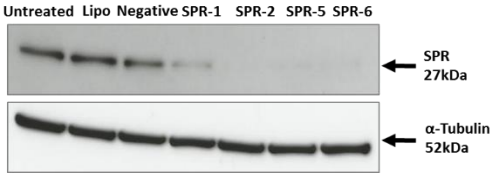

(ii)

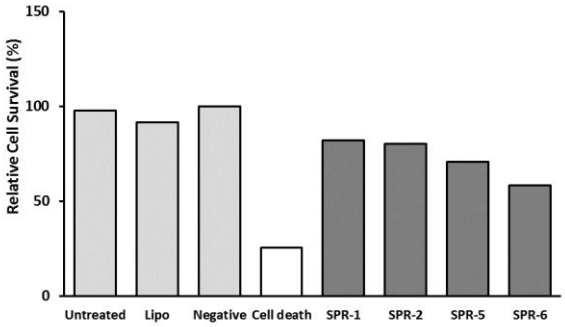

(b) AsPc-1

(i)

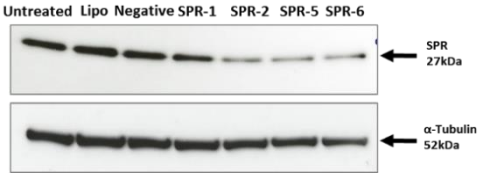

(ii)

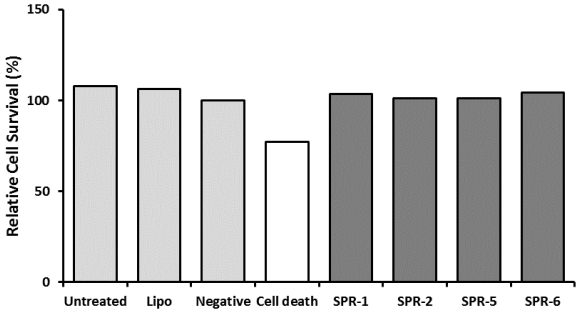

Figure 3.4-25:- SPR knockdown reduces the growth of MiaPaca2 clone 3.
Representative immunoblot showing efficient knockdown of SPR 72hrs post-transfection in **(a)** (i) MiaPaca2 Clone3 and **(b)** (i) AsPc-1 cells (α-Tubulin served as loading control). Proliferation assays on siRNA transfected **(a)** (ii) MiaPaCa2 clone3 and **(b)** (ii) AsPc-1 cells. Results graphed as percent cell survival relative to negative control. Data plotted represents a mean ±standard deviation of duplicate wells from one biological experiment (n=1).

(a) MiaPaCa2 Clone3

i.

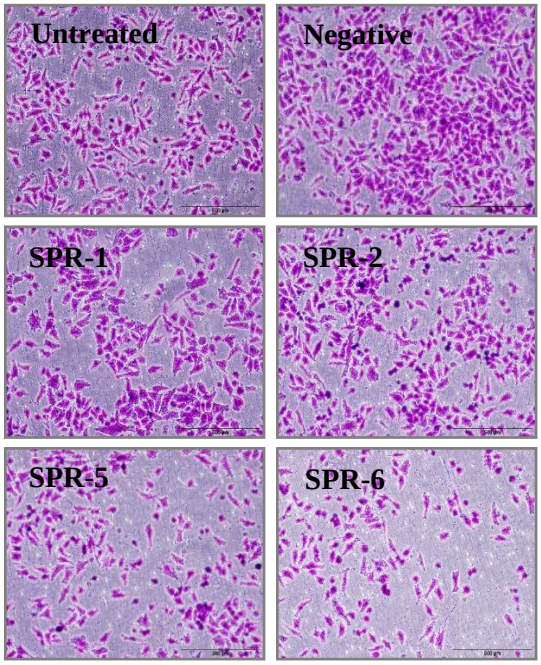

ii.

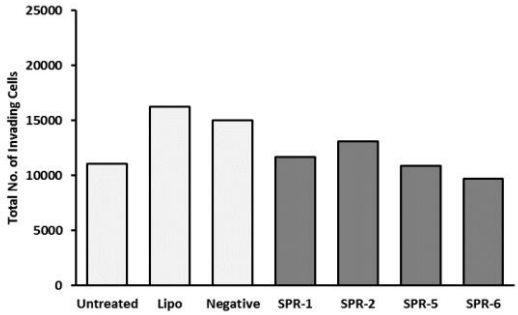

(b) AsPc-1

i.

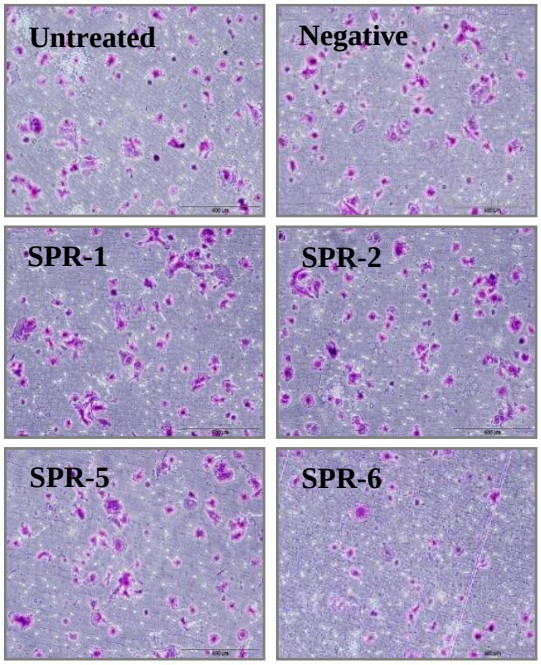

ii.

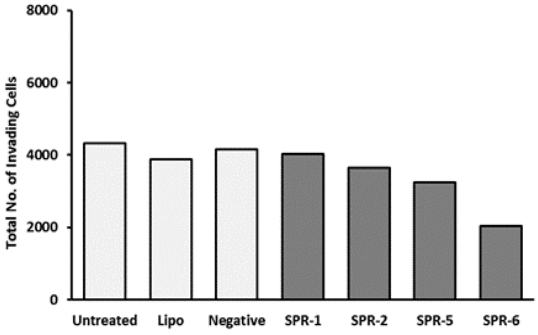

Figure 3.4-26:- SPR knockdown reduces the invasive capacity of MiaPaCa2 Clone3 and AsPc-1.

Invasion assays of **(a)** (i) MiaPaCa2 clone3 and **(b)** (i) AsPc-1 cells following siRNA transfection with SPR-1, SPR-2, SPR-5 and SPR-6 siRNAs (magnification, x100; *scale-bar* = 500µm). Histogram showing a reduction in the total number of invading cells of **(a)** (ii) MiaPaCa2 Clone3 and **(b)** (ii) AsPc-1, following transfection with SPR-6 siRNA. Data plotted represents the mean ± standard deviation of two inserts from one individual experiment (n=1).

(a) MiaPaca2 Clone3

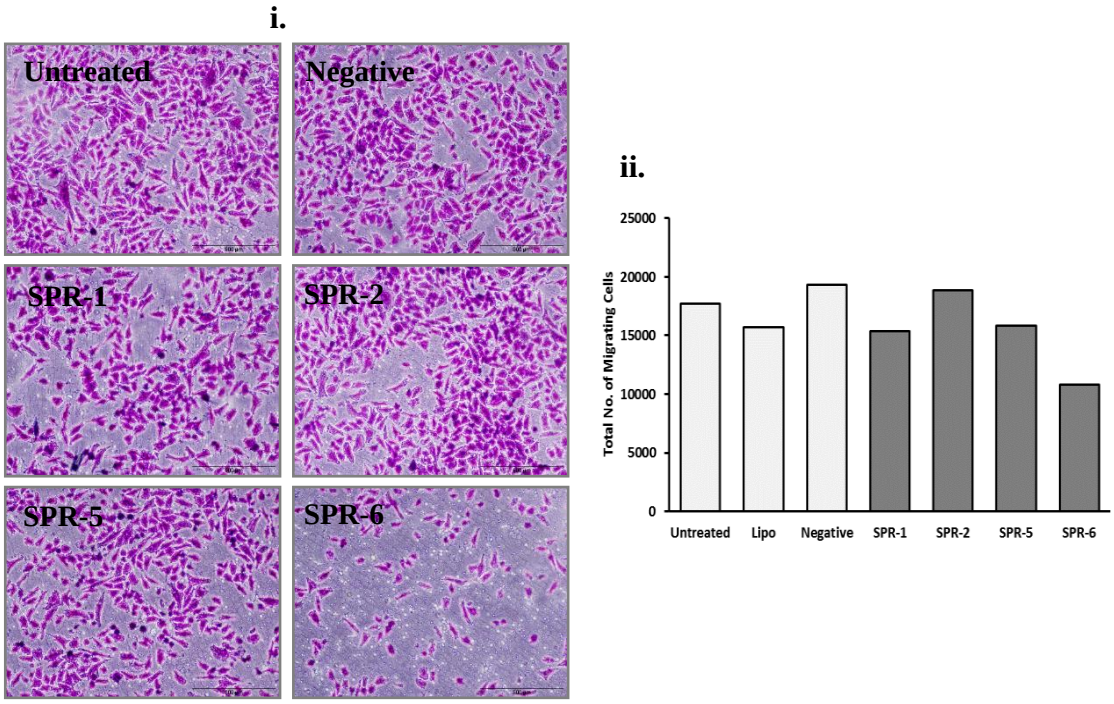

(a) AsPc-1

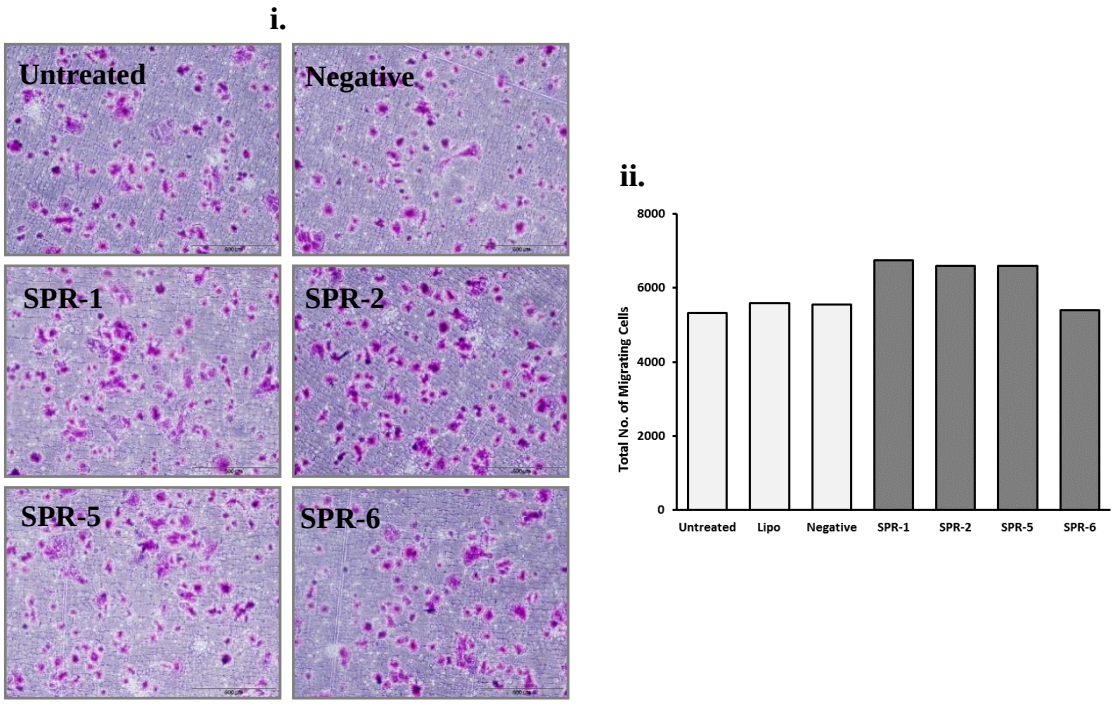

Figure 3.4-27:- SPR knockdown reduces the migratory capacity of MiaPaCa2 clone 2. Migration assays of **(a)** (i) MiaPaCa2 clone3 and **(b)** (i) AsPc-1 cells following siRNA transfection with SPR-1, SPR-2, SPR-5 and SPR-6 siRNAs (magnification, x100; *scalebar* = 500µm). Histogram showing a reduction in the total number of migrating cells of **(a)** (ii) MiaPaCa2 Clone3, following transfection with SPR-6 siRNA. Data plotted represents the mean ± standard deviation of two inserts from one individual experiment (n=1).

3.4.5 Summary of functional analyses

- ALCAM is highly expressed in DLKPI compared to DLKPSQ and DLKPM, indicating its potential use as a marker for DLKPI. Knockdown of ALCAM resulted in a significant decrease in the invasive capacity of DLKPM and a significant increase in the invasive capacity of DLKPSQ-mitox-BCRP-6P. ALCAM may, therefore, have dual invasion roles in these cell lines.
- DLKPSQ displayed the highest expression levels of INA and SPR compared to DLKPI and DLKPM, indicating their potential use as markers for DLKPSQ. Both INA and SPR were also expressed in DLKPM cells.
- Knockdown of INA and SPR resulted in a significant reduction in the invasion and migration capacities of DLKPM. Reduced invasive capacity of MDA-MB-468 was also observed following knockdown of SPR.
- Potential roles for INA and SPR in the invasion and migration capacity of these cell lines was shown through silencing of their respective genes. In addition, generation of ROS in DLKPM cells was reduced following knockdown of SPR which may indicate a potential link between SPR and ROS.

3.4.6 Immunohistochemical analysis of INA and SPR expression in lung cancer

Western blot analysis of INA showed that expression was highest in DLKPSQ and DLKP and a lower level in DLKPM, while increased SPR expression was established in DLKPSQ and DLKPM compared to DLKP and DLKPI. Expression of INA had been associated with pancreatic neuroendocrine cancer while little Immunohistochemical analysis of the distribution of SPR in human cancers has been reported. To look at the distribution of INA and SPR expression in lung cancer, tissue microarrays (TMA) (Biomax, LC1502) were immunohistochemically stained using primary antibodies specific for INA and SPR. The arrays contained: 2 cases of normal lung, 23 cases of squamous cell carcinoma, 21 cases of adenocarcinoma, 5 cases of adenosquamous carcinoma, 5 cases of bronchioloalveolar carcinoma, 7 cases of small cell undifferentiated carcinoma and 3 cases of neuroendocrine carcinoma. Other cases on the TMA that showed negative to weak immunoreactivity included large cell carcinoma undifferentiated carcinoma, malignant mesothelioma, carcinosarcoma, chronic bronchitis, lobar pneumonia, pulmonary tuberculosis where negligible staining for INA was observed. There were duplicate cores per case providing 75 cases (total 150 TMA cores). TMA cores were scored semi-quantitatively, according to the intensity of the INA immunoreactivity observed (weak, moderate, strong).

Expression of INA (Table 3.4-1) and SPR (Table 3.4-2) in human lung cancer was investigated further. Immunoreactivity for INA and SPR was observed in a number of tumour types. The overall immunoreactivity on the TMA displayed very specific membrane reactivity of isolated cells. Figure 3.4-28 illustrates negligible staining for INA in normal lung, while isolated cells displayed immunoreactivity in adenocarcinoma. Squamous cell carcinoma also shows immunoreactivity but the most intense staining was observed in the sections of neuroendocrine cancer. Overall staining for SPR on the lung cancer TMA displayed was variable across the lung cancer tumour, however, moderate to strong cytoplasmic immunoreactivity was observed in lung squamous tumour cases. Figure 3.4-29 illustrates negligible staining for SPR in normal lung, while moderate to strong immunoreactivity was observed in squamous carcinoma, while the other tumour types displayed a lower level of immunoreactivity.

Tumour Type	INA staining intensity
Squamous cell carcinoma	17/23 - negative 4/23 - weak 2/23- moderate
Adenocarcinoma	16/21 - negative 5/21 – weak
Adenosquamous	1/5 - negative 2/5- weak 2/5 - moderate
Bronchioalveolar	4/5 - negative 1/5 – weak
Small cell undifferentiated	6/7- negative 1/7 - weak
Neuroendocrine	1/3 - negative 2/3 – moderate

Table 3.4-1:- Immunoreactivity of INA on lung cancer TMA.
The table above shows the results from staining of squamous, adenocarcinoma, adenosquamous, bronchioalveolar, small cell lung and neuroendocrine primary tumours using an antibody specific to INA.

Tumour Type	SPR staining intensity
Squamous cell carcinoma	8/23 - negative 11/23 - weak 2/23- moderate 1/23 - strong
Adenocarcinoma	4/21 - negative 14/21 - weak 2/21- moderate 1/21 - strong
Adenosquamous	4/5 - weak 1/5- moderate
Bronchioalveolar	5/5 - weak
Small cell undifferentiated	5/7- negative 2/7 - weak
Neuroendocrine	2/3 - negative 1/3 - weak

Table 3.4-2:- Immunoreactivity of SPR on lung cancer TMA.
The table above shows the results from staining of squamous, adenocarcinoma, adenosquamous, bronchioalveolar, small cell lung and neuroendocrine primary tumours using an antibody specific to SPR.

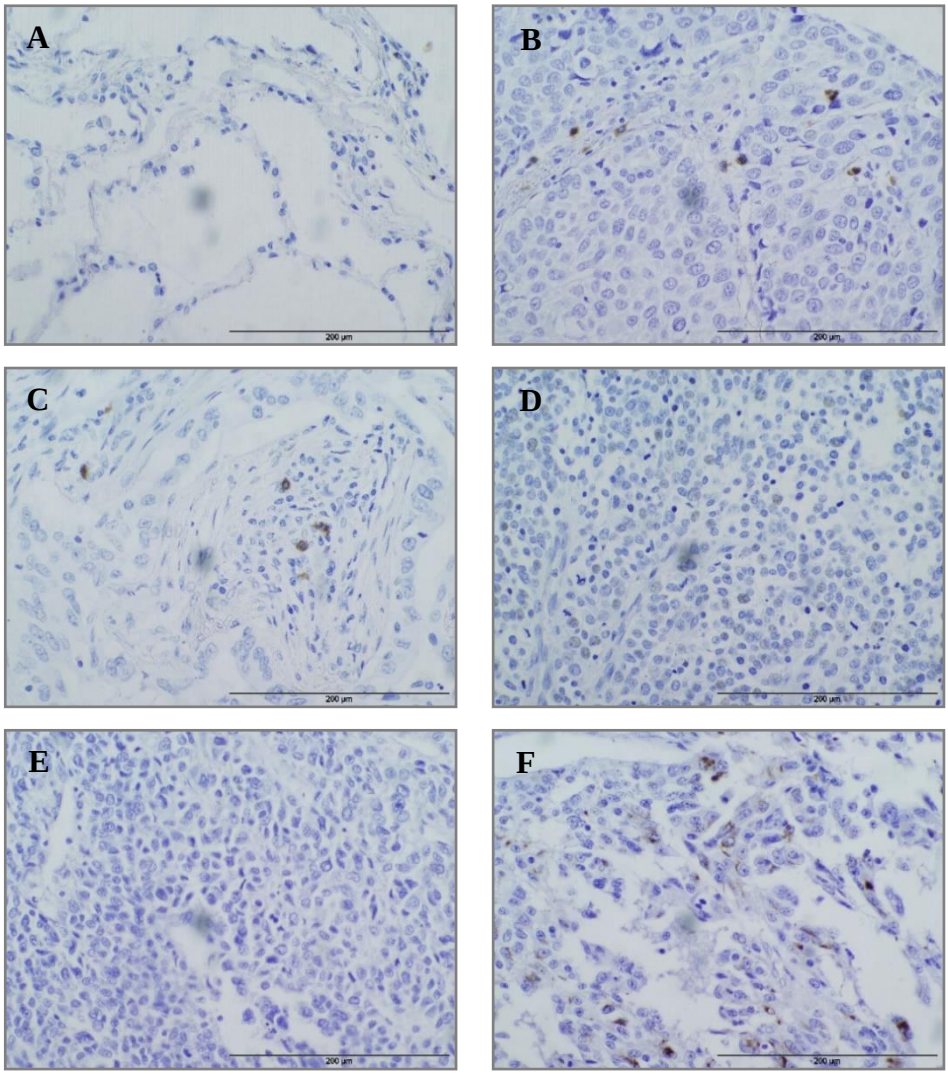

Figure 3.4-28:- Immunohistochemical analysis of INA expression in human lung cancer.
A TMA containing normal lung, squamous, adeno, small cell, large cell and neuroendocrine carcinoma was immunohistochemically stained using a primary antibody specific to INA. Representative photomicrographs are shown (A) Negligible staining is observed in normal lung tissue, (B) Isolated cells staining in Squamous, (C) Isolated cells staining in adenocarcinoma, (D) & (E), negligible staining in small cell and Large cell, in contrast to (F) strong isolated staining in neuroendocrine. Neuroendocrine carcinoma shows distinct immunoreactivity for INA (Original magnification of all photomicrographs, 400×, *scale bar* = 200 μm).

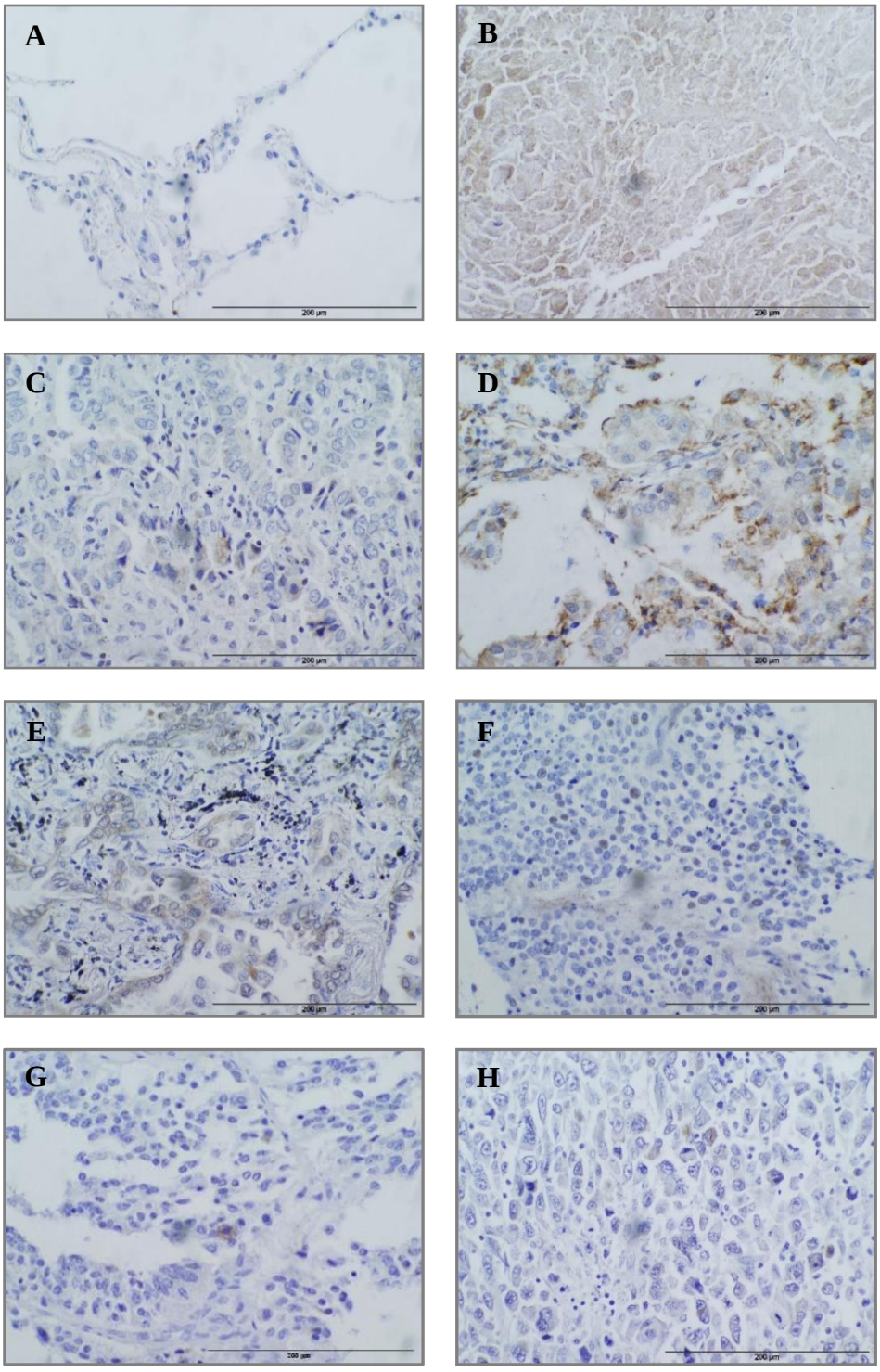

Figure 3.4-29:- Immunohistochemical analysis of SPR expression in human lung cancer. A TMA containing normal lung, squamous, adeno, small cell, large cell and neuroendocrine carcinoma was immunohistochemically stained using a primary antibody specific to SPR. Representative photomicrographs are shown; (A) Negligible staining is observed in normal lung tissue, (B) Intense staining in squamous, (C) weak staining in adenocarcinoma, (D) intense staining in mucinous and (E) strong staining for bronchioalveolar, (F) isolated cells staining in small cell, (G) neuroendocrine and (H) Large cell carcinomas. Squamous carcinoma shows moderate to strong immuno-reactivity for SPR (Original magnification of all photomicrographs, 400×, *scale bar* = 200 μm).

3.4.7 Immunohistochemical analysis of SPR in Breast cancer

BreastMark analysis of SPR indicated that low expression of SPR may be associated with poor prognosis of Luminal A and Basal-like molecular subtypes of breast cancer. SPR expression was then investigated in a breast cancer TMA (A712 (18)) containing 12 invasive ductal breast carcinomas with their corresponding adjacent normal tissues. Immunoreactivity of SPR was observed in a number of breast cancer cases (Table 3.4-3), while weak immunoreactivity was observed in a number of adjacent normal tissues. Figure 3.4-30 shows representative staining of TMA cores that were scored semi-quantitatively, according to the intensity of the SPR immunoreactivity observed (weak, moderate, strong). In addition, SPR expression was also investigated in a small panel of patient tumours tissues of unknown subtypes, Figure 3.4-31 shows negligible immunoreactivity in normal breast tissue and representative immunoreactivity for SPR in grade 1, grade 2 and a 3 grade breast cancer of unknown subtypes, evidence of membrane localisation was also observed.

Breast tissue type	SPR staining Intensity
Normal	Negative – 8/12 Weak – 4/12
Invasive ductal	Negative – 4/12 Weak – 4/12 Moderate - 4/12

Table 3.4-3:- Immunoreactivity of SPR in invasive ductal breast cancer tissues with corresponding adjacent normal tissue.

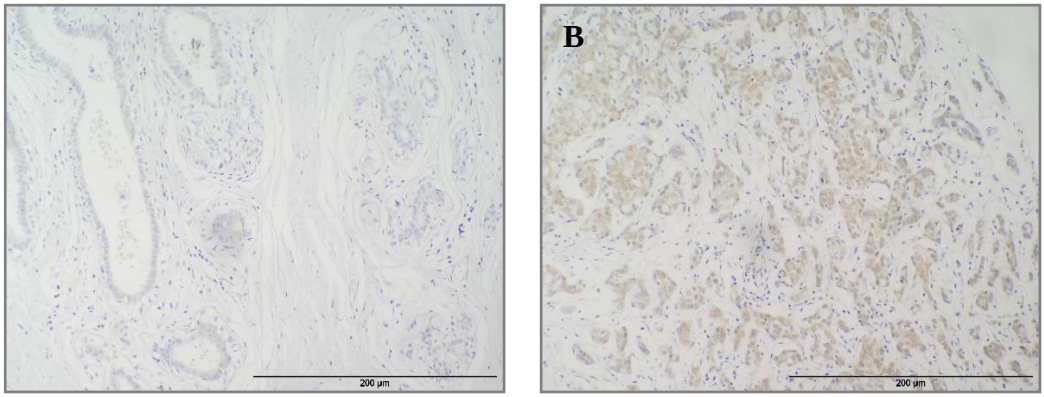

Figure 3.4-30:- Immunohistochemical analysis of SPR expression in human breast cancer. A TMA containing invasive ductal breast and adjacent Normal breast, immunohistochemically stained using a primary antibody specific for SPR. Representative photomicrographs are shown (A) Negligible staining is observed in normal breast tissue, (B) Intense staining in invasive ductal breast (ER (-), PR (+), C *erb* B2 (2+/3), shows moderate immunoreactivity for SPR (Original magnification of all photomicrographs, 200×, *scale bar* = 200 µm).

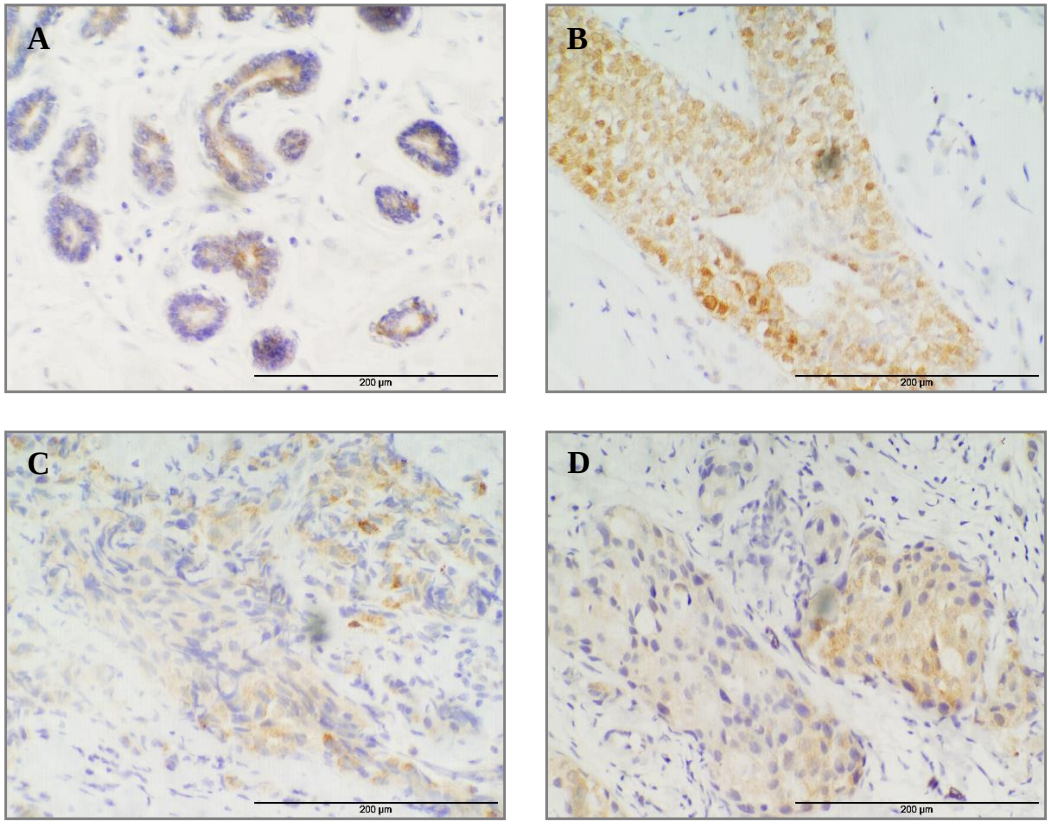

Figure 3.4-31:- Immunohistochemical analysis of SPR in a panel of breast cancer tissues. Staining for SPR observed in seven out of eight breast cancer tissues. Representative images showing immunoreactivity in: **(A)** normal breast tissue, **(B)** Histological Grade 1, **(C)** Histological Grade 2 and **(D)** Histological grade 3 breast cancer (subtypes unknown) (magnification x400, *scale-bar* = 200µm.

3.5 The investigation into the growth and tumour development of DLKP and its clonal subpopulations *in vivo*.

3.5.1 Background to DLKP clones

Lung Squamous cell line DLKP was originally established from a tumour histologically diagnosed as "poorly differentiated Squamous carcinoma" and later found to contain at least three morphologically and phenotypically distinct clonal subpopulations [93]. DLKPSQ, DLKPI and DLKPM are the three established clones of DLKP and all have the ability to grow on monolayers. DLKPSQ are squamous-like and form colonies with distinct cell boundaries and account for approximately 70% of the DLKP parent. DLKPM make up approximately 5% of DLKP parent, are more irregular in shape with a fibroblastoid-like morphology and do not form colonies. DLKPI grow in colonies but their boundaries are less distinct in appearance and account for approximately 25% of the DLKP. DLKPSQ, DLKPI and DLKPM display different growth and invasion characteristics but also distinctly different morphologies. However, a model of interconversion (shown in Figure 3.5-1 below) between these clonal subpopulations was previously described, the model suggested that interconversion can occur between DLKPSQ and DLKPI, DLKPI and DLKPM and vice versa but not between DLKPSQ and DLKPM.

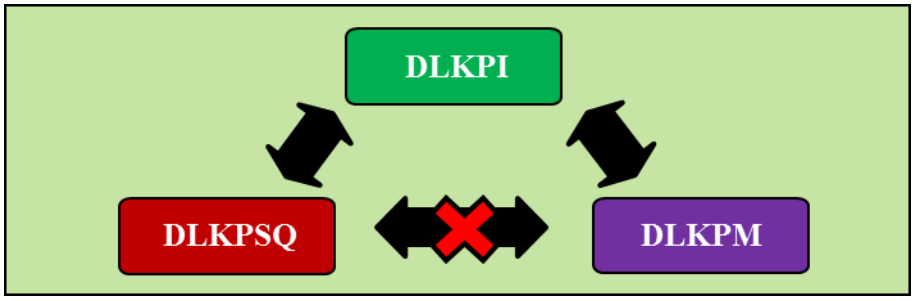

Figure 3.5-1:- Proposed model of interconversion between DLKPSQ, DLKPI and DLKPM.

Further characterisation of the clones found that the *in vitro* invasion (ability to breakdown extracellular matrix components and invade) and anoikis (ability to survive in anchorage-independent conditions) abilities of the clones were also different. DLKPSQ was found to be poorly invasive and anoikis resistant, DLKPM was highly invasive and is anoikis sensitive, while the intermediate, DLKPI, appears most sensitive to anoikis and dies more readily. Interestingly, DLKPM appears to use autophagy as cell survival mechanism before dying [93, 95, 96]. Autophagy is a general term for the degradation of cytoplasmic components within lysosomes and mediated by an organelle known as an autophagosome [118].

3.5.2 The *in vivo* investigation of DLKP

The heterogeneous nature of DLKP and the distinct characteristics displayed between the clones make DLKP an ideal cell line model to investigate their growth and behaviour in vivo. A pilot study to investigate growth and development of cell line based tumours was carried out by sub-cutaneous injection of DLKP, DLKPSQ, DLKPI and DLKPM cell lines at two sites in 4 groups of 4 CB17/lcr-PrkdcSCID/Crl mice (4 mice per cell line), in collaboration with Prof. Robert Straubinger, Ms Ninfa Straubinger, Dr. Fiona O'Neill and Dr. Sandra Roche. Three different cell numbers were used in this study (1x106 cells in 250 µl, 5x106 cells in 250 µl and 1x107 cells in 500 µl), cells were prepared in matrigel and injected into mice as described in section 2.8. There are a number of potential animal models that could be used for this study, however as mentioned in section 2.8 our collaborator has extensive experience and publishing history using SCID mice for in vivo modelling [101, 102], which is one of the main reasons why this animal model was chosen. A schematic showing a summary of the experimental approach is outlined in Figure 3.5-2.

After injection, animals were monitored until tumours had developed, once palpable tumours formed, one mouse from each group was sacrificed for exploratory surgery (indicated on schematic by blue boxes). The organs from this group of animals were paraffin embedded, sectioned and examined using haematoxylin and eosin (H&E) staining by a pathologist, Prof. Susan Kennedy at Royal Victoria Eye and Ear Hospital for evidence of metastasis. This examination did not find any evidence of metastasis within the organs, however, the xenograft tumours were described as "poorly differentiated squamous carcinoma". The description of these tumours is in line with the diagnosis of the original DLKP tumour. The remaining 12 animal cohort were allowed to progress to experimental finality or until a guideline tumour volume of 2000mm3 had been reached. Animals were monitored daily and measurements were taken twice weekly to determine tumour volume. At the end of the experiment, representative tumours were embedded in paraffin and OCT medium for examination by immunohistochemistry (indicated on the schematic by red boxes). This study also provided a unique opportunity to characterise the cells within the xenograft tumours, this was performed using explant culture (indicated on the schematic by green boxes). Tumour growth curves from tumours produced by DLKP, DLKPSQ, DLKPI and DLKPM cell lines in mice were determined using average measurements obtained from three different inoculation densities (1x106 cells (n=2), 5x106 cells (n=4) and 1x107 cells (n=2)).

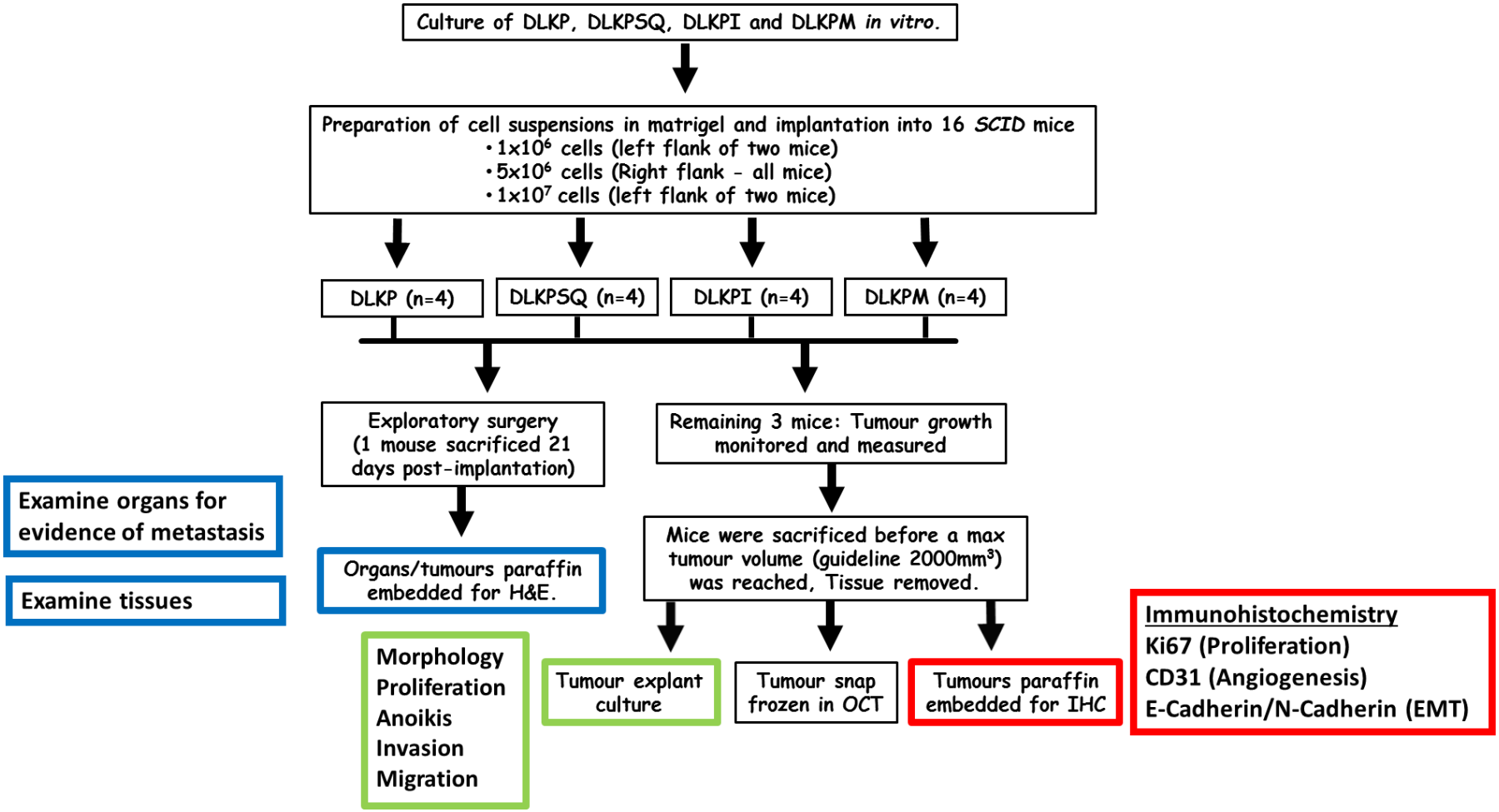

Figure 3.5-2:- Schematic showing development of xenografts derived from DLKP and its clones.
Outline of the steps involved in the generation of the cell line derived tumours and tumour xenografts from DLKP, DLKPSQ, DLKPI and DLKPM cells. Organs from one group of mice were examined for evidence of metastasis (Blue), explant culture was performed on tumours and recovered cells were examined (green) and tumours were immunohistochemically examined for expression of markers of proliferation, angiogenesis and EMT (Red).

3.5.2.1 Examination of the growth of DLKP *in vivo*

Four 28-35 day old SCID mice received subcutaneous injections of DLKP cells at cell densities of $1x10^6$ cells, $5x10^6$ cells and $1x10^7$ cells. All four mice displayed tumour formation across the three different inoculation densities of DLKP at both injection sites. Exploratory surgery performed on one mouse (mouse 3) to look for evidence of metastasis after 21 days of growth revealed no evidence of metastasis. Figure 3.5-3 gives a representation of the tumours produced by DLKP and their locations (indicated by red arrows).

Measurements for the tumours produced by DLKP and for each of the cell densities used in this study are presented in Table 3.5-1 **(a)** $1x10^6$ cells (n=2), **(b)** $5x10^6$ cells (n=4) and **(c)** $5x10^7$ cells (n=2). Tumours produced by DLKP appeared to be fast growing and large tumours. The growth curves (Figure 3.5-4) highlights the size of tumours produced by DLKP in SCID mice over 32 days.

A

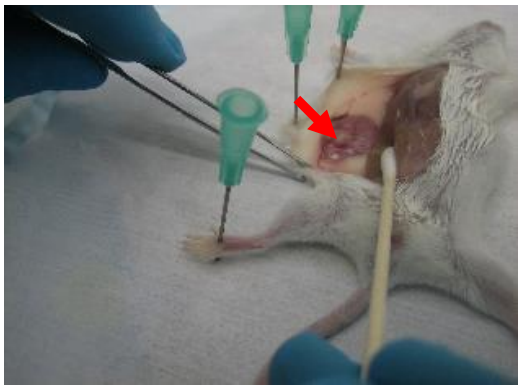

B

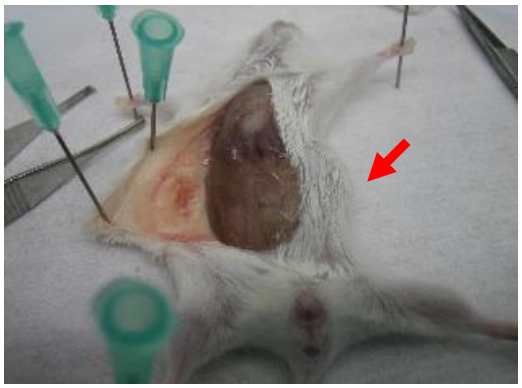

Figure 3.5-3:- Growth of xenograft tumours from DLKP cells.
Representative images showing xenograft tumours following subcutaneous injection of DLKP cells at inoculation densities of $5x10^6$ cells (Image A) and $1x10^7$ cells (image B) in SCID mice. Red arrows indicate tumour location on both sides of the mouse.

(a)

Mouse no	DLKP: Tumour growth measurements (mm^3) from mice inoculated with $1x10^6$ cells (Days)			
	21	**25**	**29**	**32**
1	107.64	241.28	782.93	696.7
2	129.4	209.58	296.7	484.84

(b)

Mouse No	DLKP: Tumour growth measurements (mm^3) from mice inoculated with $5x10^6$ cells (Days)			
	21	25	29	*32*
1	166.12	295.12	457.52	505.68
2	185.2	787.52	535.13	818.7
3	209.3	**Mouse sacrificed at day 21**		
4	124.03	410	829.6	910.2

(c)

Mouse No	DLKP: Tumour growth measurements (mm^3) from mice inoculated with $1x10^7$ cells (Days)			
	21	**25**	**29**	**32**
3	378.324	**Mouse sacrificed at day 21**		
4	192.19	494.5	778.04	985.71

Table 3.5-1:- DLKP xenograft tumour measurements.
The growth of xenograft tumours following subcutaneous injection of DLKP cells. Measurements of the tumours in SCID mice inoculated with DLKP at cell densities of **(a)** $1x10^6$ cells (n=2), **(b)** $5x10^6$ cells (n=4) and **(c)** $1x10^7$ cells (n=2).

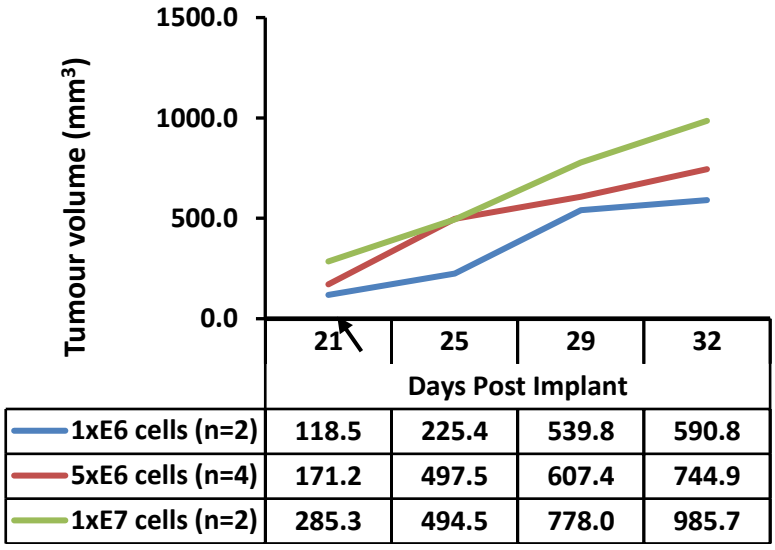

Figure 3.5-4:- Xenograft tumour growth curves for DLKP.
Xenografts tumours were developed following subcutaneous injection of DLKP cells in SCID mice over 32days post injection. Tumour growth curves for DLKP. Cell numbers injected: $1x10^6$ cells (n=2), $5x10^6$ cells (n=4), $1x10^7$ cells (n=2). Black arrow indicates when a mouse was sacrificed, reducing the numbers continuing on in the experiment.

3.5.2.2 Examination of the growth of DLKPSQ *in vivo*

Four 28-35 day old SCID mice received subcutaneous injections of DLKPSQ cells at cell densities of $1x10^6$ cells, $5x10^6$ cells and $1x10^7$ cells. All four mice displayed tumour formation across the three different inoculation densities of DLKPSQ at both injection sites.

Exploratory surgery was performed on one mouse (mouse 1) to look for evidence of metastasis after 21 days of growth. Figure 3.5-5 gives a visual representation of tumours produced by DLKPSQ and their locations (indicated by red arrows). Measurements for the tumours produced by DLKPSQ at each of the cell densities used in this study are presented in Table 3.5-2 **(a)** $1x10^6$ cells (n=2), **(b)** $5x10^6$ cells (n=4) and **(c)** $1x10^7$ cells (n=2). Tumours produced by DLKPSQ appeared to vary in size (indicated by the red arrows in images A, B, D, E and G), but displayed increased vascularisation and angiogenesis compared to tumours produced by DLKP, DLKPI and DLKPM (indicated by blue arrows in images B, D, E, G and H).

Upon dissection, two out of four mice were found to have small white masses distributed within the peritoneal cavity, suggesting evidence of suspected metastasis (image E, F and H - green arrows) and an enlarged lymph node was also noted (Image C- yellow arrow). The growth curves (Figure 3.5-6) highlights the size of tumours produced by DLKPSQ in SCID mice over 32 days.

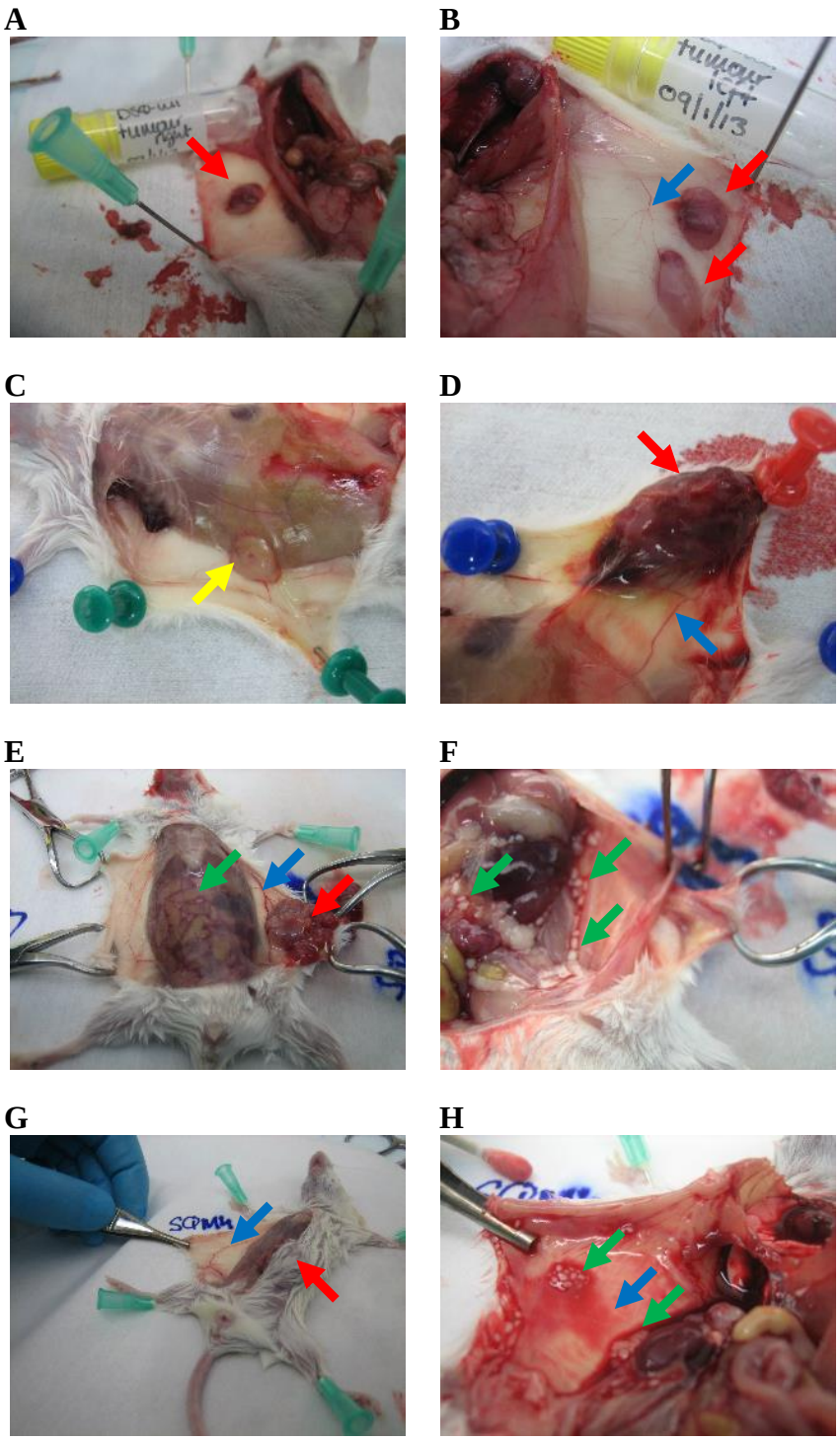

Figure 3.5-5:- Growth of xenograft tumours from DLKPSQ cells.
Representative images showing xenograft tumours following subcutaneous injection of DLKPSQ cells at inoculation densities $1x10^6$ cells (images B and D), $5x10^6$ cells (images A, C, E and G) and $1x10^7$ cells (images F and H) in 28-35 day old SCID mice. Red arrows indicate tumour locations.

(a)

Mouse no	DLKPSQ: Tumour growth measurements (mm^3) from mice inoculated with $1x10^6$ cells (Days)			
	21	**25**	**29**	**32**
1	63.96	**Mouse sacrificed at day 21**		
2	0	449.31	426.88	663.17

(b)

Mouse No	DLKPSQ: Tumour growth measurements (mm^3) from mice inoculated with $5x10^6$ cells (Days)			
	21	**25**	**29**	***32***
1	54	**Mouse sacrificed at day 21**		
2	60.39	310.38	574.19	663.26
3	0	0	0	0
4	0	0	0	0

(c)

Mouse No	DLKPSQ: Tumour growth measurements (mm^3) from mice inoculated with $1x10^7$ cells (Days)			
	21	**25**	**29**	**32**
3	61.64	406.12	1045.90	1951.82
4	69.79	280.30	508.38	762.96

Table 3.5-2:- DLKPSQ xenograft tumour measurements.
The growth of xenograft tumours following subcutaneous injection of DLKPSQ cells. Measurements of the tumours in SCID mice inoculated with DLKPSQ at cell densities of **(a)** $1x10^6$cells (n=2), **(b)** $5x10^6$cells (n=4) and **(c)** $1x10^7$cells (n=2).

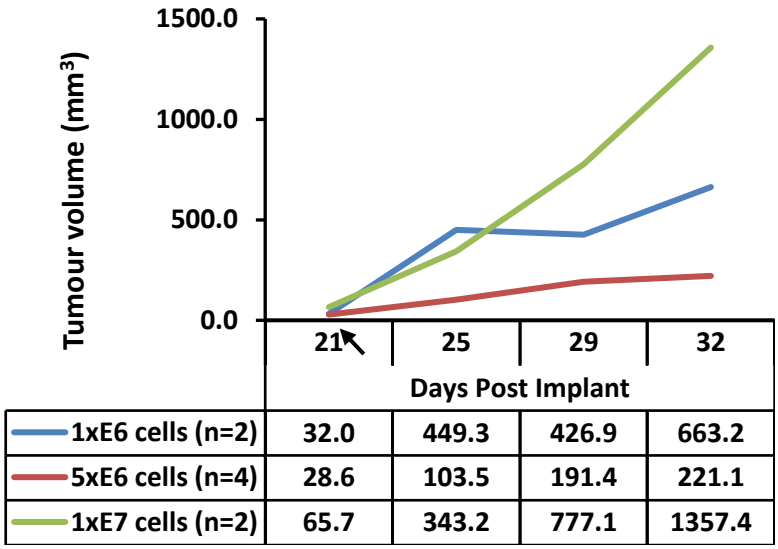

Figure 3.5-6:- Xenograft tumour growth curves for DLKPSQ.
Xenograft tumours were developed following subcutaneous injection of DLKPSQ cells in SCID mice over 32 days post injection. Tumour growth curves for DLKPSQ. Cell numbers injected: $1x10^6$ cells (n=2), $5x10^6$ cells (n=4), $1x10^7$ cells (n=2). Black arrow indicates when a mouse was sacrificed, reducing the numbers continuing on in the experiment.

3.5.2.3 Examination of the growth of DLKPI *in vivo*

Four 28-35 day old SCID mice received subcutaneous injections of DLKPI cells at cell densities of $1x10^6$ cells, $5x10^6$ cells and $1x10^7$ cells.

All four mice displayed tumour formation across the three different inoculation densities of DLKPI at both injection sites. Exploratory surgery performed on one mouse (mouse 3) to look for evidence of metastasis after 21 days of growth revealed no evidence of metastasis. The rapidly growing tumours produced by DLKPI cells in mouse 4 had exceeded guideline measurement of $2000mm^2$, so it was necessary to sacrifice this mouse. Figure 3.5-7 gives a visual representation of tumours produced by DLKPSQ and their locations (indicated by red arrows). DLKPI appeared to produce the largest tumours and more quickly than those produced by DLKP, DLKPSQ and DLKPM. The DLKPI tumours appeared to resemble those produced by the DLKP parent.

There was variation observed in the growth of tumours from DLKPI cells. The measurements for the tumours and each of the cell densities used in this study are presented in Table 3.5-3 **(a)** $1x10^6$ cells (n=2), **(b)** $5x10^6$ cells (n=4) and **(c)** $1x10^7$ cells (n=2). The growth curves (Figure 3.5-8) highlights the large size of tumours produced by DLKPI in SCID mice over 32 days, it appears that tumour growth an inoculation cell density of $1x10^6$cells would be optimal for DLKPI cells for further *in vivo* studies.

A

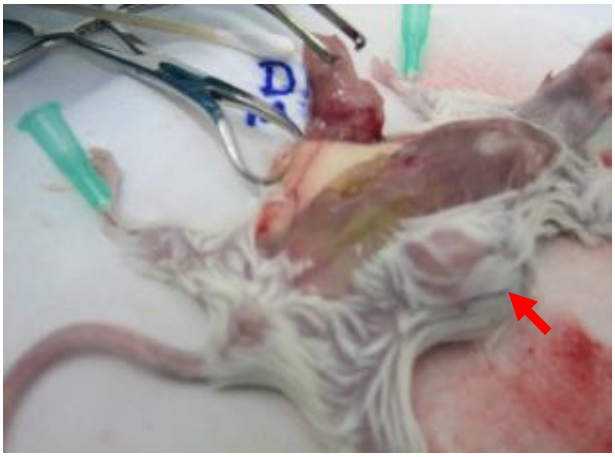

B

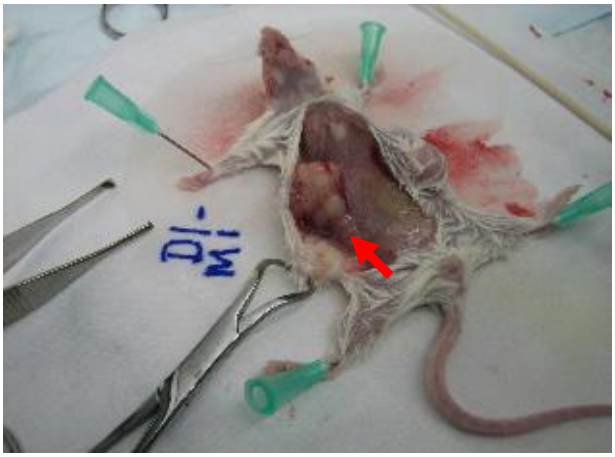

Figure 3.5-7:- Growth of xenograft tumours from DLKPI cells.
Representative images showing xenograft tumours following subcutaneous injection of DLKPI cells at inoculation densities of $5x10^6$ cells (Image A) and $1x10^7$ cells (image B) in 28-35 day old SCID mice. Red arrows indicate tumour location on both sides of the mouse.

(a)

Mouse no	DLKPI: Tumour growth measurements (mm^3) from mice inoculated with $1x10^6$ cells (Days)			
	21	**25**	**29**	**32**
1	117.20	398.36	584.06	807.79
2	65.80	251.16	564.37	563.70

(b)

Mouse No	DLKPI: Tumour growth measurements (mm^3) from mice inoculated with $5x10^6$ cells (Days)			
	21	**25**	**29**	***32***
1	286.65	692.20	711.62	1080.54
2	554.40	766.26	1498.65	1602.84
3	460.04	**Mouse sacrificed at day 21**		
4	491.39	970.22	1670.92	**Mouse sacrificed**

(c)

Mouse No	DLKPI: Tumour growth measurements (mm^3) from mice inoculated with $1x10^7$ cells (Days)			
	21	**25**	**29**	**32**
3	266.13	**Mouse sacrificed at day 21**		
4	149.50	435.24	907.26	**Mouse sacrificed**

Table 3.5-3:- DLKPI xenograft tumour measurements.
The growth of xenograft tumours following subcutaneous injection of DLKPI cells. Measurements of the tumours in SCID mice inoculated with DLKPI cells at cell densities of **(a)** $1x10^6$ cells (n=2), **(b)** $5x10^6$ cells (n=4) and **(c)** $1x10^7$ cells (n=2).

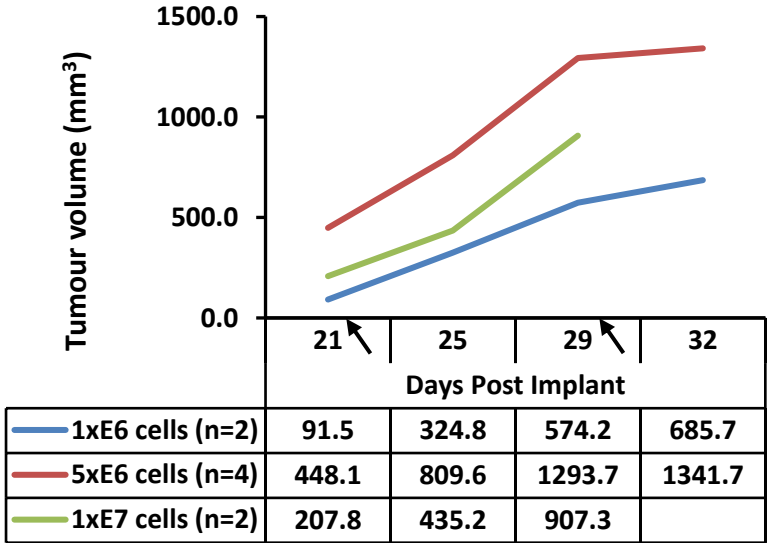

Figure 3.5-8:- Xenograft tumour growth curves for DLKPI.
Xenografts tumours were developed following subcutaneous injection of DLKPI cells in SCID mice over 32 days post injection. Tumour growth curves for DLKPI. Cell numbers injected: $1x10^6$ cells (n=2), $5x10^6$ cells (n=4), $1x10^7$ cells (n=2). Black arrow indicates when a mouse was sacrificed, reducing the numbers continuing on in the experiment.

3.5.2.4 Examination of the growth of DLKPM *in vivo*

Four 28-35 day old SCID mice received subcutaneous injections of DLKPM cells at cell densities of $1x10^6$ cells, $5x10^6$ cells and $1x10^7$ cells.

Three out of four mice displayed tumour formation across the three different inoculation densities of DLKPM at both injection sites. Exploratory surgery performed to look for evidence of metastasis in one mouse (mouse 4) inoculated with DLKPM cells after 21 days of growth revealed no evidence of metastasis. Figure 3.5-9 (A) and (B) gives a visual representation of tumours produced by DLKPM and their location (indicated by red arrows).

Tumours produced by DLKPM were the slowest growing, smallest and were more solid compared to those produced by DLKP, DLKPSQ and DLKPI. However, the most successful tumours to be produced by DLKPM were those injected with $1x10^7$ cells, indicating an optimal cell number could be required for tumour growth of DLKPM.

Measurements for the tumours produced by DLKPM for each of the cell densities used in this study are presented in Table 3.5-4 **(a)** $1x10^6$ cells (n=2), **(b)** $5x10^6$ cells (n=4) and **(c)** $1x10^7$ cells (n=2). The growth curves (Figure 3.5-10) highlights the size of tumours produced by DLKPM in SCID mice over 35 days.

A

B

Figure 3.5-9:- Growth of xenograft tumours from DLKPM cells.
Representative images showing xenograft tumours following subcutaneous injection of DLKPM cells at inoculation densities of $5x10^6$ cells (Image A) and $1x10^7$ cells (image B) in 28-35 day old SCID mice. Red arrows indicate tumour location on both sides of the mouse.

(a)

Animal No	DLKPM: Tumour growth measurements (mm^3) from mice inoculated with $1x10^6$ cells (Days)				
	21	**25**	**29**	**32**	**35**
1	0	0	0	470.20	698.15
2	0	0	0	0	0

(a)

Animal No	DLKPM: Tumour growth measurements (mm^3) from mice inoculated with $5x10^6$ cells (Days)				
	21	**25**	**29**	**32**	**35**
1	0	0	0	391.04	603.65
2	0	0	0	0	0
3	79.67	0	0	327.63	1324.56
4	224.40	**Mouse sacrificed at day 21**			

(b)

Animal No	DLKPM: Tumour growth measurements (mm^3) from mice inoculated with $1x10^7$ cells (Days)				
	21	**25**	**29**	**32**	**35**
3	102.25	196.56	304.29	367.08	807.40
4	253.34	**Mouse sacrificed at day 21**			

Table 3.5-4:- DLKPM xenograft tumour measurements.
The growth of xenograft tumours following subcutaneous injection of DLKPM cells. Measurements of the tumours in SCID mice inoculated with DLKPM cells at cell densities of **(a)** $1x10^6$ cells (n=2), (b) $5x10^6$ cells (n=4) and (c) $1x10^7$ cells (n=2).

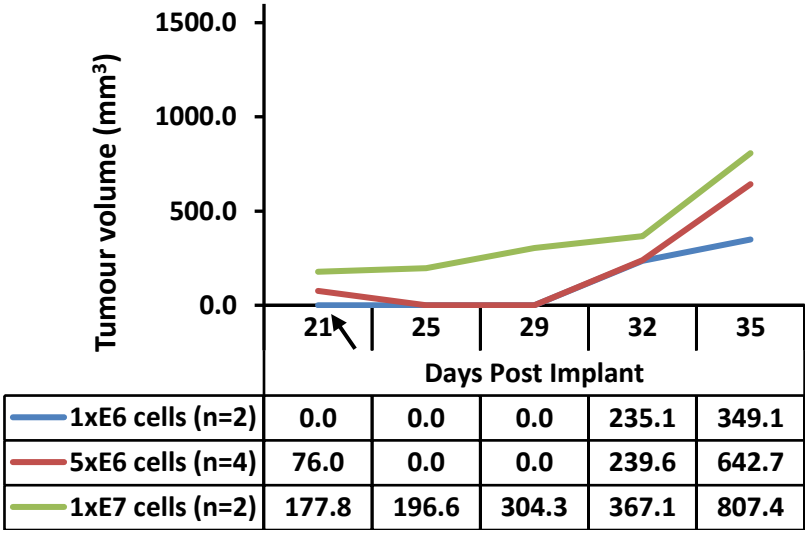

Figure 3.5-10:- Xenograft tumour growth curves for DLKPM.
Tumour xenografts were developed following subcutaneous injection of DLKPM cells in SCID mice over 35 days post injection. Tumour growth curves for DLKPM. Cell numbers injected: $1x10^6$ cells (n=2), $5x10^6$ cells (n=4), $1x10^7$ cells (n=2). Black arrow indicates when a mouse was sacrificed, reducing the animal numbers continuing on in the experiment.

3.5.2.5 Summary of xenograft tumour growth from the DLKP *in vivo* study

Growth curves of tumours developed by DLKP, DLKPSQ, DLKPI and DLKPM (Figure 3.5-11) in mice were determined using average measurements obtained from the chosen three different inoculation densities ($1x10^6$ cells (n=2), $5x10^6$ cells (n=4) and $1x10^7$ cells (n=2)). Tumour formation was clearly visible at all inoculation densities for DLKP, DLKPSQ, DLKPI and DLKPM cell lines indicating that this cell line model was deemed compatible with the mouse model used in this study.

- DLKP, DLKPSQ, DLKPI and DLKPM cell lines were all capable of producing tumours.
- DLKP and DLKPI appeared to grow fastest giving rise to the largest tumours (DLKPI appeared to be marginally faster).
- DLKP & DLKPI appeared to respond similarly with tumours produced on both injection sites at all cell densities by day 21.
- DLKPM showed a range in response: at 21 days 0 out of 2 mice inoculated with $1x10^6$ cells had tumours, 2 out of 4 mice inoculated with $5x10^6$ cells had tumours, while 2 out of 2 mice inoculated with $1x10^7$cells had tumours).
- DLKPI and DLKP tumours appeared to look similar, while DLKPM tumours were smaller and more solid.
- Tumours produced by DLKPSQ appeared to be much more vascularised and angiogenic. In 2 out of 4 mice inoculated with DLKPSQ, small growths were produced in the peritoneal cavity (suggesting evidence of potential metastasis). Mr Vincent Lynch suggested that these growths were carcinomatosis of the peritoneal cavity. In a follow up experiment, the masses were produced in 1 out of 6 mice (data not shown).

A

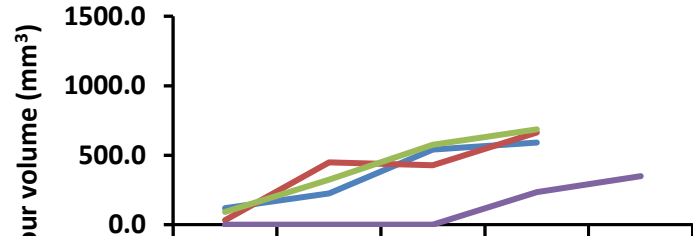

	21	25	29	32	35
DLKP	118.5	225.4	539.8	590.8	
DLKPSQ	32.0	449.3	426.9	663.2	
DLKPI	91.5	324.8	574.2	685.7	
DLKPM	0.0	0.0	0.0	235.1	349.1

B

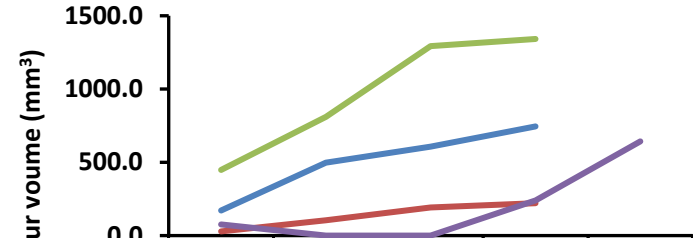

	21	25	29	32	35
DLKP	171.2	497.5	607.4	744.9	
DLKPSQ	28.6	103.5	191.4	221.1	
DLKPI	448.1	809.6	1293.7	1341.7	
DLKPM	76.0	0.0	0.0	239.6	642.7

C

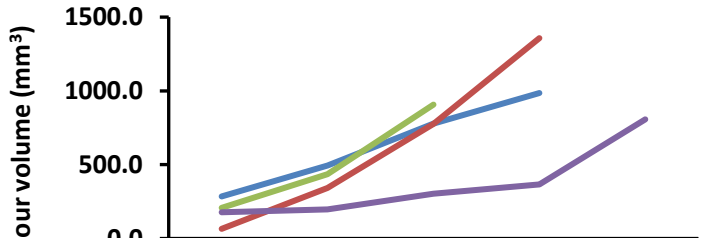

	21	25	29	32	35
DLKP	285.3	494.5	778.0	985.7	
DLKPSQ	65.7	343.2	777.1	1357.4	
DLKPI	207.8	435.2	907.3		
DLKPM	177.8	196.6	304.3	367.1	807.4

Figure 3.5-11:- Summary growth curves of xenografts tumours developed by DLKP and its clones.

(A) Tumour growth curve for DLKP, DLKPSQ, DLKPI and DLKPM in *SCID* mice at an inoculation density of $1x10^6$ cells, (n=2). **(B)** Tumour growth curve for DLKP, DLKPSQ, DLKPI and DLKPM in *SCID* mice at an inoculation density of $5x10^6$ cells, (n=4). **(C)** Tumour growth curve for DLKP, DLKPSQ, DLKPI and DLKPM in *SCID* mice at an inoculation density of $1x10^7$ cells, (n=2). Black arrow indicates where a mouse was sacrificed, reducing the animal numbers continuing on in the experiment.

3.6 Characteristics of DLKP, DLKPSQ, DLKPI and DLKPM cell lines post tumour explant culture

DLKP has at least three morphologically and phenotypically distinct clonal subpopulations (DLKPSQ, DLKPI and DLKPM). In culture, the ratios of these subpopulations in DLKP appear to remain balanced. Shirley McBride previously described a model for interconversion between the clonal subpopulations (i.e. DLKPSQ convert to DLKPI and DLKPI convert to DLKPM, but DLKPSQ cannot convert to DLKPM). One of the aims of this investigation was to establish if the DLKP clones developed different characteristics as a result of their growth in tumours compared to their growth under control conditions. The *in vivo* study presented an opportunity to recover DLKP and its clones from the tumours produced in SCID mice and to assess their characteristics post tumour growth.

3.6.1 Isolation of DLKP clones from Xenograft tumours by explant culture

Explant culture is a technique where by cells are isolated from a piece or pieces of tissue. Explant culture was carried out on xenograft tumours to investigate any changes in the *in vitro* characteristics of DLKP, DLKPSQ, DLKPI and DLKPM, post tumour growth. Table 3.6-1 indicates the names assigned to cell lines recovered from xenograft tumours and masses of the peritoneal cavity. This nomenclature was established to differentiate between the original DLKP cell lines and the DLKP cell lines established from the xenograft tumours, eliminating the risk of cross-contamination. The newly established tumour derived cell lines were initially cultured in serum free DMEM-Hams-F12 + 1% pen-strep to reduce the outgrowth of fibroblasts and contamination. Tumour derived cell lines were subsequently maintained in DMEM-Hams-F12 with 5% FCS**.** Established tumour cell lines were examined for changes in morphology, monolayer growth, anoikis, invasion and migration.

Control culture	Re-cultured cells	Source
DLKP	DLKPt	DLKP xenograft tumours
DLKPSQ (1)	DLKPSQta	DLKPSQ xenograft tumours
DLKPSQ (2)	DLKPSQtn	Growths from DLKSQ mice
DLKPI	DLKPIt	DLKPI xenograft tumours
DLKPM	DLKPMt	DLKPM xenograft tumours

Table 3.6-1:- Nomenclature of DLKP and its clones in control culture *vs.* DLKP and its clones recovered from mouse xenografts.

3.6.2 Examination of the morphology of explanted tumour cells

Once explant culture was complete, all cell lines were trypsinised from 6 well-plates into 12.5cm^2 where images were taken (early culture). Established recovered cell lines were then monitored for the subsequent 5 passages (late culture). Figure 3.6-1 shows the morphology of DLKPSQ, DLKPI and DLKPM cell lines pre-tumour growth (control) compared to recovered DLKPSQta, DLKPSQtn, DLKPIt and DLKPMt cell lines from xenograft tumours (early culture and late culture).

Early culture (passage 1): Compared to control culture, all clones appeared to have an obvious morphological difference in appearance compared to control cells. Most notable for DLKPSQtn and DLKPMt was that individual cells appeared to be more elongated, late culture (between passage 3 and passage 5), DLKPSQtn and DLKPIt appeared to revert back to the morphology seen in control culture. However, DLKPMt appeared to retain a more elongated appearance.

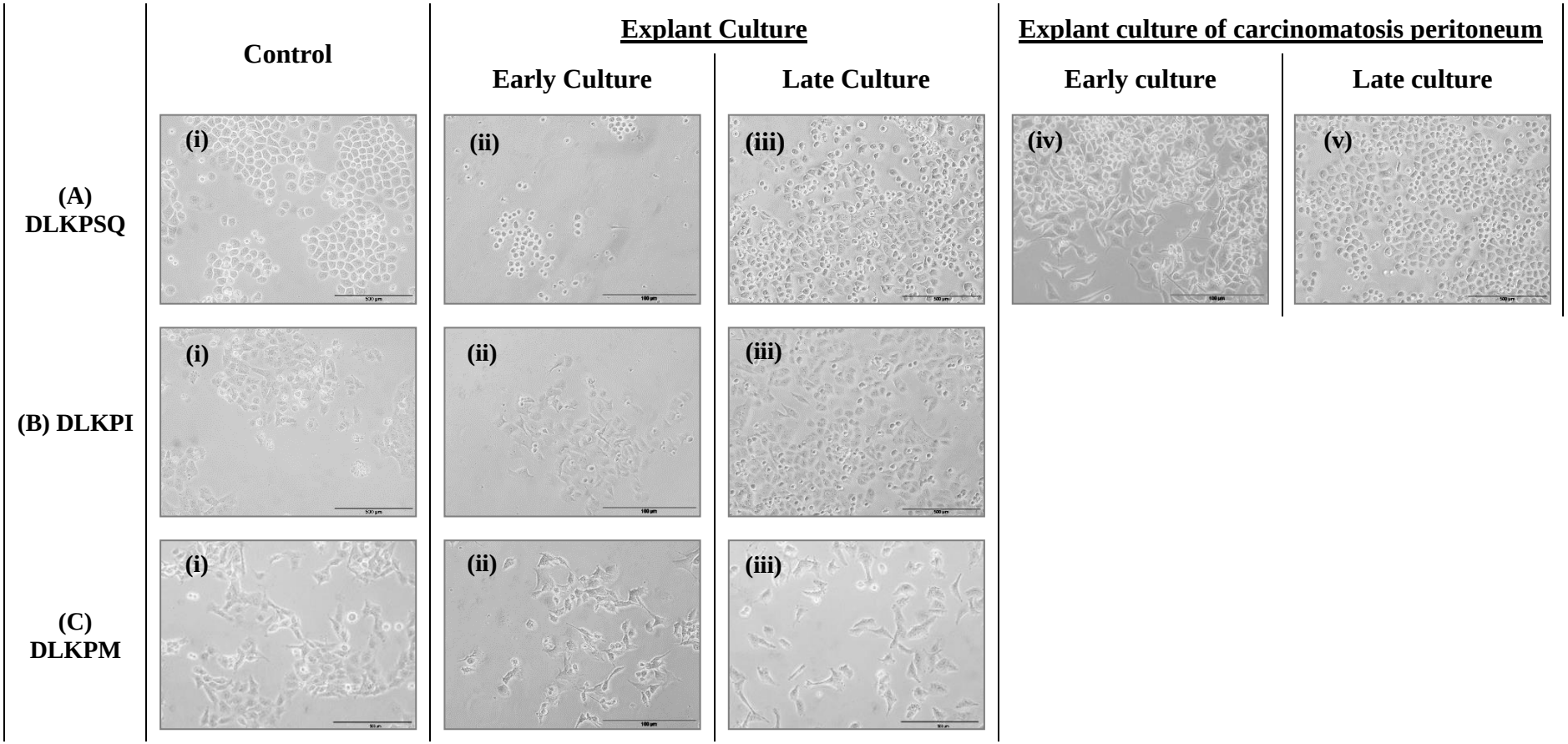

Figure 3.6-1:- Morphology of DLKP clones preimplantation *vs.* DLKP clones post explant culture.
Explant culture was performed on xenograft tumours implanted with DLKPSQ, DLKPI and DLKPM. **(A)** DLKPSQ (i) Control, (ii) Early culture post explant, (iii) Late culture post explant (DLKPSQta), cells from suspected Carcinomatosis: (iv) early culture, (v) Late culture (DLKPSQtn). **(B)** DLKPI (i) Control, (ii) Early culture post explant, (iii) Late culture post explant (DLKPIt). **(C)** DLKPM (i) Control, (ii) Early culture post explant, (iii) Late culture post explant (DLKPMt). (Original magnification, x400; *scale bar* = 100 & 500µm).

3.6.3 Examination of growth of explanted tumour cells

Recovered cell lines from xenograft tumours were examined for changes in growth. Figure 3.6-2 (A) shows a preliminary examination of the growth of explanted cells DLKPt, DLKPSQta, DLKPIt and DLKPMt compared to cells pre-tumour growth. Generally, all explanted cell lines grew in a similar fashion to control cells. However, a 90% decrease in growth of DLKPSQtn (cells from carcinomatosis peritoneum) relative to DLKPSQ control cells was observed.

3.6.3.1 Anoikis ability of explanted tumour cells

Recovered cell lines from xenograft tumours were examined for changes in anoikis resistance. Figure 3.6-2 (B) shows a preliminary examination of growth under anoikis conditions of explanted DLKPt, DLKPSQta, DLKPIt and DLKPMt *vs.* control cells. Under anoikis conditions, explanted DLKP clones grew similar to DLKP control clones. However, an increase in anoikis sensitivity was observed for DLKP, from 17% in control cells to 43% in explanted DLKPt cells.

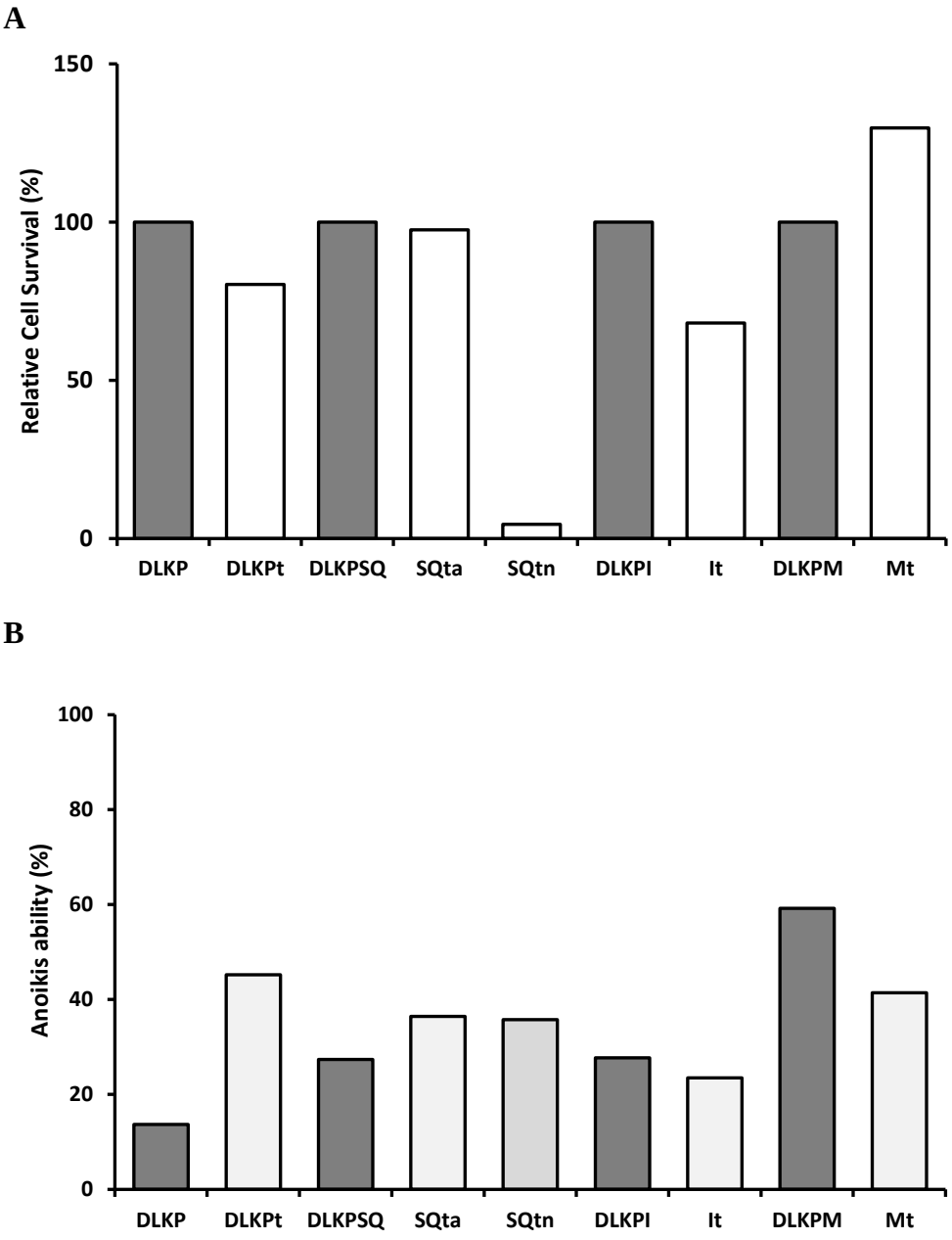

Figure 3.6-2:- Growth and anoikis capabilities of the DLKP clones post tumour growth.
DLKP and its clones under control conditions (grey) *vs.* recovered DLKP and clones from xenografts (white). DLKPt and clones from tumour explant culture were compared to DLKP and its clones under control conditions for changes in **(A)** growth (acid phosphase) and **(B)** anoikis ability (using alamar blue). Data plotted represents the single technical replicate from one biological assay (n=1).

3.6.4 Examination of invasive and migratory capacity of explanted tumour cells

Recovered cell lines from xenografts tumours were examined for changes in invasion and migration capacity. To assess whether the growth of DLKP and subpopulations in xenografts effected their invasive capacity, *in vitro* invasion assay were performed (as described in section 2.4.1), on explanted cells. Representative photomicrographs in Figure 3.6-3 show the invasive capacity of DLKP and its clones post tumour explant compared to cells in control culture, while Figure 3.6-4 shows the total number of invading DLKPt, DLKPSQta, DLKPIt and DLKPMt cells through matrigel compared to control cells. This preliminary examination of explanted cells indicates an increase in the invasion of DLKPt *vs.* DLKP control cells, while a reduction in invasion was observed for explanted DLKPSQta and DLKPMt cells compared to control cells.

Further examination of the invasive and migratory capacity of explanted DLKPSQta and DLKPMt were carried out. Figure 3.6-5 (B) (iii) shows a significant reduction in migratory capacity was observed for DLKPSQta (p=0.00605) *vs.* control DLKPSQ cells, while a significant reduction in **(C)** (iii) invasive capacity (p=0.000976) and **(D)** (iii) migratory capacity (p=0.008014) of DLKPMt *vs.* control DLKPM cells (Figure 3.6-5).

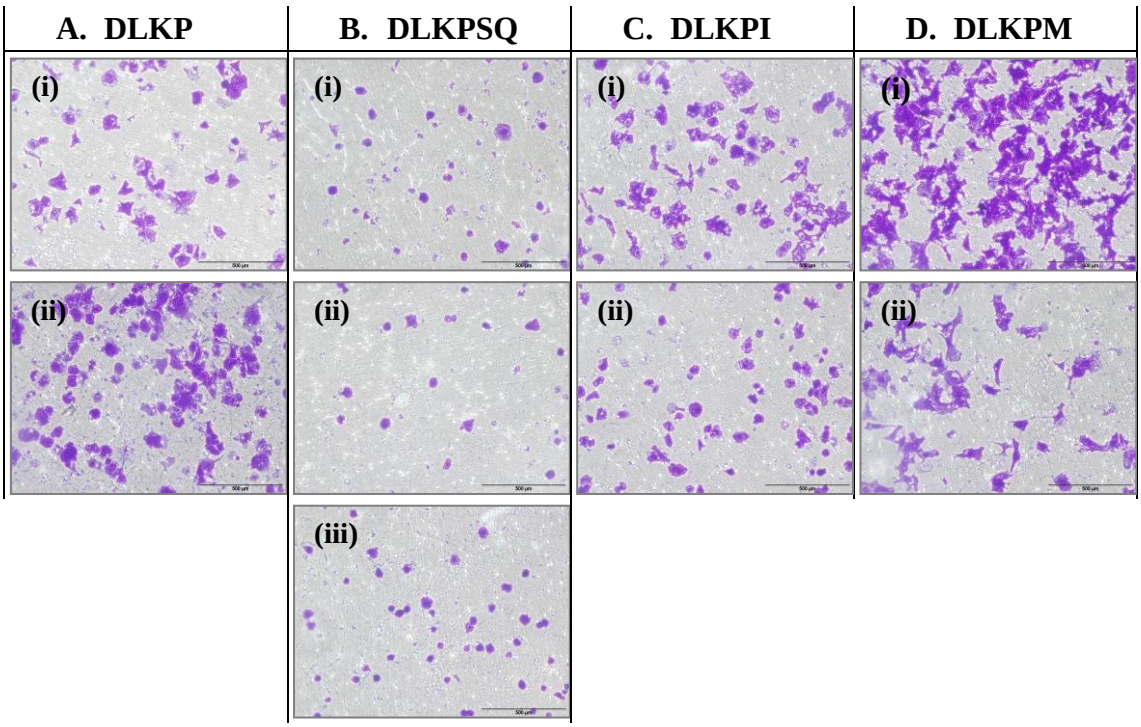

Figure 3.6-3:- The invasive capacity of DLKP and its clones post tumour growth.
DLKP and clones pre-implantation (Top row) *vs.* recovered DLKP and clones (bottom row) post explant culture. Explanted cell lines from xenograft tumours were examined for changes in levelss of invasion **(A)** (i) DLKP (ii) recovered DLKPt, **(B)** (i) DLKPSQ (ii) recovered DLKPSQta (iii) recovered DLKPSQtn, (**C)** (i) DLKPI (ii) recovered DLKPIt and **(D)** (i) DLKPM (ii) recovered DLKPMt (Original magnification x100, *scale-bar* = 200µm).

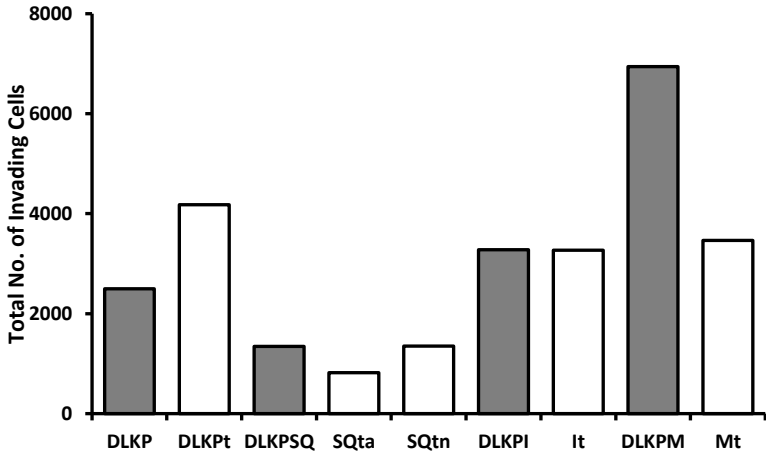

Figure 3.6-4:- The invasive capacity of DLKP and its clones post tumour explant culture.
Preliminary invasion assays showing: DLKP and its clones (grey) compared to DLKP post tumour growth (white). Explanted cell lines from xenograft tumours were examined for changes in levels of invasion. An increase was observed for DLKPt cells, while a reduction was observed for DLKPMt cells compared to control cells. The total number of invading cells is shown. Data plotted represents mean ± standard deviation of duplicate inserts, (n=1).

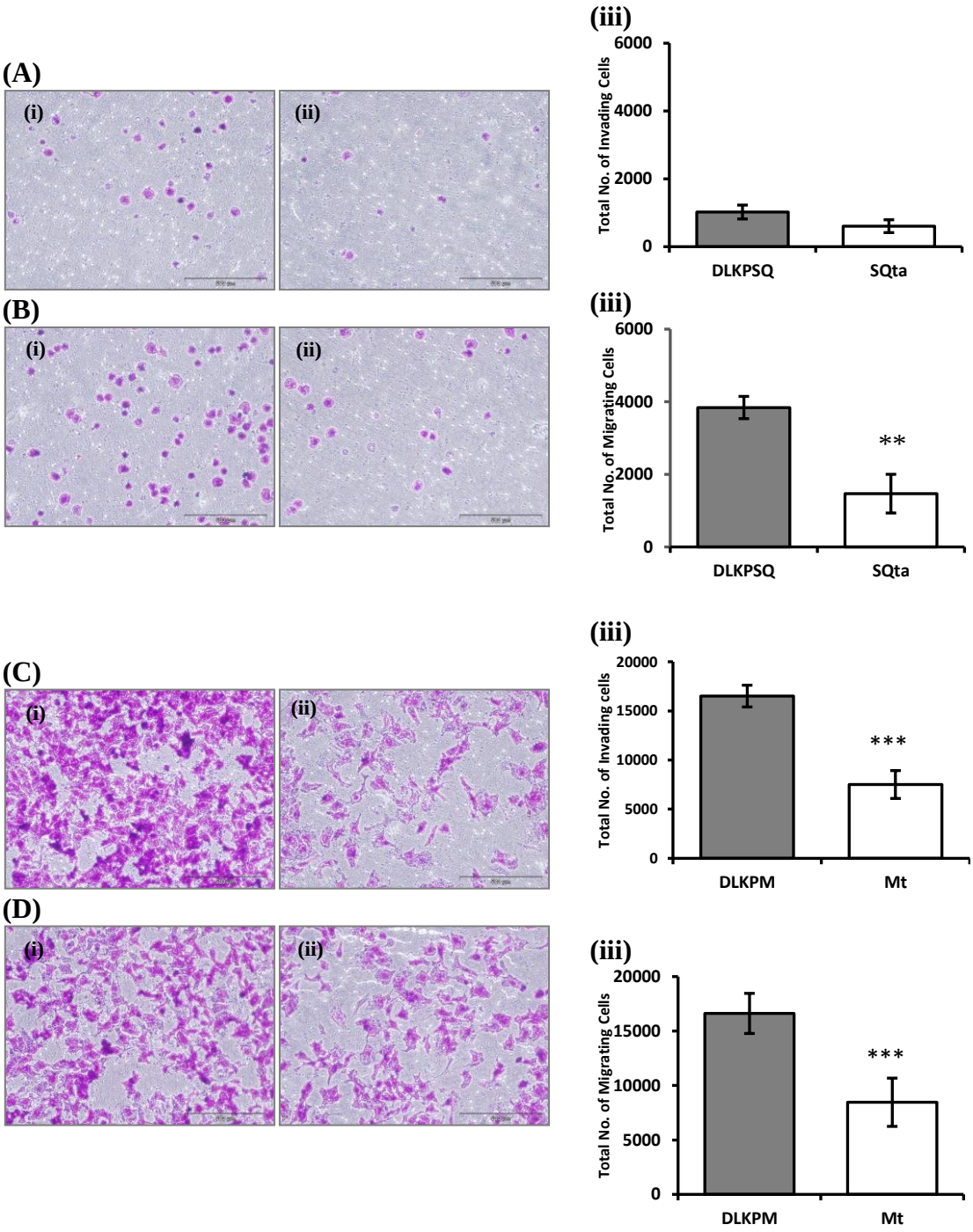

Figure 3.6-5:- Invasive and migratory capacity of DLKPSQ and DLKPM post tumour growth.

Invasion and migration assays were carried out on DLKPSQ and DLKPM pre-implantation and post explant culture. **(A)** Invasive capacity of DLKPSQ (i) pre-implantation (ii) post explant culture (iii) Total invading cells: preimplantation *vs.* explant culture invasive capacity. **(B)** Migratory capacity of DLKPSQ (i) pre-implantation (ii) post explant culture (iii) Total migrating cells: preimplantation *vs.* explant culture (p=0.00605). **(C)** Invasive capacity of DLKPM (i) pre-implantation (ii) post explant culture (iii) Total invading cells: preimplantation *vs.* explant culture invasive capacity (p=0.000976). **(D)** Migration of DLKPM (i) pre-implantation (ii) post explant culture (iii) Total migrating cells: preimplantation *vs.* explant culture (p=0.008014). Data plotted represents the mean +/- standard deviation duplicate inserts from triplicate biological assays. Statistics ** $p \leq 0.01$ and *** $p \leq 0.005$. Student's *t* test (two tailed with equal variance, unpaired, n=3).

3.7 Immunohistochemical analysis of xenograft tumours

An *in vivo* investigation was carried out where DLKP, DLKPSQ, DLKPI and DLKPM cell lines were implanted into mice. Section 3.5.2 outlines the capacity of each cell line to form tumours *in vivo* over a 32 - 35-day period post implantation of cells. After this period (or once the guideline tumour volume of 2000mm^2 was reached) the mice were sacrificed and the tumours were harvested. One mouse from each cell line was sacrificed for exploratory surgery at day 21, the tumours from this mouse were formalin-fixed-paraffin embedded and sectioned for immunohistochemical analysis. This investigation would allow us to characterise tumours for the expression of angiogenesis and proliferation markers, but also to evaluate any differences in expression of validated proteins from section 3.2 as a result of growth in tumours.

An immunohistochemical survey was carried out using antibodies specific to a small number of protein markers known to be involved in cancer progression. For all xenograft tumours, the same tumour block was used throughout this study, however, fresh sections were cut when required. Antibodies targeted against the protein targets were used to stain xenograft tumours derived from DLKP, DLKPSQ, DLKPI and DLKPM cell lines. Tumours used for IHC were established from an inoculation density of 1x10^6 cells and 5x10^6 cells.

3.7.1 Human mitochondrial protein

Human cells were used to form human tumours, however, the tumours were allowed to form in mice, these tumours may recruit murine tissue in order for the tumours to form. Before starting any immunohistochemical analysis, it was necessary to determine the amount of infiltrating murine tissue present in each of the tumours. The xenograft tissues were therefore stained using a commercial antibody specific to human mitochondrial proteins.

Paraffin embedded sections of DLKP, DLKPSQ, DLKPI and DLKPM xenograft tissue sections were examined for reactivity to Human mitochondrial protein. Intense staining was observed in all tumours from all cell line derived tumours, some areas of the tumours displayed weaker expression (Figure 3.7-1).

3.7.2 Ki-67

Ki-67 antigen is a protein present in the nuclei of proliferating cells. It is widely used as a marker of proliferating tumour cells [119]. An antibody specific to Ki-67 was used to examine Ki67 expression in paraffin-embedded sections of xenograft tumours from the

in vivo study. Strong staining was observed in all tumours, however possibly more intense staining was found to be in tumours derived from DLKP and DLKPI cells (Figure 3.7-2). There appear to be more cells staining positive for Ki67 in the tumours compared to staining observed for human mitochondria proteins. Strong Ki-67 staining indicates that the xenograft tumours derived by DLKP, DLKPSQ, DLKPI and DLKPM cells were highly proliferative.

3.7.3 CD31

CD31 (PECAM-1) is found on the surface of endothelial cells and has been used routinely as a marker for angiogenesis [120]. An antibody specific to CD31 was used to examine the expression of CD31 in paraffin-embedded sections of xenograft tumours from our DLKP *in vivo* study. In xenograft tumours derived from DLKP, DLKPSQ, DLKPI and DLKPM, weak/low level staining of CD31 was observed (Figure 3.7-3).

3.7.4 E-cadherin and N-cadherin

E-cadherin and N-cadherin are proteins known to be involved in processes such as cell-cell adhesion, differentiation, migration and invasion. Their involvement in epithelium to mesenchymal transition (EMT) has also been suggested. During an EMT, E-cadherin is downregulated while N-cadherin is upregulated during a process known as cadherin switching [121]. Expression of both E-cadherin and N-cadherin were examined in paraffin embedded sections of xenograft tumours from our DLKP *in vivo* study.

In the xenograft tumours associated with DLKPSQ, low-level staining in small areas of the tumours was observed for E-cadherin, however, tumours derived from DLKP, DLKPI and DLKPM showed very low to negative immunoreactivity for E-cadherin (Figure 3.7-4). Staining was not observed in explanted cells from the tumour xenografts (Figure 3.7-5). N-cadherin expression was previously established in DLKP and the clones. As expected strong staining was observed in tumours associated with DLKP, DLKPI and DLKPM with low level staining in tumours associated with DLKPSQ (Figure 3.7-6). Interestingly, in explanted cells, the intensity of expression of N-cadherin was increased in explanted DLKPt cells and DLKPSQta cells and is reduced in explanted DLKPMt cells compared to control cells (Figure 3.7-7). Tissue section associated with DLKPI (inoculation density of $1x10^6$ cells) is not shown because the section did not stain correctly. A summary of the immunohistochemical analysis of markers outlined above is presented in Table 3.7-1.

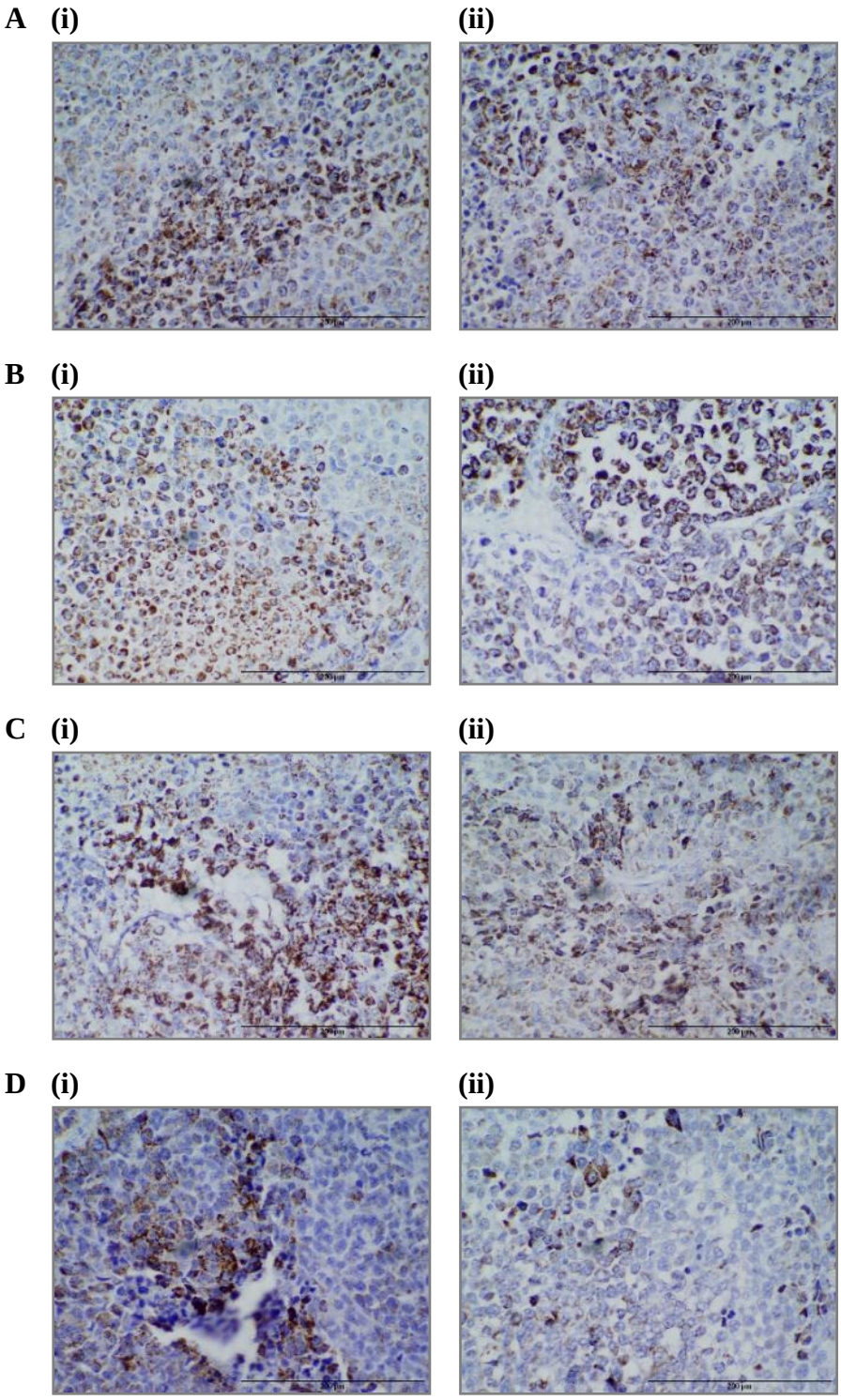

Figure 3.7-1:- Expression of human mitochondrial protein in xenograft tumours.
Xenograft tumours derived from; **(A)** DLKP implanted with (i) $1x10^6$ cells (ii) $5x10^6$ cells, **(B)** DLKPSQ implanted with (i) $1x10^6$ cells (ii) $5x10^6$ cells, **(C)** DLKPI implanted with (i) $1x10^6$ cells (ii) $5x10^6$ cells and **(D)** DLKPM implanted with (i) $1x10^6$ cells (ii) $5x10^6$ cells. Strong staining was observed in all xenograft tumours using an antibody specific to a human mitochondrial protein. (Magnification, x400; *scale bar* = 200µm).

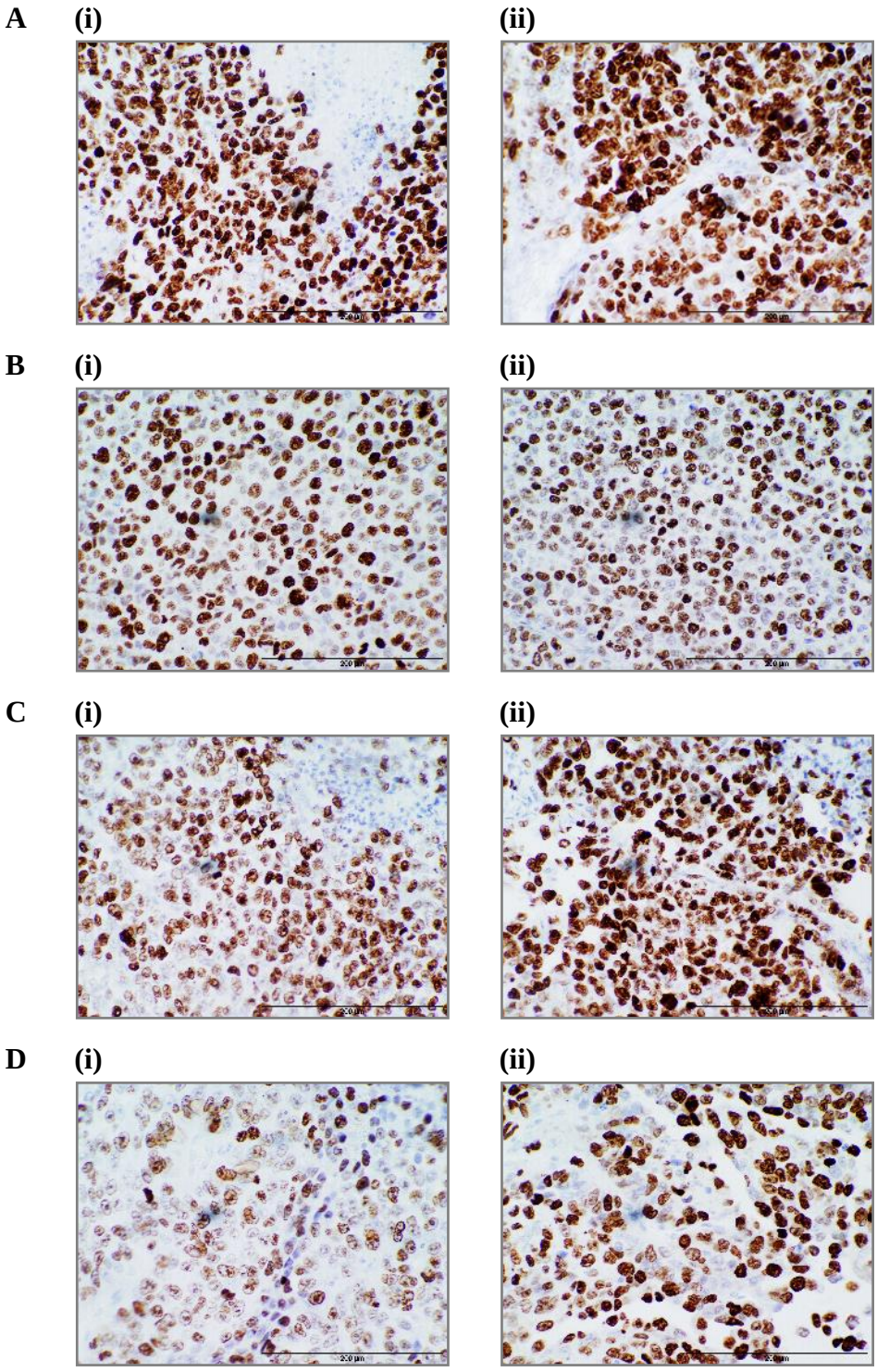

Figure 3.7-2:- Expression of Ki-67 in xenograft tumours.
Xenograft tumours derived from; **(A)** DLKP implanted with (i) $1x10^6$ cells (ii) $5x10^6$ cells, **(B)** DLKPSQ implanted with (i) $1x10^6$ cells (ii) $5x10^6$ cells, **(C)** DLKPI implanted with (i) $1x10^6$ cells (ii) $5x10^6$ cells and **(D)** DLKPM implanted with (i) $1x10^6$ cells (ii) $5x10^6$ cells, intense staining was observed in all tumours, using an antibody specific to Ki67. (Magnification, x400; *scale bar* = 200µm).

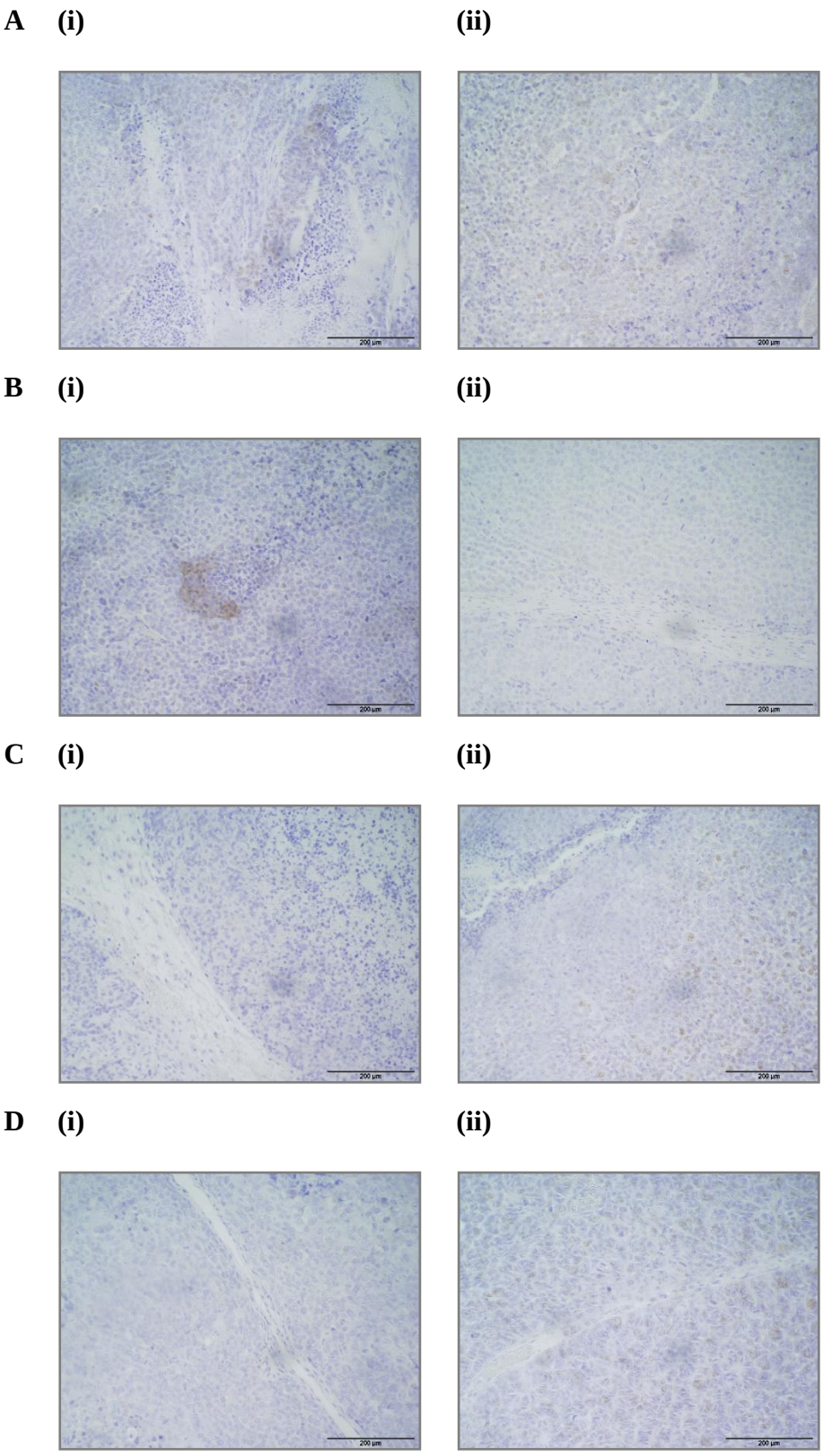

Figure 3.7-3:- Representative images of xenograft tumours stained for the expression of CD31.
Xenograft tumours derived from; **(A)** DLKP (i) $1x10^6$ (ii) $5x10^6$, **(B)** DLKPSQ (i) $1x10^6$ cells (ii) $5x10^6$ cells, **(C)** DLKPI ((i) $1x10^6$ cells (ii) $5x10^6$ cells and **(D)** DLKPM (i) $1x10^6$ cells (ii) $5x10^6$ cells, weak/low level staining was observed in all xenograft tumours, using an antibody specific to CD31 (Magnification, x400; *scale bar* = 200µm).

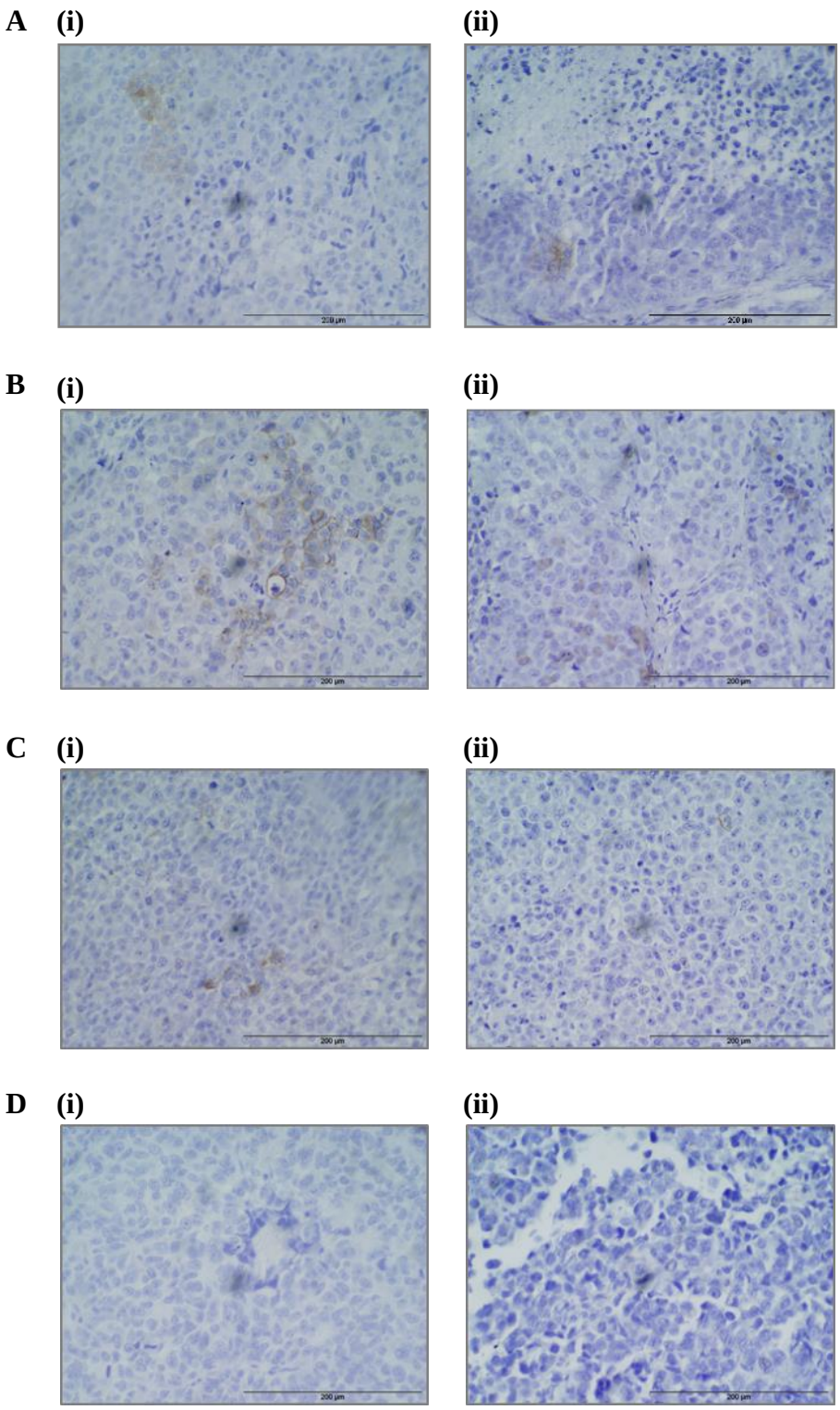

Figure 3.7-4:- Representative images of xenograft tumours stained for the expression of E-cadherin.
Xenograft tumours derived from; **(A)** DLKP implanted with (i) $1x10^6$ cells (ii) $5x10^6$ cells, **(B)** DLKPSQ implanted with (i) $1x10^6$ cells (ii) $5x10^6$ cells, **(C)** DLKPI implanted with (i) $1x10^6$ cells (ii) $5x10^6$ cells and **(D)** DLKPM implanted with (i) $1x10^6$ cells (ii) $5x10^6$ cells. Low level staining for E-cadherin observed in DLKPSQ tumours, using an antibody specific to E-cadherin. (Magnification, x400; *scale bar* = 200µm).

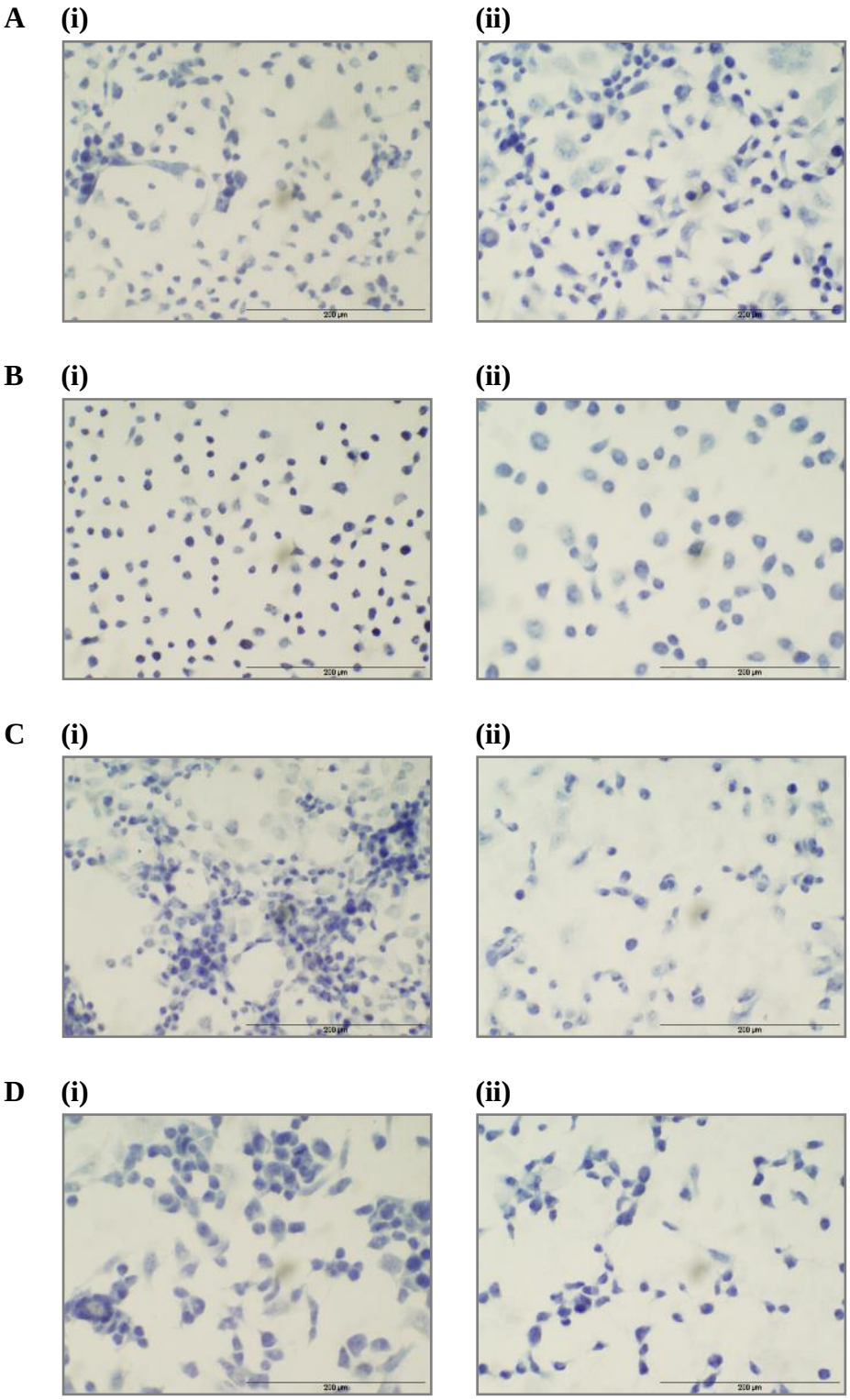

Figure 3.7-5:- Representative images of control cells *vs.* explanted cells stained for expression of E-cadherin.
Control cells compared to explanted cell lines from xenograft tumours. **(A)** DLKP (i) control cells (ii) explanted cells, **(B)** DLKPSQ (i) control cells (ii) explanted cells, **(C)** DLKPI (i) control cells (ii) explanted cells and **(D)** DLKPM (i) control cells (ii) explanted cells. Using an antibody specific to E-cadherin, staining was not observed in explanted tumour cells. (Magnification, x400; *scale bar* = 200µm).

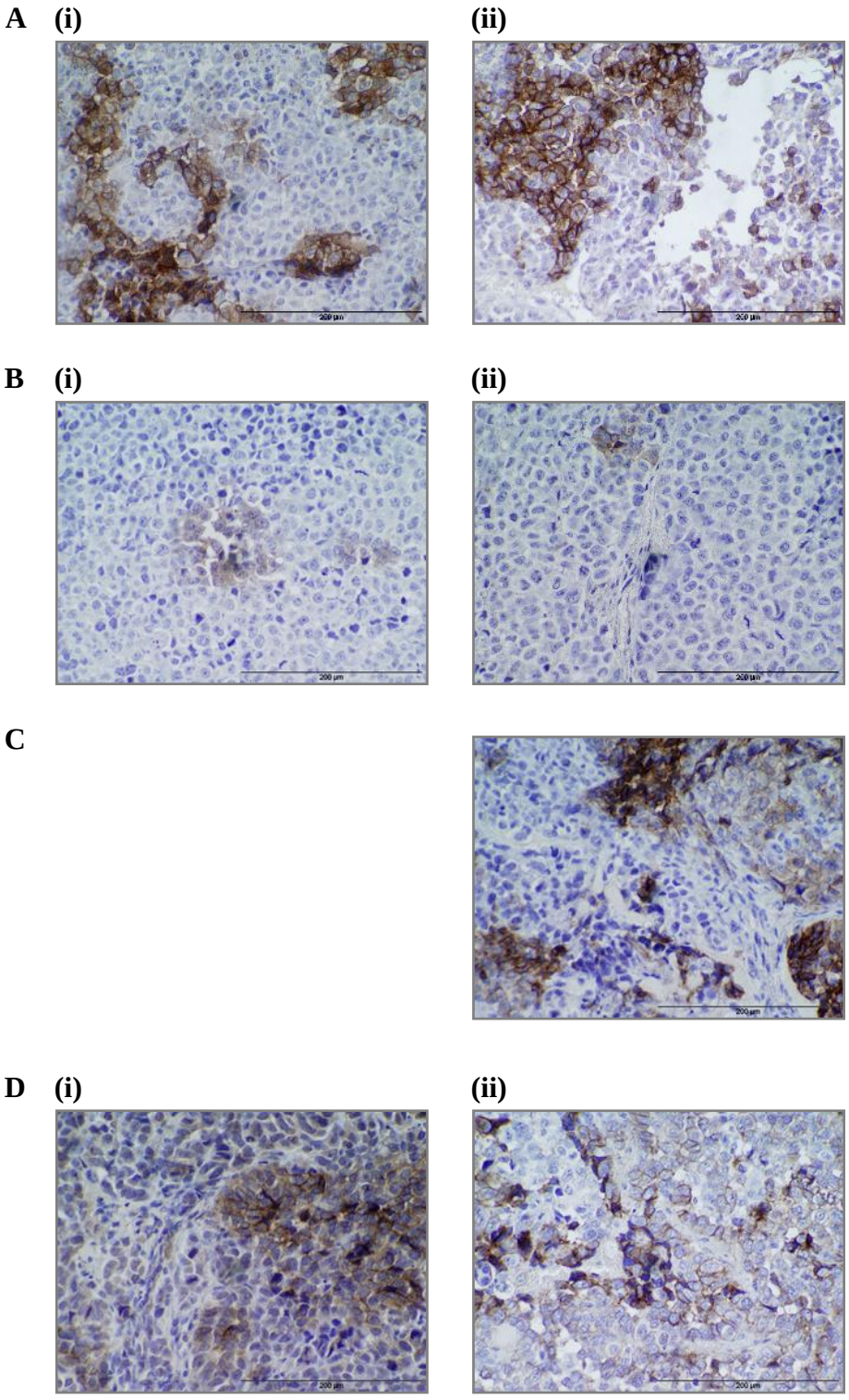

Figure 3.7-6:- Expression of N-cadherin in xenograft tumours
Xenograft tumours derived from; **(A)** DLKP implanted with (i) $1x10^6$ cells (ii) $5x10^6$ cells, **(B)** DLKPSQ implanted with (i) $1x10^6$ cells (ii) $5x10^6$ cells, **(C)** DLKPI implanted with $5x10^6$ cells and **(D)** DLKPM implanted with (i) $1x10^6$ cells (ii) $5x10^6$ cells. Staining was observed in all xenograft tumours using an antibody specific to N-cadherin. (Magnification, x400; *scale bar* = 200µm).

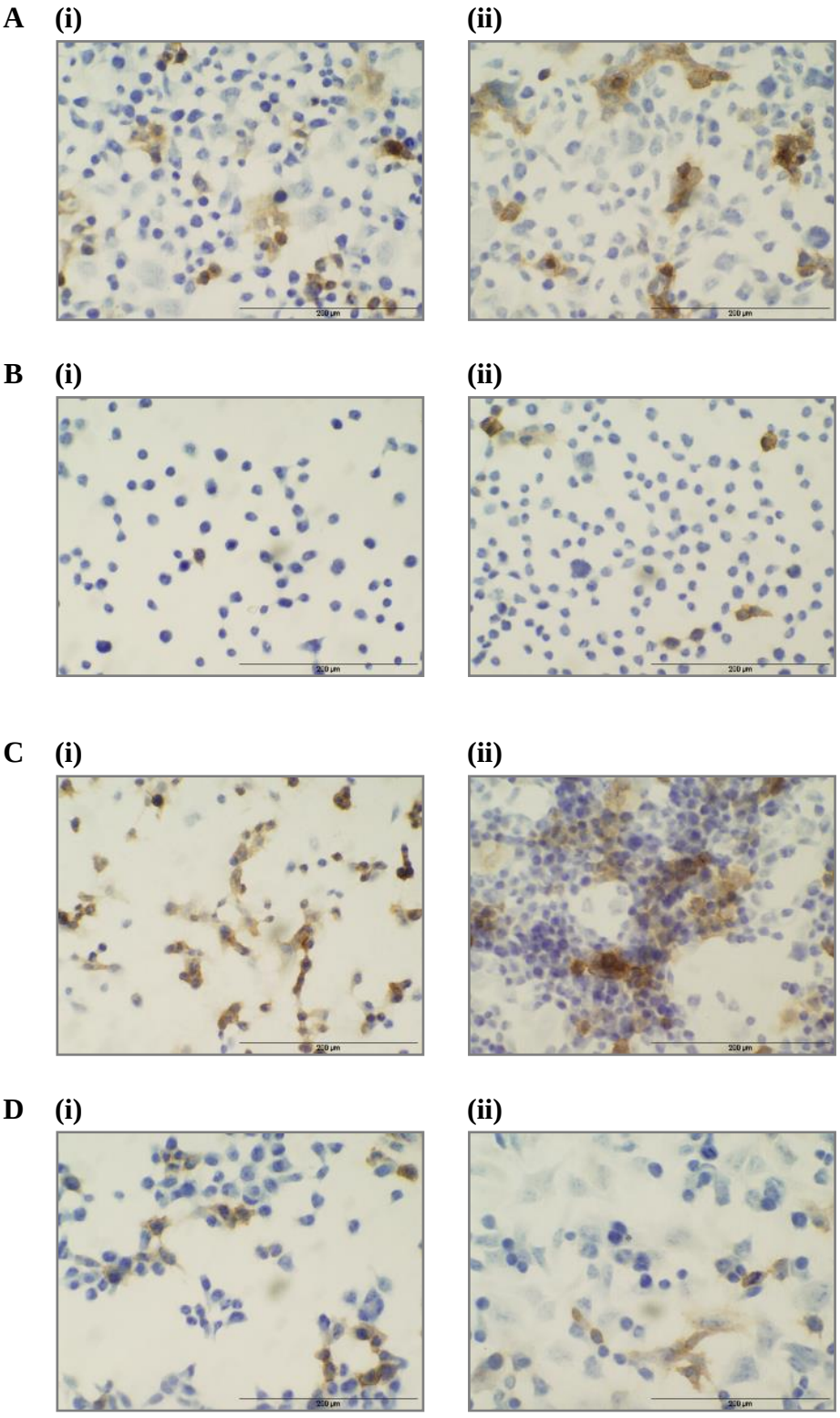

Figure 3.7-7:- Expression of N-cadherin in cells derived from xenograft tumours.
Xenograft tumours derived from; **(A)** DLKP (i) control cells (ii) explanted cells, **(B)** DLKPSQ (i) control cells (ii) explanted cells, **(C)** DLKPI (i) control cells (ii) explanted cells and **(D)** DLKPM (i) control cells (ii) explanted cells (ii) $5x10^6$ cells, using an antibody specific to E-cadherin. (Magnification, x400; *scale bar* = 200µm).

3.7.5 Summary of staining observed in cell line derived-xenografts

Target protein	Cell line derived Xenografts			
	DLKP	DLKPSQ	DLKPI	DLKPM
Human Mitochondrial protein	+++	+++	+++	+++
Ki-67	+++	++	++	++
CD31 (PECAM-1)	-	-/+	-	-
E-cadherin	+	-/+	+	-
N-cadherin	+	-/+	++	+

Table 3.7-1:- Summary of Immunohistochemical analysis carried out on xenograft tumours. Representative analysis of tumours formed after implantation of cells at $1x10^6$ and $5 x10^6$ cells. +++ very intense positivity, ++ intense positivity, +weak positivity: +/- some very weak positivity, - Negative.

3.8 Immunohistochemical analysis of differentially expressed proteins in xenograft tumours derived from DLKP clones

DLKP, DLKPSQ, DLKPI and DLKPM cell lines were all shown to be able to produce tumours in SCID mice. In this section, Western blot analysis and Immunohistochemistry were used to investigate the expression of the differentially expressed proteins which were identified by comparative proteomics analysis (section 3.1.3 and section 3.1.4), in explanted cells and xenograft tissues. Representative tumour blocks were prepared from tumours derived from inoculation densities of $1x10^6$ cells and $5x10^6$ cells, fresh sections were prepared as required.

3.8.1 Expression of SLIT2 and ROBO2 *in vivo*.

SLIT2 ligand and its receptor ROBO2 were previously studied in DLKP and its clones (see section 3.2.3). The expression of SLIT2 and ROBO2 was examined in explanted tumour cells and xenograft tumours derived from DLKP and its clones.

Western blot analysis was carried out to establish the expression of SLIT2 in membrane enriched fractions which were prepared from cells recovered from xenograft tumours via explant culture. Expression of SLIT2 was examined in recovered cells (DLKPt, DLKPSQta, DLKPIt and DLKPMt) and control cells (DLKP, DLKPSQ, DLKPI and DLKPM). A potential loss of SLIT2 was observed with DLKPSQta compared to control DLKPSQ cells, while a potential increase in expression of SLIT2 was observed in DLKPt compare to control DLKP (Figure 3.8-1), DLKPIt and DLKPMt cells appear to maintain expression compared to control cells. This was a preliminary investigation and would need to be repeated with the inclusion of appropriate loading controls.

Immunohistochemistry was carried out to determine the expression of SLIT2 and its receptor ROBO2 in paraffin embedded sections of the xenograft tissues. Figure 3.8-2 shows strong staining for SLIT2 in xenograft tissues in (A) DLKP, (B) DLKPI, (C) DLKPSQ and (D) DLKPM. The expression pattern of SLIT2 in xenografts is broadly in line with expression seen in Western blot validations in section 3.2.3. The *in vivo* expression of ROBO2 appears to show the same pattern of expression seen for SLIT2, increased expression in DLKP and DLKPM xenograft and lower expression levels for DLKPSQ and DLKPI (Figure 3.8-3).

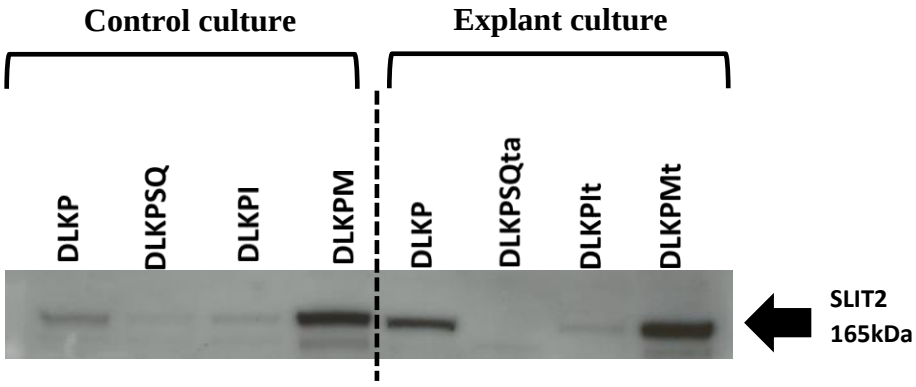

Figure 3.8-1:- Expression of SLIT2 in the explanted DLKP tumour cells
Represents expression of SLIT2 in membrane enriched fractions from explanted tumour cells (DLKPt, DLKPSQta, DLKPIt and DLKPMt) compared to control cells (DLKP, DLKPSQ, DLKPI and DLKPM), using an antibody specific to SLIT2 (n=1).

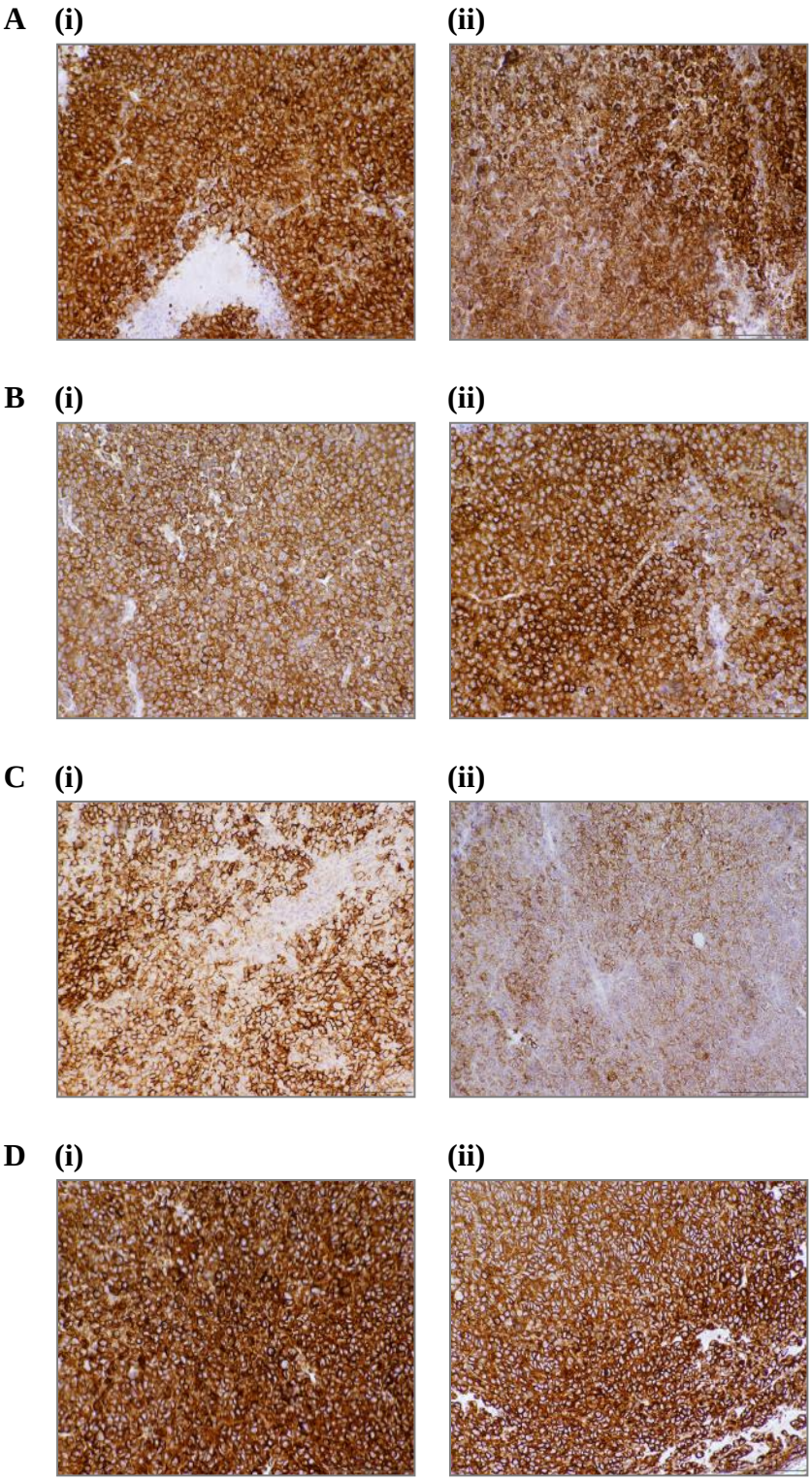

Figure 3.8-2:- Expression of SLIT2 in the xenograft tumours.
Xenograft tumours derived from; **(A)** DLKP implanted with (i) $1x10^6$ cells (ii) $5x10^6$ cells, **(B)** DLKPSQ implanted with (i) $1x10^6$ cells (ii) $5x10^6$ cells, **(C)** DLKPI implanted with (i) $1x10^6$ cells (ii) $5x10^6$ cells and **(D)** DLKPM implanted with (i) $1x10^6$ cells (ii) $5x10^6$ cells, Strong immunoreactivity was observed in all tumours using an antibody specific to a SLIT2 (Magnification, x400; *scale bar* = 200µm).

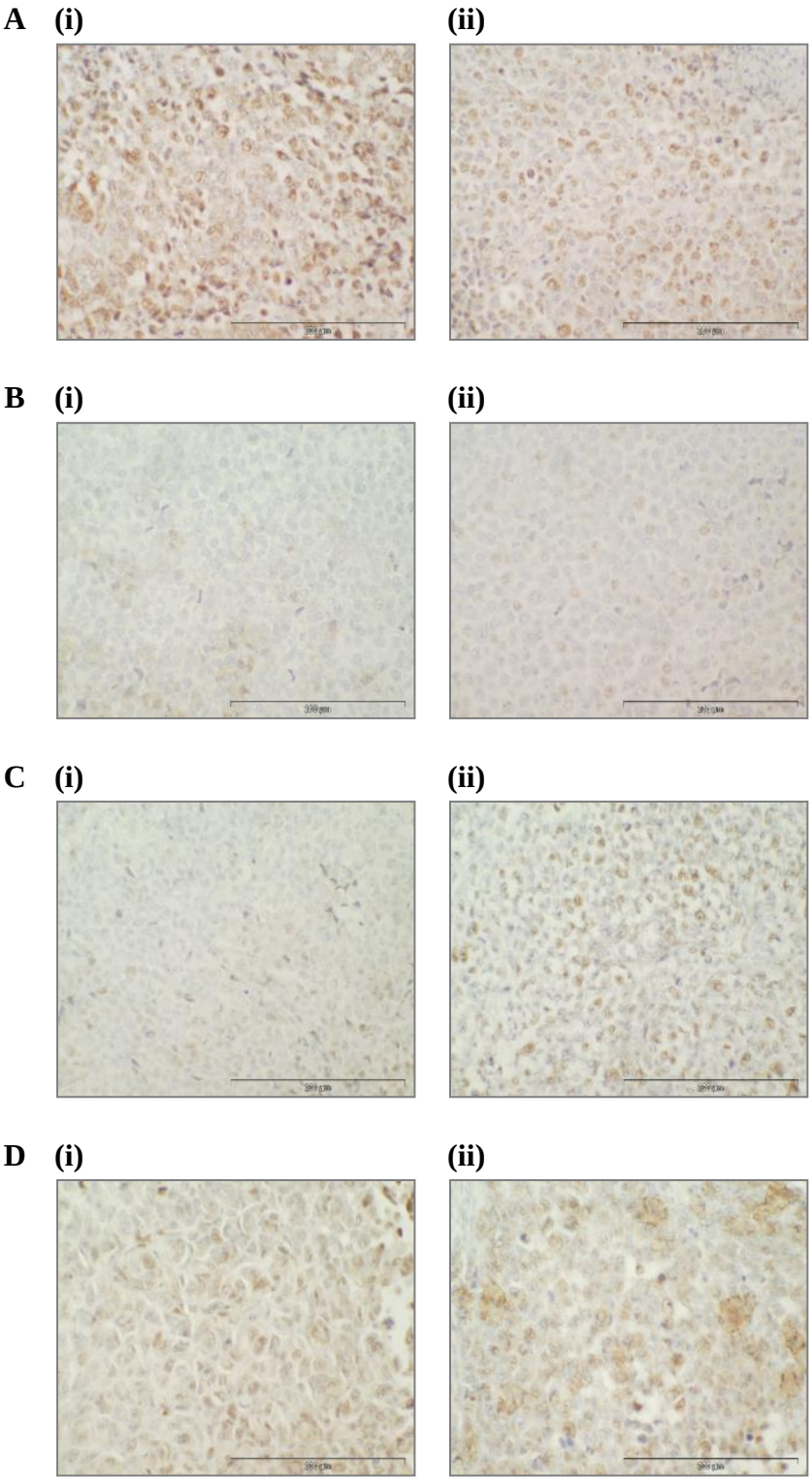

Figure 3.8-3:- Expression of ROBO2 in the xenograft tumours.
Xenograft tumours derived from; **(A)** DLKP implanted with (i) $1x10^6$ cells (ii) $5x10^6$ cells, **(B)** DLKPSQ implanted with (i) $1x10^6$ cells (ii) $5x10^6$ cells, **(C)** DLKPI implanted with (i) $1x10^6$ cells (ii) $5x10^6$ cells and **(D)** DLKPM implanted with (i) $1x10^6$ cells (ii) $5x10^6$ cells. Immunoreactivity was observed in all tumours using an antibody specific to a ROBO2 (Magnification, x400; *scale bar* = 200µm).

3.8.2 Expression of ALCAM *in vivo*.

ALCAM expression was previously studied in DLKP and its clones (see section 3.2.4). The expression of ALCAM was investigated in explanted tumour cells and xenograft tumours derived from DLKP and its clones.

Western blot analysis was carried out to establish the expression of ALCAM in membrane-enriched fractions which were prepared from cells recovered from xenograft tumours via explant culture. Figure 3.8-4 confirms expression of ALCAM to be maintained strongly in recovered cells from DLKPIt xenografts tumours compared to cells under control conditions. In the control cells, ALCAM is expressed at a notably lower level in DLKP, DLKPSQ and DLKPM compared to DLKPI, this expression pattern is also maintained *in vivo*. This was a preliminary investigation carried out on membrane enriched fractions of the and would need to be repeated but also examined in whole cell lysates of the cell lines with the inclusion of appropriate loading controls.

Immunohistochemical analysis was carried out to determine the expression of ALCAM in paraffin embedded sections of the xenograft tissues. Representative images showing staining of ALCAM in xenografts tumours derived from DLKP and its clones (Figure 3.8-5), intense expression was maintained throughout DLKPI xenograft tumour, while smaller areas of staining were observed for DLKP, DLKPSQ and DLKPM xenograft tissues.

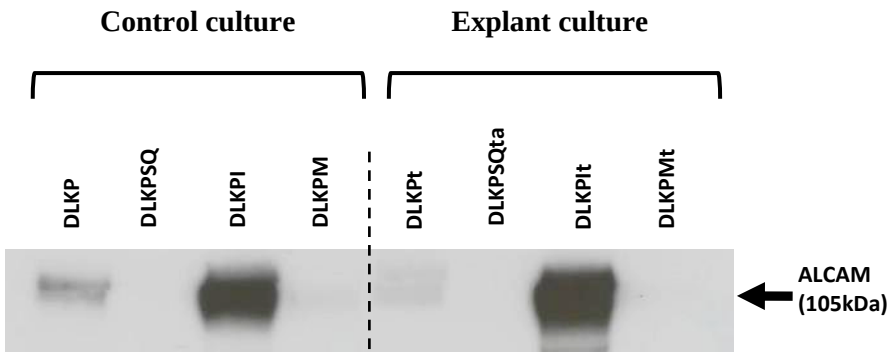

Figure 3.8-4:- Expression of ALCAM in the explanted DLKP tumour cells.
Represents expression of ALCAM in membrane enriched fractions from explanted tumour cells (DLKPt, DLKPSQta, DLKPIt and DLKPMt) compared to control cells (DLKP, DLKPSQ, DLKPI and DLKPM), using an antibody specific to ALCAM (n=1).

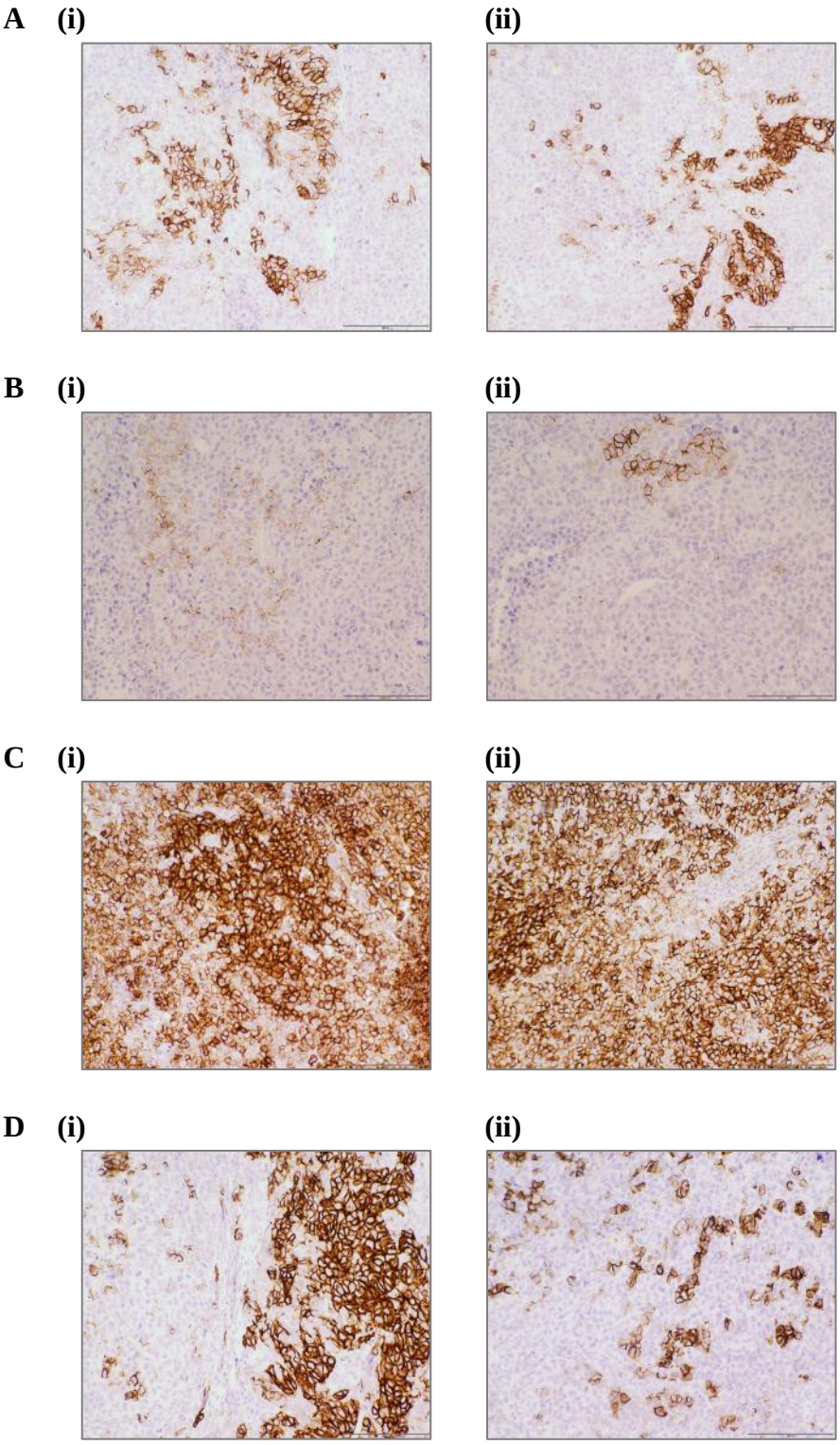

Figure 3.8-5:- Expression of ALCAM in the xenograft tumours.
Xenograft tumours derived from; **(A)** DLKP implanted with (i) $1x10^6$ cells (ii) $5x10^6$ cells, **(B)** DLKPSQ implanted with (i) $1x10^6$ cells (ii) $5x10^6$ cells, **(C)** DLKPI implanted with (i) $1x10^6$ cells (ii) $5x10^6$ cells and **(D)** DLKPM implanted with (i) $1x10^6$ cells (ii) $5x10^6$ cells, staining was observed in all tumours with DLKPI showing most intense immunoreactivity, using an antibody specific to a ALCAM (Magnification, x400; *scale bar* = 200µm).

3.8.3 Expression of IQGAP1 *in vivo*

Expression of IQGAP1 was previously studied in DLKP and its clones (see section 3.2.5). The expression of IQGAP1 was examined in explanted tumour cells and xenograft tumours derived from DLKP and its clones. Western blot analysis was carried out to establish expression of IQGAP1 in membrane enriched fractions which were prepared from cells recovered from xenograft tumours via explant culture. Figure 3.8-6 confirmed expression of IQGAP1 in recovered cells (DLKPt, DLKPSQta, DLKPIt and DLKPMt) compared to cells cultured under control conditions (DLKP, DLKPSQ, DLKPI and DLKPM). Post tumour explantation, expression of IQGAP1 appears to be decreased in DLKPSQta, DLKPIt and DLKPMt compared to control cells, while expression in DLKPt appears to be increased compared to control DLKP. This was a preliminary investigation and would need to be repeated with the inclusion of appropriate loading controls.

Immunohistochemistry was carried out to determine the expression of IQGAP1 in paraffin embedded sections of the xenograft tissues. Figure 3.8-7 shows strong immunoreactivity for IQGAP1 in all xenograft tissues with DLKPI and DLKPM showing marginally higher levels of expression compared to DLKP and DLKPSQ. Expression IQGAP1 appears to be maintained under *in vivo* conditions.

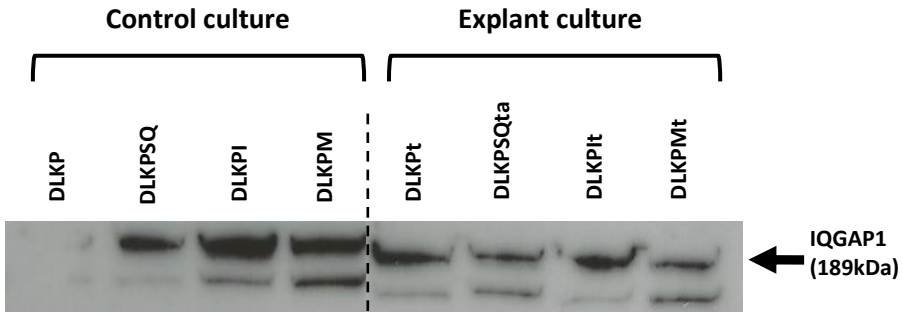

Figure 3.8-6:- Expression of IQGAP1 in the explanted DLKP tumour cells.
Represents expression of IQGAP1 in membrane enriched fractions from explanted tumour cells (DLKPt, DLKPSQta, DLKPIt and DLKPMt) compared to control cells (DLKP, DLKPSQ, DLKPI and DLKPM), using an antibody specific to IQGAP1 (n=1).

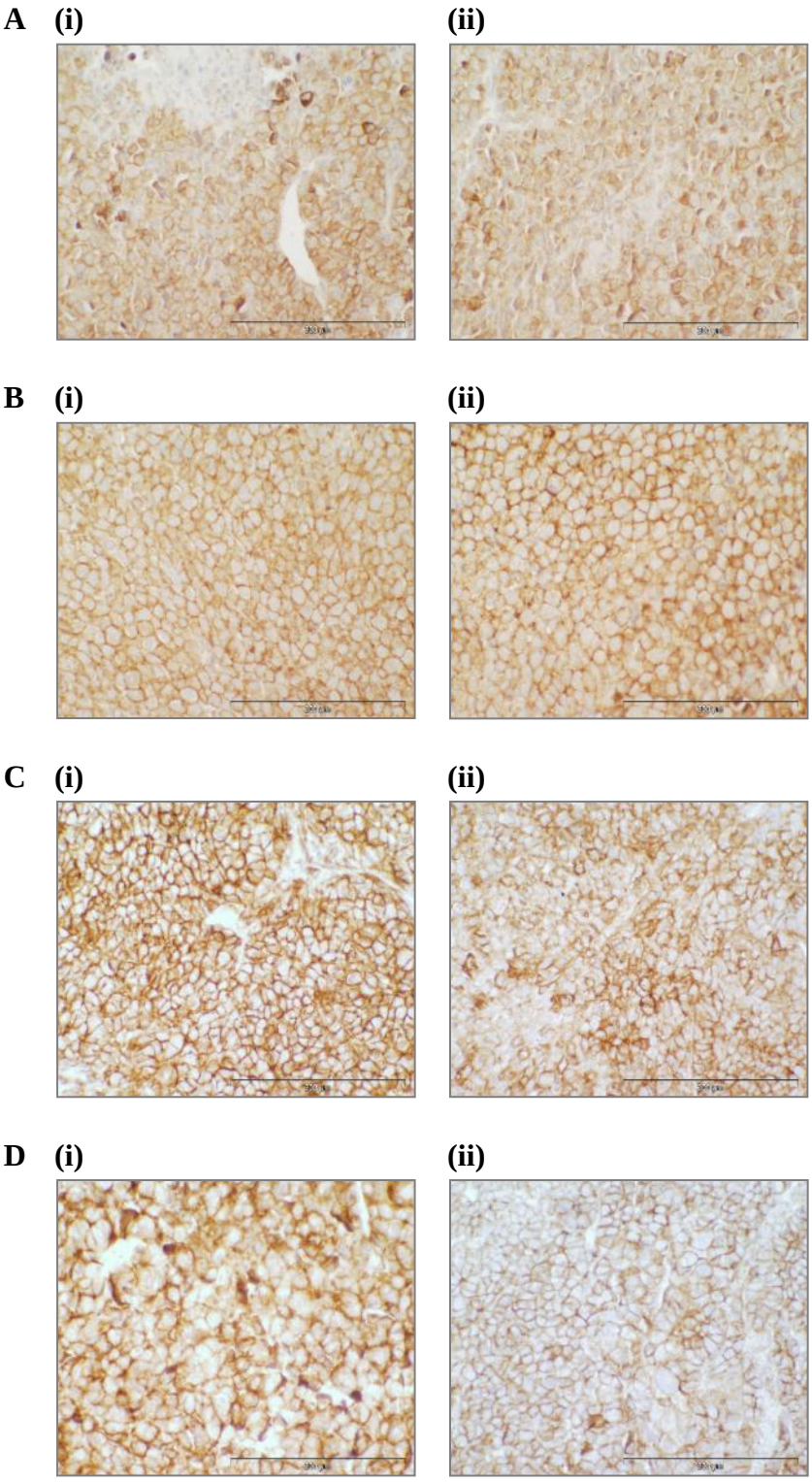

Figure 3.8-7:- Expression of IQGAP1 in the xenograft tumours.
Xenograft tumours derived from; **(A)** DLKP implanted with (i) $1x10^6$ cells (ii) $5x10^6$ cells, **(B)** DLKPSQ implanted with (i) $1x10^6$ cells (ii) $5x10^6$ cells, **(C)** DLKPI implanted with (i) $1x10^6$ cells (ii) $5x10^6$ cells and **(D)** DLKPM implanted with (i) $1x10^6$ cells (ii) $5x10^6$ cells. Immunoreactivity was observed in all tumours, using an antibody specific to a IQGAP1 (Magnification, x400; *scale bar* = 200µm).

3.8.4 Expression of INA *in vivo*

Expression of INA was previously studied in DLKP and its clones (see section 3.2.6). The expression of INA was examined in xenograft tumours derived from DLKP and its clones.

Immunohistochemistry was carried out to determine the expression of INA in paraffin embedded sections of the xenograft tissues. Figure 3.8-8, shows staining for INA in xenograft tissues in (A) DLKP, (B) DLKPSQ, (C) DLKPI and (D) DLKPM. The expression pattern of INA in the xenografts is in line with expression observed by Western blot validations of cultured cells, with expression observed in tumours derived from DLKP, DLKPSQ and DLKPM. Highest expression appears to be in DLKP and is absent in DLKPI, this indicates that DLKP and its clones retained their expression of INA under *in vivo*.

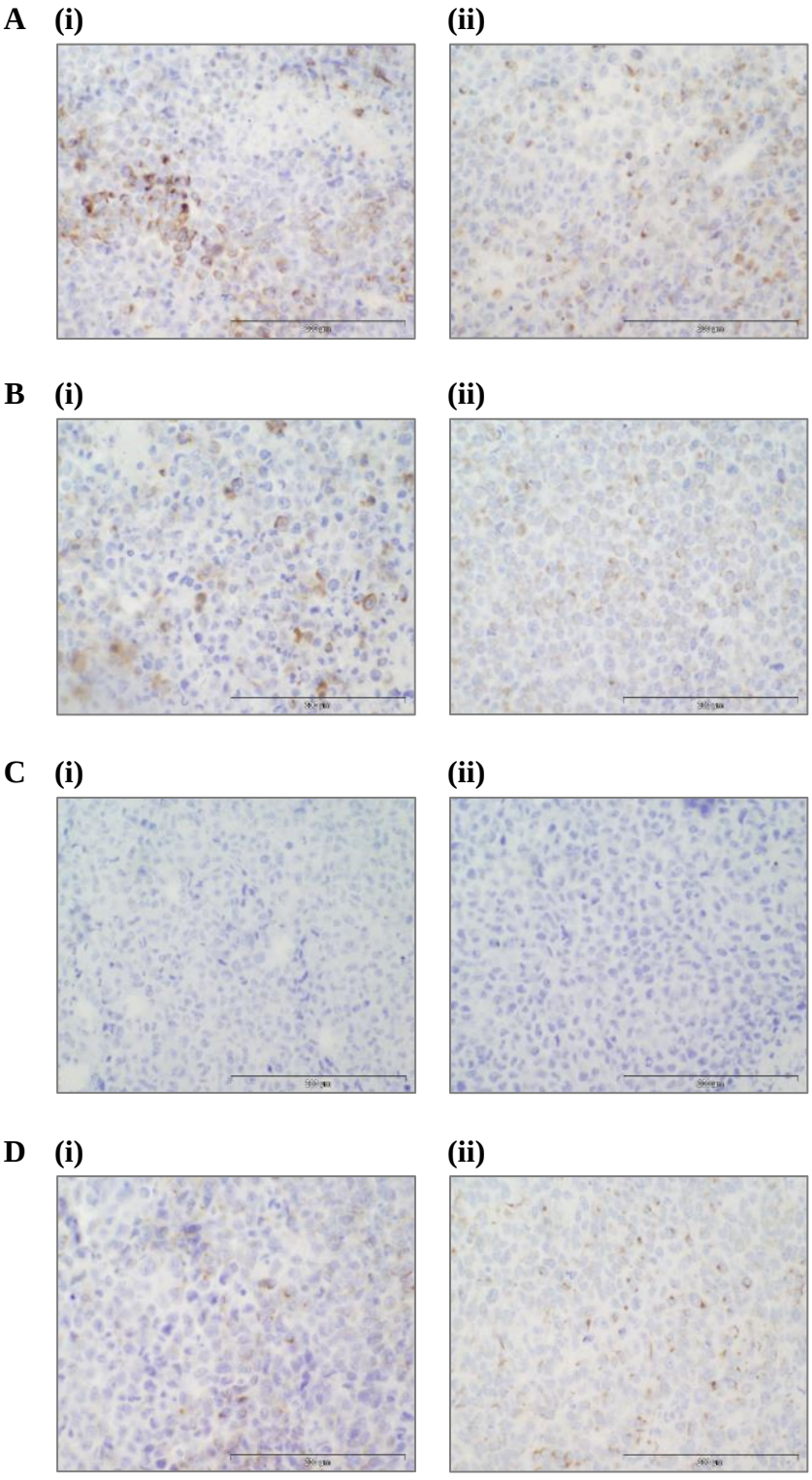

Figure 3.8-8:- Expression of INA in the xenograft tumours.
Xenograft tumours derived from; **(A)** DLKP implanted with (i) $1x10^6$ cells (ii) $5x10^6$ cells, **(B)** DLKPSQ implanted with (i) $1x10^6$ cells (ii) $5x10^6$ cells, **(C)** DLKPI implanted with (i) $1x10^6$ cells (ii) $5x10^6$ cells and **(D)** DLKPM implanted with (i) $1x10^6$ cells (ii) $5x10^6$ cells. Immunoreactivity was observed in tumours derived DLKP, DLKPSQ and DLKPM, with the strongest staining observed in DLKPSQ tumours, using an antibody specific to INA (Magnification, x400; *scale bar* = 200µm).

3.8.5 Expression SPR *in vivo*

Expression of SPR was previously studied in DLKP and its clones (see section 3.2.7). The expression of SPR was examined in explanted tumour cells and xenograft tumours derived from DLKP and its clones.

Western blot analysis was carried out to establish the expression of SPR in membrane enriched fractions which were prepared from cells recovered from xenograft tumours via explant culture. Figure 3.8-9 confirmed expression of SPR in recovered cells (DLKPt, DLKPSQta, DLKPIt and DLKPMt) compared to cells cultured under control conditions (DLKP, DLKPSQ, DLKPI and DLKPM). Expression of SPR was maintained in all cell lines derived from tumours, with explanted DLKPt and DLKPSQta having highest expression.

Immunohistochemistry was carried out to determine the expression of SPR in paraffin embedded sections of the xenograft tissues. Figure 3.8-10 shows strong staining for SPR in xenograft tissues in (A) DLKP, (B) DLKPSQ, (C) DLKPSQ and (D) DLKPM. The expression pattern of SPR in xenografts is broadly in line with expression seen in Western blot validations, indicating all cell lines maintained expression of SPR *in vivo*.

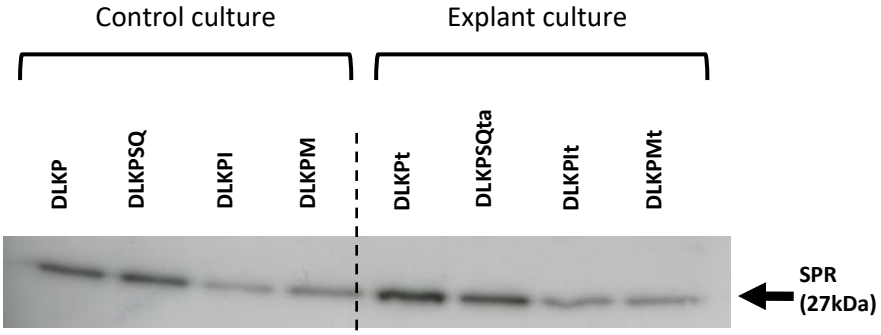

Figure 3.8-9:- Expression of SPR in the explanted DLKP tumour cells.
Represents expression of SPR in membrane enriched fractions from explanted tumour cells (DLKPt, DLKPSQta, DLKPIt and DLKPMt) compared to control cells (DLKP, DLKPSQ, DLKPI and DLKPM), using an antibody specific to SPR (n=1).

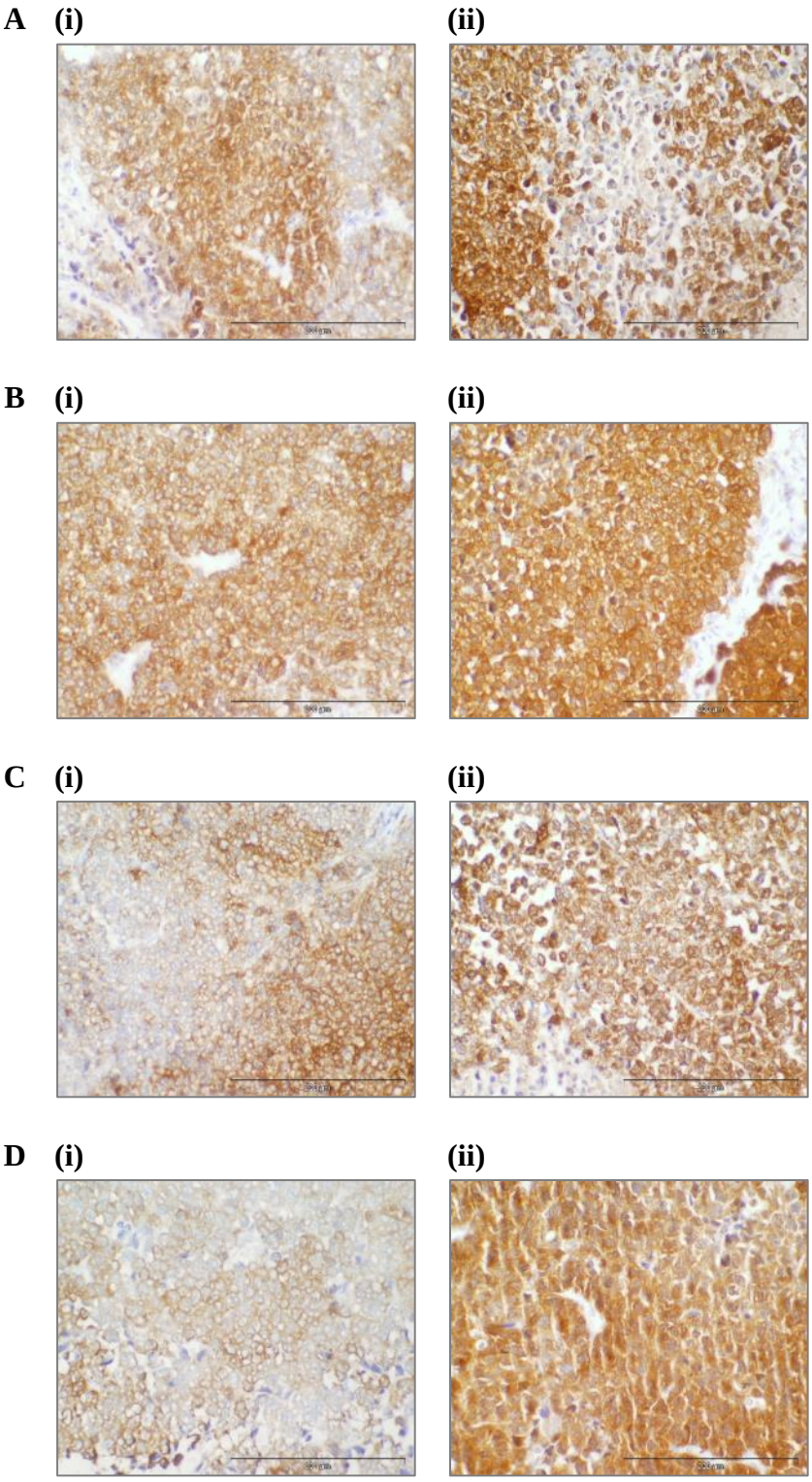

Figure 3.8-10:- Expression of SPR in the xenograft tumours.
Xenograft tumours derived from; **(A)** DLKP implanted with (i) $1x10^6$ cells (ii) $5x10^6$ cells, **(B)** DLKPSQ implanted with (i) $1x10^6$ cells (ii) $5x10^6$ cells, **(C)** DLKPI implanted with (i) $1x10^6$ cells (ii) $5x10^6$ cells and **(D)** DLKPM implanted with (i) $1x10^6$ cells (ii) $5x10^6$ cells. immunoreactivity was observed in all cell lines with DLKPSQ and DLKPM derived tumours showing strongest staining, using an antibody specific to SPR (Magnification, x400; *scale bar* = 200µm).

Chapter 4 DISCUSSION

4.1 DLKP and its clonal subpopulations

It is well established that primary and metastatic tumours are heterogeneous in nature and are home to subpopulations of cancer cells that differ in their genetic, phenotypic and behaviour characteristics. Two theories have been described to explain the establishment and maintenance of tumour heterogeneity; the cancer stem cell (CSC) theory and the clonal evolution/selection model. Both had been thought to be exclusive from each other, however, the processes are now believed to be potentially complementary. Heterogeneity in tumours can limit therapeutic efficacy and lead to resistance to therapies [88-90].

DLKP is a cell line established from the lymph node metastasis of a primary lung tumour histologically, described as a poorly differentiated squamous cell carcinoma. In early studies, DLKP was found to contain at least three morphologically distinct subpopulations, DLKPSQ, DLKPI and DLKPM. DLKPSQ resembled a squamous like morphology, with distinct cell boundaries and a cobble stone appearance. DLKPM resembled mesenchymal appearance with and fibroblast-like morphology, while DLKPI grew in tightly packed colonies with indistinct cell boundaries. The ratio of clones present within the DLKP parental cell line seems to be tightly controlled through a proposed model of interconversion [93]. This model proposed that DLKPSQ may convert to DLKPI and DLKPI may convert with DLKPM (and vice versa). Initial observations suggest that DLKPSQ and DLKPM they must pass through the DLKPI 'phase' first. The mechanism that allows the DLKP clones to interconvert remains unknown, but further investigations should be carried out in order to investigate interconversion in the DLKP clones. However, this model of interconversion could suggest also that DLKP may also represent a possible *in vitro* model of EMT. These observations suggested that DLKPI may resemble a potential stem cell-like population in DLKP given its ability to interconvert and give rise to both DLKPSQ and DLKPM cells. A core property of a stem cell is one with a self-renewal capacity and expression of specific cell surface markers. A number of different markers have been identified for lung cancer stem cells including ALDH1A1, CD177 and EpCAM. ALCAM has also been suggested as a putative stem cell marker for NSCLC [122, 123]. ALCAM is expressed in the DLKP clones but is expressed strongest in DLKPI and may, with further investigation, help confirm DLKPI as a stem cell population within DLKP (Figure 3.2-4). Expression of the cancer stem marker, ALCAM, may also suggest that the cancer stem cell model may fit the DLKP cell line model.

The initial studies also indicated that DLKP should be classified as either; variant small cell lung carcinoma (vSCLC) or non-small cell lung carcinoma with neuroendocrine differentiation [93]. vSCLC is distinguished from classic SCLC by having large cell undifferentiated carcinoma, with large cells and prominent nucleoli [124]. One of the interesting findings of the comparative proteomic study performed in this thesis, was that the identified proteins were associated with a variety of cellular processes, some of the proteins that were identified and subsequently validated appear to have strong neuronal association (e.g. INA, SPR, AHNAK), but also that their expression appeared to be strongest in SCLC cell lines (see section 3.3.1). These findings appear to correlate with these suggestions made by McBride 1998. In addition, later studies carried out on DLKP and its clonal variants indicated that the clones displayed differences in the levels of *in vitro* invasion, migration and anoikis resistance. Also, differences in its expression of key proteins associated with cancer progression were also found to be different between the clones. The DLKPSQ clone displays a poor invasive and migratory capacity, is anoikis resistant *in vitro* and displays low level expression of integrin αv. The DLKPM clone displays a high invasive and migratory capacity but is anoikis sensitive. The DLKPI clone displays an intermediate level of invasive and migratory capacity, with an intermediate ability to resist anoikis [95]. Anoikis is a Greek word used to describe the loss of a 'home' or 'homelessness'[125]. Effectively, anoikis is a form of apoptosis which is induced by loss of attachment of cells from its ECM or by attachment to the incorrect ECM. However, some tumour cells have the ability to 'resist anoikis'. Anoikis resistance is one of the hallmarks of cancer progression. If tumour cells resist anoikis they may develop the ability to survive in suspension or under anchorage-independent conditions. Cells given the ability to grow under these conditions may be able to disseminate throughout the body and give rise to metastasis [126]. Under normal conditions, anoikis is a control mechanism to prevent cells from colonizing elsewhere in the body, for this reason, the process of anoikis has been described as a physiologically relevant process in tissue homeostasis and development [127]. In gastric and ovarian cancers, it has been reported that anoikis is important for the peritoneal dissemination of cells [128, 129]. Interestingly, results from the DLKP *in vivo* study appear to suggest that the anoikis resistant cell line, DLKPSQ, appeared to display peritoneal dissemination of cells. There are a number of mechanisms whereby cells develop the ability to resist anoikis, one of those is through the loss of adhesion through integrin mediated cell-matrix attachment [130, 131].

DLKPI and DLKPM both display high adherence capacity to bind fibronectin and vitronectin, potentially explained by their increased expression of integrin αv. Integrins are heterodimeric cell surface receptors that are involved in signal transduction. In addition, integrins also function to mediate attachment of cells to their substratum, e.g. integrin αvβ3 functions as a receptor for proteins with exposed Arg-Gly-ASP tripeptide, examples of such proteins include; fibronectin, vitronectin, fibrinogen, laminins and collagens. It has been reported that integrin αvβ3 binds MMP-2 and co-localises with degraded collagen type 1 [132]. Matrix metalloproteases (MMPs) are a diverse family of endopeptidases, which are enzymes capable of breaking down components of extracellular matrix (ECM). Common properties of MMPs are their dependence on zinc in the catalytic site for activity but also they are generally synthesised as inactive zymogens that require proteolytic cleaving to become active. They are known to be expressed in normal tissues only when and where they are required e.g. wound healing and embryonic development. However, aberrant expression of MMPs has been associated with roles tumour cell invasion and metastasis [133]. Differences in expression of MMP2 and MMP10 was observed between the DLKP clones [96].

Previous attempts were made to identify specific markers for the clones, through Immunocytochemical methods. A marker would serve to identify the individual clones from each other in a mixed population. Therefore, to select a protein that is specific to one of the clones (i.e. a marker), ideally, it would be expressed in one or two of the clones, not in all three. To date, no specific markers have been identified that can allow us to distinguish the individual DLKP clones. Quantitative proteomic analysis potentially allows for the identification of differentially expressed proteins between the DLKP clones and thus could potentially act as markers for the individual clones. Also, identification of such membrane protein markers could provide the means to study the previously proposed model of interconversion between the clones, as well as their potential involvement in cell invasion and migration. This study also presents an opportunity to identify potentially novel membrane associated proteins that could be associated with lung cancer. The phenotypic differences of DLKP and its clones present a prime opportunity to investigate both heterogeneity in lung cancer, but also the mechanisms associated with lung heterogeneity, *in vitro*.

4.2 Proteomic analysis of DLKP and its subpopulations

To identify proteins that could act as potential markers for the DLKP clones and also potentially novel proteins associated with lung cancer, the comparative proteomic analysis was carried out on DLKP, DLKPSQ, DLKPI and DLKPM cell lines. In this study, the four cell lines were grown in triplicate under standard culture conditions until approx. 90% confluent. To ensure cells were healthy, the cell culture media was changed the day before processing (section 2.2.1). Isolated proteins were then prepared for LC-MS/MS as described in section 2.2.2 and 2.2.3. Peptide identification was performed using proteome discoverer 2.0 against MASCOT and SEQUEST databases against the UniProtKB-SwissProt database. Comparative proteomic analysis was performed using Progenesis label-free software to identify proteins from 3 biologicals and 3 technical replicates of the 4 cell lines (DLKP, DLKPSQ, DLKPI and DLKPM) (section 2.2.4). Principle component analysis (PCA) revealed good separation of the cell lines and each of the replicates into their corresponding groups, indicating that the isolation and subsequent proteomic analysis performed in this study was robust and reproducible (section 3.1.2).

A proteomic profile of proteins associated with the cell membrane of the DLKP and its clones was developed *in vitro*. Six lists of differentially expressed protein lists were generated from comparative proteomic analysis of DLKP *vs.* DLKPSQ, DLKP *vs.* DLKPI, DLKP *vs.* DLKPM, DLKPSQ *vs.* DLKPI, DLKPSQ *vs.* DLKPM and DLKP *vs.* DLKPI. Six statistically significant differentially expressed proteins were identified in DLKP and the DLKP clones (SQ, I and M); AHNAK, ROBO2, ALCAM, IQGAP1 and SPR (see section 3.1.3),), less stringent criteria revealed HDGF as having statistical significance (p= 0.0302) and was also chosen for validation studies (see section 3.1.4). The objective of this analysis was to find proteins that could potentially be used as markers for the DLKP clones and, in addition, identify novel proteins associated with lung cancer. Proteins showing membrane association could be (with further investigation and validation) extrapolated to other tumour types and may lead to the identification of novel targets for treatment of other lethal cancers such as pancreatic cancer. Table 4.2-1 below indicates the comparison from which each protein was identified. Two further proteins INA and SLIT2 were added to the panel of proteins selected for validation studies. Early studies suggested that DLKP could be classified as a non-small cell lung carcinoma with neuroendocrine differentiation. Another comparative proteomic study found INA to be increased in DLKPSQ *vs.* DLKPM (~2.5-fold). Increased INA

expression was recently associated with pancreatic neuroendocrine cancer tumour aggressiveness [104], hence why INA was selected for validation. ROBO2 acts as a receptor for SLIT2 and both of these genes were identified by microarray analysis of the DLKP clones previously carried out in our laboratory, thus both proteins were validated in this thesis [96].

Selected proteins for validation studies: identified from comparative proteomic analysis of DLKP and its clones							
Gene name	**Protein Name**	**DLKP *vs.* DLKPSQ**	**DLKP *vs.* DLKPI**	**DLKP *vs.* DLKPM**	**DLKPSQ *vs.* DLKPI**	**DLKPSQ *vs.* DLKPM**	**DLKPI *vs.* DLKPM**
AHNAK	Neuroblast differentiation associated protein	5.0	5.5	---	10	8.0	---
ALCAM	Activated leukocyte cell adhesion molecule	---	---	5.9	24.3	---	30.2
HDGF	Hepatoma derived growth factor	---	2.2	---	---	---	---
IQGAP1	Ras GTPase activating-like protein 1	1.7	7.6	8.9	---	---	---
ROBO2	Roundabout Homolog 2	---	---	60.6	21.8	---	26.9
SPR	Sepiapterin Reductase	---	---	---	3.6	---	---

Table 4.2-1:- Summary of all proteins selected for validation studies.
The table above indicates the proteins identified from the comparative proteomic analysis as potential markers for DLKP. Proteins are organised in alphabetical order, the list/s from which they came and their fold change.

4.2.1 Neuroblast differentiation-associated protein

Neuroblast differentiation-associated protein (AHNAK) or desmoyokin, is an exceptionally large protein (~629kDa), originally identified as a nuclear phosphoprotein in human neuroblastomas and skin epithelial cells. It has been reported as a membrane scaffold protein with three structurally distinct regions; an amino-terminal (500 amino acids), a large central region (4388 amino acids) and a carboxyl-terminal 1003 amino acids [134]. The specific localisation of AHNAK is controversial, with studies reporting localisation to the nucleus, Golgi apparatus, cytoplasm and association with the plasma

membrane. Its translocation from the cytoplasm and the plasma membrane in the $Ca2^{+}$ and Protein Kinase C dependent manner in keratinocytes may potentially explain AHNAK's ability to localise to different sites in the cell [135]. It has also been reported that in the presence of arachidonic acid, AHNAK binds and activates phospholipase C-γ1 [136], a protein believed to play a key role in cell migration and invasion [137]. It also acts as a key molecular switch in the regulation of tumour migration [138]. AHNAK was recently found to be essential for pseudopodia formation and tumoural migration/invasion [134]. One study in mesothelioma showed that siRNA knockdown of AHNAK induced pseudopodia retraction, inhibited cell migration and invasion, reduced actin cytoskeleton dynamics and induced mesenchymal to epithelial transition [139]. Chen *et al.,* reported that the AHNAK gene was among eight genes to show an association with relapse-free survival in lung and breast cancer patients treated with chemotherapy [140].

AHNAK was chosen as a potential marker for DLKPI or DLKPM, based on its comparative proteomic analysis carried out in section 3.1.3. AHNAK protein expression was increased in DLKP *vs.* SQ (increased in DLKP 5 fold), DLKP *vs.* DLKPI (increased in DLKPI 5.5 fold), DLKPSQ *vs.* DLKPI (increased in DLKPI 9.3 fold) and DLKPSQ *vs.* DLKPM (increased in DLKPM 8 fold). The large size of AHNAK made it difficult for validation by Western blot analysis and Immunohistochemistry. A number of attempts were made using gels that allow for the separation of high molecular weight proteins and the use of two separate antibodies targeting AHNAK. It was not possible to identify the AHNAK reactive band and staining of formalin fixed paraffin embedded tissues did not reveal AHNAK immunoreactivity. However, Immunofluorescence staining did show membrane immunoreactivity for AHNAK (see section 3.2.1), with high expression observed in both DLKPI and DLKPM compared to DLKP. Also, lower expression levels were observed in DLKPSQ, where individual cells showed strong membrane immunoreactivity. This could indicate a potential subpopulation within DLKPSQ. Survival analysis was carried out using the BreastMark algorithm to evaluate AHNAK expression in Luminal A, Luminal B, Her2+ and Basal-like molecular subtypes of breast cancer. The analysis indicates a significant association of AHNAK expression with outcome in patients with Luminal B (p=0.032) breast cancer (Figure 3.2-8). AHNAK has been reported to function as a tumour suppressor in breast cancer due to its involvement as a mediator of TGFβ signalling leading to cell cycle arrest. Mechanistic studies performed by Lee *et al.,* indicated that TGFβ-induced nuclear translocation of AHNAK

leads to potentiation of R-Smad function and downregulation of c-Myc and cyclin D1/D2 as well as inhibition of cell growth [141]. While the comparative proteomic analysis indicated differential expression of AHNAK within the DLKP clones, the subsequent validation studies confirmed high expression in DLKPI and DLKPM cells. AHNAK expression was also observed in DLKP and DLKPSQ cell lines, but membrane immunoreactivity was only observed in a specific population of these cell lines (see Figure 3.2-1). This may indicate the presence of further subpopulations in DLKP and DLKPSQ. Further investigations could include cell sorting using a fluorescent-activated cell sorting (FACS) to characterise any potential subpopulations. However, AHNAK would not serve as a good marker for identification of the individual DLKP clones. There is still little known about the role of AHNAK in lung cancer and could be investigated further in the DLKP cell line model by use of inhibitors targeting PI3K/MAK/MTOR pathways or through the use of siRNA mediated knockdown of the AHNAK gene.

4.2.2 Hepatoma-derived growth factor

Hepatoma-derived growth factor (HDGF) has a molecular weight of approximately 37kDa. HDGF is a heparin-binding growth factor originally purified from media conditioned with the human hepatoma cell line HuH-7. Its precise function is unclear, however, HDGF is believed to translocate to the nucleus which is essential for its effect on cell growth by binding to DNA using its PWWP motif [142]. HDGF lacks the N-terminal hydrophobic sequence that is characteristic of most signal proteins, therefore suggesting that HDGF is secreted via an alternative pathway and is independent of the golgi secretion system. [143-145].

HDGF was selected as a potential marker for DLKP based on its comparative proteomic data which compared protein expression in DLKP *vs.* DLKPI (see appendix 1.1). A putative receptor for HDGF has not been established [105]. However, part of the HATH region, containing 80-100 amino acids, has been proposed as a potential receptor binding site [146]. Immunocytochemical analysis and Western blot analysis subsequently confirmed highest expression of HDGF in DLKP compared to DLKPSQ, DLKPI and DLKPM (Figure 3.2-2). Levels of expression in the clones appear to be similar. HDGF was initially isolated from conditioned medium (CM) of HuH-7 cells and its secretory expression seems to correlate with the high levels of HDGF in CM generated from DLKP and its clones.

There are accumulating findings suggesting that HDGF is closely related to the aggressive biological potential of cancer cells and could be of prognostic value for patients with pancreatic cancer [147]. In the studies presented in this thesis, HDGF expression was investigated across representative tumour cell line panels from lung cancer (Figure 3.3-1), TNBC (Figure 3.3-6), pancreatic cancer (Figure 3.3-9), colon, glioma and melanoma (Figure 3.3-12). Results indicate that higher expression of HDGF may be associated with a more invasive/metastatic phenotype, *in vitro*. The invasive MiaPaCa2 Clone3 showed increased expression compared to the less invasive MiaPaCa2 parent and high expression was also observed in AsPc-1; a pancreatic cancer cell line derived from a metastatic ascites (www.atcc.org) and in the metastatic colon cell line (SW620) compared to its primary cell line counterpart (SW480). High expression was observed in LoxIVMI, a cell line derived from a metastatic melanoma. Survival analysis was carried out using the BreastMark algorithm to evaluate HDGF expression in Luminal A, Luminal B, Her2+ and Basal-like molecular subtypes of breast cancer. The analysis indicated that low expression of HDGF was associated with better outcome in patients with Luminal A breast cancer (Figure 3.2-9). High expression of HDGF was observed across a representative panel of cell lines: basal-like 1, basal like 2, mesenchymal and mesenchymal-like TNBC cancer cell lines. Validation studies confirmed increased expression of HDGF in DLKP and similar levels observed across the clones. Therefore, HDGF could not act as a selective marker to distinguish the individual DLKP clones. However, the preliminary evidence relating to HDGF expression in TNBC suggest a potential association with invasiveness, *in vitro* (Figure 3.3-6). Further investigations into the role for HDGF in metastatic cancers such as pancreatic, breast, colon or lung cancer should be performed.

4.2.3 SLIT2 and ROBO2

SLIT2 belongs to the Slit family of large extracellular matrix-secreted glycoproteins and consists of 3 genes (*slit1*, *slit2*, and *slit3*). The *slit2* gene is located on chromosome 4p15.2 and acts as a ligand for the repulsive guidance receptors, the *robo* gene family (*robo1-4*) [148]. SLIT2 interacts with ROBO1 and possibly ROBO2 receptors. SLIT–ROBO interactions are believed to play an important role in axon guidance in the central nervous system, but in human cancers, the *slit2* gene is frequently inactivated by hypermethylation in its promoter region or allele loss in the lung, breast, colorectal cancers and malignant gliomas. This suggests a tumour-suppressive role for SLIT2, which inhibits cell migration and invasion in breast cancer and medulloblastoma [149].

Studies in breast cancer and lung cancer have shown that SLIT2 elicits its tumour suppressor effects by its regulation of β-catenin and PI3K/Akt signalling pathways. In breast cancer, this regulation has shown to enhance β-catenin/E-cadherin-mediated cell-cell adhesion [148, 150].

ROBO2 was selected as a potential marker for DLKPI based on the comparative proteomic data analysis of DLKP *vs.* DLKPSQ (increased in DLKP ~57-fold), DLKP *vs.* DLKPM (increased in DLKP ~61-fold), DLKPSQ *vs.* DLKPI (increased in DLKPI ~22-fold) and DLKPI *vs.* DLKPM (increased in DLKPI ~27-fold), see section 3.1.3. Not only did ROBO2 appear in this differentially expressed proteomic analysis, but also in microarray analysis previously carried out by Dr. Helena Joyce indicated that ROBO2 was overexpressed in DLKPI cells. Unpublished proteomic analysis performed on CM of DLKP and the clones also suggests secreted ROBO2 is increased in DLKPSQ and DLKPM compared to DLKP and DLKPI, providing supporting evidence for carrying out validation studies.

The expression of both SLIT2 and ROBO2 was investigated in the DLKP cell line model using Immunofluorescence, Western blot analysis and Immunocytochemistry. SLIT2 and ROBO2 expression was highly varied across the DLKP clones. High expression of SLIT2 was observed in DLKP and DLKPM only, with a lower level of expression observed in DLKPSQ and DLKPI. Western blot analysis indicated that expression of SLIT2 is highest in DLKPM and suggesting a potential use as a marker for DLKPM (Figure 3.2-3). SLIT2 is a secreted protein and this was confirmed by Immunofluorescence and Immunocytochemical analysis, where immunoreactivity was visually observed in the extracellular space surrounding DLKP, DLKPI and DLKPM cells. To investigate a potential role for SLIT2 in the invasive process of DLKPI and DLKPM, siRNA transfections targeting SLIT2 were carried out. However, inconclusive results were observed following invasion assays (data not shown). Further investigations should be carried out to establish a functional role, if any, for the SLIT/ROBO signalling system in DLKP (e.g. this could include overexpression of SLIT2 in DLKPSQ). SLIT2 and ROBO2 were investigated in parallel as potential markers for the DLKP clones. Following validation studies, expression was confirmed in DLKP and its clones. While a correlation of expression was observed between ROBO2 and SLIT2 in the DLKP cell line model, both, SLIT2 and ROBO2 expression was not considered specific enough to be able to identify the individual clones and was not carried forward as a potential marker for DLKP clones.

4.2.4 Ras-GTPase-activating-like protein 1

Ras-GTPase-activating-like protein 1 (IQGAP1) is a scaffolding protein that binds to actin, which functions to cross-link and stabilise actin filaments through its calponin homology domain. IQGAP1 is approximately 189kDa and is a member of the IQGAP family of proteins of which three isoforms have been described in humans: IQGAP1, IQGAP2 and IQGAP3. IQGAP1 is the best characterized and the most widely studied. It is believed that they interact with signalling and structural molecules and are usually overexpressed in metastatic breast cancer [111] and advanced colorectal cancer [151]. IQGAP1 localizes to sites of cell–cell contact in epithelial cells and has been shown to regulate E-cadherin-mediated cell–cell adhesion as well as a number of signal transduction pathways, including Ca2+/ calmodulin, CDC42 and Rac MAPK and mTORC1–Akt. IQGAP1 shows elevated levels in a variety of cancer types, including pancreatic cancer [152, 153]. Jameson *et al.,* investigated tumour formation in IQGAP1 -/- mice with RAS-driven cancer and their studies indicated that there was diminished tumour formation in the knock out mice [154].

IQGAP1 was selected as a potential marker for the DLKP clones based on comparative proteomic analysis of DLKP *vs.* DLKPSQ (increased in DLKPSQ ~1.7-fold), DLKP *vs.* DLKPI (increased in DLKPI ~8-fold), DLKP *vs.* DLKPM ~9-fold) and DLKPSQ *vs.* DLKPM (increased in DLKPM ~6.2-fold) see section 3.1.3. Unpublished proteomic analysis performed by Dr. Joanne Keenan in our laboratory also indicated that IQGAP1 was present in CM of DLKP and the clones. A further reason for selecting IQGAP1 for validation studies was its reported interaction with ALCAM [112].

Immunofluorescence, Western Blot analysis and Immunocytochemical analysis confirmed that expression of IQGAP1 was highest in DLKPI and DLKPM compared to both DLKP and DLKPSQ (Figure 3.2-5). A good marker would theoretically allow for the identification of one clone from another in a mixed culture because IQGAP1 was expressed in all DLKP cell lines it would therefore not serve as a good choice. Jannie (2012) reported that ALCAM co-localised with N-cadherin, and, with IQGAP1 bound to the cytoplasmic tail of ALCAM, it elicits an effect on β-catenin. High expression of N-cadherin had been previously shown in DLKPI, but also at lower levels in DLKP, DLKPSQ and DLKPM. ALCAM and N-cadherin appear to display a similar pattern of expression in DLKP and the clones. This suggests that, as proposed by Jannie (2012), IQGAP1 may interact with ALCAM and NCAD in DLKP, this potential interaction would need to be compared through immunoprecipitation.

4.2.5 Activated Leukocyte Cell Adhesion Molecule

Activated leukocyte cell adhesion molecule (ALCAM) is a 105kDa protein that belongs to the immunoglobulin superfamily and is expressed by epithelial cells in several organs with reported functions in embryogenesis, angiogenesis, haematopoiesis and the immune response [155]. Originally, ALCAM was discovered as a ligand for CD6 in leukocytes [156] and is known to mediate both heterophilic (ALCAM-CD6) and homophilic (ALCAM-ALCAM) cell-cell interactions. ALCAM expression has been correlated with invasiveness of malignant melanoma and has been proposed as a prognostic marker of melanoma, prostate cancer, breast cancer, colorectal cancer, bladder cancer, oesophageal squamous cell carcinoma and ovarian cancer [157]. However, reports relating to tumour expression of ALCAM are conflicting, with one study suggesting that membranous expression in colorectal cancer appears to correlate with a shortened patient survival [158]. However, another suggests cytoplasmic localisation in breast cancer correlates with poorer patient outcome [159]. To investigate the association of ALCAM with survival in breast cancer, we used the BreastMark algorithm to evaluate ALCAM expression in Luminal A, Luminal B, Her2+ and Basal-like molecular subtypes of breast cancer. The analysis did not indicate significance in association with ALCAM expression in the molecular subtypes of breast cancer (Figure 3.2-12), therefore ALCAM was not investigated in the panel of TNBC cell lines.

ALCAM was selected as a potential marker for DLKPI based on its comparative proteomic analysis of DLKP *vs.* DLKPI (increased in DLKPI ~19 fold), DLKP *vs.* DLKPM (increased in DLKP ~6-fold), DLKPSQ *vs.* DLKPI (increased in DLKPI ~24-fold) and DLKPI *vs.* DLKPM (increased in DLKPI ~30-fold) see section 3.1.3. The stem cell theory proposes that a subpopulation of tumour cells initiates and maintains the tumour due to its ability to undergo asymmetrical divisions [122]. A number of studies have identified ALCAM as a lung cancer stem cell marker, other markers include aldehyde dehydrogenase isoform 1 (ALDH1), CD133 and CD44. The proteins have also been investigated as potential stem cell markers in colorectal cancer, melanoma, glioblastoma, ovarian and breast cancer. [110]. ALCAM has also been associated with colorectal cancer stem cells [160, 161]. Tachezy *et al.*, reported that ALCAM expression was more frequent in smaller tumours without lymph node metastasis and with a benign grading that didn't affect patient survival. They suggested that this was not consistent with a cancer stem cell, but instead reported ALCAM as an 'inert' cancer stem cell marker for NSCLC [122]. As an intermediate subpopulation in DLKP and with a potential ability

to give rise to DLKPSQ and DLKPM cells through interconversion, it was previously proposed that the DLKPI resembled a stem cell population in DLKP. There is little known about the function of ALCAM in lung cancer, so we wanted to investigate if ALCAM played a role in the invasion process in DLKP. Previous microarray and proteomic analyses indicate that ALCAM was highly overexpressed in DLKPI only and increased shedding of ALCAM from DLKPSQ and DLKPM cells was observed compared to DLKP and DLKPI, in conditioned media. sALCAM is a soluble isoform of ALCAM that is thought to be produced by alternative splicing. It is believed to play a regulatory effect on ALCAM may function but also potentially modulate endothelial function through ALCAM-dependent and ALCAM-independent pathways [109]. Immunofluorescence, Western blot analysis and immunocytochemical analyses confirmed that expression of ALCAM was highest in DLKPI while DLKP, DLKPSQ and DLKPM showed low levels of expression. Expression in CM did correlate with expression observed in the whole cell lysate and membrane enriched fractions (Figure 3.2-4). Soluble ALCAM (sALCAM) is believed to have a lower molecular weight than ALCAM [109]. Western blot analysis, using an ALCAM specific antibody revealed an additional band at approximately 60kDa (data not shown) in CM of DLKP, DLKPSQ, DLKPI and DLKPM and with higher expression in DLKPSQ. This band may represent sALCAM and potentially indicate its presence in the conditioned medium. To confirm this result, a Western blot analysis could be carried out using an antibody specific to sALCAM.

We investigated a possible role for ALCAM in the invasive process of DLKPM, DLKPI and DLKPSQ-mitox-BCRP-6P, using siRNA knockdown of ALCAM. As previously shown in the validation experiments in section 3.2.4; DLKPI displayed the highest levels of ALCAM, while DLKPM showed lower expression levels compared to DLKPI. Dr Helena Joyce developed the DLKPSQ-mitox-BCRP-6P cell line after pulsing DLKPSQ with mitoxantrone. Subsequent characterisation of this cell line by Western blot analysis and Immunofluorescence analysis indicated increased expression of ALCAM in the drug resistant variant compared to DLKPSQ, its parental cell line (Helena Joyce PhD). In addition, DLKPSQ-mitox-BCRP-6P was also shown to have an increased ability to invade *in vitro*. It was therefore thought that DLKPSQ-mitox-BCRP-6P would be a good candidate cell line to investigate the role of ALCAM in lung cancer. There was no effect on proliferation in both DLKPSQ and DLKPM cell lines following siRNA knockdown of ALCAM, indicating that ALCAM does not appear to play a role in the growth of DLKP SQ or DLKPM.

4.2.5.1 Effect of ALCAM siRNA knockdown in DLKP

High expression of ALCAM in DLKPI made it challenging for transient siRNA knockdown studies. Western blot analysis showed only a partial reduction of ALCAM at the protein level, with very little functional effect on proliferation and invasion. However, a reduction in protein levels occurred in both DLKPSQ-mitox-BCRP and in DLKPM, showing opposing roles in these cell lines. In DLKPSQ-mitox-BCRP-6P, an increase in invasion was observed following knockdown of ALCAM, with a significant increase observed using ALCAM-2 siRNA (p=0.0040) see section 3.4.1.1. A reduction in invasion was observed following siRNA knockdown of ALCAM in DLKPM, with a significant decrease shown using ALCAM-2 siRNA (p= 0.0041) see section 3.4.1.2. As discussed, there are contradictive roles for sALCAM and ALCAM in human cancers. sALCAM is reported to attenuate invasion of metastatic melanoma BLM cells [161, 162] but promotes invasion of glioblastoma [163]. In breast cancer ALCAM expression has been associated with suppression of invasion of breast cancer cells [164], while ALCAM promotes tumour cell invasion of glioblastoma cells. Membranous expression of ALCAM enhanced invasion and migration of NSCLC cells *in vitro* and was associated with poor survival of patients with NSCLC [165]. In this study, we have shown that invasion is significantly reduced in DLKPM and significantly increased in drug resistant cell line DLKPSQ-mitox-BCRP-6P. Our results suggest that siRNA knockdown of ALCAM does not affect cell growth but may have opposing roles in cancer cell invasion within a lung cancer cell line model, thus reflecting the contradicting roles for ALCAM reported in the literature.

4.2.6 Alpha-Internexin

Alpha-Internexin (INA) is a 66-kDa intermediate filament protein that maps to chromosome 10q24.33. It is a component of the primary neurofilament triplet proteins of the central nervous system which include neurofilament subunits of low molecular weight (68kDa), a middle molecular weight (160kDa) and a high molecular weight (205kDa). To date, INA has mainly been investigated in cancers related to the brain such as Glioblastoma [166], Oligodendroglioma [113, 167] and medulloblastoma [168]. Using gene expression arrays, Ducray *et al* (2011) found that neuronal associated proteins were preferentially expressed in gliomas that were 1p19q codeleted and of these genes INA was one of the most differentially expressed [169], suggesting that INA may act as a surrogate marker for the 1p19q co-deletion. However, a recent study hypothesized that INA could be expressed in pancreatic neuroendocrine tumours (PNETs) [104]. Shirley

McBride initially characterised DLKP and suggested that DLKP should be classified as either a variant small cell lung carcinoma or non-small cell lung carcinoma with neuroendocrine differentiation [93]. This association led us to investigate the expression and a potential role of INA in the lung cancer cell line model DLKP. Presently, there are no reports relating to a functional role for INA in lung cancer.

4.2.6.1 Effect of siRNA knockdown of INA on DLKPSQ and DLKPM

Increased expression of INA has been associated with pancreatic neuroendocrine cancer tumour aggressiveness. A previous comparative proteomic study carried on DLKP cell line model in our laboratory found INA to be increased in DLKPSQ *vs.* DLKPM (~2.5-fold). As previously stated, early studies suggested that DLKP could be characterised as a non-small cell lung carcinoma with neuroendocrine differentiation. INA was chosen for validation based on its recent association with PNETs.

Western blot analysis, Immunofluorescence and Immunocytochemical analysis confirmed expression of INA was highest in DLKPSQ compared to both DLKP and DLKPM, with the lowest expression seen in DLKPI, see section 3.2.6. To investigate whether INA expression had a functional role in invasion and migration in the DLKP lung cancer cell line model, siRNA knockdown of the INA gene was carried out in two of the DLKP clones, DLKPSQ and DLKPM. DLKPSQ displays highest levels of INA expression and DLKPM which showed lower INA expression. There was no effect on proliferation in both DLKPSQ and DLKPM cell lines following siRNA knockdown of INA, indicating that INA does not appear to play a role in the growth of both cell lines.

Two independent siRNAs were used to knockdown INA in DLKPSQ. The invasive and migratory ability of DLKPSQ, using both INA-6 and INA-8 siRNAs remained unchanged following transfection (see section 3.4.2.1). By comparison, siRNA knockdown in DLKPM using four independent siRNAs resulted in a variety of effects. Firstly, a morphological change was observed with two out of four siRNAs. Under normal conditions, DLKPM cells are irregularly shaped with fibroblastoid-like morphology and do not appear to form colonies. This morphology has been suggested to be typical of highly invasive and motile cancer cells. However, in DLKPM cells that were transfected with INA-7, the cells appeared to display a more elongated morphology, whilst cells transfected with INA-9 cells became more isolated and lost their fibroblastoid-like morphology (see section 3.4.2.2). One of the biological functions of INA is its involvement in cellular differentiation (www.uniprot.org) and it has been shown to be

expressed in neuronal cells as they begin to differentiate [170]. This observation may be evidence of potential differentiation of DLKPM from a highly invasive to a less invasive phenotype. We then looked at the effect on invasion and migration following knockdown of INA in DLKPM. A reduction in the invasive capacity of DLKPM was observed following INA knockdown, a significant reduction using INA-7 (p=0.0021) and INA-9 (p=0.0016), while a reduction was also observed for INA-6 (n=2). Migratory ability was also reduced following INA knockdown, significantly with INA-6 (p=0.024). However, an increase in the invasive and migratory ability was noted using INA-8 siRNA, significantly for migration using INA-8 (p=0.015 (n=3)). A decreased migratory ability was also noted for the remaining two siRNAs (INA-7 and INA-9 (n=2)) see section 3.4.2.2. This, to our knowledge, is the first report associating INA with both invasion /migration of lung cancer *in vitro*, suggesting that INA may have a potential role in the invasion and migratory process of lung cancer.

INA expression was investigated by Western blot analysis in panels of cell lines representing various tumour types including lung cancer (Figure 3.3-4), TNBC (Figure 3.3-7), neuroblastoma and glioma (Figure 3.3-14). Investigation of INA expression across a panel of pancreatic ductal adenocarcinoma (PDAC) cell lines appeared to show no detectable levels of expression (results not shown). This is not surprising considering the only reported association of INA with pancreatic cancer has been an association with the aggressiveness of PNETs [104]. In addition, Immunohistochemical analysis performed on a small number of pancreatic cancer tissues were negative for INA immunoreactivity. These findings suggest that INA may not play a role in PDAC, but further investigation would need to be carried out in order to confirm this finding. In the panel lung cancer of cell lines, there was also a low level of expression of INA, with the exception of NCI-H69, a SCLC cell line. Expression of INA in NCI-H69 is not unexpected considering it is reported to express neuronal markers such as neuronal cell adhesion molecule and neuroendocrine markers such as neuronal specific enolase, chromogranin A and synaptophysin [171]. In addition, a lung cancer tissue microarray (TMA) was immunohistochemically stained for INA expression. Overall immunoreactivity on the TMA showed very specific reactivity of individual cells in lung adenocarcinoma and squamous cell carcinoma. However, the most intense staining was observed in the lung neuroendocrine tissues see Figure 3.4-28. This result could potentially suggest specificity of INA for neuroendocrine cells within different lung tumour types and thus suggest that INA may represent a potential marker for neuroendocrine lung cancer. Further

immunohistochemical analysis would need to be carried out on a larger number of neuroendocrine tissues of different tumour types.

To date, there have been no reports of INA expression in breast cancer. TNBC is an aggressive form of breast cancer with high rates of relapse and overall poor prognosis. Survival analysis using the BreastMark algorithm was carried out and indicated that high expression of INA was associated with better outcome in patients with Luminal B breast cancer (Figure 3.2-14). This was a surprising result since increased INA expression had been reported as a marker for tumour aggressiveness in PNETs. The expression of INA was investigated in a panel of cell lines representing various TNBC sub-types. INA specific bands were detected at ~60kda in 4 out of 10 cell lines; HCC-1937, HCC-1143 (BL-1), HDQP-1 (BL-2) and MDA-MB-157 (MSL), whereas the remaining 6 cell lines displayed very low expression of INA (Figure 3.3-7). In the remaining cell lines, INA expression was also observed in the neuroblastoma (SK-N-SH) cell line relative to glioma (SNB-19) as shown in Figure 3.3-14. The findings in relation to INA appear to suggest that INA expression could be associated with neuroendocrine cancer and that INA has potential as a marker for neuroendocrine cancer. Schimmack *et al.,* have investigated the clinical relevance of INA as a potential marker for gastroenteropancreatic neuroendocrine neoplasms [172]. It is tempting to suggest that the four TNBC cell lines showing reactivity for INA, could indicate a neuroendocrine association. To verify this association, further investigation would need to be carried out to confirm expression of neuronal markers in these cell lines. In addition to breast cancer, INA should be investigated further as a potential neuroendocrine marker in other cancers.

4.2.6.2 Summary

In summary, we have shown that siRNA knockdown of INA in DLKPM; (i) does not affect cell growth, (ii) induces morphological changes to a potentially less invasive phenotype that may be associated with differentiation and (iii) results in significant reduction of invasion and migration. Western blot analysis indicates that INA is expressed at low levels across representative tumour cell line panels including lung cancer and TNBC cell lines. IHC analysis of a lung TMA also indicates that INA is expressed at low levels in various lung tumours. We have shown through IHC analysis that expression of INA may be associated with neuroendocrine cancer and that INA has the potential for use as a marker of neuroendocrine cancer. We have shown that targeting INA, through siRNA silencing may potentially indicate a role for INA in the invasive and migratory processes of lung cancer. This investigation may also support early findings suggesting that DLKP

should be classified as non-small cell lung carcinoma with neuroendocrine differentiation, through its expression of INA.

4.2.7 Sepiapterin Reductase

The SPR gene encodes for a 27kDa cytoplasmic enzyme. SPR is a homodimeric enzyme belonging to the family of short chain dehydrogenase/reductases and is inhibited by N-acetyl derivatives of both serotonin and dopamine. The SPR gene, which is located on chromosome 2p14-p12 and disease causing mutations, can cause a rare inherited error in pterin metabolism leading to Levodopa-responsive disorder [173, 174]. Individuals with this disorder frequently manifest motor disorders, cognitive delays and more frequently neurological disorders [175]. SPR is localised to the cytoplasm where it functions as an aldo-keto reductase catalysing the NADPH-dependent formation of dihydrobiopterin (BH_2), a precursor for tetrahydrobiopterin (BH_4) [176]. BH_4 is an essential co-factor for enzymes such as nitric oxide synthase (NOS), Phenylalanine-3-3-hydroxylase, and catecholamine, but also for serotonin-biosynthesis enzymes tyrosine-4-hydroxylase and tryptophan-5-hyrdoxylase [174]. BH_4 production appears to be crucial for normal cell functions with richest sources of SPR found in erythrocytes, the liver and the brain. Biosynthesis of BH_4 (Figure 4.2-1) is regulated by the BH_4 *de novo* synthesis pathway, the BH_4 salvage pathway and a BH_4 regeneration system [177]. It has been reported that homeostasis of BH_4, dopamine, norepinephrine, serotonin and phenylalanine were greatly disturbed in SPR-/- mice leading to dwarfism and impaired body movement. The study did not investigate the activities of nitric oxide (NO) in the SPR mutant [178].

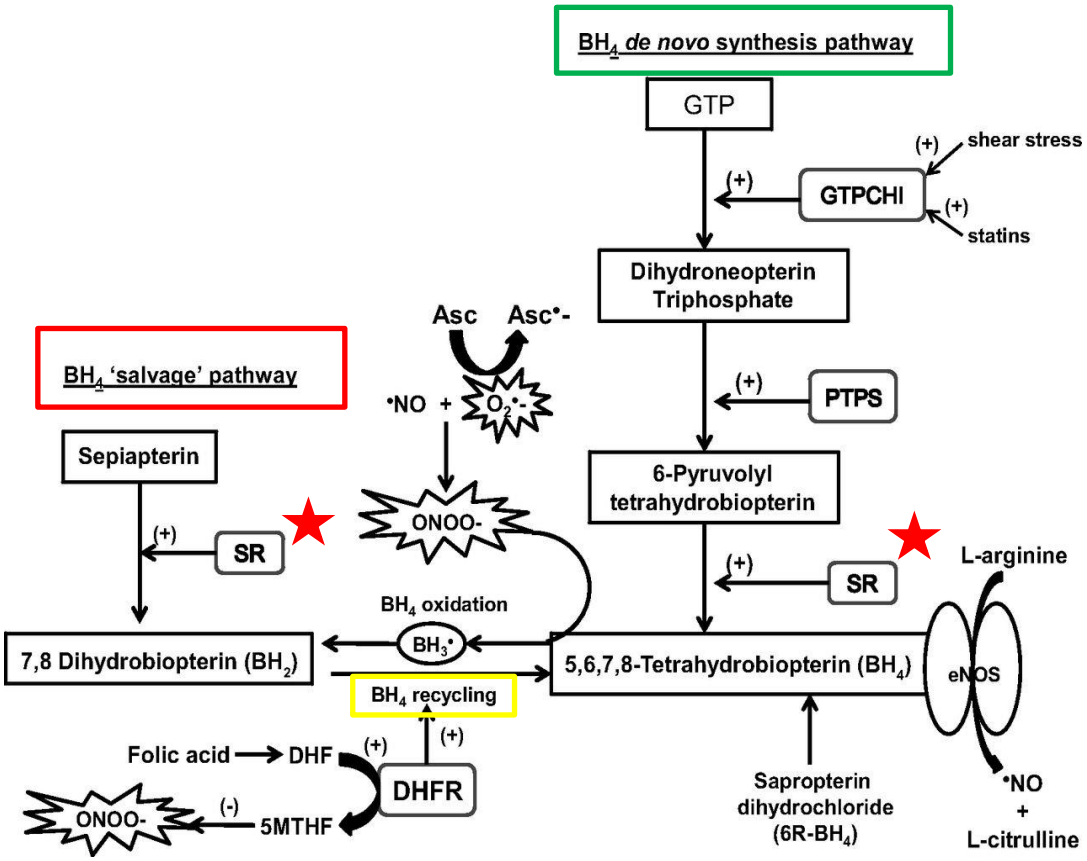

Figure 4.2-1:- Mechanisms of BH_4 biosynthesis.
BH_4 is synthesised through the de-novo pathway (green), salvage pathway (red) and BH_4 recycling (yellow). BH_4 biosynthesis is regulated by the de novo pathway in which guanidine triphosphate (GTP) is converted to BH_4 under the control of the rate-limiting enzyme GTP cyclohyrolase I (GTPCHI) and two intermediate enzymes pyruvoyl tetrahydrobiopterin synthase (PTPS) and sepiapterin reductase (SR - red star). BH_4 is also synthesized by a "salvage pathway," whereby sepiapterin is converted to 7,8-dihydrobiopterin (BH_2) via SR and subsequently reduced to BH_4 by dihydrofolate reductase (DHFR) [179].

4.2.7.1 Effect of siRNA knockdown of SPR on DLKPSQ and DLKPM

SPR was selected as a potential marker for DLKPSQ based on its comparative proteomic analysis of DLKPSQ *vs.* DLKPI (increased in DLKPSQ ~3.6-fold). Western Blot analysis confirmed expression of SPR was highest in DLKPSQ compared to DLKP and DLKPM, with the lowest expression seen in DLKPI (see section 3.1.3). Proteomic analysis and subsequent Western blot analysis of conditioned medium (CM) did not indicate expression of SPR in DLKP or its clones (data not shown). SPR is primarily localised to the cytoplasm. Immunofluorescence staining confirmed cytoplasmic staining in all four cell lines. membrane immunoreactivity was observed in a small population of DLKPSQ cells.

There is limited knowledge related to the potential functional role of SPR in cancer. One study presented data demonstrating a functional role in proliferation for SPR in neuroblastoma through a novel association with Ornithine Decarboxylase (ODC) [180], see Figure 4.2-2. Two independent studies have associated Sepiapterin (SP) with proliferation and migration in ovarian cancer through downregulation of p70S6K-dependent VEGFR2 expression [181] and in lung cancer through an association with Sepiapterin and integrin α3β1 and p53 [182]. Whilst these studies have reported findings directly related to proliferation and migration, presently there is no report in the literature associating SPR with cancer invasion, *in vitro*. A lung cancer TMA was immunohistochemically stained to examine SPR expression across different lung cancers. Variable staining was observed across the lung tumour types. The most intense and strongest staining was observed in the lung squamous cell carcinoma tumours (Figure 3.4-29). DLKP was established from a "poorly differentiated squamous carcinoma", so the intense staining in this tumour type was expected [92]. We wanted to see if SPR had a functional role in invasion and migration in the DLKP lung cancer cell line model. Knockdown of SPR was carried out in DLKPSQ and DLKPM because both cell lines show different levels of invasion and migration. There was a negligible effect on cell growth of both cell lines, however, one siRNA significantly (SPR-6, p=0.015) reduced cell growth of DLKPM.

Two independent siRNAs were used to knockdown SPR in DLKPSQ. The invasive and migratory abilities using SPR-6 siRNA were reduced, but a high degree of variability was observed within a single biological replicate. By carrying out siRNA knockdown in a lowly invasive cell line, we were hoping to observe an increase in the invasion levels of DLKPSQ. Invasion levels of DLKPSQ are very low, so we were unable to determine if

the decrease was as a result of the knockdown or due to the low invasive and migratory capacity of DLKPSQ (see section 3.4.3.1). It was therefore decided to focus on DLKPM. Four independent siRNAs were used to knockdown SPR in DLKPM (SPR-1, SPR-2, SPR-5 and SPR-6). The invasive capacity of DLKPM cells was significantly reduced; SPR-1 (p=0.0031) and SPR-6 siRNA (p=0.0014) and the migratory ability was also significantly reduced using SPR-1 (p=0.0054) and SPR-6 (p=0.0048) see section 3.4.3.2. This is to our knowledge, the first report associating SPR with invasion and migration *in vitro*, suggesting that SPR may have a potential role in the invasive and migratory process of lung cancer.

4.2.7.2 Effect of SPR knockdown in TNBC and pancreatic cancer

Survival analysis using the BreastMark algorithm indicated that low expression of SPR was significantly associated with poor outcome in patients with Luminal A (p=0.0019) and Basal-like (p=0.022) breast cancer (section 3.2.8). Currently, there are no available targeted therapies for triple negative breast cancer (TNBC). SPR expression was investigated in a panel of cell lines representing various TNBC sub-types. SPR specific bands were detected at ~27kDa in TNBC cell lines, with the highest level of expression observed in MDA-MB-468, a basal-like 1 breast cancer subtype (Figure 3.3-8). PDAC is the most common type of pancreatic cancer, accounting for up to 90% of cases. Several mutations have been associated with pancreatic cancer development; KRAS, TP53, CDKN2A, EGFR and SMAD4. These mutations may lead to pancreatic tumour development and potentially chemo-resistance [183]. A role for SPR in the invasion or migration processes is not currently described in TNBC or pancreatic cancer. Preliminary siRNA knockdown studies were carried out to investigate a potential role for SPR in TNBC (MDA-MB-468: BL-1) and pancreatic cancer (MiaPaCa2 Clone3 and AsPc-1). These cell lines were selected based on their increased expression profile of SPR in representative TNBC and PDAC cell line panel (Figure 3.3-8 and Figure 3.3-11). siRNA knockdown studies in MDA-MD-468 cells resulted in a reduction in invasion using at least two siRNAs targeting SPR, a significant reduction for SPR-6 (p=0.000908). Preliminary transfections were also carried out on MiaPaCa2 clone3 and AsPc-1 cells; reduced invasion and migration was observed for MiaPaCa2 clone 3 cells, while migration was only reduced for AsPc-1 cells. Although further investigations will need to be carried out in these pancreatic cancer cell lines, preliminary results indicate a potential role for SPR in breast and pancreatic cancer (Figure 3.4-26). BreastMark analysis indicated that SPR expression may be significant in relation to survival of

patients with breast cancer. SPR expression was examined in a small panel of breast cancer tissues (subtypes unknown), we found increased expression of SPR in these tissues compared to normal. In addition, a TMA containing 12 invasive ductal breast carcinomas also showed moderate to weak membrane staining (see section 3.4.7). This study aimed to evaluate SPR expression in a small cohort of breast cancer tissues, however, a larger number of tissues would need to be stained to verify the distribution of SPR in breast cancer.

4.2.7.3 Hypoxia and tumour progression

Tumour hypoxia occurs as a result of inadequate supply of blood borne oxygen to tumours due to the rapid cell proliferation that exceeds the development of the tumours blood supply. This can cause changes in the expression pattern of certain proteins in the tumours can induce hypoxia. Such proteins can act as makers for hypoxia, for example, Hypoxia-inducible factors (HIFs) transcription factors that respond to a decrease in oxygen in the cellular environment. Activation of HIF-l (hypoxia-inducible factor 1) in cancer can increase the transcription of genes involved in glucose metabolism, apoptosis resistance, proliferation, invasion, metastasis and angiogenesis. Elevated levels of HIF-1α and or HIF-2α have been found in the majority of human cancers and their metastases and has been associated with higher patient mortality. Two other proteins have been described as intrinsic markers of hypoxia: Glucose-transport protein-1 (GLUT-1) and Carbonic anhydrase 9 (CAIX). Hypoxic conditions can lead to changes in characteristics of cells within a tumour and potentially lead to tissue heterogeneity, some cells may adapt and escape leading to potential local invasion and metastatic spread [184, 185]. Some of the changes in hypoxic conditions may result in increased sensitivity of cells as well as increased resistance to chemotherapy, the latter presenting a major clinical challenge in the treatment of certain cancers [186].

4.2.7.4 Reactive oxygen species

Reactive oxygen species (ROS) are derived from the metabolism of molecular oxygen and are highly reactive. The major source of endogenous ROS is hydrogen peroxide and superoxide anion, which are generated as by-products of cellular metabolism such as mitochondrial respiration. ROS can be categorized into two groups. The first group include free oxygen radicals e.g. superoxide, hydroxyl radical, nitric oxide, organic radicals, peroxyl radicals, alkoxyl radicals, thiyl radicals, sulfonyl radicals, thiyl peroxyl radicals and disulphides. The second group are non-radical ROS which include: hydrogen peroxide, singlet oxygen, ozone/trioxygen, organic hydroperoxide, hypochloride,

peroxynitrite, nitrosoperoxycarbonate anion, nitrocarbonate anion, dinitrogen dioxide, nitronium, and highly reactive lipid-or carbohydrate derived carbonyl compounds. ROS exists in all aerobic cells but is tightly balanced by biochemical antioxidants. When this critical balance is disrupted oxidative stress occurs due to excess production of ROS coupled with depletion of antioxidants [187].

ROS are potential carcinogens because they facilitate mutagenesis, tumour promotion and progression [188]. The growth promoting effects of ROS are related to redox-responsive cell signalling cascades and have been implicated in the regulation of the mitogen-activated protein (MAP) kinase/Erk cascade, phosphoinositide-3-kinase (PI3K)/Akt-regulated signalling cascades, as well as the IκB kinase (IKK)/nuclear factor κ-B (NF-κB)-activating pathways). [187, 188]. In addition to this, DFMO used to inhibit invasion in DLKPM cells (see section 3.4.3.3) has been implicated in two opposing cellular actions (cell survival and cell cycle arrest) in neuroblastoma through the inhibition of ornithine decarboxylase (ODC), leading to the activation of both AKT/Protein kinase B and p27Kip1 [189].

4.2.7.5 Effect of SPR knockdown on generation of ROS in DLKPM

To investigate the effect of SPR on the generation of reactive oxygen species (ROS). DLKPM cells were transfected using four independent siRNAs targeting SPR and were then tested for generation of ROS. There was a reduction in ROS generation in SPR transfected cells using four independent siRNAs when compared to negative control cells. For SPR-1, SPR-5 and SPR-6, a 22% (p= 0.04), 32% (p= 0.006) and 31% (p= 0.009). The results in section 3.4.3.5, indicate that ROS generation may be potentially impaired as a result of knockdown of SPR.

4.2.7.6 Investigation of the role of NOS and ODC in invasion of DLKPM

To further develop our understanding of the role of SPR in the invasive process of the lung cancer cell line DLKPM, we performed preliminary studies to investigate the role of NOS and ODC in the invasion of DLKPM. We used two inhibitors; Nω-Nitro-L-arginine (L-NNA) and DL-α-Difluoromethylornithine (DFMO) inhibitors for this study. An appropriate concentration was established for each inhibitor prior to carrying out invasion assays.

4.2.7.7 Effect of L-NNA on DLKPM invasion

As mentioned earlier, SPR is an enzyme that catalyses the final one or two steps in the production of BH_4. BH_4 is an essential co-factor for a number of enzymes including NOS.

There are three isoforms of NOS in mammalian tissues NOS-1 or nNOS was first purified from neuronal tissue, NOS-3 or eNOS was first found in endothelial cells. Both are constitutively expressed in epithelial tissues and are dependent on the transient influx of calcium to activate calmodulin. NOS-2 or iNOS permanently binds calmodulin and functions independent of calcium, its inducible by pro-inflammatory stimuli and once induced, NO is produced in high concentrations for longer periods. Also, sustained high levels can contribute to stroke and neurotoxic effects. NO is generally a short lived, endogenously produced gas and is responsible for numerous physiological functions such as vasodilation, inhibition of platelet aggregation and neurotransmission in central and peripheral nervous systems. However, it has been reported that components of the tumour microenvironment of breast cancer, may be important in the regulation of NOS *in vitro*. IL-8, TLR4, TIMP1, S100A8 and IL-6 were all implicated in this regard [190]

L-NNA is a competitive inhibitor for all isoforms of NOS, it interacts non-covalently with all NOS'es but its coupling with iNOS is reported to be immediate and rapidly reversible with arginine. The role of NOS was investigated using the inhibitor L-NNA. The cell viability of DLKPM cells following treatment with L-NNA was determined by the acid phosphatase assay as described in section 2.5. Three different concentrations of L-NNA inhibitor were used (50μM, 100μM and 150μM) over a 5-day period. Results indicate that the growth inhibitory effects of L-NNA at all concentrations were negligible. In fact, at the higher concentration of 150μM, L-NNA treatment resulted in an increase cell growth of DLKPM. This concentration range of between 50μM and 150μM was used to investigate the effect of NO on the invasive capacity of DLKPM. Invasion assays were performed using two approaches. Firstly, a co-treatment, whereby L-NNA was added directly to the cells in the invasion assay and secondly, whereby the cells were treated for 24hrs prior to invasion assay. The results indicate that there was no inhibitory effect following co-treatment with L-NNA. However, a 37% reduction in invasion (Figure 3.4-21) was observed following the 24hr pre-treatment, indicating a potential role for NO in lung cancer cell invasion, *in vitro*.

4.2.7.8 Effect of DFMO on DLKPM invasion

Ornithine decarboxylase (ODC) is an enzyme that catalyses the first step of polyamine biosynthesis in humans: the decarboxylation of ornithine to putrescine. ODC is indispensable because of its central role in polyamine biosynthesis and because polyamines play essential roles in normal cell growth and differentiation. The resulting low molecular weight polyamines, spermidine, spermine and putrescine, are known to

interact with various macromolecules and have a variety of cellular effects. Polyamines are known to be involved in cell growth and have also been implicated in the process of cell transformation. In cancer, elevated levels of polyamine biosynthesis and accumulation have been associated with rapid tumour growth [191, 192]. SPR has been previously shown to interact with and activate ODC in order to elicit an effect on proliferation in neuroblastoma, the proposed mechanism for crosstalk between SPR and ODC is illustrated in Figure 4.2-2 [180]. We have also shown a potential role for SPR in the invasive and migration processes of DLKPM cells (section 3.4.3.3).

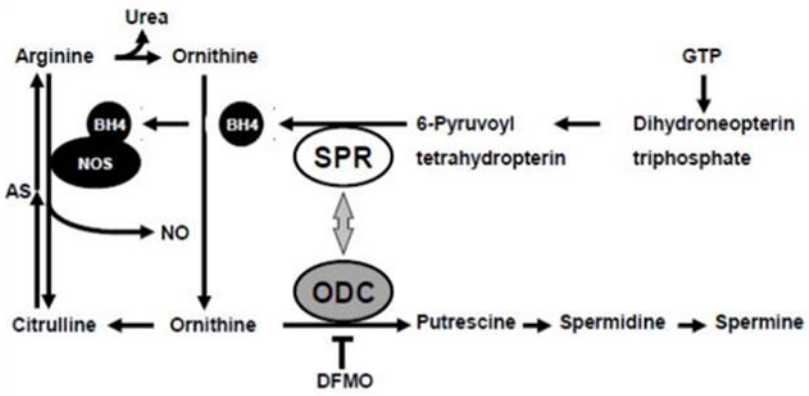

Figure 4.2-2:- Proposed crosstalk between polyamine and nitric oxide (NO) pathways.
Arginine is converted to ornithine by the action of arginase in the urea cycle. The enzyme ODC converts ornithine to putrescine and is a key enzyme in the biosynthesis of higher polyamines (spermidine, spermine). The NO pathway enzyme sepiapterin reductase (SPR) converts 6-pyruvoyl tetrahydropterin to tetrahydrobiopterin (BH_4), a cofactor for NO synthase (NOS) which converts arginine to citrulline. In reverse, citrulline converts to arginine via argininosuccinate (AS). ODC forms a heterodimer complex with SPR which activates ODC and stimulates cell proliferation.

The role of ODC was investigated using the inhibitor, L-α-difluoromethylornithine (DFMO). DFMO is an irreversible inhibitor of ODC which is used to induce the depletion of polyamines. Three different concentrations of the DFMO inhibitor were used (1mM, 2.5mM and 5mM) over a 5-day period. Results indicate that there were growth inhibitory effects of associated with DFMO at 1mM and 2.5mM, (between 40-47% reduction in growth), while the highest concentration of 5mM showed little or no inhibitory effects on DLKPM cells. To investigate a potential role for ODC in the invasion of DLKPM cells, 2.5mM and 5mM of DFMO was used. Invasion assays were performed using the same approach as used for L-NNA, a co-treatment and a 24hr pre-treatment. There was a significant reduction in the invasive capacity (p=0.04) of DLKPM following co-treatment

with the DFMO inhibitor, indicating that ODC (and potentially the production of polyamines) may be important for invasion of DLKPM (Figure 3.4-20).

4.2.7.9 Summary

In summary, the effect of SPR silencing was investigated in the invasive cell line, DLKPM. We have shown that siRNA knockdown of SPR; (i) does not appear to affect cell growth but (ii) results in a significant reduction of invasion and migration in DLKPM. We also suggest a potential association with MDA-MB-468 (TNBC) and MiaPaCa3 Clone3 and AsPc-1 (PDAC). We have indicated that NOS and ODC (through the use of inhibitors) may also have a role in the invasive process of DLKPM cells.

4.3 Investigation of the growth of DLKP and its clones, *in vivo*

A pilot study was carried out to investigate the growth of DLKP and its clones *in vivo*. DLKP, DLKPSQ, DLKPI and DLKPM cell lines were previously used in the *in vitro* generation of xenografts, no tumours were produced in this case. However, unlike the previous study SCID mice were selected for use in this study, so it was not known whether these cell lines would grow and result in the formation of tumours. The main aims of this study were to see if DLKP and the clones would grow and result in tumour formation in SCID mice.

4.3.1 Examination of DLKP and its clones *in vivo*

In vitro observations of the growth of DLKP and the clones indicated that they display different growth rates. DLKPSQ appears to be the slowest growing and DLKPM appears to grow the fastest, with DLKP and DLKPI displaying similar growth patterns [93]. Since an *in vivo* study such as this had not previously been carried out using DLKP and the clones, it was decided to use three different cell densities ($1x10^6$cells, $5x10^6$cells and $1x10^7$cells) for implantation. When the cell lines were implanted into the mice, they appeared to show an initial lag in their growth, this characteristic also resembles their growth *in vitro*. Up to day 21, small palpable tumours were present in mice inoculated with DLKP, DLKPSQ and DLKPI cells, after this period the tumours appeared to grow at a rapidly (see section 3.5.2), while DLKPM cells produce tumours but at a slower rate to the other clones. The growth of DLKP and its clones *in vitro* is well established, they appear to exhibit slow growth for up to 2 days post trypsinisation, after which they appear to show an increased rate of growth. However, tumours developed using all cell lines, but DLKP and DLKPI cells appeared to behave similarly *in vivo*. DLKP (Figure 3.5-3 and Figure 3.5-4) and DLKPI (Figure 3.5-7 and Figure 3.5-8) were the fastest growing and largest, giving rise to tumours of over $100mm^3$ by 21 days, DLKPI were marginally faster. In contrast, DLKPSQ also gave rise to large tumours that were highly vascularised and angiogenic tumours (Figure 3.5-5 and Figure 3.5-6), while tumours produced by DLKPM were small, compact and more 'solid' in appearance (Figure 3.5-9 and Figure 3.5-10).

The size of the tumours produced by the cell lines may be reflected in the expression of Ki67. Ki67 is a marker for proliferation and is expressed by proliferating cells in all active phases of the cell cycle (G (1), S, G (2), and mitosis), [193, 194]. Strong expression of Ki67 was observed in all tumours, a reduced level was observed in DLKPM derived tumours. The relatively high levels of ki67 expression observed in the xenograft tumours indicate that cells are actively proliferating and suggest a reason why such large tumours

were produced with DLKP, DLKPSQ and DLKPI. Ki67 expression in DLKPM derived tumours were reduced relative to the other tumours and thus potentially explaining why small tumours were produced for DLKPM cells. The large size of the tumours produced by DLKP and DLKPI indicated evidence of necrosis or potential hypoxia (Figure 3.5-3 and Figure 3.5-7). This was not surprising due to the lack of visible vasculature in these tumours. Immunohistochemical analysis of the tumours for markers of hypoxia (e.g. HIF-1α or Glut-1) would help confirm the presence of a hypoxic environment in these tumours.

Use of different cell numbers for subcutaneous injection of cell lines allowed for examination of potential dose responses relating to tumour growth of the cell lines. In the case of DLKP and DLKPI, large tumours formed with all cell numbers, however, a lower cell number of $1x10^6$ cells may be optimal for the *in vivo* growth of DLKP and DLKPI in future experiments. It appears that DLKPSQ produced tumours at each cell number, but failed to produce tumours in two mice out of four at $5x10^6$ cells, however, an optimal cell number for DLKPSQ would be between $1x10^6$ cells and $5x10^6$ cells. DLKPM seemed to be cell density dependent showing optimal tumour growth using an inoculation density of $1x10^7$cells. While all cell lines produced tumours, tumours were not produced at all three cell densities, indicating that there may be an optimal seeding density tot could be used for further experimentation. However, where tumours were produced by DLKP, DLKPSQ and DLKPI, they very large tumours and were produced very quickly. DLKPM appeared to be the exception producing smaller more solid tumours. An optimal cell number for tumour growth would prevent excessively large tumours being produced in future studies and potentially allow for the examination of the effect of drugs on tumour growth over a longer period of time. The fact that all four cell lines produced tumours indicates that DLKP is an invaluable cell line model that could be used to carry out further *in vivo* experiments. A role for INA and SPR in tumour growth and development could be investigated through stable knockdown of DLKPSQ or DLKPM, shRNA transfected cells could be implanted into SCID mice as performed in this study and examined for effects on tumour growth. But also the effect of potential drug candidates on lung cancer tumour growth could also be examined using this cell line model.

To examine the animals for evidence of potential metastasis, at day 21 one animal was sacrificed. The organs of each animal in this group were embedded in paraffin wax, sectioned and examined by a pathologist (Prof. Susan Kennedy) for evidence of metastasis. In this group of animals, there was no evidence of metastasis found in these

organs. The organs from the remaining mice in this study should be examined for metastasis. Tumours from one group of mice were also examined using Haematoxylin and Eosin staining, the xenografts were described as "poorly differentiated squamous cell carcinoma". This description of the xenograft tumours is consistent with the original tumour from which DLKP was isolated. When harvesting the organs and tumours, the mice were examined for potential metastasis in the abdomen. Upon inspection one injection site inoculated with DLKPSQ at an inoculation density of $5x10^6$ cells failed to produce a tumour, this mouse in addition to one other produced small growths throughout their abdomen, indicating evidence of suspected metastasis or peritoneal carcinomatosis as described by Mr. Vincent Lynch (Figure 3.5-5). Carcinomatosis is very rare and is detected in about 10% of patients at the time of primary resection. The mechanisms causing carcinomatosis include dissemination of free cancer cells as a result of serosal involvement of the primary tumour, implantation of free cancer cells or the presence of cancer cells in the lymph fluid or venous blood retained in the peritoneal cavity [195]. Interestingly these growths did not appear in mice inoculated with DLKP, DLKPI or DLKPM, which would be considered to have moderate to high levels of invasion *in vitro*.

CD31 is an established marker for angiogenesis [196], CD31 that has been associated with multiple cellular functions including adhesion, apoptosis, coagulation, host response, and protein synthesis that could influence tumour growth [197]. CD31 expression was examined in the xenograft tumours, while the xenograft tumours showed extremely low expression in all tumours, DLKPSQ derived tumours did show some CD31 immunoreactivity. The low expression of CD31 in DLKPSQ derived tumours may indicate why evidence of potential metastasis was observed in only three out of ten mice and why there was no observed evidence of potential metastases in mice inoculated with DLKP, DLKPI and DLKPM (Figure 3.7-3).

The observation of potential evidence of metastasis in a total of three out of ten mice inoculated with DLKPSQ was an unexpected result due to the poorly invasive nature of this cell line. One possible explanation for the distribution of these growths may be the ability of DLKPSQ to survive in suspension or rather its ability to resist anoikis [95]. Anoikis is an important process that contributes to cancer metastasis and is a particular type of apoptosis that occurs as a result of detachment or the absence of attachment to extracellular matrix (ECM), or to an inappropriate ECM [198, 199]. Evasion of anoikis is mainly regulated by integrins. Integrins protect the cell from anoikis, and so also do several kinases activated by integrins, like SRC, FAK and ILK [200]. Some tumour cells

use ROS to avoid anoikis through oxidative stress, where by the production of ROS leads to the oxidation/activation of tyrosine kinase SRC leading to the activation of mechanisms that promotes survival and metastasis [201]. In a follow-up experiment, six mice were inoculated with DLKPSQ with the aim of replicating the original experiment i.e. to the production of growths in the peritoneal cavity. This study resulted in production growths in just one out of the six mice, this time, the growths were smaller than previously observed. In total 3 out of 10 mice produced evidence of potential metastasis. This result could indicate that not all DLKPSQ cells have the capacity to produce these growths and possibly suggesting that there may be potential tumorigenic and non-tumorigenic subpopulations in DLKPSQ [202]. This could indicate potential cellular heterogeneity within DLKPSQ.

This study indicated that DLKP, DLKPSQ, DLKPI and DLKPM cell lines were all capable of forming tumours *in vivo* (section 3.5.2). Apart from the growths produced by DLKPSQ, there was no other evidence of metastasis. However only organs from one mouse inoculated with each cell line were examined for metastasis, it would, therefore, be important to examine the organs from the remaining animals for evidence of metastasis. It is possible that the tumour microenvironment, which comprises of a complex network of tumour cells, immune cells, stromal cells and extracellular matrix, may have favoured the growth of a stem-like subpopulation within DLKPSQ, that resulted in the dissemination of DLKPSQ cells throughout the peritoneal cavity. This study provided a unique opportunity to study each of the cell lines under *in vitro* conditions but after a period of time in a tumour. We wanted to examine DLKP and its clones post tumour growth for changes in their invasive and migratory capabilities. Explant culture was performed by placing small pieces of the tumours into dishes containing serum free media and allowing the tumour cells migrate outward over a number of days. During the initial culture of cells derived from tumours, DLKPSQta appeared to display a more rounded morphology and had difficulty bedding down, while DLKPMt appeared to be smaller and more elongated and was capable of bedding down. Interestingly cells explanted from the DLKPSQ growths displayed marked changes in their morphology, while DLKPIt became slightly more fibroblastoid-like. However, after culturing over a number of passages, cells derived from DLKPSQ and DLKPI tumours appeared to revert to a morphology that resembled their original culture. Cells derived from DLKPM tumour appeared to retain its newly established morphology (Figure 3.6-1). In addition, cells derived from DLKPM tumours exhibited a reduced invasive and

migratory capacity (Figure 3.6-5) over prolonged growth in culture but also showed reduced expression of N-cadherin, this could be evidence of a move to a less aggressive cell type [202]. Perhaps this reduced expression of N-cadherin is indicative of reduced tumorigenic capacity of DLKPM cells. In contrast, cells derived from DLKP parental showed large tumour production, whilst an increased N-cadherin expression was observed in the explanted cells (Figure 3.7-6). N-cadherin is a known marker for EMT [203, 204]. The change in N-cadherin expression could indicate the start of the processes of epithelial to mesenchymal transition (EMT) in the case of DLKP or potentially mesenchymal to epithelial transition (MET) the case of DLKPM. It could also indicate potential interconversion of DLKPM to DLKPI-like cells. There was no change in E-cadherin expression in xenograft tumours or in explanted cells (Figure 3.7-4 and Figure 3.7-5). The EMT model indicates that cancer cells with an EMT phenotype can invade and intravasatate, but cannot form metastatic nodules. Cancer cells without an EMT phenotype cannot invade, but are able to form metastatic nodules. Cancer cells with a mixed EMT and non-EMT phenotype can complete the entire process of spontaneous metastasis. However, an additional model of EMT has been described and may be relevant to the results obtained in our *in vivo* study, where DLKPSQ, poorly invasive cell line produced evidence of metastasis *in vivo*. The model indicates, EMT cells with an enhanced invasive and migratory phenotype are responsible for degrading the surrounding ECM and penetrating the local tissues and blood or lymphatic vessels (intravasation). It is thought that the non-EMT cells migrate with EMT cells and thereby follow them into the circulation [205]. We suggested earlier that there may be an additional subpopulation present in DLKPSQ that was responsible for producing evidence of metastasis. That subpopulation may have played a role in initiating the process that led to the production of the growths in the peritoneal cavity.

4.3.2 Investigation of the expression of validated proteins *in vivo*

Eight proteins selected for validation studies in section 3.2, were also examined in xenograft tumours that were produced from the growth of DLKP, DLKPS, DLKPI and DLKPM in SCID mice. Proteins were identified from the comparative proteomic analysis carried out as part of this thesis (section 3.1.3), but also from an examination of other analyses performed in the NICB. Xenograft tumours were immunohistochemically examined using antibodies specific to each of the proteins and also by Western blot analysis of the cells recovered from the tumours. Table 4.3-1 shows overall expression of SLIT2, ROBO2, ALCAM, IQGAP1, INA and SPR from both xenograft tumours, while

Table 4.3-2 shows the expression of SLIT2, ALCAM, IQGAP1 and SPR in explanted cells recovered from tumours compared to control cells.

Overall expression in xenograft tumours				
	DLKP	**DLKPSQ**	**DLKPI**	**DLKPM**
ALCAM	++	+	++++	++
INA	+	+	-	+
IQGAP1	+	+	++	+++
ROBO2	++	+	+	++
SLIT2	+++	++	++	+++
SPR	+++	+++	++	++

Table 4.3-1:- Expression of validated protein in xenograft tumours.
Scoring reflects overall expression in tumours from two injection sites ($1x10^6$ cells and $5x10^6$ cells). ++++ Very Strong; +++ Strong; ++ Intermediate; + weak; +/- very weak; - negative

Expression of proteins in control *vs.* explanted cells					
		DLKP	**DLKPSQ**	**DLKPI**	**DLKPM**
ALCAM	**Control**	+	+/-	++++	+/-
	Explant	+/+	+/-	++++	+/-
IQGAP1	**Control**	+/-	+	++	+++
	Explant	++	+	++	++
SLIT2	**Control**	++	+/-	+	+++
	Explant	+	+/-	+	+++
SPR	**Control**	++	++	+	+
	Explant	++	++	+	+

Table 4.3-2:- Expression of validated proteins was maintained in recovered cells from DLKP *in vivo* study.
Expression of proteins in control cells was compared to expression in cells recovered by explant culture from DLKP tumours. ++++ Very Strong; +++ Strong; ++ Intermediate; + weak; +/- very weak; - negative

ROBO2 and SLIT2 expression was examined in xenograft tumours (section 3.8.1). Expression trends *in vivo* appear to be similar to that seen in culture. For SLIT2, strong expression was observed in all cell line derived tumours with DLKP and DLKPM showing the most intense level of expression, whilst DLKPSQ and DLKPI showed lower levels of expression.

ALCAM expression was confirmed by Western blot analysis in DLKP and its clones (section 3.8.2), with the highest expression observed in DLKPI and lower levels observed in DLKP and DLKPM cells. Investigation of ALCAM expression in xenograft tumours appears to show similar trends in the expression of ALCAM between each of the cell line derived tumours. Briefly, DLKPSQ shows the lowest level of expression. However, strong expression was observed in isolates areas of both tumours produced from $1x10^6$ and $5x10^6$ cells. DLKPI shows the strongest expression throughout both tumours while DLKPI and DLKPM shows a moderate level of expression in areas of each tumour (summarised in Table 4.3-1 and Table 4.3-2). Fujiwara *et al.*, carried out a study to investigate the significance of ALCAM expression in pancreatic cancer. They found that $ALCAM^{+ve}$ pancreatic cancer cells exhibited stronger tumourigenicity than that of $ALCAM^{-ve}$ cells, whereas $ALCAM^{-ve}$ pancreatic cancer cells exhibited comparatively stronger invasive and migratory activities [206]. The DLKP cell line model shows varied levels of expression of ALCAM and all cell lines produced tumours *in vivo*, it could further indicate the contradictory role of ALCAM in cancer, as discussed previously.

Validation studies (Section 3.2) confirmed that expression of IQGAP1 is lowest in DLKP with increasing levels in DLKPSQ, DLKPI and in DLKPM. Examination of IQGAP1 expression observed in xenograft tumours appears to show similar trends in its expression *in vivo vs. in vitro* expression (see section 3.8.3). Strong membrane reactivity was observed in tumours from all cell lines, however, DLKP showed the lowest level of expression in both tumours produced from $1x10^6$ and $5x10^6$ cells. DLKPM shows the most intense membrane immunoreactivity throughout both tumours, while DLKPSQ and DLKPI shows a more moderate level of expression (Table 4.3-1). As mentioned earlier Jameson *et al.*, investigated tumour formation in $IQGAP1^{-/-}$ mice and showed that there was diminished tumour formation in the knock-out mice [154]. We have a cell line model showing strong expression of IQGAP1, which appears to be maintained *in vivo*, suggesting that IQGAP1 may play an important role in tumourigenicity of DLKP, DLKPSQ, DLKPI and DLKPM cell lines *in vivo*. For confirmation of the role of IQGAP1

in tumour growth of DLKP and its clones, further investigations would need to be performed.

INA expression in xenograft tumours shows similar trends to that seen in culture. Briefly, DLKP, DLKPSQ and DLKPM appear to show moderate levels of expression of INA, while DLKPI shows an absence of expression in both tumours produced from $1x10^6$ and $5x10^6$ cells (see section 3.8.4, Figure 3.8-8). It is unlikely that INA is required for tumour growth, given that DLKP and its clones were all capable of tumour development in SCID mice.

In vivo expression of SPR in xenograft tumours (see section 3.8.5) appears to show similar expression trends to that seen in culture. However strong immunoreactivity was observed in all four cell lines, DLKP and DLKPSQ showed the highest immunoreactivity for SPR, while DLKPI and DLKPM appear to show a lower level of expression - especially in tumours derived from $1x10^6$ cells. A number of different dilutions of the SPR antibody were used to stain the xenograft tumours and all concentrations resulted in extremely strong staining. The antibody dilution used for the purposes of this these was 1:3000. A more optimal concentration of SPR antibody should be used to examine fully the extent of expression of SPR in the tumours. However, there is evidence of membrane staining within tumours developed from DLKP, DLKPSQ and DLKPI. Preliminary Western blot analysis of membrane enriched samples appears to show maintenance of SPR expression in cells recovered from the tumours compared to cells in control culture. High expression of SPR in the xenografts may indicate that SPR is important for the development of tumours. Evidence of membrane expression of SPR in the xenograft tissues indicates that SPR may be important for use as a potential membrane target for therapy.

4.3.3 Summary

The *in vivo* study presented here shows that DLKP, DLKPSQ, DLKPI and DLKPM are all capable of forming tumours in SCID mice. We have shown that the expression of proteins identified from the comparative proteomic analysis was maintained in both recovered cells and also in xenograft tumours. We have shown DLKP and its clones display tumorigenic abilities in SCID mice and at certain cell densities, these conditions will make it easier to perform further *in vivo* studies using the DLKP cell line as a model. DLKP and its clones having distinctly different levels of invasion and other phenotypical characteristics could, therefore, prove to be an invaluable model to study the efficacy of chemotherapy drugs or monoclonal antibody therapies for lung cancer *in vivo*.

Chapter 5 CONCLUSIONS AND FUTURE WORK

5.1 Conclusions

1. Proteomic profiling of membrane associated proteins of DLKP, DLKPSQ, DLKPI and DLKPM cell lines identified a number of statistically significant differentially expressed proteins: AHNAK, ALCAM, IQGAP1, HDGF, ROBO2 and SPR. All candidate membrane proteins including two further proteins; INA and SLIT2 were validated in DLKP and its clones, indicating that the method used in this study successfully isolated potentially biologically relevant membrane proteins.

2. A dual invasion role for ALCAM was demonstrated through siRNA silencing of the ALCAM gene, a significant decrease in the invasive potential of DLKPM was observed, while a significant increase in the invasive potential was observed in the DLKPSQ-mitox-BCRP-6P cell line.

3. A functional role for SPR and INA in invasion/migration of DLKPM cells was demonstrated through siRNA silencing of their respective genes, a significant decrease in the invasive and migratory potential of DLKPM was observed. In addition, a role for ROS was shown through a significant reduction in ROS generation following siRNA knockdown of SPR in DLKPM cells.

4. Survival analysis using the BreastMark algorithm indicated that low expression of SPR was associated with poor outcome of Luminal A breast cancer and TNBC. A significant reduction in the invasive capacity of MDA-MB-468 (TNBC cell line) was also demonstrated following siRNA knockdown of SPR gene, indicating a potential role for SPR in breast cancer invasion. IHC analysis of SPR in a small panel of breast cancer tissues showed evidence of membrane reactivity, suggesting that SPR could be used as a potential therapeutic target.

5. The differentially expressed proteins markers; HDGF, SLIT2, ALCAM, INA and SPR were all shown to be highly expressed in DLKP and SCLC cell lines, indicating an association of DLKP with SCLC. In addition, IHC analysis of INA carried out on lung cancer tumours indicated expression was observed mainly in lung neuroendocrine, suggesting that INA could serve as a marker for neuroendocrine cancers.

6. A study indicated that DLKP, DLKPSQ, DLKPI and DLKPM were highly tumorigenic in SCID mice. DLKP and DLKPI produced the largest and fastest growing tumours. DLKPSQ produced large, but extremely vascularised tumours with three out of ten mice showing evidence of potential metastasis in the peritoneal cavity. Immunohistochemical analysis of xenografts revealed strong Ki67 immunoreactivity in xenografts derived from all four cell lines, suggesting that all cell lines were highly proliferative *in vivo*, particularly for DLKP, DLKPSQ and DLKPI.

7. Explant culture revealed a significant decrease in the migratory potential of DLKPSQ cells, but also a significant decrease in both invasive and migratory potential of DLKPM cells. Western blot analysis of explanted cells and immunohistochemical analysis of xenograft tumours revealed that the expression of the differentially expressed proteins was maintained *in vivo*.

8. We have shown that DLKP and its clones display tumorigenic abilities in SCID mice, the conditions used in this study will make it easier to perform further *in vivo* studies using the DLKP cell line as a model.

5.2 Future work

1. Immunohistochemical analysis should be carried out to determine the distribution of ALCAM in a range of human cancer tissues (e.g. lung cancer, pancreatic cancer). To explore the mechanism responsible for the dual invasion role of ALCAM in the DLKP cell line model, further investigations should be carried out using siRNA knockdown followed by analysis of protein expression (e.g. E-cadherin, N-Cadherin, Vimentin, β-catenin, T-ERK/P-ERK etc.) by western blot analysis.

2. BreastMark survival analysis indicated that SPR expression was significant in relation to survival of patients with Luminal A and Basal-like breast cancers. To further investigate a functional role for SPR in TNBC, siRNA knockdown studies should be carried out on additional cell lines associated with these cancer subtypes. SPR also displayed evidence of membrane association in a number of breast cancer tissues. Further immunohistochemical analysis should be carried out on a larger cohort of breast tumour types (including triple negative, HER2+, ER+, invasive and non-invasive) to further investigate if SPR is amenable as a potential drug target.

3. To further examine the involvement of Nitric Oxide Synthase and Ornithine decarboxylase as a mechanism by which SPR decreased invasion and migration in DLKPM cells, further assays could be carried out using additional inhibitors of ODC and NOS. Inhibitors could be used in combination to establish a synergistic role. In addition to inhibitor studies, siRNA knockdown studies could to carried out to further evaluate a role for NOS (eNOS, nNOS, iNOS) or ODC in invasion and migration of the DLKPM cell line and TNBC cell lines.

4. SPR and INA should be investigated in representative colon cancer cell lines to establish potential differences in their expression between primary and metastatic cell types (e.g. SW480 and SW620). Immunohistochemistry should be performed to establish the expression of these proteins in non-cancerous tissues and in other tumour types such as melanoma or glioma.

5. Using commercially available antibodies, immunoprecipitation should be performed to identify potential binding partners of SPR and INA, which would help us to further understand the mechanism by which they effect invasion and migration in DLKPM

cells. Immunoprecipitation studies may also help identify further potentially novel proteins involved in cancer.

6. Functional roles for target proteins should be investigated in other cellular processes such as anoikis, adhesion, through siRNA knockdown. Use of 3D assays could be useful to look at the effect of transfected cells on cellular growth *in vitro.*

7. DLKPSQ produced evidence of potential metastasis in the peritoneal cavity of a number of mice in the pilot *in vivo* study. A further *in vivo* study with DLKPSQ using a larger number of mice should be performed to further investigate DLKPSQ as having a potential metastatic subgroup or subpopulation capable of producing metastasis. DLKP and its clones could, therefore, prove to be an invaluable model to study the efficacy of chemotherapy or monoclonal antibody therapies for lung cancer *in vivo*.

Bibliography

[1] Zellmer, V.,R.and Zhang, S., (2014), "Evolving concepts of tumor heterogeneity 2014**4**:69", *Cell & Bioscience,* Vol.4 (69),.

[2] Durrett, R., et al. (2011), "Intratumor heterogeneity in evolutionary models of tumor progression", *Genetics,* Vol.188 (2), pp. 461-477.

[3] Marusyk, A., Almendro, V.and Polyak, K., (2012), "Intra-tumour heterogeneity: a looking glass for cancer?", *Nat.Rev.Cancer.,* Vol.12 (5), pp. 323-334.

[4] Burrell, R.A., et al. (2013), "The causes and consequences of genetic heterogeneity in cancer evolution", *Nature,* Vol.501 (7467), pp. 338-345.

[5] Magee, J.A., Piskounova, E.and Morrison, S.J., (2012), "Cancer stem cells: impact, heterogeneity, and uncertainty", *Cancer.Cell.,* Vol.21 (3), pp. 283-296.

[6] Michor, F.and Polyak, K., (2010), "The origins and implications of intratumor heterogeneity", *Cancer.Prev.Res.(Phila),* Vol.3 (11), pp. 1361-1364.

[7] Fulawka, L., Donizy, P.and Halon, A., (2014), "Cancer stem cells--the current status of an old concept: literature review and clinical approaches", *Biol.Res.,* Vol.47 pp. 66-6287-47-66.

[8] Wang, A., et al. (2015), "Heterogeneity in cancer stem cells", *Cancer Lett.,* Vol.357 (1), pp. 63-68.

[9] Burrell, R.A.and Swanton, C., (2014), "The evolution of the unstable cancer genome", *Curr.Opin.Genet.Dev.,* Vol.24 pp. 61-67.

[10] Junttila, M.R.and de Sauvage, F.J., (2013), "Influence of tumour micro-environment heterogeneity on therapeutic response", *Nature,* Vol.501 (7467), pp. 346-354.

[11] Govindan, R. (2014), "Cancer. Attack of the clones", *Science,* Vol.346 (6206), pp. 169-170.

[12] Gatenby, R.A., Gillies, R.J.and Brown, J.S., (2010), "Evolutionary dynamics of cancer prevention", *Nat.Rev.Cancer.,* Vol.10 (8), pp. 526-527.

[13] Ahrendt, S.A., et al. (2003), "p53 mutations and survival in stage I non-small-cell lung cancer: results of a prospective study", *J.Natl.Cancer Inst.,* Vol.95 (13), pp. 961-970.

[14] Shen, Z. (2011), "Genomic instability and cancer: an introduction", *J.Mol.Cell.Biol.,* Vol.3 (1), pp. 1-3.

[15] Blair, B.G., Bardelli, A.and Park, B.H., (2014), "Somatic alterations as the basis for resistance to targeted therapies", *J.Pathol.,* Vol.232 (2), pp. 244-254.

[16] Ferguson, L.R., et al. (2015), "Genomic instability in human cancer: Molecular insights and opportunities for therapeutic attack and prevention through diet and nutrition", *Semin.Cancer Biol.,* Vol.35 Suppl pp. S5-24.

[17] Allison, K.H.and Sledge, G.W., (2014), "Heterogeneity and cancer", *Oncology (Williston Park),* Vol.28 (9), pp. 772-778.

[18] Wao, H., et al. (2013), "Survival of patients with non-small cell lung cancer without treatment: a systematic review and meta-analysis", *Syst.Rev.,* Vol.2 pp. 10-4053-2-10.

[19] Torre, L.A., et al. (2015), "Global cancer statistics, 2012", *CA Cancer.J.Clin.,* Vol.65 (2), pp. 87-108.

[20] Shames, D.S.and Wistuba, I.I., (2014), "The evolving genomic classification of lung cancer", *J.Pathol.,* Vol.232 (2), pp. 121-133.

[21] Staaf, J., et al. (2013), "Landscape of somatic allelic imbalances and copy number alterations in human lung carcinoma", *Int.J.Cancer,* Vol.132 (9), pp. 2020-2031.

[22] Furak, J., et al. (2003), "Bronchioloalveolar lung cancer: occurrence, surgical treatment and survival", *Eur.J.Cardiothorac.Surg.,* Vol.23 (5), pp. 818-823.

[23] Subramanian, J.and Govindan, R., (2007), "Lung cancer in never smokers: a review", *J.Clin.Oncol.,* Vol.25 (5), pp. 561-570.

[24] Ismail-Khan, R., et al. (2006), "Malignant pleural mesothelioma: a comprehensive review", *Cancer Control,* Vol.13 (4), pp. 255-263.

[25] Molina, J.R., et al. (2008), "Non-small cell lung cancer: epidemiology, risk factors, treatment, and survivorship", *Mayo Clin.Proc.,* Vol.83 (5), pp. 584-594.

[26] Vignot, S., et al. (2012), "Discrepancies between primary tumor and metastasis: a literature review on clinically established biomarkers", *Crit.Rev.Oncol.Hematol.,* Vol.84 (3), pp. 301-313.

[27] Govindan, R., et al. (2012), "Genomic landscape of non-small cell lung cancer in smokers and never-smokers", *Cell,* Vol.150 (6), pp. 1121-1134.

[28] Lee, H., et al. (2013), "A novel imidazopyridine PI3K inhibitor with anticancer activity in non-small cell lung cancer cells", *Oncol.Rep.,* Vol.30 (2), pp. 863-869.

[29] Ferrara, N., Hillan, K.J.and Novotny, W., (2005), "Bevacizumab (Avastin), a humanized anti-VEGF monoclonal antibody for cancer therapy", *Biochem.Biophys.Res.Commun.,* Vol.333 (2), pp. 328-335.

[30] Hsu, J.Y.and Wakelee, H.A., (2009), "Monoclonal antibodies targeting vascular endothelial growth factor: current status and future challenges in cancer therapy", *BioDrugs,* Vol.23 (5), pp. 289-304.

[31] Calbo, J., et al. (2011), "A functional role for tumor cell heterogeneity in a mouse model of small cell lung cancer", *Cancer.Cell.,* Vol.19 (2), pp. 244-256.

[32] Osann, K.E., Lowery, J.T.and Schell, M.J., (2000), "Small cell lung cancer in women: risk associated with smoking, prior respiratory disease, and occupation", *Lung Cancer,* Vol.28 (1), pp. 1-10.

[33] Cook, R.M., Miller, Y.E.and Bunn, P.A.,Jr., (1993), "Small cell lung cancer: etiology, biology, clinical features, staging, and treatment", *Curr.Probl.Cancer,* Vol.17 (2), pp. 69-141.

[34] Azim, H.A.,Jrand Ganti, A.K., (2007), "Treatment options for relapsed small-cell lung cancer", *Anticancer Drugs,* Vol.18 (3), pp. 255-261.

[35] Asai, N., et al. (2014), "Relapsed small cell lung cancer: treatment options and latest developments", *Ther.Adv.Med.Oncol.,* Vol.6 (2), pp. 69-82.

[36] Rosti, G., et al. (2006), "Small cell lung cancer", *Ann.Oncol.,* Vol.17 Suppl 2 pp. ii5-10.

[37] Travis, W.D. (2012), "Update on small cell carcinoma and its differentiation from squamous cell carcinoma and other non-small cell carcinomas", *Mod.Pathol.,* Vol.25 Suppl 1 pp. S18-30.

[38] Chong, S., et al. (2006), "Neuroendocrine tumors of the lung: clinical, pathologic, and imaging findings", *Radiographics,* Vol.26 (1), pp. 41-57; discussion 57-8.

[39] Wagner, P.L., et al. (2009), "Combined small cell lung carcinomas: genotypic and immunophenotypic analysis of the separate morphologic components", *Am.J.Clin.Pathol.,* Vol.131 (3), pp. 376-382.

[40] Petitjean, A., et al. (2007), "TP53 mutations in human cancers: functional selection and impact on cancer prognosis and outcomes", *Oncogene,* Vol.26 (15), pp. 2157-2165.

[41] Sermeus, A.and Michiels, C., (2011), "Reciprocal influence of the p53 and the hypoxic pathways", *Cell.Death Dis.,* Vol.2 pp. e164.

[42] Siegel, R.L., Miller, K.D.and Jemal, A., (2016), "Cancer statistics, 2016", *CA Cancer.J.Clin.,* Vol.66 (1), pp. 7-30.

[43] Lehmann, B.D., et al. (2011), "Identification of human triple-negative breast cancer subtypes and preclinical models for selection of targeted therapies", *J.Clin.Invest.,* Vol.121 (7), pp. 2750-2767.

[44] Inic, Z., et al. (2014), "Difference between Luminal A and Luminal B Subtypes According to Ki-67, Tumor Size, and Progesterone Receptor Negativity Providing Prognostic Information", *Clin.Med.Insights Oncol.,* Vol.8 pp. 107-111.

[45] Ford, C.H., et al. (2011), "Reassessment of estrogen receptor expression in human breast cancer cell lines", *Anticancer Res.,* Vol.31 (2), pp. 521-527.

[46] Catalanotti, V., et al. (2014), "Treatment of Advanced Breast Cancer (ABC): The Expanding Landscape of Targeted Therapies. ", *J Cancer Biol Res,* Vol.2 (1), pp. 1036.

[47] Brown-Glaberman, U., Dayao, Z.and Royce, M., (2014), "HER2-targeted therapy for early-stage breast cancer: a comprehensive review", *Oncology (Williston Park),* Vol.28 (4), pp. 281-289.

[48] Martinez, M.T., et al. (2016), "Treatment of HER2 positive advanced breast cancer with T-DM1: A review of the literature", *Crit.Rev.Oncol.Hematol.,* Vol.97 pp. 96-106.

[49] Boyraz, B., et al. (2013), "Trastuzumab emtansine (T-DM1) for HER2-positive breast cancer", *Curr.Med.Res.Opin.,* Vol.29 (4), pp. 405-414.

[50] Yardley, D.A., et al. (2015), "Trastuzumab Emtansine (T-DM1) in Patients With HER2-Positive Metastatic Breast Cancer Previously Treated With Chemotherapy and 2 or More HER2-Targeted Agents: Results From the T-PAS Expanded Access Study", *Cancer J.,* Vol.21 (5), pp. 357-364.

[51] Penault-Llorca, F.and Viale, G., (2012), "Pathological and molecular diagnosis of triple-negative breast cancer: a clinical perspective", *Ann.Oncol.,* Vol.23 Suppl 6 pp. vi19-22.

[52] Holliday, D.L.and Speirs, V., (2011), "Choosing the right cell line for breast cancer research", *Breast Cancer Res.,* Vol.13 (4), pp. 215.

[53] Granados-Principal, S., et al. (2015), "Inhibition of iNOS as a novel effective targeted therapy against triple-negative breast cancer", *Breast Cancer Res.,* Vol.17 pp. 25-015-0527-x.

[54] Wahba, H.A.and El-Hadaad, H.A., (2015), "Current approaches in treatment of triple-negative breast cancer", *Cancer.Biol.Med.,* Vol.12 (2), pp. 106-116.

[55] Nagini, S. (2016), "Breast Cancer: Current Molecular Therapeutic Targets and New Players", *Anticancer Agents Med.Chem.,* .

[56] Kramer, N., et al. (2013), "In vitro cell migration and invasion assays", *Mutat.Res.,* Vol.752 (1), pp. 10-24.

[57] Larue, L.and Bellacosa, A., (2005), "Epithelial-mesenchymal transition in development and cancer: role of phosphatidylinositol 3' kinase/AKT pathways", *Oncogene,* Vol.24 (50), pp. 7443-7454.

[58] Lamouille, S., Xu, J.and Derynck, R., (2014), "Molecular mechanisms of epithelial-mesenchymal transition", *Nat.Rev.Mol.Cell Biol.,* Vol.15 (3), pp. 178-196.

[59] Kalluri, R.and Weinberg, R.A., (2009), "The basics of epithelial-mesenchymal transition", *J.Clin.Invest.,* Vol.119 (6), pp. 1420-1428.

[60] Fidler, I.J. (2003), "The pathogenesis of cancer metastasis: the 'seed and soil' hypothesis revisited", *Nat.Rev.Cancer.,* Vol.3 (6), pp. 453-458.

[61] Perlikos, F., Harrington, K.J.and Syrigos, K.N., (2013), "Key molecular mechanisms in lung cancer invasion and metastasis: a comprehensive review", *Crit.Rev.Oncol.Hematol.,* Vol.87 (1), pp. 1-11.

[62] Alizadeh, A.M., Shiri, S.and Farsinejad, S., (2014), "Metastasis review: from bench to bedside", *Tumour Biol.,* Vol.35 (9), pp. 8483-8523.

[63] Wang, S.H.and Lin, S.Y., (2013), "Tumor dormancy: potential therapeutic target in tumor recurrence and metastasis prevention", *Exp.Hematol.Oncol.,* Vol.2 (1), pp. 29-3619-2-29.

[64] Yeh, A.C.and Ramaswamy, S., (2015), "Mechanisms of Cancer Cell Dormancy--Another Hallmark of Cancer?", *Cancer Res.,* Vol.75 (23), pp. 5014-5022.

[65] Aguirre-Ghiso, J.A. (2007), "Models, mechanisms and clinical evidence for cancer dormancy", *Nat.Rev.Cancer.,* Vol.7 (11), pp. 834-846.

[66] Sleeman, J.P., Nazarenko, I.and Thiele, W., (2011), "Do all roads lead to Rome? Routes to metastasis development", *Int.J.Cancer,* Vol.128 (11), pp. 2511-2526.

[67] Collado, M., Blasco, M.A.and Serrano, M., (2007), "Cellular senescence in cancer and aging", *Cell,* Vol.130 (2), pp. 223-233.

[68] Sosa, M.S., Bragado, P.and Aguirre-Ghiso, J.A., (2014), "Mechanisms of disseminated cancer cell dormancy: an awakening field", *Nat.Rev.Cancer.,* Vol.14 (9), pp. 611-622.

[69] Luo, J., Manning, B.D.and Cantley, L.C., (2003), "Targeting the PI3K-Akt pathway in human cancer: rationale and promise", *Cancer.Cell.,* Vol.4 (4), pp. 257-262.

[70] Vivanco, I.and Sawyers, C.L., (2002), "The phosphatidylinositol 3-Kinase AKT pathway in human cancer", *Nat.Rev.Cancer.,* Vol.2 (7), pp. 489-501.

[71] Gillet, J.P., Varma, S.and Gottesman, M.M., (2013), "The clinical relevance of cancer cell lines", *J.Natl.Cancer Inst.,* Vol.105 (7), pp. 452-458.

[72] Hahn, W.C.and Weinberg, R.A., (2002), "Modelling the molecular circuitry of cancer", *Nat.Rev.Cancer.,* Vol.2 (5), pp. 331-341.

[73] Cheon, D.J.and Orsulic, S., (2011), "Mouse models of cancer", *Annu.Rev.Pathol.,* Vol.6 pp. 95-119.

[74] Richmond, A.and Su, Y., (2008), "Mouse xenograft models vs GEM models for human cancer therapeutics", *Dis.Model.Mech.,* Vol.1 (2-3), pp. 78-82.

[75] Bosma, M., Schuler, W.and Bosma, G., (1988), "The scid mouse mutant", *Curr.Top.Microbiol.Immunol.,* Vol.137 pp. 197-202.

[76] Xie, X., et al. (1992), "Comparative studies between nude and scid mice on the growth and metastatic behavior of xenografted human tumors", *Clin.Exp.Metastasis,* Vol.10 (3), pp. 201-210.

[77] Chen, Z., et al. (2014), "Non-small-cell lung cancers: a heterogeneous set of diseases", *Nat.Rev.Cancer.,* Vol.14 (8), pp. 535-546.

[78] Corpet, D.E.and Pierre, F., (2003), "Point: From animal models to prevention of colon cancer. Systematic review of chemoprevention in min mice and choice of the model system", *Cancer Epidemiol.Biomarkers Prev.,* Vol.12 (5), pp. 391-400.

[79] White, R.D., Previte, S.and Olsson, C.A., (1978), "A new animal model for testing the effectiveness of chemotherapeutic agents on renal adenocarcinoma", *Surg.Forum,* Vol.29 pp. 629-631.

[80] Havens, A.M., et al. (2008), "An in vivo mouse model for human prostate cancer metastasis", *Neoplasia,* Vol.10 (4), pp. 371-380.

[81] Kwon, M.and Berns, A., (2013), "Mouse models for lung cancer", *Molecular Oncology,* Vol.7 (2), pp. 165-177.

[82] Meuwissen, R.and Berns, A., (2005), "Mouse models for human lung cancer", *Genes Dev.,* Vol.19 (6), pp. 643-664.

[83] O'Hagan, R.C.and Heyer, J., (2011), "KRAS Mouse Models: Modeling Cancer Harboring KRAS Mutations", *Genes Cancer.,* Vol.2 (3), pp. 335-343.

[84] Chu, P.C., et al. (2016), "Regulation of oncogenic KRAS signaling via a novel KRAS-integrin-linked kinase-hnRNPA1 regulatory loop in human pancreatic cancer cells", *Oncogene,* Vol.35 (30), pp. 3897-3908.

[85] Jackson, E.L., et al. (2005), "The differential effects of mutant p53 alleles on advanced murine lung cancer", *Cancer Res.,* Vol.65 (22), pp. 10280-10288.

[86] Oliver, T.G., et al. (2010), "Chronic cisplatin treatment promotes enhanced damage repair and tumor progression in a mouse model of lung cancer", *Genes Dev.,* Vol.24 (8), pp. 837-852.

[87] Singh, M., et al. (2010), "Assessing therapeutic responses in Kras mutant cancers using genetically engineered mouse models", *Nat.Biotechnol.,* Vol.28 (6), pp. 585-593.

[88] Martelotto, L.G., et al. (2014), "Breast cancer intra-tumor heterogeneity", *Breast Cancer Res.,* Vol.16 (3), pp. 210.

[89] Janku, F. (2014), "Tumor heterogeneity in the clinic: is it a real problem?", *Ther.Adv.Med.Oncol.,* Vol.6 (2), pp. 43-51.

[90] Zhang, J., et al. (2014), "Intratumor heterogeneity in localized lung adenocarcinomas delineated by multiregion sequencing", *Science,* Vol.346 (6206), pp. 256-259.

[91] Law, E., et al. (1992), "Cytogenetic comparison of two poorly differentiated human lung squamous cell carcinoma lines", *Cancer Genet.Cytogenet.,* Vol.59 (2), pp. 111-118.

[92] McBride, S., et al. (1998), "Human lung carcinoma cell line DLKP contains 3 distinct subpopulations with different growth and attachment properties", *Tumour Biol.,* Vol.19 (2), pp. 88-103.

[93] McBride, S. , (1995), "Characterisation of Clonal Variants in a Human Lung Carcinoma Cell Iine: Investigation into Control of Growth and Differentiation", Dublin City University,.

[94] McBride, S., et al. (1999), "Bromodeoxyuridine induces keratin protein synthesis at a posttranscriptional level in human lung tumour cell lines", *Differentiation,* Vol.64 (3), pp. 185-193.

[95] Keenan, J., et al. (2012), "Olfactomedin III expression contributes to anoikis-resistance in clonal variants of a human lung squamous carcinoma cell line", *Exp.Cell Res.,* Vol.318 (5), pp. 593-602.

[96] Joyce, H. , (2014), "Molecular mechanisms of drug resistance and invasion in a human lung carcinoma cell line", Dublin City University,.

[97] Keenan, J., et al. (2009), "Proteomic analysis of multidrug-resistance mechanisms in adriamycin-resistant variants of DLKP, a squamous lung cancer cell line", *Proteomics,* Vol.9 (6), pp. 1556-1566.

[98] Holland, A., et al. (2015), "Comparative Label-Free Mass Spectrometric Analysis of Mildly versus Severely Affected mdx Mouse Skeletal Muscles Identifies Annexin, Lamin, and Vimentin as Universal Dystrophic Markers", *Molecules,* Vol.20 (6), pp. 11317-11344.

[99] Linge, A., et al. (2014), "Identification and functional validation of RAD23B as a potential protein in human breast cancer progression", *J.Proteome Res.,* Vol.13 (7), pp. 3212-3222.

[100] Albini, A., et al. (1987), "A rapid in vitro assay for quantitating the invasive potential of tumor cells", *Cancer Res.,* Vol.47 (12), pp. 3239-3245.

[101] Roy Chaudhuri, T., et al. (2016), "Tumor-Priming Smoothened Inhibitor Enhances Deposition and Efficacy of Cytotoxic Nanoparticles in a Pancreatic Cancer Model", *Mol.Cancer.Ther.,* Vol.15 (1), pp. 84-93.

[102] Pawaskar, D.K., et al. (2013), "Physiologically based pharmacokinetic models for everolimus and sorafenib in mice", *Cancer Chemother.Pharmacol.,* Vol.71 (5), pp. 1219-1229.

[103] Ocak, S., et al. (2014), "Discovery of new membrane-associated proteins overexpressed in small-cell lung cancer", *J.Thorac.Oncol.,* Vol.9 (3), pp. 324-336.

[104] Liu, B., et al. (2014), "Alpha-internexin: a novel biomarker for pancreatic neuroendocrine tumor aggressiveness", *J.Clin.Endocrinol.Metab.,* pp. jc20132874.

[105] Abouzied, M.M., et al. (2005), "Hepatoma-derived growth factor. Significance of amino acid residues 81-100 in cell surface interaction and proliferative activity", *J.Biol.Chem.,* Vol.280 (12), pp. 10945-10954.

[106] Abouzied, M.M., et al. (2004), "Expression patterns and different subcellular localization of the growth factors HDGF (hepatoma-derived growth factor) and HRP-3 (HDGF-related protein-3) suggest functions in addition to their mitogenic activity", *Biochem.J.,* Vol.378 (Pt 1), pp. 169-176.

[107] Schmid, B.C., et al. (2007), "The neuronal guidance cue Slit2 induces targeted migration and may play a role in brain metastasis of breast cancer cells", *Breast Cancer Res.Treat.,* Vol.106 (3), pp. 333-342.

[108] Chang, P.H., et al. (2012), "Activation of Robo1 signaling of breast cancer cells by Slit2 from stromal fibroblast restrains tumorigenesis via blocking PI3K/Akt/beta-catenin pathway", *Cancer Res.,* Vol.72 (18), pp. 4652-4661.

[109] Ikeda, K.and Quertermous, T., (2004), "Molecular isolation and characterization of a soluble isoform of activated leukocyte cell adhesion molecule that modulates endothelial cell function", *J.Biol.Chem.,* Vol.279 (53), pp. 55315-55323.

[110] Miyata, T., et al. (2015), "Cancer stem cell markers in lung cancer", *Personalized Medicine Universe,* Vol.4 pp. 40-45.

[111] Jadeski, L., et al. (2008), "IQGAP1 stimulates proliferation and enhances tumorigenesis of human breast epithelial cells", *J.Biol.Chem.,* Vol.283 (2), pp. 1008-1017.

[112] Jannie, K. , (2012), "Activated leukocyte cell adhesion molecule (ALCAM) regulation of tumour cell behavior and neuronal targeting", University of Iowa,.

[113] Suh, J.H., Park, C.K.and Park, S.H., (2013), "Alpha internexin expression related with molecular characteristics in adult glioblastoma and oligodendroglioma", *J.Korean Med.Sci.,* Vol.28 (4), pp. 593-601.

[114] Munagala, R., Aqil, F.and Gupta, R.C., (2011), "Promising molecular targeted therapies in breast cancer", *Indian.J.Pharmacol.,* Vol.43 (3), pp. 236-245.

[115] Polyak, K. (2011), "Heterogeneity in breast cancer", *J.Clin.Invest.,* Vol.121 (10), pp. 3786-3788.

[116] Longo, R., Torino, F.and Gasparini, G., (2007), "Targeted therapy of breast cancer", *Curr.Pharm.Des.,* Vol.13 (5), pp. 497-517.

[117] Madden, S.F., et al. (2013), "BreastMark: an integrated approach to mining publicly available transcriptomic datasets relating to breast cancer outcome", *Breast Cancer Res.,* Vol.15 (4), pp. R52.

[118] Mizushima, N. (2007), "Autophagy: process and function", *Genes Dev.,* Vol.21 (22), pp. 2861-2873.

[119] Scholzen, T.and Gerdes, J., (2000), "The Ki-67 protein: from the known and the unknown", *J.Cell.Physiol.,* Vol.182 (3), pp. 311-322.

[120] Pusztaszeri, M.P., Seelentag, W.and Bosman, F.T., (2006), "Immunohistochemical expression of endothelial markers CD31, CD34, von Willebrand factor, and Fli-1 in normal human tissues", *J.Histochem.Cytochem.,* Vol.54 (4), pp. 385-395.

[121] Maeda, M., Johnson, K.R.and Wheelock, M.J., (2005), "Cadherin switching: essential for behavioral but not morphological changes during an epithelium-to-mesenchyme transition", *J.Cell.Sci.,* Vol.118 (Pt 5), pp. 873-887.

[122] Tachezy, M., et al. (2014), "Activated Leukocyte Cell Adhesion Molecule (CD166): An "Inert" Cancer Stem Cell Marker for Non-Small Cell Lung Cancer?", *Stem Cells,* Vol.32 (6), pp. 1429-1436.

[123] Zakaria, N., et al. (2015), "Human non-small cell lung cancer expresses putative cancer stem cell markers and exhibits the transcriptomic profile of multipotent cells", *BMC Cancer,* Vol.15 pp. 84-015-1086-3.

[124] Doyle, L.A., et al. (1989), "Differentiation of human variant small cell lung cancer cell lines to a classic morphology by retinoic acid", *Cancer Res.,* Vol.49 (23), pp. 6745-6751.

[125] Paoli, P., Giannoni, E.and Chiarugi, P., (2013), "Anoikis molecular pathways and its role in cancer progression", *Biochim.Biophys.Acta,* Vol.1833 (12), pp. 3481-3498.

[126] Guadamillas, M.C., Cerezo, A.and Del Pozo, M.A., (2011), "Overcoming anoikis--pathways to anchorage-independent growth in cancer", *J.Cell.Sci.,* Vol.124 (Pt 19), pp. 3189-3197.

[127] Kim, Y.N., et al. (2012), "Anoikis resistance: an essential prerequisite for tumor metastasis", *Int.J.Cell.Biol.,* Vol.2012 pp. 306879.

[128] Masoumi Moghaddam, S., et al. (2012), "Significance of vascular endothelial growth factor in growth and peritoneal dissemination of ovarian cancer", *Cancer Metastasis Rev.,* Vol.31 (1-2), pp. 143-162.

[129] Uekita, T., et al. (2008), "CUB-domain-containing protein 1 regulates peritoneal dissemination of gastric scirrhous carcinoma", *Am.J.Pathol.,* Vol.172 (6), pp. 1729-1739.

[130] Frisch, S.M.and Ruoslahti, E., (1997), "Integrins and anoikis", *Curr.Opin.Cell Biol.,* Vol.9 (5), pp. 701-706.

[131] Frisch, S.M.and Screaton, R.A., (2001), "Anoikis mechanisms", *Curr.Opin.Cell Biol.,* Vol.13 (5), pp. 555-562.

[132] Nisato, R.E., et al. (2005), "Dissecting the role of matrix metalloproteinases (MMP) and integrin alpha(v)beta3 in angiogenesis in vitro: absence of hemopexin C domain bioactivity, but membrane-Type 1-MMP and alpha(v)beta3 are critical", *Cancer Res.,* Vol.65 (20), pp. 9377-9387.

[133] Rundhaug, J.E. (2003), "Matrix metalloproteinases, angiogenesis, and cancer: commentary re: A. C. Lockhart et al., Reduction of wound angiogenesis in patients treated with BMS-275291, a broad spectrum matrix metalloproteinase inhibitor. Clin. Cancer Res., 9: 00-00, 2003", *Clin.Cancer Res.,* Vol.9 (2), pp. 551-554.

[134] Dumitru, C.A., et al. (2013), "AHNAK and Inflammatory Markers Predict Poor Survival in Laryngeal Carcinoma", *PLoS One,* Vol.8 (2), pp. e56420. doi:10.1371/journal.pone.0056420.

[135] Hashimoto, T., et al. (1995), "Regulation of translocation of the desmoyokin/AHNAK protein to the plasma membrane in keratinocytes by protein kinase C", *Exp.Cell Res.,* Vol.217 (2), pp. 258-266.

[136] Shtivelman, E.and Bishop, J.M., (1993), "The human gene AHNAK encodes a large phosphoprotein located primarily in the nucleus", *J.Cell Biol.,* Vol.120 (3), pp. 625-630.

[137] Lattanzio, R., Piantelli, M.and Falasca, M., (2013), "Role of phospholipase C in cell invasion and metastasis", *Adv.Biol.Regul.,* Vol.53 (3), pp. 309-318.

[138] Wells,Alanand Grandis,JenniferRubin., (2003), "Phospholipase C-Î³1 in tumor progression", *Clinical & Experimental Metastasis,* Vol.20 (4), pp. 285-290.

[139] Sudo, H., et al. (2014), "AHNAK is highly expressed and plays a key role in cell migration and invasion in mesothelioma", *Int.J.Oncol.,* Vol.44 (2), pp. 530-538.

[140] Hsu, Y.C., et al. (2013), "Genome-wide analysis of three-way interplay among gene expression, cancer cell invasion and anti-cancer compound sensitivity", *BMC Med.,* Vol.11 pp. 106-7015-11-106.

[141] Lee, I.H., et al. (2014), "Ahnak functions as a tumor suppressor via modulation of TGFbeta/Smad signaling pathway", *Oncogene,* Vol.33 (38), pp. 4675-4684.

[142] Kishima, Y., et al. (2002), "Hepatoma-derived growth factor stimulates cell growth after translocation to the nucleus by nuclear localization signals", *J.Biol.Chem.,* Vol.277 (12), pp. 10315-10322.

[143] Meng, J., et al. (2010), "shRNA targeting HDGF suppressed cell growth and invasion of squamous cell lung cancer", *Acta Biochim.Biophys.Sin.(Shanghai),* Vol.42 (1), pp. 52-57.

[144] Zhang, J., et al. (2006), "Down-regulation of hepatoma-derived growth factor inhibits anchorage-independent growth and invasion of non-small cell lung cancer cells", *Cancer Res.,* Vol.66 (1), pp. 18-23.

[145] Guo, H., et al. (2014), "MiR-195 targets HDGF to inhibit proliferation and invasion of NSCLC cells", *Tumour Biol.,* Vol.35 (9), pp. 8861-8866.

[146] Enomoto, H., et al. (2015), "Hepatoma-Derived Growth Factor: Its Possible Involvement in the Progression of Hepatocellular Carcinoma", *Int.J.Mol.Sci.,* Vol.16 (6), pp. 14086-14097.

[147] Uyama, H., et al. (2006), "Hepatoma-Derived Growth Factor Is a Novel Prognostic Factor for Patients with Pancreatic Cancer", *Clinical Cancer Research,* Vol.12 (20), pp. 6043-6048.

[148] Prasad, A., et al. (2008), "Slit-2 induces a tumor-suppressive effect by regulating beta-catenin in breast cancer cells", *J.Biol.Chem.,* Vol.283 (39), pp. 26624-26633.

[149] Yiin, J., et al. (2009), "Slit2 inhibits glioma cell invasion in the brain by suppression of Cdc42 activity", *Neuro-oncology,* Vol.11 (6), pp. 779-789.

[150] Tseng, R.C., et al. (2010), "SLIT2 attenuation during lung cancer progression deregulates beta-catenin and E-cadherin and associates with poor prognosis", *Cancer Res.,* Vol.70 (2), pp. 543-551.

[151] Hayashi, H., et al. (2010), "Overexpression of IQGAP1 in advanced colorectal cancer correlates with poor prognosis-critical role in tumor invasion", *Int.J.Cancer*, Vol.126 (11), pp. 2563-2574.

[152] Tanos, B.E., et al. (2015), "IQGAP1 controls tight junction formation through differential regulation of claudin recruitment", *J.Cell.Sci.*, Vol.128 (5), pp. 853-862.

[153] Zhao, H., et al. (2014), "Coexpression of IQ-domain GTPase-activating protein 1 (IQGAP1) and Dishevelled (Dvl) is correlated with poor prognosis in non-small cell lung cancer", *PLoS One*, Vol.9 (12), pp. e113713.

[154] Jameson, K.L., et al. (2013), "IQGAP1 scaffold-kinase interaction blockade selectively targets RAS-MAP kinase-driven tumors", *Nat.Med.*, Vol.19 (5), pp. 626-630.

[155] Minner, S., et al. (2011), "Low activated leukocyte cell adhesion molecule expression is associated with advanced tumor stage and early prostate-specific antigen relapse in prostate cancer", *Hum.Pathol.*, Vol.42 (12), pp. 1946-1952.

[156] Bowen, M.A., et al. (1995), "Cloning, mapping, and characterization of activated leukocyte-cell adhesion molecule (ALCAM), a CD6 ligand", *J.Exp.Med.*, Vol.181 (6), pp. 2213-2220.

[157] Kahlert, C., et al. (2009), "Increased expression of ALCAM/CD166 in pancreatic cancer is an independent prognostic marker for poor survival and early tumour relapse", *Br.J.Cancer*, Vol.101 (3), pp. 457-464.

[158] Weichert, W., et al. (2004), "ALCAM/CD166 is overexpressed in colorectal carcinoma and correlates with shortened patient survival", *J.Clin.Pathol.*, Vol.57 (11), pp. 1160-1164.

[159] Burkhardt, M., et al. (2006), "Cytoplasmic overexpression of ALCAM is prognostic of disease progression in breast cancer", *J.Clin.Pathol.*, Vol.59 (4), pp. 403-409.

[160] Horst, D., et al. (2009), "Prognostic significance of the cancer stem cell markers CD133, CD44, and CD166 in colorectal cancer", *Cancer Invest.*, Vol.27 (8), pp. 844-850.

[161] Weidle, U.H., et al. (2010), "ALCAM/CD166: cancer-related issues", *Cancer.Genomics Proteomics*, Vol.7 (5), pp. 231-243.

[162] van Kilsdonk, J.W., et al. (2008), "Attenuation of melanoma invasion by a secreted variant of activated leukocyte cell adhesion molecule", *Cancer Res.*, Vol.68 (10), pp. 3671-3679.

[163] Kijima, N., et al. (2012), "CD166/activated leukocyte cell adhesion molecule is expressed on glioblastoma progenitor cells and involved in the regulation of tumor cell invasion", *Neuro Oncol.*, Vol.14 (10), pp. 1254-1264.

[164] Jezierska, A., et al. (2006), "Activated Leukocyte Cell Adhesion Molecule (ALCAM) is associated with suppression of breast cancer cells invasion", *Med.Sci.Monit.*, Vol.12 (7), pp. BR245-56.

[165] Ishiguro, F., et al. (2013), "Membranous expression of activated leukocyte cell adhesion molecule contributes to poor prognosis and malignant phenotypes of non-small-cell lung cancer", *J.Surg.Res.*, Vol.179 (1), pp. 24-32.

[166] Durand, K., et al. (2011), "Alpha-internexin expression in gliomas: relationship with histological type and 1p, 19q, 10p and 10q status", *J.Clin.Pathol.*, Vol.64 (9), pp. 793-801.

[167] Mokhtari, K., et al. (2011), "Alpha-internexin expression predicts outcome in anaplastic oligodendroglial tumors and may positively impact the efficacy of chemotherapy: European organization for research and treatment of cancer trial 26951", *Cancer*, Vol.117 (13), pp. 3014-3026.

[168] Kaya, B., et al. (2003), "Alpha-internexin expression in medulloblastomas and atypical teratoid-rhabdoid tumors", *Clin.Neuropathol.*, Vol.22 (5), pp. 215-221.

[169] Ducray, F., et al. (2011), "Diagnostic and prognostic value of alpha internexin expression in a series of 409 gliomas", *Eur.J.Cancer*, Vol.47 (5), pp. 802-808.

[170] Fliegner, K.H., et al. (1994), "Expression of the gene for the neuronal intermediate filament protein α-internexin coincides with the onset of neuronal differentiation in the developing rat nervous system ", *J.Comp.Neurol.*, Vol.342 (2), pp. 161-173.

[171] Walker, C.and Wright-Perkins, S., (1992), "Expression of neuroendocrine and epithelial markers in an adherent subline derived from a classic small cell lung cancer cell line", *Oncol.Res.*, Vol.4 (10), pp. 419-429.

[172] Schimmack, S., et al. (2012), "The clinical implications and biologic relevance of neurofilament expression in gastroenteropancreatic neuroendocrine neoplasms", *Cancer*, Vol.118 (10), pp. 2763-2775.

[173] Thony, B.and Blau, N., (2006), "Mutations in the BH4-metabolizing genes GTP cyclohydrolase I, 6-pyruvoyl-tetrahydropterin synthase, sepiapterin reductase, carbinolamine-4a-dehydratase, and dihydropteridine reductase", *Hum.Mutat.*, Vol.27 (9), pp. 870-878.

[174] Bonafe, L., et al. (2001), "Mutations in the sepiapterin reductase gene cause a novel tetrahydrobiopterin-dependent monoamine-neurotransmitter deficiency without hyperphenylalaninemia", *Am.J.Hum.Genet.*, Vol.69 (2), pp. 269-277.

[175] Friedman, J., et al. (2012), "Sepiapterin reductase deficiency: a treatable mimic of cerebral palsy", *Ann.Neurol.*, Vol.71 (4), pp. 520-530.

[176] Yang, S., et al. (2013), "Sepiapterin reductase mediates chemical redox cycling in lung epithelial cells", *J.Biol.Chem.*, Vol.288 (26), pp. 19221-19237.

[177] Auerbach, G., et al. (1997), "The 1.25 A crystal structure of sepiapterin reductase reveals its binding mode to pterins and brain neurotransmitters", *EMBO J.*, Vol.16 (24), pp. 7219-7230.

[178] Yang, S., et al. (2006), "A murine model for human sepiapterin-reductase deficiency", *Am.J.Hum.Genet.*, Vol.78 (4), pp. 575-587.

[179] Pierce, G.L. (2013), "Oral BH4: A novel remedy for age-related skin microvascular impairment during heat stress or fool's elixir?", *J.Appl.Physiol.*, Vol.115 (7), pp. 951-953.

[180] Lange, I., et al. (2014), "Novel interaction of ornithine decarboxylase with sepiapterin reductase regulates neuroblastoma cell proliferation", *J.Mol.Biol.*, Vol.426 (2), pp. 332-346.

[181] Cho, Y.R., et al. (2011), "Sepiapterin inhibits cell proliferation and migration of ovarian cancer cells via down-regulation of p70S6K-dependent VEGFR-2 expression", *Oncol.Rep.*, Vol.26 (4), pp. 861-867.

[182] Cho,Young-Rak, Choi,ShinWookand Seo,Dong-Wan., (2011), "Sepiapterin regulates cell proliferation and migration: its association with integrin Î±3Î²1 and p53 in human lung cancer cells", *Genes & Genomics*, (33), pp. 577-582.

[183] Kim, Y., et al. (2014), "Comparative proteomic profiling of pancreatic ductal adenocarcinoma cell lines", *Mol.Cells*, Vol.37 (12), pp. 888-898.

[184] Airley, R.E., et al. (2003), "GLUT-1 and CAIX as intrinsic markers of hypoxia in carcinoma of the cervix: relationship to pimonidazole binding", *Int.J.Cancer*, Vol.104 (1), pp. 85-91.

[185] Guan, X. (2015), "Cancer metastases: challenges and opportunities", *Acta Pharm.Sin.B.*, Vol.5 (5), pp. 402-418.

[186] Wilson, W.R.and Hay, M.P., (2011), "Targeting hypoxia in cancer therapy", *Nat.Rev.Cancer.*, Vol.11 (6), pp. 393-410.

[187] Liou, G.Y.and Storz, P., (2010), "Reactive oxygen species in cancer", *Free Radic.Res.*, Vol.44 (5), pp. 10.3109/10715761003667554. doi:10.3109/10715761003667554.

[188] Waris, G.and Ahsan, H., (2006), "Reactive oxygen species: role in the development of cancer and various chronic conditions", *J.Carcinog.*, Vol.5 pp. 14-3163-5-14.

[189] Koomoa, D.L.T., et al. (2008), "Ornithine Decarboxylase Inhibition by DFMO Activates Opposing Signaling Pathways via Phosphorylation of both Akt/PKB and p27(Kip1) in Neuroblastoma", *Cancer Res.*, Vol.68 (23), pp. 9825-9831.

[190] Heinecke, J.L., et al. (2014), "Tumor microenvironment-based feed-forward regulation of NOS2 in breast cancer progression", *Proc.Natl.Acad.Sci.U.S.A.*, Vol.111 (17), pp. 6323-6328.

[191] Wu, D., et al. (2015), "Structural basis of Ornithine Decarboxylase inactivation and accelerated degradation by polyamine sensor Antizyme1", *Sci.Rep.*, Vol.5 pp. 14738.

[192] Zhang, Y., et al. (2005), "Antitumor effect of antisense ODC adenovirus on human prostate cancer cells", *Prostate Cancer.Prostatic Dis.*, Vol.8 (3), pp. 280-286.

[193] Scholzen, T.and Gerdes, J., (2000), "The Ki-67 protein: from the known and the unknown", *J.Cell.Physiol.,* Vol.182 (3), pp. 311-322.

[194] Urruticoechea, A., Smith, I.E.and Dowsett, M., (2005), "Proliferation marker Ki-67 in early breast cancer", *J.Clin.Oncol.,* Vol.23 (28), pp. 7212-7220.

[195] Glehen, O., Mohamed, F.and Gilly, F.N., (2004), "Peritoneal carcinomatosis from digestive tract cancer: new management by cytoreductive surgery and intraperitoneal chemohyperthermia", *Lancet Oncol.,* Vol.5 (4), pp. 219-228.

[196] Majchrzak, K., et al. (2013), "Markers of angiogenesis (CD31, CD34, rCBV) and their prognostic value in low-grade gliomas", *Neurol.Neurochir.Pol.,* Vol.47 (4), pp. 325-331.

[197] Salva, K.A., et al. (2014), "Expression of CD31/PECAM-1 (platelet endothelial cell adhesion molecule 1) by blastic plasmacytoid dendritic cell neoplasms", *JAMA Dermatol.,* Vol.150 (1), pp. 73-76.

[198] Paoli, P., Giannoni, E.and Chiarugi, P., (2013), "Anoikis molecular pathways and its role in cancer progression", *Biochimica et Biophysica Acta (BBA) - Molecular Cell Research,* Vol.1833 (12), pp. 3481-3498.

[199] Liotta, L.A.and Kohn, E., (2004), "Anoikis: cancer and the homeless cell", *Nature,* Vol.430 (7003), pp. 973-974.

[200] Perlikos, F., Harrington, K.J.and Syrigos, K.N., (2013), "Key molecular mechanisms in lung cancer invasion and metastasis: A comprehensive review", *Crit.Rev.Oncol.,* Vol.87 (1), pp. 1-11.

[201] Taddei, M.L., et al. (2012), "Anoikis: an emerging hallmark in health and diseases", *J.Pathol.,* Vol.226 (2), pp. 380-393.

[202] Jessani, N., et al. (2005), "Breast cancer cell lines grown in vivo: what goes in isn't always the same as what comes out", *Cell.Cycle,* Vol.4 (2), pp. 253-255.

[203] Ishimine, H., et al. (2013), "N-Cadherin is a prospective cell surface marker of human mesenchymal stem cells that have high ability for cardiomyocyte differentiation", *Biochem.Biophys.Res.Commun.,* Vol.438 (4), pp. 753-759.

[204] Kallergi, G., et al. (2011), "Epithelial to mesenchymal transition markers expressed in circulating tumour cells of early and metastatic breast cancer patients", *Breast Cancer Res.,* Vol.13 (3), pp. R59.

[205] Tsuji, T., Ibaragi, S.and Hu, G.F., (2009), "Epithelial-mesenchymal transition and cell cooperativity in metastasis", *Cancer Res.,* Vol.69 (18), pp. 7135-7139.

[206] Fujiwara, K., et al. (2014), "CD166/ALCAM expression is characteristic of tumorigenicity and invasive and migratory activities of pancreatic cancer cells", *PLoS One,* Vol.9 (9), pp. e107247.

Appendix

Appendix 1.1

Comparative proteomic analysis: DLKP *vs.* DLKPSQ

Description	Accession	Anova (p)	Max fold change
Roundabout homolog 2	Q9HCK4	2.51E-02	56.88
Intercellular adhesion molecule 1	P05362	1.40E-02	56.16
Catenin alpha-1	P35221	9.23E-03	30.84
Fumarylacetoacetase	P16930	4.53E-03	19.87
Fascin	Q16658	1.41E-03	14.08
Catenin beta-1	P35222	1.98E-02	12.58
Cathepsin Z	Q9UBR2	1.60E-03	6.85
Neutral cholesterol ester hydrolase 1	Q6PIU2	4.15E-03	6.39
Neuroblast differentiation-associated protein AHNAK	Q09666	1.02E-02	5.00
D-3-phosphoglycerate dehydrogenase	O43175	1.43E-03	4.52
Serpin H1	P50454	2.14E-04	4.21
Shootin-1	A0MZ66	2.49E-04	3.87
Procollagen galactosyltransferase 1	Q8NBJ5	1.40E-03	3.31
Hydroxymethylglutaryl-CoA synthase, cytoplasmic	Q01581	1.57E-03	3.10
Protein CutA	O60888	1.46E-04	2.59
Melanoma-associated antigen 4	P43358	5.30E-03	2.44
RNA-binding protein 14	Q96PK6	2.29E-02	2.40
Myosin-9	P35579	9.02E-03	2.33
GDP-fucose protein O-fucosyltransferase 1	Q9H488	1.46E-02	2.33
Microtubule-associated protein 2	P11137	2.22E-02	2.24
Nucleolar RNA helicase 2	Q9NR30	6.24E-03	2.24
Non-POU domain-containing octamer-binding protein	Q15233	1.11E-02	2.21
Transcription intermediary factor 1-beta	Q13263	7.40E-03	2.15
Barrier-to-autointegration factor	O75531	3.05E-02	2.15
Glucose-6-phosphate isomerase	P06744	2.94E-02	2.12
Protein disulfide-isomerase A6	Q15084	1.79E-02	2.06
Leucine-rich PPR motif-containing protein, mitochondrial	P42704	2.49E-02	2.05
Protein disulfide-isomerase	P07237	1.42E-02	2.04
Tubulin beta-6 chain	Q9BUF5	3.23E-03	2.01
X-ray repair cross-complementing protein 5	P13010	3.60E-02	1.97
Filamin-A	P21333	5.35E-03	1.97
Importin-5	O00410	1.33E-02	1.96
Elongation factor 1-gamma	P26641	5.09E-03	1.87
Endoplasmin	P14625	1.33E-03	1.81
Peroxiredoxin-1	Q06830	5.97E-03	1.75
Neutral alpha-glucosidase AB	Q14697	1.00E-02	1.74
Ras GTPase-activating-like protein IQGAP1	P46940	2.32E-02	1.73
Endoplasmic reticulum resident protein 29	P30040	1.66E-04	1.72
Exportin-2	P55060	7.60E-03	1.71
78 kDa glucose-regulated protein	P11021	7.71E-04	1.71
Kinectin	Q86UP2	3.73E-03	1.68
Calponin-3	Q15417	1.20E-02	1.65
Glyceraldehyde-3-phosphate dehydrogenase	P04406	1.37E-02	1.62
Far upstream element-binding protein 1	Q96AE4	8.71E-03	1.58
Fatty acid synthase	P49327	2.49E-03	1.56

Talin-1	Q9Y490	1.99E-02	1.56
Membrane-associated progesterone receptor component 1	O00264	3.16E-02	1.54
ATP-dependent RNA helicase A	Q08211	1.34E-02	1.54
Peroxiredoxin-6	P30041	9.64E-03	1.54

Appendix 1.2

Comparative proteomic analysis: DLKP *vs.* DLKPI

Description	Accession	Anova (p)	Max fold change
Chondroitin sulfate proteoglycan 4	Q6UVK1	1.65E-02	82.94
Intercellular adhesion molecule 1	P05362	1.18E-02	55.65
Receptor-type tyrosine-protein phosphatase C	P08575	1.52E-02	37.62
Peroxiredoxin-2	P32119	4.59E-04	31.26
CD166 antigen	Q13740	3.79E-02	18.80
Collagen alpha-1(XIV) chain	Q05707	1.58E-02	15.61
Cathepsin Z	Q9UBR2	4.18E-03	9.26
Prohibitin	P35232	1.15E-02	7.71
Prohibitin-2	Q99623	1.28E-02	7.64
Ras GTPase-activating-like protein IQGAP1	P46940	1.78E-03	7.61
Filamin-B	O75369	2.19E-02	7.44
Ras-related protein Ral-A	P11233	1.21E-02	6.55
Prelamin-A/C	P02545	2.12E-02	5.75
Neuroblast differentiation-associated protein AHNAK	Q09666	7.38E-04	5.55
Tubulin-specific chaperone A	O75347	6.18E-03	5.34
Ran-specific GTPase-activating protein	P43487	1.06E-03	5.21
Creatine kinase B-type	P12277	2.80E-03	4.63
Extended synaptotagmin-1	Q9BSJ8	4.04E-02	4.61
Filamin-A	P21333	1.38E-02	4.59
PDZ and LIM domain protein 5	Q96HC4	7.21E-03	4.55
Exportin-2	P55060	6.62E-03	4.48
Aconitate hydratase, mitochondrial	Q99798	5.66E-03	4.00
ATP synthase subunit d, mitochondrial	O75947	2.92E-03	3.81
Prosaposin	P07602	6.87E-03	3.63
Lamin-B1	P20700	1.57E-04	3.57
Superoxide dismutase [Cu-Zn]	P00441	2.74E-03	3.57
Eukaryotic initiation factor 4A-II	Q14240	1.22E-03	3.53
Alpha-aminoadipic semialdehyde dehydrogenase	P49419	7.26E-04	3.48
Glutathione S-transferase P	P09211	5.78E-03	3.43
Calponin-3	Q15417	4.24E-02	3.42
Macrophage migration inhibitory factor	P14174	1.13E-03	3.41
Annexin A2	P07355	9.00E-03	3.30
Glutathione reductase, mitochondrial	P00390	5.35E-03	3.30
Heat shock protein beta-1	P04792	5.91E-04	3.25
Pirin	O00625	3.21E-02	3.18
Cystatin-B	P04080	3.49E-02	3.10
Vimentin	P08670	1.53E-02	3.09
Calnexin	P27824	2.49E-02	3.07
Lamina-associated polypeptide 2, isoform alpha	P42166	2.73E-04	3.05
Serpin H1	P50454	1.78E-03	3.03
Spectrin beta chain, non-erythrocytic 1	Q01082	2.00E-02	2.94
Chloride intracellular channel protein 1	O00299	1.05E-02	2.93
GDP-fucose protein O-fucosyltransferase 1	Q9H488	4.07E-03	2.91
Enoyl-CoA delta isomerase 1, mitochondrial	P42126	3.37E-03	2.90
Calreticulin	P27797	1.48E-03	2.88
Actin, cytoplasmic 1	P60709	1.97E-02	2.83

Spectrin alpha chain, non-erythrocytic 1	Q13813	2.65E-02	2.78
Platelet-activating factor acetylhydrolase IB subunit gamma	Q15102	3.17E-03	2.75
Thioredoxin-dependent peroxide reductase, mitochondrial	P30048	9.13E-03	2.75
Heat shock protein 105 kDa	Q92598	7.11E-03	2.73
Thioredoxin domain-containing protein 12	O95881	1.51E-02	2.68
Band 4.1-like protein 2	O43491	1.70E-03	2.68
Ubiquitin-conjugating enzyme E2 variant 1	Q13404	2.18E-02	2.66
Crk-like protein	P46109	2.06E-03	2.64
6-phosphogluconate dehydrogenase, decarboxylating	P52209	5.00E-03	2.60
Triosephosphate isomerase	P60174	1.47E-02	2.59
ADP/ATP translocase 2	P05141	9.57E-03	2.58
Phosphoglycerate kinase 1	P00558	4.28E-03	2.57
ATP synthase subunit O, mitochondrial	P48047	9.10E-03	2.57
X-ray repair cross-complementing protein 5	P13010	3.30E-03	2.57
Thioredoxin domain-containing protein 5	Q8NBS9	4.01E-02	2.56
Histone H4	P62805	2.06E-02	2.56
Leucine-rich repeat-containing protein 59	Q96AG4	1.59E-02	2.51
Rho GDP-dissociation inhibitor 1	P52565	4.65E-03	2.50
Neutral alpha-glucosidase AB	Q14697	6.76E-03	2.44
Nuclear autoantigenic sperm protein	P49321	4.16E-03	2.38
Nucleoside diphosphate kinase A	P15531	5.95E-03	2.37
Ataxin-10	Q9UBB4	6.54E-03	2.34
Leucine-rich PPR motif-containing protein, mitochondrial	P42704	1.35E-02	2.34
Fatty acid synthase	P49327	3.28E-02	2.30
Cytosolic acyl coenzyme A thioester hydrolase	O00154	8.01E-03	2.30
Fumarate hydratase, mitochondrial	P07954	4.22E-03	2.27
DNA-dependent protein kinase catalytic subunit	P78527	4.32E-02	2.27
Myosin-11	P35749	8.06E-03	2.25
Nucleophosmin	P06748	8.09E-03	2.21
Electron transfer flavoprotein subunit alpha, mitochondrial	P13804	3.05E-02	2.19
Hepatoma-derived growth factor	P51858	3.02E-02	2.19
L-lactate dehydrogenase B chain	P07195	8.46E-04	2.18
Puromycin-sensitive aminopeptidase	P55786	6.70E-03	2.13
ATP synthase subunit alpha, mitochondrial	P25705	6.55E-03	2.13
Transitional endoplasmic reticulum ATPase	P55072	1.76E-02	2.10
Putative nucleoside diphosphate kinase	O60361	1.24E-02	2.08
Phosphoglycerate mutase 1	P18669	7.31E-03	2.07
ATP synthase subunit beta, mitochondrial	P06576	1.07E-02	2.04
10 kDa heat shock protein, mitochondrial	P61604	2.17E-02	2.04
60 kDa heat shock protein, mitochondrial	P10809	9.79E-03	2.04
Transaldolase	P37837	7.76E-03	2.03
Ubiquitin carboxyl-terminal hydrolase isozyme L1	P09936	9.89E-03	2.03
ATP-dependent RNA helicase A	Q08211	8.30E-03	2.01
Glucose-6-phosphate isomerase	P06744	5.91E-03	1.98
Malate dehydrogenase, cytoplasmic	P40925	1.11E-02	1.94

Heat shock protein HSP 90-beta	P08238; Q58FF8; Q58FG1	1.11E-02	1.94
Ubiquitin-like modifier-activating enzyme 1	P22314	3.68E-02	1.93
Myosin-9	P35579	1.44E-03	1.93
Aspartate aminotransferase, mitochondrial	P00505	4.33E-03	1.90
Polypyrimidine tract-binding protein 1	P26599; Q9UKA9	1.43E-02	1.88
Annexin A1	P04083	3.37E-02	1.88
Actin-related protein 3	P61158	4.77E-03	1.86
Protein disulfide-isomerase A6	Q15084	6.06E-03	1.86
Adenosylhomocysteinase	P23526	2.50E-02	1.85
Heterogeneous nuclear ribonucleoprotein H	P31943	9.34E-04	1.82
Tumor protein D52	P55327	1.60E-02	1.81
Rab GDP dissociation inhibitor beta	P50395	3.65E-03	1.78
Microtubule-associated protein 2	P11137	1.14E-02	1.77
Peptidyl-prolyl cis-trans isomerase A	P62937	1.26E-02	1.75
Cytochrome c	P99999	9.35E-03	1.72
Transketolase	P29401	5.12E-03	1.71
Heat shock 70 kDa protein 1A/1B	P08107	1.42E-02	1.69
Stress-70 protein, mitochondrial	P38646	1.63E-02	1.67
78 kDa glucose-regulated protein	P11021; P17066	1.89E-02	1.64
Melanoma-associated antigen 4	P43358	1.31E-02	1.63
Heat shock cognate 71 kDa protein	P11142	1.55E-02	1.63
Cytosol aminopeptidase	P28838	1.95E-02	1.59
LETM1 and EF-hand domain-containing protein 1, mitochondrial	O95202	1.93E-02	1.52

Appendix 1.3

Comparative proteomic analysis: DLKP *vs.* DLKPM

Description	Accession	Anova (p)	Max fold change
Receptor-type tyrosine-protein phosphatase F	P10586	4.00E-02	89.23
Intercellular adhesion molecule 1	P05362	1.09E-02	61.31
Roundabout homolog 2	Q9HCK4	1.93E-02	60.59
Chondroitin sulfate proteoglycan 4	Q6UVK1	2.28E-02	45.49
Plexin-B2	O15031	3.79E-02	27.33
Nectin-2	Q92692	2.59E-02	25.06
Hematopoietic progenitor cell antigen CD34	P28906	1.29E-02	24.97
PDZ and LIM domain protein 5	Q96HC4	1.48E-03	13.80
Collagen alpha-1(XIV) chain	Q05707	6.85E-04	12.64
Inactive tyrosine-protein kinase 7	Q13308	4.86E-02	10.40
Cathepsin Z	Q9UBR2	5.08E-04	10.01
Ras GTPase-activating-like protein IQGAP1	P46940	4.89E-03	8.99
Keratin, type II cytoskeletal 6A	P02538	3.68E-03	8.81
Ras-related protein Ral-A	P11233	1.92E-02	8.81
Prohibitin-2	Q99623	8.46E-03	8.35
Probable 28S rRNA (cytosine(4447)-C(5))-methyltransferase	P46087	9.45E-03	8.25
U5 small nuclear ribonucleoprotein 200 kDa helicase	O75643	1.99E-02	8.00
Prohibitin	P35232	1.18E-02	7.83
Cytoskeleton-associated protein 5	Q14008	3.39E-03	7.80
Filamin-B	O75369	2.67E-02	7.75
Importin-5	O00410	1.53E-03	7.44
Histone H4	P62805	3.39E-02	6.86
Alpha-2-macroglobulin receptor-associated protein	P30533	8.30E-03	6.68
Protein disulfide-isomerase A6	Q15084	1.95E-02	6.05
CD166 antigen	Q13740	2.10E-02	5.97
Paraspeckle component 1	Q8WXF1	2.73E-03	5.90
Hypoxia up-regulated protein 1	Q9Y4L1	9.52E-03	5.83
Splicing factor, proline- and glutamine-rich	P23246	2.81E-03	5.65
Caldesmon	Q05682	4.35E-02	5.60
Voltage-dependent anion-selective channel protein 2	P45880	1.55E-02	5.54
Spectrin beta chain, non-erythrocytic 1	Q01082	1.91E-02	5.52
Band 4.1-like protein 2	O43491	2.41E-04	5.44
Neutral cholesterol ester hydrolase 1	Q6PIU2	1.74E-03	5.23
Neuroblast differentiation-associated protein AHNAK	Q09666	2.80E-03	5.04
Spectrin alpha chain, non-erythrocytic 1	Q13813	2.51E-02	5.02
Heat shock 70 kDa protein 1A/1B	P08107	1.51E-03	4.88
60S ribosomal protein L13	P26373	4.41E-02	4.81
Cleavage and polyadenylation specificity factor subunit 6	Q16630	9.95E-03	4.79
Non-POU domain-containing octamer-binding protein	Q15233	5.05E-03	4.75
Keratin, type II cytoskeletal 1	P04264	1.38E-02	4.61
Ornithine aminotransferase, mitochondrial	P04181	2.04E-02	4.51
ATP-dependent RNA helicase DDX3X	O00571	4.86E-03	4.40
ATP synthase subunit alpha, mitochondrial	P25705	1.92E-02	4.26
Heat shock 70 kDa protein 1-like	P34931	2.76E-03	4.22
Exportin-1	O14980	6.30E-03	4.19

60S ribosomal protein L12	P30050	3.04E-02	4.00
Dolichyl-diphosphooligosaccharide--protein glycosyltransferase subunit 1	P04843	3.39E-02	3.90
Exportin-2	P55060	5.86E-03	3.90
Nucleolar RNA helicase 2	Q9NR30	9.75E-03	3.79
Barrier-to-autointegration factor	O75531	5.20E-04	3.79
ATP synthase subunit O, mitochondrial	P48047	1.43E-02	3.76
Phospholipase D3	Q8IV08	4.30E-03	3.70
ATP synthase subunit beta, mitochondrial	P06576	2.83E-02	3.69
Cytosolic acyl coenzyme A thioester hydrolase	O00154	2.38E-03	3.66
Annexin A2	P07355	1.86E-02	3.55
60S ribosomal protein L4	P36578	3.57E-02	3.55
60S acidic ribosomal protein P0-like	Q8NHW5	1.95E-02	3.52
Calnexin	P27824	1.83E-02	3.50
Trifunctional enzyme subunit beta, mitochondrial	P55084	3.50E-02	3.49
Proliferation-associated protein 2G4	Q9UQ80	9.76E-03	3.48
Calreticulin	P27797	7.16E-03	3.47
Cadherin-2	P19022	2.10E-02	3.39
Glutathione S-transferase kappa 1	Q9Y2Q3	2.99E-03	3.30
Tropomyosin alpha-4 chain	P67936	3.87E-03	3.27
Keratin, type I cytoskeletal 9	P35527	3.17E-02	3.26
Fumarate hydratase, mitochondrial	P07954	4.26E-03	3.22
RNA-binding protein 14	Q96PK6	1.23E-02	3.21
Peroxisomal multifunctional enzyme type 2	P51659	4.03E-02	3.18
Hydroxymethylglutaryl-CoA synthase, cytoplasmic	Q01581	1.74E-03	3.13
60S ribosomal protein L5	P46777	1.05E-02	3.12
Inorganic pyrophosphatase	Q15181; Q9H2U2	2.40E-02	3.06
Prolyl 3-hydroxylase 1	Q32P28	2.84E-03	3.03
Peroxiredoxin-6	P30041	1.38E-02	3.02
Protein CutA	O60888	1.96E-02	3.00
Nucleophosmin	P06748	1.18E-02	2.99
Protein disulfide-isomerase A4	P13667	5.68E-03	2.97
Cytoplasmic dynein 1 heavy chain 1	Q14204	6.08E-03	2.94
Lamin-B1	P20700	1.20E-03	2.94
Prelamin-A/C	P02545	2.19E-02	2.90
60S ribosomal protein L7a	P62424	3.04E-02	2.89
Drebrin-like protein	Q9UJU6	5.69E-03	2.85
Fructose-bisphosphate aldolase C	P09972	2.83E-02	2.82
THO complex subunit 4	Q86V81	9.47E-03	2.80
Transitional endoplasmic reticulum ATPase	P55072	2.31E-02	2.78
Adenylyl cyclase-associated protein 1	Q01518	1.80E-03	2.78
Annexin A1	P04083	3.11E-02	2.77
Adenylate kinase 2, mitochondrial	P54819	2.79E-02	2.74
Fructose-bisphosphate aldolase A	P04075	2.13E-02	2.74
Valine--tRNA ligase	P26640	4.78E-03	2.72
Receptor-type tyrosine-protein phosphatase C	P08575	1.39E-02	2.65
26S proteasome non-ATPase regulatory subunit 2	Q13200	3.17E-03	2.64

Thioredoxin domain-containing protein 12	O95881	2.21E-02	2.63
DNA replication licensing factor MCM7	P33993	1.22E-02	2.63
F-actin-capping protein subunit beta	P47756	7.98E-04	2.61
60S acidic ribosomal protein P1	P05386	2.71E-02	2.60
6-phosphogluconate dehydrogenase, decarboxylating	P52209	2.87E-03	2.60
Adenosylhomocysteinase	P23526	1.38E-02	2.53
Myosin-9	P35579	2.74E-02	2.45
X-ray repair cross-complementing protein 5	P13010	4.32E-05	2.45
Heat shock protein beta-1	P04792	1.33E-02	2.44
Malate dehydrogenase, mitochondrial	P40926	4.96E-03	2.42
Serine/arginine-rich splicing factor 7	Q16629	1.30E-02	2.39
Alpha-enolase	P06733	5.48E-03	2.38
Dihydrolipoyllysine-residue succinyltransferase component of 2-oxoglutarate dehydrogenase complex, mitochondrial	P36957	4.13E-03	2.35
Isoleucine--tRNA ligase, mitochondrial	Q9NSE4	2.15E-02	2.31
Putative heat shock protein HSP 90-beta-3	Q58FF7	2.57E-02	2.31
78 kDa glucose-regulated protein	P11021; O95399	1.00E-03	2.30
Bifunctional glutamate/proline--tRNA ligase	P07814	4.45E-04	2.29
Fatty acid synthase	P49327	3.99E-03	2.29
Protein SET	Q01105	7.34E-03	2.26
Heat shock protein HSP 90-beta	P08238; Q58FG1	5.16E-03	2.23
Heterogeneous nuclear ribonucleoprotein U	Q00839	3.31E-04	2.23
Ran-specific GTPase-activating protein	P43487	6.93E-03	2.22
60S ribosomal protein L24	P83731	1.56E-02	2.22
Serpin H1	P50454	9.30E-03	2.13
T-complex protein 1 subunit beta	P78371	2.98E-02	2.12
Proteasome subunit alpha type-3	P25788	1.59E-02	2.11
Hypoxanthine-guanine phosphoribosyltransferase	P00492	2.82E-02	2.09
Heat shock protein HSP 90-alpha	P07900	2.61E-03	2.09
Neutral alpha-glucosidase AB	Q14697	3.13E-03	2.07
Far upstream element-binding protein 1	Q96AE4	6.99E-03	2.05
Endoplasmin	P14625	1.97E-03	2.03
Glucosidase 2 subunit beta	P14314	5.14E-04	2.01
Heat shock protein 105 kDa	Q92598	1.54E-02	2.00
C-1-tetrahydrofolate synthase, cytoplasmic	P11586	2.43E-02	2.00
Protein disulfide-isomerase	P07237	1.14E-02	1.97
Elongation factor 1-gamma	P26641	1.02E-02	1.91
Nucleoprotein TPR	P12270	7.77E-03	1.90
Heterogeneous nuclear ribonucleoprotein Q	O60506	1.67E-03	1.89
Tubulin beta-6 chain	Q9BUF5	1.96E-03	1.88
T-complex protein 1 subunit theta	P50990	9.30E-03	1.87
Transcription intermediary factor 1-beta	Q13263	1.11E-02	1.85
T-complex protein 1 subunit eta	Q99832	1.91E-03	1.84
Endoplasmic reticulum resident protein 29	P30040	5.94E-03	1.84
Leucine-rich PPR motif-containing protein, mitochondrial	P42704	4.71E-03	1.81

Heterogeneous nuclear ribonucleoprotein M	P52272	2.32E-02	1.75
Actin-related protein 2/3 complex subunit 4	P59998	3.49E-02	1.74
Protein phosphatase 1G	O15355	6.27E-03	1.74
Glyceraldehyde-3-phosphate dehydrogenase	P04406	2.61E-02	1.70
T-complex protein 1 subunit gamma	P49368	1.40E-02	1.64
Retinal dehydrogenase 1	P00352	2.07E-03	1.57
Transketolase	P29401	1.28E-02	1.57
Peroxiredoxin-1	Q06830	2.86E-02	1.55
Heat shock cognate 71 kDa protein	P11142	2.90E-02	1.53

Appendix 1.3

Comparative proteomic analysis: DLKPSQ *vs.* DLKPI

Description	Accession	Anova (p)	Max fold change
Receptor-type tyrosine-protein phosphatase C	P08575	1.43E-02	42.10
Cadherin-2	P19022	4.13E-02	29.00
Splicing factor, proline- and glutamine-rich	P23246	3.07E-02	28.92
Catenin beta-1	P35222	5.52E-03	26.80
CD166 antigen	Q13740	2.75E-02	24.30
Roundabout homolog 2	Q9HCK4	1.66E-02	21.85
BH3-interacting domain death agonist	P55957	1.82E-03	18.07
RNA-binding protein 14	Q96PK6	3.22E-02	17.52
Desmoglein-2	Q14126	2.62E-02	17.34
Non-POU domain-containing octamer-binding protein	Q15233	3.02E-02	14.81
Fascin	Q16658	4.17E-02	14.34
Catenin alpha-1	P35221	1.42E-02	10.81
Prohibitin-2	Q99623	6.30E-03	10.26
Prohibitin	P35232	7.57E-03	10.06
Neuroblast differentiation-associated protein AHNAK	Q09666	5.60E-05	9.29
Kinectin	Q86UP2	1.26E-02	8.37
Prelamin-A/C	P02545	4.68E-02	7.38
D-3-phosphoglycerate dehydrogenase	O43175	1.08E-03	7.36
Filamin-A	P21333	6.95E-03	7.07
Pirin	O00625	2.06E-04	6.45
Ataxin-10	Q9UBB4	1.59E-03	6.23
Extended synaptotagmin-1	Q9BSJ8	1.77E-02	6.23
Creatine kinase B-type	P12277	5.94E-04	6.08
Ran-specific GTPase-activating protein	P43487	3.38E-03	5.89
Filamin-B	O75369	2.30E-02	5.68
Ras GTPase-activating-like protein IQGAP1	P46940	3.27E-03	5.50
Nucleolar RNA helicase 2	Q9NR30	8.07E-03	5.36
3-hydroxyisobutyrate dehydrogenase, mitochondrial	P31937	3.09E-03	5.12
Superoxide dismutase [Cu-Zn]	P00441	3.46E-03	5.07
Tropomyosin alpha-1 chain	P09493	2.19E-02	4.78
Heat shock protein beta-1	P04792	3.03E-04	4.76
Serine hydroxymethyltransferase, mitochondrial	P34897	2.04E-03	4.68
Tubulin-specific chaperone A	O75347	1.76E-02	4.44
Glutathione S-transferase P	P09211	9.46E-03	4.41
Glutathione reductase, mitochondrial	P00390	6.73E-03	4.31
U5 small nuclear ribonucleoprotein 200 kDa helicase	O75643	2.03E-02	4.20
Hydroxymethylglutaryl-CoA synthase, cytoplasmic	Q01581	2.22E-02	4.15
Prosaposin	P07602	2.62E-02	4.14
Phosphoglycerate kinase 1	P00558	5.72E-03	4.13
Lamin-B1	P20700	1.51E-04	4.06
Ras-related protein Ral-A	P11233	1.06E-02	4.03
Proliferating cell nuclear antigen	P12004	9.88E-03	3.86
Tumor protein D54	O43399	5.08E-03	3.72
Sepiapterin reductase	P35270	2.61E-02	3.64
Crk-like protein	P46109	1.46E-02	3.64
Lamina-associated polypeptide 2, isoform alpha	P42166	1.49E-02	3.60

Macrophage migration inhibitory factor	P14174	3.81E-04	3.56
Puromycin-sensitive aminopeptidase	P55786	9.45E-03	3.46
Actin, cytoplasmic 1	P60709	2.94E-02	3.45
Spermidine synthase	P19623	2.89E-02	3.45
Melanoma-associated antigen 4	P43358	9.84E-03	3.44
Adenine phosphoribosyltransferase	P07741	2.50E-02	3.39
Annexin A2	P07355	1.52E-02	3.37
Histone H4	P62805	4.78E-03	3.34
Peptidyl-prolyl cis-trans isomerase A	P62937	2.96E-02	3.31
Actin, aortic smooth muscle	P62736	2.86E-02	3.26
Spectrin alpha chain, non-erythrocytic 1	Q13813	1.11E-02	3.23
PDZ and LIM domain protein 5	Q96HC4	1.20E-02	3.19
Ubiquitin carboxyl-terminal hydrolase isozyme L1	P09936	2.41E-02	3.02
Alanine--tRNA ligase, cytoplasmic	P49588	5.42E-03	2.98
Alpha-actinin-4	O43707	1.14E-02	2.93
Alpha-aminoadipic semialdehyde dehydrogenase	P49419	3.32E-03	2.93
Carbonyl reductase [NADPH] 1	P16152	3.27E-02	2.90
Electron transfer flavoprotein subunit alpha, mitochondrial	P13804	1.15E-02	2.80
Phosphoglycerate mutase 1	P18669	6.68E-03	2.79
Puromycin-sensitive aminopeptidase-like protein	A6NEC2	1.62E-02	2.76
Ubiquitin-conjugating enzyme E2 variant 1	Q13404	1.39E-02	2.74
Aconitate hydratase, mitochondrial	Q99798	1.20E-02	2.73
Heat shock protein 105 kDa	Q92598	1.53E-02	2.70
ATP-dependent RNA helicase A	Q08211	3.92E-03	2.70
Calnexin	P27824	1.91E-02	2.70
Heterogeneous nuclear ribonucleoprotein H3	P31942	2.77E-03	2.67
Transitional endoplasmic reticulum ATPase	P55072	3.92E-03	2.56
Exportin-2	P55060	3.40E-02	2.49
Alpha-enolase	P06733	1.67E-02	2.49
C-1-tetrahydrofolate synthase, cytoplasmic	P11586	4.56E-04	2.48
Stathmin	P16949	2.68E-02	2.44
Microtubule-associated protein 2	P11137	1.93E-02	2.42
Aspartate aminotransferase, mitochondrial	P00505	1.59E-03	2.37
Heat shock protein 75 kDa, mitochondrial	Q12931	1.06E-02	2.37
L-lactate dehydrogenase B chain	P07195	3.60E-02	2.34
Ubiquitin-like modifier-activating enzyme 1	P22314	8.50E-03	2.31
60 kDa heat shock protein, mitochondrial	P10809	4.17E-03	2.31
Succinyl-CoA ligase [GDP-forming] subunit beta, mitochondrial	Q96I99	1.38E-02	2.23
Peptidyl-prolyl cis-trans isomerase B	P23284	1.32E-02	2.22
Nuclear autoantigenic sperm protein	P49321	1.40E-02	2.16
Malate dehydrogenase, cytoplasmic	P40925	2.08E-02	2.15
Nucleophosmin	P06748	2.93E-02	2.07
Bifunctional purine biosynthesis protein PURH	P31939	1.38E-02	1.99
Transketolase	P29401	2.08E-02	1.94
Stress-70 protein, mitochondrial	P38646	1.00E-02	1.92
Peroxiredoxin-1	Q06830	3.52E-03	1.80

ATP synthase subunit alpha, mitochondrial	P25705	2.16E-02	1.74
Malate dehydrogenase, mitochondrial	P40926	5.91E-03	1.56

Appendix 1.5

Comparative proteomic analysis: DLKPSQ *vs.* DLKPM

Description	Accession	Anova (p)	Max fold change
Probable 28S rRNA (cytosine(4447)-C(5))-methyltransferase	P46087	1.70E-03	12.26
U5 small nuclear ribonucleoprotein 200 kDa helicase	O75643	1.44E-02	11.69
Prohibitin-2	Q99623	5.54E-03	11.52
Splicing factor, proline- and glutamine-rich	P23246	5.15E-03	10.66
Non-POU domain-containing octamer-binding protein	Q15233	2.00E-03	10.17
PDZ and LIM domain protein 5	Q96HC4	1.77E-03	9.67
Prohibitin	P35232	1.41E-02	9.45
Neuroblast differentiation-associated protein AHNAK	Q09666	5.56E-04	8.04
Histone H4	P62805	1.63E-02	7.84
RNA-binding protein 14	Q96PK6	4.59E-03	7.59
Ras-related protein Ral-A	P11233	9.63E-03	7.46
Shootin-1	A0MZ66	1.29E-03	7.02
Caprin-1	Q14444	1.26E-02	6.91
D-3-phosphoglycerate dehydrogenase	O43175	2.51E-04	6.70
Ras GTPase-activating-like protein IQGAP1	P46940	8.84E-03	6.17
Catenin beta-1	P35222	2.19E-02	5.71
Kinectin	Q86UP2	8.39E-03	5.30
Glutathione S-transferase kappa 1	Q9Y2Q3	1.28E-02	5.22
Nucleolar RNA helicase 2	Q9NR30	2.41E-03	5.13
Guanine nucleotide-binding protein G(i) subunit alpha-1	P63096; Q03113	1.91E-02	5.01
Pirin	O00625	3.10E-04	4.95
Heat shock 70 kDa protein 1A/1B	P08107	2.36E-03	4.84
Filamin-B	O75369	2.61E-02	4.72
Tumor protein D54	O43399	1.76E-02	4.31
Calreticulin	P27797	9.51E-03	4.12
Cytoskeleton-associated protein 5	Q14008	1.60E-02	4.10
Collagen alpha-1(XIV) chain	Q05707	9.72E-03	4.05
Filamin-A	P21333	3.83E-02	4.04
Heat shock 70 kDa protein 1-like	P34931	4.09E-03	3.98
Exportin-1	O14980	1.43E-02	3.96
Spectrin alpha chain, non-erythrocytic 1	Q13813	3.00E-02	3.93
Adenosylhomocysteinase	P23526	6.64E-03	3.86
Tropomyosin alpha-4 chain	P67936; P07951	5.00E-04	3.74
Importin-5	O00410	1.27E-03	3.65
Putative heat shock protein HSP 90-beta-3	Q58FF7; Q58FF8	3.55E-03	3.58
Cleavage and polyadenylation specificity factor subunit 6	Q16630	1.76E-02	3.57
Serpin H1	P50454	3.21E-03	3.52
Heat shock protein beta-1	P04792	5.26E-03	3.52
Calnexin	P27824	5.69E-03	3.48

Lamin-B1	P20700	9.74E-04	3.35
Neutral alpha-glucosidase AB	Q14697	7.90E-03	3.25
Nucleophosmin	P06748	2.05E-02	3.24
Cytosolic acyl coenzyme A thioester hydrolase	O00154	2.46E-03	3.11
Exportin-2	P55060	3.95E-03	3.10
ATP-dependent RNA helicase DDX3X	O00571	1.30E-02	3.08
Annexin A2	P07355	8.36E-03	3.05
Probable ATP-dependent RNA helicase DDX5	P17844	1.57E-02	3.02
ATP synthase subunit alpha, mitochondrial	P25705	1.09E-02	3.02
Serine hydroxymethyltransferase, mitochondrial	P34897	6.34E-03	2.99
Receptor-type tyrosine-protein phosphatase C	P08575	2.13E-02	2.94
Protein disulfide-isomerase A4	P13667	1.29E-03	2.94
Peroxiredoxin-6	P30041	3.40E-03	2.92
60S ribosomal protein L5	P46777	1.77E-02	2.90
F-actin-capping protein subunit beta	P47756	1.33E-03	2.90
Fumarate hydratase, mitochondrial	P07954	3.48E-03	2.90
Myotrophin	P58546	1.13E-02	2.90
60S acidic ribosomal protein P0-like	Q8NHW5	3.35E-02	2.89
Tropomyosin alpha-1 chain	P09493	2.93E-02	2.87
Drebrin-like protein	Q9UJU6	3.40E-03	2.84
Hypoxanthine-guanine phosphoribosyltransferase	P00492	5.74E-04	2.84
Histone H2A type 1-B/E	P04908	5.36E-03	2.81
Phosphoglycerate kinase 1	P00558	2.78E-02	2.75
THO complex subunit 4	Q86V81	2.62E-02	2.69
Acetyl-CoA acetyltransferase, mitochondrial	P24752	4.15E-03	2.69
6-phosphogluconate dehydrogenase, decarboxylating	P52209	7.68E-03	2.69
Probable ATP-dependent RNA helicase DDX6	P26196	5.91E-03	2.68
Protein disulfide-isomerase A6	Q15084	9.22E-03	2.64
Adenylate kinase 2, mitochondrial	P54819	1.13E-02	2.62
Ran-specific GTPase-activating protein	P43487	1.20E-02	2.60
Alpha-enolase	P06733; P13929	1.68E-02	2.58
26S proteasome non-ATPase regulatory subunit 2	Q13200	4.17E-03	2.57
Inorganic pyrophosphatase	Q15181; Q9H2U2	3.23E-02	2.56
Peroxiredoxin-1	Q06830	6.14E-03	2.46
Keratin, type II cuticular Hb4	Q9NSB2	1.70E-03	2.42
Isoleucine--tRNA ligase, mitochondrial	Q9NSE4	1.05E-02	2.42
Importin subunit beta-1	Q14974	1.08E-02	2.39
Band 4.1-like protein 2	O43491	3.31E-02	2.34
Keratin, type II cytoskeletal 1	P04264	4.95E-02	2.34
Retinal dehydrogenase 1	P00352	2.33E-02	2.32
Valine--tRNA ligase	P26640	8.10E-03	2.31
Far upstream element-binding protein 1	Q96AE4	3.33E-03	2.25
Heat shock protein HSP 90-beta	P08238	6.96E-03	2.23
Heterogeneous nuclear ribonucleoprotein K	P61978	2.28E-02	2.21
Heat shock protein 105 kDa	Q92598	1.36E-02	2.20
Alpha-actinin-1	P12814	3.55E-02	2.19

Cytoplasmic dynein 1 heavy chain 1	Q14204	2.09E-03	2.18
Catenin alpha-1	P35221	2.08E-02	2.17
Calcyclin-binding protein	Q9HB71	1.45E-02	2.16
Pyruvate kinase PKM	P14618	2.08E-02	2.15
Actin, aortic smooth muscle	P62736	2.57E-02	2.13
Heterogeneous nuclear ribonucleoprotein Q	O60506	1.67E-03	2.08
Ras-related protein Rab-2A	P61019	2.71E-02	2.04
Malate dehydrogenase, mitochondrial	P40926	2.11E-02	2.03
Peptidyl-prolyl cis-trans isomerase A	P62937	1.45E-02	2.01
Actin, cytoplasmic 1	P60709	1.17E-02	2.01
Ubiquitin-like modifier-activating enzyme 1	P22314	1.20E-02	1.97
ATP-citrate synthase	P53396	1.69E-03	1.97
Dihydrolipoyllysine-residue succinyltransferase component of 2-oxoglutarate dehydrogenase complex, mitochondrial	P36957	6.17E-04	1.97
T-complex protein 1 subunit theta	P50990	9.15E-03	1.92
Puromycin-sensitive aminopeptidase-like protein	A6NEC2	3.35E-02	1.90
78 kDa glucose-regulated protein	P11021	4.48E-04	1.90
Fructose-bisphosphate aldolase A	P04075	2.44E-02	1.89
Multifunctional protein ADE2	P22234	2.02E-02	1.85
40S ribosomal protein S19	P39019	1.85E-02	1.85
Fatty acid synthase	P49327	5.49E-04	1.84
X-ray repair cross-complementing protein 5	P13010	1.75E-02	1.81
Aspartate aminotransferase, mitochondrial	P00505	4.59E-03	1.69
Stress-70 protein, mitochondrial	P38646	1.50E-02	1.61
3-hydroxyacyl-CoA dehydrogenase type-2	Q99714	2.94E-03	1.54
Heat shock cognate 71 kDa protein	P11142	9.38E-03	1.54

Appendix 1.6

Comparative proteomic analysis: DLKPI v DLKPM

Description	Accession	Anova (p)	Max fold change
Receptor-type tyrosine-protein phosphatase C	P08575	2.77E-02	41.79
CD166 antigen	Q13740	2.54E-02	30.15
Roundabout homolog 2	Q9HCK4	6.95E-03	26.95
Receptor-type tyrosine-protein phosphatase F	P10586	1.78E-02	25.10
Desmoglein-2	Q14126	1.68E-02	24.70
Cadherin-2	P19022	3.44E-02	20.87
Alpha-2-macroglobulin receptor-associated protein	P30533	1.59E-02	9.17
Nectin-2	Q92692	3.12E-02	7.93
Catenin beta-1	P35222	1.42E-02	7.93
3-hydroxyisobutyrate dehydrogenase, mitochondrial	P31937	4.57E-03	7.33
Creatine kinase B-type	P12277	1.72E-03	7.29
Tubulin-specific chaperone A	O75347	4.50E-03	4.52
Peroxisomal acyl-coenzyme A oxidase 1	Q15067	2.86E-02	4.48
Hydroxymethylglutaryl-CoA synthase, cytoplasmic	Q01581	2.39E-02	4.26
Alpha-aminoadipic semialdehyde dehydrogenase	P49419	2.51E-03	4.12
Glutathione S-transferase kappa 1	Q9Y2Q3	2.52E-02	4.05
Filamin-A	P21333	1.87E-02	3.89
Heat shock 70 kDa protein 1-like	P34931	4.53E-03	3.81
L-lactate dehydrogenase B chain	P07195	2.29E-02	3.47
Adenine phosphoribosyltransferase	P07741	7.56E-03	3.45
Annexin A5	P08758	9.87E-04	3.45
Ran-specific GTPase-activating protein	P43487	1.31E-03	3.43
Nucleoprotein TPR	P12270	3.79E-02	3.35
Glutathione S-transferase P	P09211	1.28E-02	3.33
Peroxisomal multifunctional enzyme type 2	P51659	1.07E-02	3.32
Carbonyl reductase [NADPH] 1	P16152	4.63E-03	3.22
Serpin H1	P50454	1.46E-02	3.18
F-actin-capping protein subunit beta	P47756	1.56E-03	3.07
PDZ and LIM domain protein 5	Q96HC4	3.98E-02	3.03
Peptidyl-prolyl cis-trans isomerase A	P62937	2.28E-02	3.02
Heat shock 70 kDa protein 1A/1B	P08107	7.65E-03	2.93
Superoxide dismutase [Cu-Zn]	P00441	1.45E-02	2.88
Macrophage migration inhibitory factor	P14174	6.15E-03	2.79
Band 4.1-like protein 2	O43491	3.50E-03	2.75
ATP-dependent RNA helicase A	Q08211	1.70E-02	2.74
Dihydrolipoyllysine-residue succinyltransferase component of 2-oxoglutarate dehydrogenase complex, mitochondrial	P36957	1.73E-03	2.72
Keratin, type II cytoskeletal 1	P04264	2.59E-02	2.68
Malate dehydrogenase, cytoplasmic	P40925	2.30E-02	2.66
Tumor protein D52	P55327	1.62E-02	2.58
Electron transfer flavoprotein subunit alpha, mitochondrial	P13804	3.03E-03	2.49
Phosphoglycerate mutase 1	P18669	4.10E-03	2.46
C-1-tetrahydrofolate synthase, cytoplasmic	P11586	5.35E-03	2.41
Phosphoglycerate kinase 1	P00558	1.07E-02	2.39
Actin-related protein 2/3 complex subunit 4	P59998	3.45E-03	2.37

Heat shock cognate 71 kDa protein	P11142	1.35E-02	2.33
Ubiquitin carboxyl-terminal hydrolase isozyme L1	P09936	2.45E-02	2.25
Heat shock protein HSP 90-alpha	P07900	9.74E-03	2.20
Aconitate hydratase, mitochondrial	Q99798	3.47E-02	2.14
Fatty acid synthase	P49327	4.08E-03	2.11
Puromycin-sensitive aminopeptidase	P55786	1.86E-03	2.09
Peptidyl-prolyl cis-trans isomerase B	P23284	4.24E-03	2.06
Calreticulin	P27797	2.68E-02	2.05
Protein disulfide-isomerase A6	Q15084	2.80E-02	1.96
Peroxiredoxin-1	Q06830	1.45E-02	1.95
Enoyl-CoA delta isomerase 1, mitochondrial	P42126	2.08E-03	1.86
Melanoma-associated antigen 4	P43358	2.93E-02	1.82
Fructose-bisphosphate aldolase A	P04075	1.90E-02	1.76
60 kDa heat shock protein, mitochondrial	P10809	1.57E-02	1.70